UNITED NATIONS EDUCATIONAL, SCIENTIFIC AND CULTURAL ORGANIZATION
INTERNATIONAL ATOMIC ENERGY AGENCY
INTERNATIONAL CENTRE FOR THEORETICAL PHYSICS

SMR: 960/7

WORKSHOP ON NONLINEAR CONTROL AND CONTROL OF CHAOS

(17 - 28 June 1996)

"Chaos Control and Chaos Synchronization in High Dimensions"

presented by:

Mingzhou Ding
Center for Complex Systems and Department of Mathematics
Florida Atlantic University
Boca Raton, FL 33431
U.S.A.

Reprinted from

PHYSICA D

Physica D 74 (1994) 386–394

Controlling chaos in a temporally irregular environment

Mingzhou Ding [a], Edward Ott [b,c], Celso Grebogi [b,d]

[a] *Center for Complex Systems and Department of Mathematics, Florida Atlantic University, Boca Raton, FL 33431, USA*
[b] *Institute for Plasma Research, University of Maryland, College Park, MD 20742, USA*
[c] *Institute for Systems Research and Departments of Physics and of Electrical Engineering, University of Maryland, College Park, MD 20742, USA*
[d] *Department of Mathematics and Institute for Physical Science and Technology, University of Maryland, College Park, MD 20742, USA*

Received 8 October 1993; revised 14 January 1994; accepted 4 February 1994; communicated by P.E. Rapp

N·H

ELSEVIER

ELSEVIER

Physica D 74 (1994) 386–394

PHYSICA D

Controlling chaos in a temporally irregular environment

Mingzhou Ding [a], Edward Ott [b,c], Celso Grebogi [b,d]

[a] Center for Complex Systems and Department of Mathematics, Florida Atlantic University, Boca Raton, FL 33431, USA

[b] Institute for Plasma Research, University of Maryland, College Park, MD 20742, USA

[c] Institute for Systems Research and Departments of Physics and of Electrical Engineering, University of Maryland, College Park, MD 20742, USA

[d] Department of Mathematics and Institute for Physical Science and Technology, University of Maryland, College Park, MD 20742, USA

Received 8 October 1993; revised 14 January 1994; accepted 4 February 1994; communicated by P.E. Rapp

Abstract

In this paper we examine the problem of controlling a chaotic system embedded in a time varying environment, where the environmental variation may be of relatively large amplitude, and may have a fairly irregular nature. Our results show that a previous method of controlling chaos, which selects and stabilizes unstable steady states or unstable periodic orbits, can be adapted to this time irregular situation, provided that one can make on-line, short-term predictions of the future evolution of the environment. We demonstrate this by using an example in which a ship is impacted by ocean waves on its side. The goal of control here is to prevent capsizing from taking place.

1. Introduction

Recently, there has been much theoretical and experimental work on the use of small controls to improve the performance of a system that behaves chaotically in the absence of control [1,2]. The basic idea in the previous work is to take advantage of the existence of naturally occurring unstable periodic orbits and unstable steady states embedded in the chaotic set in phase space. Specifically, choosing an unstable periodic orbit that yields improved system performance, one programs the control to stabilize the chosen orbit. This picture, however, presupposes the existence of a time independent autonomous system or a time periodic nonautonomous system. While noise can be accommodated, it must be small enough so that the basic picture is not invalidated [1].

In this paper, we consider cases where the system is situated in an environment that varies with time, and this variation may be of fairly large amplitude and may be quite irregular. Here the environment can be thought of as some large dynamical system whose evolution is independent of the system to be controlled, but whose state strongly effects the system to be controlled. The main point we wish to make is that the previous ideas on a temporally constant environment can still be utilized and adapted successfully to the case where the environment varies irregularly, *provided* that one can make on-line,

0167-2789/94/$07.00
SSDI 0167-2789(94)00034-N

short-term predictions of the future evolution of the environment. In particular, with prediction one is able to stabilize the motion indefinitely, thereby eliminating large uncontrolled excursions away from the desired behavior. This improvement is especially important for situations where the loss of control may lead to the collapse of the system. In the remainder of this paper, we demonstrate the above by treating a specific example: the control of a ship subject to ocean waves impinging on its side. The object is to use the control to prevent capsizing. In terms of the discussion above, the "environment" here is represented by the ocean waves. If the waves were purely periodic in time, then the previous work [1,2] would apply straightforwardly. The focus of this work, however, is on the effect introduced by significant irregular amplitude and phase variations of the waves. We emphasize that our technique is heuristic rather than rigorous in that it is not supported by convergence theorems. Thus its justification lies in how well it works when applied.

We use the following nonlinear oscillator to model the ship's rolling dynamics in lateral waves:

$$\ddot{x} + \nu\dot{x} + \omega^2(x - \alpha x^3) = W(t), \tag{1}$$

where x is a variable characterizing the angle from the ship's mast to the vertical direction, ν is the friction coefficient, ω is the eigenfrequency of small vibrations around the origin, α denotes the strength of nonlinearity, and $W(t)$ represents the effect of the ocean waves impinging on the ship. The restoring force, $-\omega^2(x - \alpha x^3)$, is derived from the potential

$$V(x) = \omega^2(\tfrac{1}{2}x^2 - \alpha\tfrac{1}{4}x^4).$$

In the absence of waves, i.e., $W(t) = 0$, for a small displacement in x, the subsequent motion damps out and the ship reverts back to its upright position. For large displacements in x, gravity overcomes buoyancy, and x tends to the attractor at $|x| = \infty$. When this occurs we say the ship has capsized. Other work on ship dynamics using similar models can be found in [3].

We suppose that the irregular wave term $W(t)$ has the following form:

$$\begin{aligned} W(t) &= f(t)[1 + \epsilon_a g(t)]\sin\phi(t) \\ &\equiv F(t)\sin\phi(t), \end{aligned} \tag{2}$$

where $F(t)$ is the amplitude, with $f(t)$ its slowly varying component and $g(t)$ its fast irregularly varying component, and $\phi(t)$ is the phase, whose evolution is determined by

$$\dot{\phi}(t) = \Omega + \epsilon_p h(t). \tag{3}$$

Here again $h(t)$ is an irregular function of time. In what follows, we (somewhat arbitrarily) model the temporally irregular functions $g(t)$ and $h(t)$ as outputs of well-known chaotic systems. Specifically, we use

$$g(t) = \frac{y(t) - \langle y(t)\rangle}{\sqrt{\langle [y(t) - \langle y(t)\rangle]^2\rangle}},$$

where $y(t)$ is a solution of the following driven Duffing system:

$$\ddot{y} + 0.05\dot{y} + y^3 = 7.5\cos t,$$

and

$$h(t) = \frac{z_1(t) - \langle z_1(t)\rangle}{\sqrt{\langle [z_1(t) - \langle z_1(t)\rangle]^2\rangle}},$$

with $z_1(t)$ taken from the Rössler system,

$$\begin{aligned} \dot{z}_1 &= -z_2 - z_3, \\ \dot{z}_2 &= z_1 + 0.398 z_2, \\ \dot{z}_3 &= 2 + z_3(z_1 - 4). \end{aligned}$$

The symbol $\langle\ \rangle$ denotes temporal average. Since $g(t)$ and $h(t)$ are normalized, ϵ_a and ϵ_p measure the relative strength of amplitude irregularity and that of phase irregularity, respectively. (We emphasize that our use of low dimensional chaotic systems to produce the irregularly varying functions $g(t)$ and $h(t)$ is merely a convenience, and there should be no essential difference in what follows if these functions are stochastic or are produced by some high dimensional chaotic process.)

The case of purely sinusoidal waves, (i.e., $\epsilon_a = \epsilon_p = 0$ and $f(t) = f_0$, where f_0 is a constant), will be used as the basis for control later when irregularities are introduced into the system. The evolution of Eq. (1) with increasing wave amplitude f_0 and $\epsilon_a = \epsilon_p = 0$ is shown in the bifurcation diagram in Fig. 1. The surface of section here is taken every time $W(t)$ crosses zero with $dW(t)/dt > 0$ (i.e., $\Omega t_n = 2n\pi$). For $0 < f_0 < 0.7$ the oscillation of the ship is periodic with the period equal to that of the wave. We henceforth call this orbit the period one orbit. Following a period doubling cascade the ship's response becomes chaotic. At $f_0 \approx 0.726$ a crisis takes place in which the bounded chaotic attractor is destroyed by colliding with its basin boundary. As the wave amplitude increases past this crisis value, since no bounded attractor exists in the system, almost all initial conditions tend to the attractor at $|x| = \infty$ (i.e., the ship capsizes). Also shown in Fig. 1 as a dashed curve is the period one orbit after it loses stability. Now suppose that $f(t)$ is a gradually increasing function of time starting from $f(t) = 0$. We anticipate that in the absence of control the ship will capsize some time after $f(t)$ exceeds the crisis value. To prevent this, one starts to apply control to stabilize the period one orbit in Fig. 1 when the wave is still small. As a result, we show that the ship survives waves whose amplitude can significantly exceed the crisis value. More importantly, by incorporating the prediction feature mentioned earlier, and suitably modifying the control procedure, we shall find that we are able to prevent capsizing in the presence of substantial wave irregularities. These results may be viewed as widening the practical applicability of the previous work on chaos control using unstable periodic orbits.

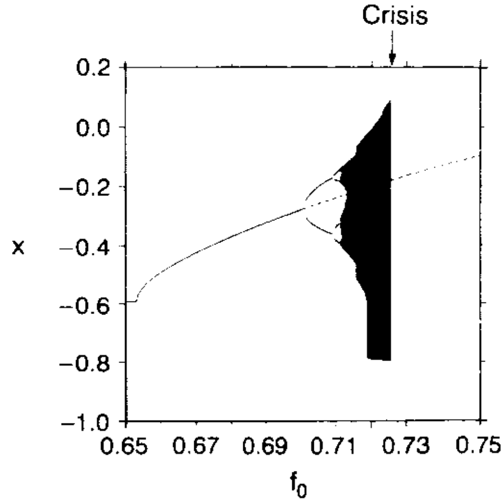

Fig. 1. Bifurcation diagram of Eq. (1). The dashed line indicates the unstable period one orbit after the period doubling bifurcation.

2. Control method

The equation of motion for the variable x, when control is applied, becomes

$$\ddot{x} + \nu\dot{x} + \omega^2(x - \alpha x^3) = W(t) + C(t), \quad (4)$$

where we take $C(t)$ to be a constant between successive crossings of the surface of section. In practical terms, $C(t)$ can be thought of as the balancing force provided by temporally shifting ballast on the ship, and the value of $C(t)$ is assumed to be bounded between $-C_0$ and C_0, i.e., $-C_0 \le C(t) \le C_0$. In fact, we shall be interested in the case where C_0 is relatively small compared to the force exerted by the waves. We take the surface of section to specify the system state at times $t = t_n$ such that $W(t) = 0$ and $dW(t)/dt > 0$. Assuming that $f(t) > 0$ and that the right hand side of Eq. (3) is positive this corresponds to $\phi(t_n) = 2n\pi$ (see Eq. (2)).

Fig. 2 shows a schematic diagram illustrating the control technique applied in the time interval $t_n \le t \le t_{n+1}$. A fixed point of the Poincaré map and its stable and unstable directions are constructed for $\epsilon_a = \epsilon_p = 0$ and $f(t) = f(t_n)$. Here we imagine that $f(t)$ can be treated as a constant in the interval $t_n < t < t_{n+1}$. (Note that

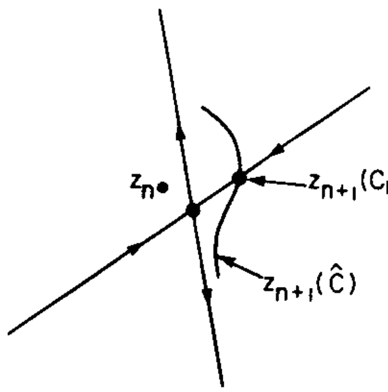

Fig. 2. Schematic of the control method.

due to the slow variation of $f(t)$ the fixed point location at $t = t_n$ changes with n.) By letting $\epsilon_a \neq 0$ and $\epsilon_p \neq 0$, we introduce irregularity into the wave. The task now is to stabilize the motion around the fixed point. Suppose that at $t = t_n$, the system state is denoted by z_n, where $z = (x, y = \dot{x})$. From observation of waves propagating toward the ship, we assume that we can make an accurate prediction of $W(t)$ for $t_n \leq t \leq t_{n+1}$. Integrating Eq. (4) with this predicted $W(t)$, and with various values of $C(t) = \hat{C}$ (the number of such values we choose in the following numerical experiments is 500), where $\hat{C}$ is a constant in the interval $[-C_0, C_0]$, we obtain images of the system state on the next surface of section at $t = t_{n+1}$, which form a curve as shown in Fig. 2. The value $\hat{C} = C_n$ of the control that we actually apply to the ship is chosen so that the system state falls on the stable direction of the fixed point constructed for $\epsilon_a = \epsilon_p = 0$ and $f(t) = f(t_n)$. As shown in the next section, repeated application of this procedure achieves the goal of stabilizing the ship's motion even for situations where the irregularity is substantial.

3. Numerical results

We select the following parameters for the numerical computations: $\nu = 0.5$, $\omega = \Omega = 1.0$, $\alpha = 1.0$, $C_0 = 0.01$ for Case 1 and $C_0 = 0.1$ for Cases 2–6. The integration step size $= 2\pi/200$.

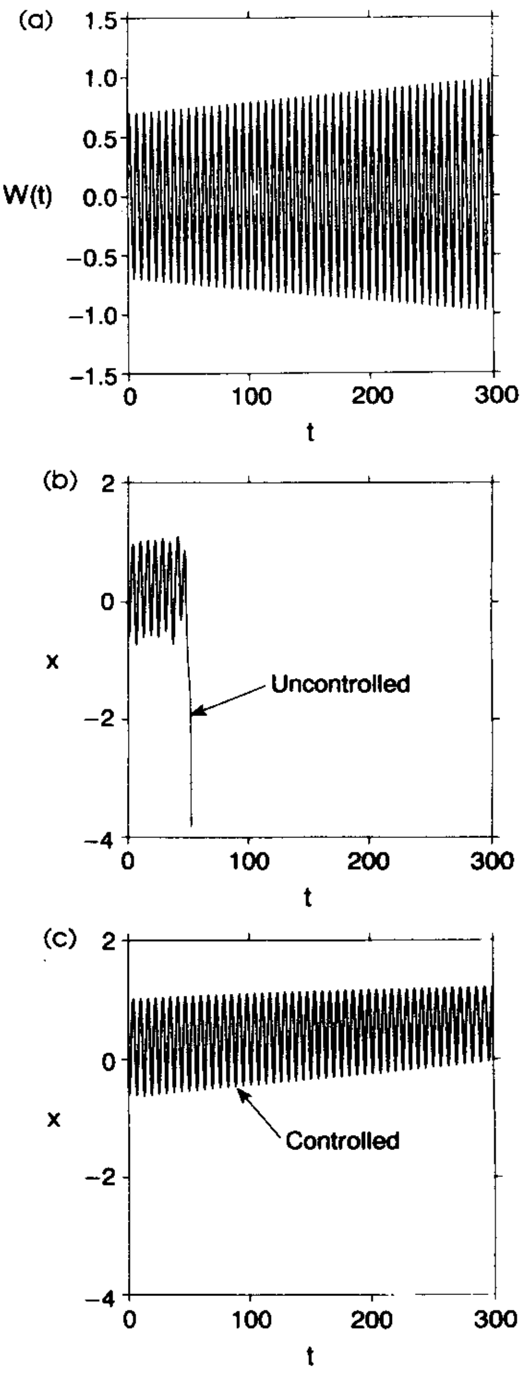

Fig. 3. (a) Segment of the increasing wave with $\epsilon_a = \epsilon_p = 0.0$, (b) uncontrolled capsizing orbit and (c) controlled orbit.

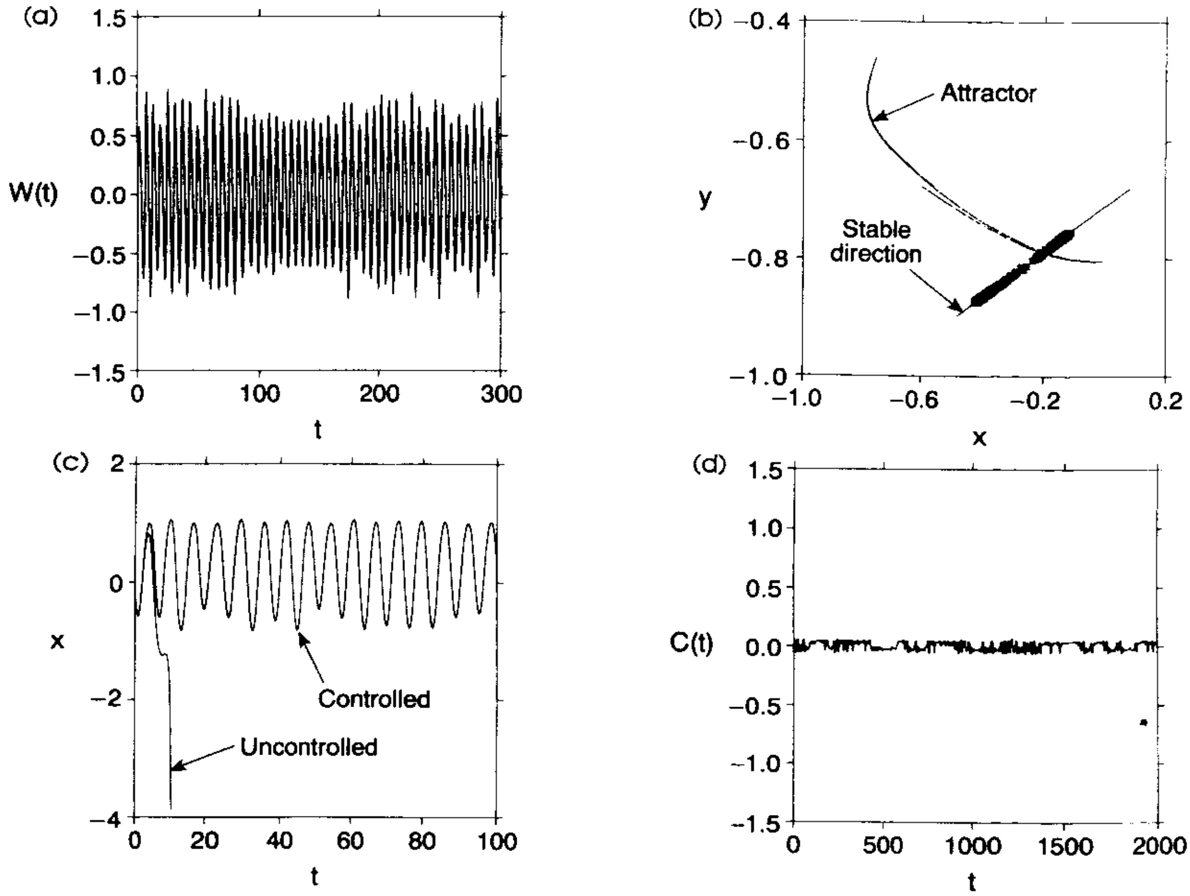

Fig. 4. (a) Segment of the irregular wave with $f(t) = f_0 = 0.72$, $\epsilon_a = 0.2$ and $\epsilon_p = 0.0$, (b) controlled orbit on the surface of section superposed on the attractor, (c) controlled together with uncontrolled orbit and (d) control function $C(t)$ versus t.

Case 1: Preventing amplitude ramping induced capsizing. Choosing $\epsilon_a = \epsilon_p = 0$, and $f(t)$ to increase linearly with time, we plot part of this gradually increasing wave in Fig. 3a in which $f(t)$ varies from 0.7 to 1.0. As can be seen in Fig. 3b, under the impact of this wave, the uncontrolled orbit capsizes once $f(t)$ exceeds the crisis value in Fig. 1. Using control, however, the ship survives the wave as shown in Fig. 3c.

Case 2: Preventing amplitude irregularity induced capsizing. For $f(t) = f_0 = 0.72$, the chaotic attractor on the surface of section for $\epsilon_a = \epsilon_p = 0$ together with the stable direction of the unstable fixed point is shown in Fig. 4b. Part of the irregular wave for $\epsilon_a = 0.2$ is shown in Fig. 4a. Using control we are able to place the successive surface of section points onto the stable direction. A total of 400 such points are shown in Fig. 4b. Fig. 4c superposes the trajectory of the controlled orbit on that of the uncontrolled one. Again, without control, capsize occurs within two cycles of the wave. With control we can sustain the ship's motion indefinitely. Fig. 4d shows $C(t)$ as a function of t. Comparing with Fig. 4a we see that $C(t)$ is much smaller than the wave amplitude $W(t)$. We mention that, since in the absence of wave irregularity there is a stable attractor in the system, the capsize cause by the irregularity in this case may be called an irregularity induced crisis, which is akin to the noise induced crisis studied in [4].

6

Case 3: Preventing capsizing with amplitude irregularity. Now we examine the situation where $f(t) = f_0 = 0.9$ which is far above the crisis value. Taking the irregularity to be carried by the amplitude, $\epsilon_a = 0.2$ and $\epsilon_p = 0$, we plot part of the irregular wave in Fig. 5a. Fig. 5b shows 400 points on the surface of section placed along the stable direction of the fixed point, and Fig. 5c shows both the controlled orbit and the uncontrolled capsizing orbit. Again the control can prevent capsizing. (Note that in the absence of prediction the control fails to prevent capsizing; see Case 6.)

Case 4: Preventing capsizing with phase irregularity. Suppose that there is only phase irregularity in the wave. For $f(t) = f_0 = 0.9$, and for $\epsilon_a = 0$ and $\epsilon_p = 0.3$, the wave is as shown in Fig. 6. Without control the ship capsizes within two cycles of the wave. The regularity seen in the wave is deceiving in this case since Eq. (3) implies that a realization of the quantity, $\phi(t) - \Omega t$, drifts with time in an irregular fashion, resembling a random walk. A consequence of this drift is that, in the long run, the wave with $\epsilon_p \neq 0$ will be severely out of phase compared to the wave with $\epsilon_p = 0$. This difference manifests itself strikingly when one attempts to apply control using two different methods of taking the surface of section. Specifically, let the nth surface of section be defined by $\phi(t_n) = 2n\pi$. Fig. 7a shows the result of placing the consecutive surface of section points on the stable direction of the fixed point using control. The control can be maintained indefinitely and a total of 400 points are plotted in the figure. Part of the controlled orbit is shown in Fig. 7b. In contrast, if we define the nth surface of section by $\Omega t_n = 2n\pi$ (i.e., by the times appropriate for $\epsilon_p = 0$), the controlled points on the resulting surface of section systematically drift away from the fixed point along the stable direction as witnessed in Fig. 8a. The control is effective only for about 25 cycles of the wave before the ship capsizes. The controlled orbit and the subsequent capsizing are shown in Fig. 8b.

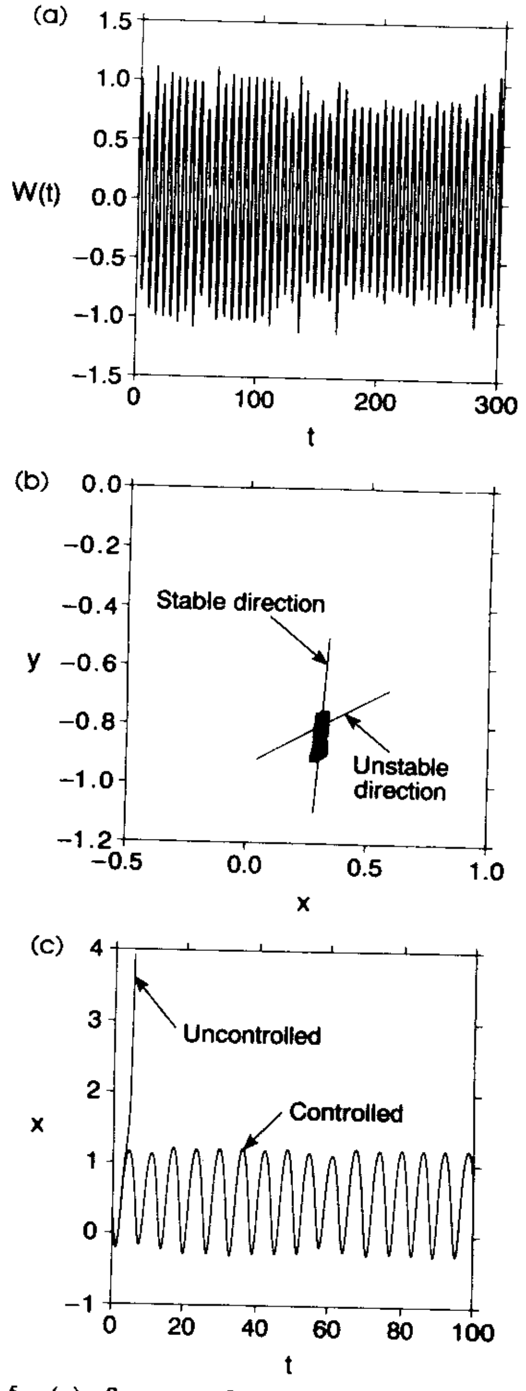

Fig. 5. (a) Segment of the irregular wave with $f(t) = f_0 = 0.9$, $\epsilon_a = 0.2$ and $\epsilon_p = 0.0$, (b) controlled orbit on the surface of section and (c) controlled together with uncontrolled orbit.

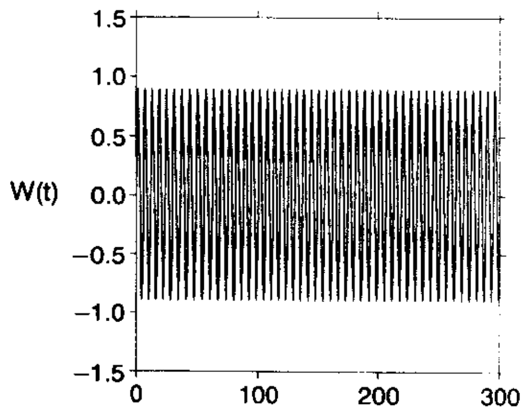

Fig. 6. Segment of the irregular wave with $f(t) = f_0 = 0.9$, $\epsilon_a = 0.0$ and $\epsilon_p = 0.3$.

8

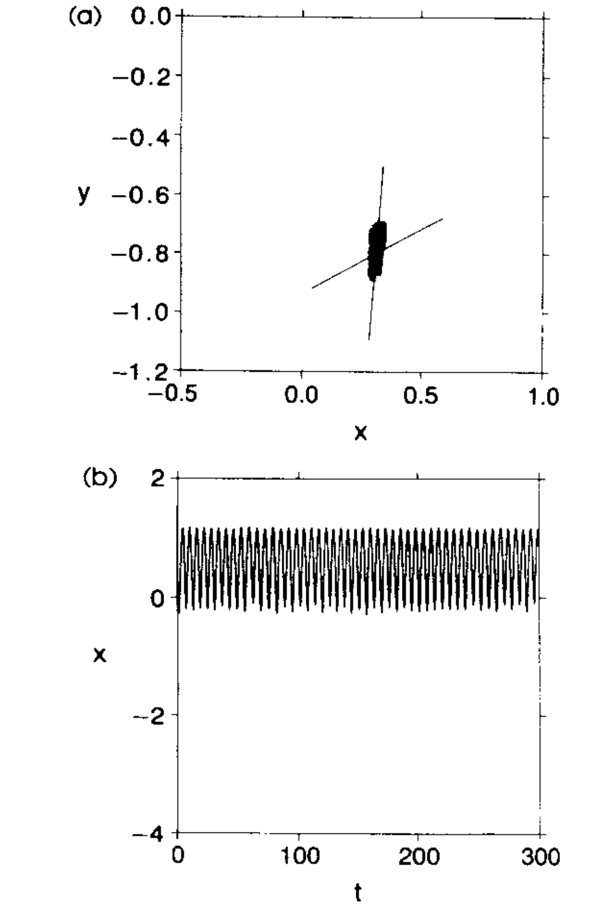

Fig. 7. Controlled orbit on the surface of section (a) and in the time domain (b) when surface of section is defined by $\phi(t_n) = 2n\pi$.

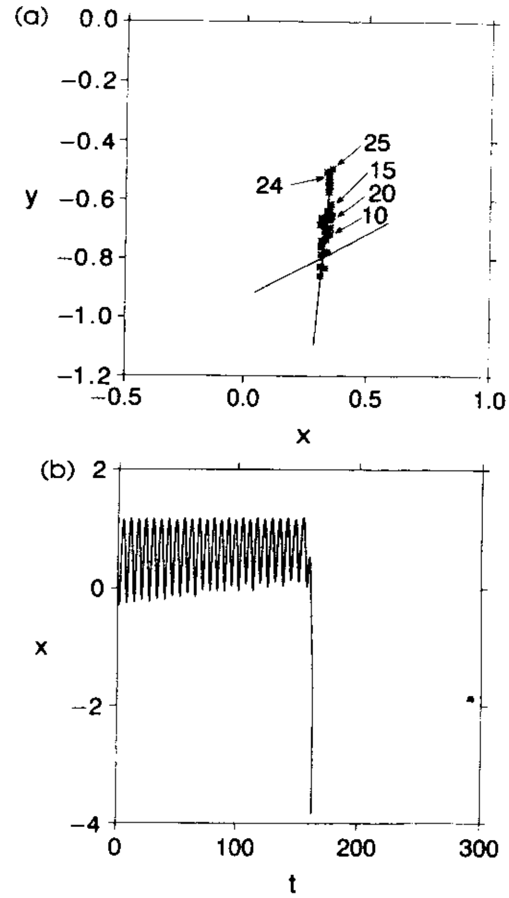

Fig. 8. Controlled orbit on the surface of section (a) and in the time domain (b) when surface of section is defined by $\Omega t_n = 2n\pi$. Capsize occurs in this case.

Case 5: Preventing capsizing with all the factors above. We study the combined effect due to the factors investigated separately in Cases 1–4. For $\epsilon_a = 0.15$, $\epsilon_p = 0.1$, and $f(t)$ a linearly increasing function of t from $f(0) = 0.7$ to $f(300) = 1.0$, the wave is as shown in Fig. 9a. The uncontrolled orbit capsizes rapidly as shown in Fig. 9b. Using control the capsizing is prevented in Fig. 9b. A more extended controlled orbit is shown in Fig. 9c.

Case 6: Effect of imperfect prediction. Thus far we have tacitly assumed that the wave $W(t)$ can be observed and predicted with certainty in the short term (i.e., from t_n to t_{n+1}). In a given application, however, a more likely situation is that

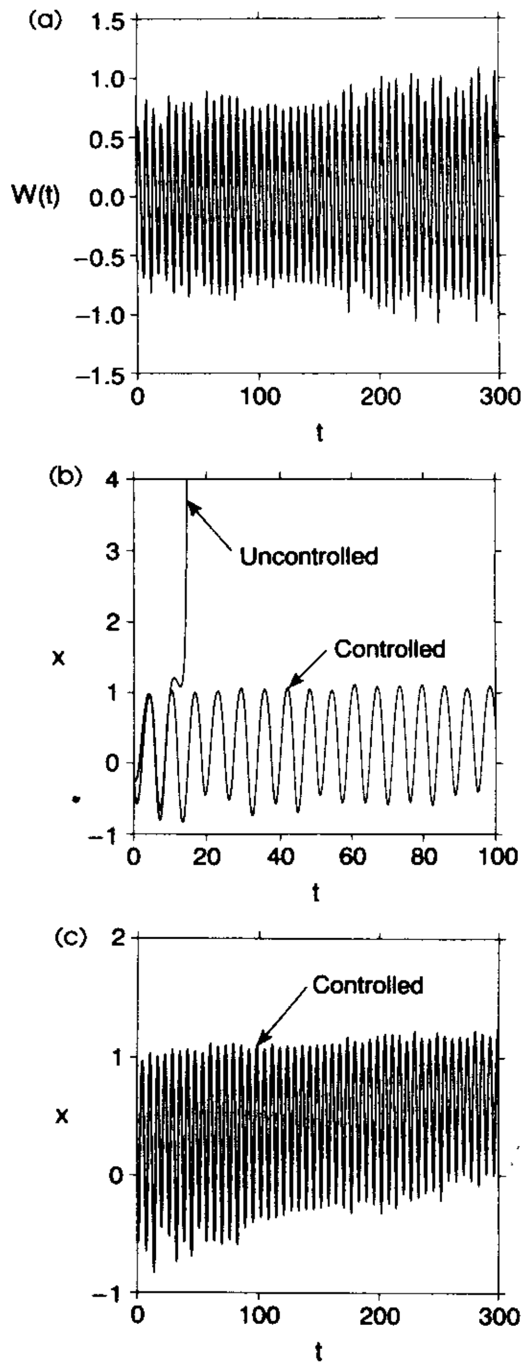

Fig. 9. (a) Segment of the irregular increasing wave with $\epsilon_a = 0.15$ and $\epsilon_p = 0.1$, (b) controlled together with uncontrolled orbit and (c) more extended plot of controlled orbit.

the prediction is imperfect. To assess the effect of this imperfection we carry out a quantitative study using the present model system. For specificity, we consider only amplitude irregularity in Eq. (2), which we assume to be

$$g(t) = \frac{(1-\gamma)g_O(t) + \gamma g_U(t)}{\sqrt{(1-\gamma)^2+\gamma^2}}, \tag{5}$$

where $g_O(t)$ and $g_U(t)$ are two different normalized trajectory realizations from the same Duffing chaotic attractor, with $g_O(t)$ being the "observed" and $g_U(t)$ the "unobserved" components of $g(t)$, and γ measures the relative strength of these two components. The imperfect prediction of $W(t)$ is assumed to be given by replacing the true $g(t)$ defined in Eq. (5) by $g_O(t)$. To design a control we integrate the equation of motion assuming $g(t) = g_O(t)$. The actual trajectory however is obtained by including $g_U(t)$ in the integration after $C(t)$ has been chosen. Let $\langle T_{\text{survival}}\rangle$ denote the average survival time in terms of the wave cycles calculated for ten different realizations of $g_O(t)$ and $g_U(t)$. Our result for $f(t) = f_0 = 0.9$ and $\epsilon_a = 0.1$ is as follows. For $\gamma \le 0.06$ we have $\langle T_{\text{survival}}\rangle \ge 400$. That is, the control method is robust with respect to less than or equal to 6% of uncertainty. The effectiveness of control deteriorates rapidly as γ increases past 0.06. In particular, we find that $\langle T_{\text{survival}}\rangle \approx 100$ for $\gamma = 0.07$; $\langle T_{\text{survival}}\rangle \approx 30$ for $\gamma = 0.08$; $\langle T_{\text{survival}}\rangle \approx 20$ for $\gamma = 0.1$; $\langle T_{\text{survival}}\rangle \approx 10$ for $\gamma = 0.3$; $\langle T_{\text{survival}}\rangle \approx 2$ for $\gamma = 1.0$.

4. Conclusion

The issue of controlling chaotic systems in temporally irregular environments is important in light of the many potential applications where chaos control may be called for. The previous method of stabilizing unstable periodic orbits can accommodate a certain amount of unpredicted irregularity if it is sufficiently small. Even so the control can sometimes be lost and the result is unwanted excursions away from the desired behavior. We propose in this paper that, if one incorporates an on-line, short-term monitoring and prediction feature of the future evolution of the environment into the control scheme, such unwanted excursions can be eliminated even in cases where the level of irregularity is substantial. This is particularly important in situations where a momentary loss of control results in a catastrophic failure of the system (e.g. capsizing of a ship). We have demonstrated the new method for a specific example where a ship is rocked from its side by lateral ocean waves. Using a small control we are able to prevent capsizing that would otherwise occur in the absence of control.

The crucial role of prediction is further illustrated by Case 6 at the end of the last section, where it was shown that the control loses its effectiveness as the level of prediction degrades.

Acknowledgements

This work was supported by the Department of Energy (Office of Scientific Computing, Office of Energy Research), and by the Office of Naval Research.

References

[1] E. Ott, C. Grebogi and J.A. Yorke, Phys. Rev. Lett. 64 (1990) 1196.

[2] T. Shinbrot, C. Grebogi, E. Ott and J.A. Yorke, Nature 363 (1993) 411, and references therein.

[3] L.N. Virgin, Appl. Ocean Res. 9 (1987) 89; J.M.T. Thompson, R.C. Rainey and M.S. Soliman, Phil. Trans. R. Soc. London Ser. A 332 (1990) 149; A.H. Nayfeh and N.E. Sanchez, Int. Shipbuild. Progr. 37 (1990) 331.

[4] J.C. Sommerer, E. Ott and C. Grebogi, Phys. Rev. A 43 (1991) 1754; J.C. Sommerer et al., Phys. Rev. Lett. 66 (1991) 1947.

10

CONTENTS ALERT™

A CURRENT AWARENESS SERVICE
FREE OF CHARGE
VIA ELECTRONIC MAIL

FOR SCIENTISTS WORKING IN THE FIELD OF SURFACES, INTERFACES AND THIN FILMS

FOR SCIENTISTS WORKING IN THE FIELD OF MATHEMATICAL & THEORETICAL METHODS IN PHYSICS

As the number of scientific publications grows daily it becomes increasingly important to trace the most interesting publications in a way that costs as little time as possible.

Elsevier Science Publishers now provides CONTENTS-Alert, ***a free electronic service*** that can assist you in carrying out time-saving searches on a regular, two-weekly basis.

CONTENTS-Alert is a current awareness service which delivers, through e-mail, the tables of contents of a selected group of journals. Not only will you receive these tables of contents ***before or upon publication*** of the journals but you can also browse through these tables of contents ***at your own terminal***, in your own time. A survey carried out among researchers using CONTENTS-Alert has shown that this free service is very convenient and time-effective.

We offer two versions of CONTENTS-Alert each covering a specific field. One version of CONTENTS-Alert includes journals on Surfaces, Interfaces and Thin Films, and one includes journals on Mathematical and Theoretical Methods in Physics.

Applied Surface Science
Chemical Physics Letters
Materials Science and Engineering: R: Reports
Nuclear Instruments and Methods in Physics Research: Section B
Surface Science (including Surface Science Letters)
Surface Science Reports
Thin Solid Films
Vacuum

Our e-mail for this version is:
RFC-822: C-ALERT@ELSEVIER.NL
X.400: C=NL;A=400NET;P=SURF;O=ELSEVIER;S=C-ALERT

Computer Physics Communications
Journal of Geometry and Physics
Nuclear Physics B
Physica A
Physica D
Physics Letters A
Physics Letters B
Physics Reports
Wave Motion

Our e-mail for this version is:
RFC-822: C-ALERT.MATHPHYS@ELSEVIER.NL
X.400: C=NL;A=400NET;P=SURF;O=ELSEVIER;
S=MATHPHYS; G=C- ALERT

Subscribe now to this *free pre-publication service* and find out how useful CONTENTS-Alert really is. Just send your full address to the e-mail number quoted above that corresponds with the CONTENTS-Alert version you wish to receive, or send it by post and we will make sure you will receive CONTENTS-Alert every two weeks.
Please allow three weeks processing time for your free subscription.

Yes, please add my name to the circulation list of.
CONTENTS-Alert.

Version: ❑ Surfaces, Interfaces and Thin Films
❑ Mathematical and Theoretical Methods in Physics

Name ______
Initials ______ Title ______ ❑ Male ❑ Female
Institute ______
Department ______
Street/ PO Box ______
City ______
Country ______
Tel: ______ Fax: ______
E-mail ______

Return to:
ELSEVIER SCIENCE PUBLISHERS B.V.,
Att: Mr. M. Stavenga,
P.O. BOX 103, 1000 AC Amsterdam, The Netherlands
Fax 31 20 5862580

ARTICLES

Controlling chaos in high dimensions: Theory and experiment

Mingzhou Ding and Weiming Yang
Program in Complex Systems and Brain Sciences, Center for Complex Systems and Department of Mathematics, Florida Atlantic University, Boca Raton, Florida 33431

Visarath In and William L. Ditto
Applied Chaos Laboratory, School of Physics, Georgia Institute of Technology, Atlanta, Georgia 30332

Mark L. Spano and Bruce Gluckman
Naval Surface Warfare Center, Carderock Division, Silver Spring, Maryland 20903
(Received 27 November 1995)

The main contribution of this work is the development of a high-dimensional chaos control method that is effective, robust against noise, and easy to implement in experiment. Assuming no knowledge of the model equations, the method achieves control by stabilizing a desired unstable periodic orbit with any number of unstable directions, using small time-dependent perturbations of a single system parameter. Specifically, our major results are as follows. First, we derive explicit control laws for time series produced by discrete maps. Second, we show how to apply this control law to continuous-time problems by introducing straightforward ways to extract from a continuous-time series a discrete time series that measures the dynamics of some Poincaré map of the original system. Third, we illustrate our approach with two examples of high-dimensional ordinary differential equations, one autonomous and the other periodically driven. Fourth, we present the result on our successful control of chaos in a high-dimensional experimental system, demonstrating the viability of the method in practical applications.

PACS number(s): 05.45.+b

12

I. INTRODUCTION

Chaotic phenomena arise ubiquitously in natural systems and in man-made devices [1]. Past work has focused mainly on the discovery and characterization of chaotic behavior occurring in situations where there is no goal-oriented intervention. Recently, ideas and techniques have been proposed to convert chaotic orbits to desired periodic ones by using temporally programmed small controls [2–9]. It is suggested that by doing so one improves the system's performance against some general classes of criteria [10]. This direction of research opens the possibility of utilizing the rich properties of chaos in practical applications and has thus attracted a great deal of interest. In the present paper we consider this chaos control paradigm in systems where the equations of motion are not known and the dynamical information is contained in a time series obtained from observing a single scalar function of the original phase space variables. Our main results are as follows.

(i) Assuming that the time series is produced by a discrete map we develop a high-dimensional chaos control method based on ideas proposed by So and Ott [7]. Here we use map-generated time series to ensure that the coefficients needed for the implementation of control are easy to estimate from experimental data. In addition, the expression of the control law involves only the knowledge about the unstable directions of the to-be-stabilized periodic orbit. This is an added practical benefit since such knowledge is often more reliably obtained from time series. It is also worth emphasizing that in this method one only needs to vary a single external parameter to control a system of arbitrary dimensionality with an arbitrary number of unstable directions.

(ii) We show that for a continuous-time system, as would be encountered in most experimental problems, simple methods can be used to extract from the continuous-time series a discrete-time series that probes the dynamics of some Poincaré map in the original phase space. Specifically, for an autonomous system, this is done by measuring the times between successive crossings of some predetermined threshold by the continuous-time series. We call these times interspike intervals. For a periodically driven system, either the interspike intervals or the more traditional stroboscopic samples can be used to form the discrete time series. In this fashion the explicit control law mentioned in (i) applies directly to continuous-time systems. Other advantages of basing the control method on discrete-time series generated by Poincaré maps are also discussed.

(iii) We illustrate our approach with two examples of ordinary differential equations, one an autonomous chemical reaction model of four variables and the other a pair of coupled Duffing oscillators with periodic forcing, a five-dimensional system. In the second example, the periodic orbit to be stabilized has two unstable directions, and in the second example, we consider the control of a period-2 orbit.

(iv) We have applied the control method to a physical system of a magnetoelastic ribbon driven by a sinusoidally varying magnetic field. We have successfully achieved the control of high-dimensional chaos where other techniques have failed to do so. We have also demonstrated the robustness of the method by showing that it works effectively in the presence of rather substantial random noise.

The rest of this paper is organized as follows. In Sec. II we present the method of chaos control. Here we leave some of the detailed calculations to the Appendix. Section III shows how to extract a Poincaré-map-generated discrete-time series from a continuous-time system. We also discuss numerical results in this section. In Sec. IV we present the control results for the magnetoelastic ribbon experiment. We summarize the paper in Sec. V.

II. THE CONTROL METHOD

A. Delay coordinates

Consider a k-dimensional map

$$\mathbf{X}_{n+1}=\mathbf{F}(\mathbf{X}_n,p), \tag{1}$$

where $\mathbf{X}\in R^k$ and p is the chosen control parameter. Suppose that for $p=\bar{p}$ Eq. (1) exhibits a chaotic attractor. Let the scalar observation function be $x=h(\mathbf{X})$. Assuming no *a priori* knowledge of the equations of motion $\mathbf{F}$, we carry out the system analysis and control by using the time series

$$\{x_n\}=\{h(\mathbf{X}_n)\}, \tag{2}$$

where $n=1,2,3,\ldots$. (In Sec. III we shall describe ways to extract such discrete-time series for both autonomous and periodically driven *continuous-time* systems.) Employing delay coordinates [11], we reconstruct the high-dimensional dynamics from $\{x_n\}$ via

$$\mathbf{z}_n=\begin{pmatrix} z_n^{(1)} \\ z_n^{(2)} \\ \vdots \\ z_n^{(m)} \end{pmatrix}=\begin{pmatrix} x_{n-m+1} \\ x_{n-m+2} \\ \vdots \\ x_n \end{pmatrix}_{m\times 1},$$

where m is the dimension of the reconstructed phase space. Results in [11] state that, for large enough m, $\mathbf{z}_n$ is a global one-to-one representation of the variable $\mathbf{X}_n$ on the original attractor. Since the application of control in this work entails that we change the value of the parameter p according to a control law at every iteration of Eq. (1), the discrete map for $\mathbf{z}_n$ is

$$\mathbf{z}_{n+1}=\mathbf{G}(\mathbf{z}_n,p_{n-m+1},p_{n-m+2},\ldots,p_n), \tag{3}$$

where $\mathbf{G}$ generally depends on all the parameter variations effective during the time interval $n-m+1\leq t\leq n$ spanned by the delay vector $\mathbf{z}_n$ [6].

Below, by taking into account of the effect of the past parameter changes specified in Eq. (3), we derive the control laws that stipulates the choice of p_n to convert the natural chaotic dynamics of Eq. (1) to a periodic orbit selected from an infinitely many contained in the chaotic attractor. The parameter variations are assumed to be small around the nominal value $p=\bar{p}$ so that no new orbits are expected to be created in the process. Thus we seek to exploit unstable periodic orbits already existing in the chaotic attractor. This control approach is also flexible in that by simply changing to a different temporal programming of the parameter p one can switch the dynamics from one periodic behavior to another without major alterations to the system.

B. Stabilizing a fixed point

We begin by considering the stabilization of a saddle fixed point that may have more than one unstable direction. In this case, the control law to be derived admits an explicit expression. Moreover, the simple setting here allows us to better illustrate the main ideas involved.

An unstable fixed point $\bar{\mathbf{X}}$ in the original chaotic attractor when $p=\bar{p}$ satisfies

$$\bar{\mathbf{X}}(\bar{p})=\mathbf{F}(\bar{\mathbf{X}}(\bar{p}),\bar{p}). \tag{4}$$

Reflected in the delay coordinate space we have

$$\bar{\mathbf{z}}(\bar{p})=\mathbf{G}(\bar{\mathbf{z}}(\bar{p}),\bar{p},\bar{p},\ldots,\bar{p}), \tag{5}$$

where $\bar{\mathbf{z}}(\bar{p})=[\bar{x}(\bar{p}),\bar{x}(\bar{p}),\ldots,\bar{x}(\bar{p})]^T$, T denoting matrix transpose, and $\bar{x}(\bar{p})=h(\bar{\mathbf{X}}(\bar{p}))$. The location of this fixed point can be extracted from the time series. The procedure for finding it is simplified by knowing that it lies on the diagonal in the m-dimensional reconstructed phase space.

To describe the effect of control parameter variations on the linear dynamics near the fixed point, we introduce the $m\times m$ Jacobian matrix

$$\mathbf{A}_n=\mathbf{D}_{\mathbf{z}_n}\mathbf{G}(\mathbf{z}_n,p_{n-m+1},p_{n-m+2},\ldots,p_n) \tag{6}$$

and a set of m-dimensional column vectors [7]

$$\mathbf{B}_n^{(m)}=D_{p_{n-m+1}}\mathbf{G}(\mathbf{z}_n,p_{n-m+1},p_{n-m+2},\ldots,p_n),$$
$$\mathbf{B}_n^{(m-1)}=D_{p_{n-m+2}}\mathbf{G}(\mathbf{z}_n,p_{n-m+1},p_{n-m+2},\ldots,p_n),$$
$$\vdots$$
$$\mathbf{B}_n^{(1)}=D_{p_n}\mathbf{G}(\mathbf{z}_n,p_{n-m+1},p_{n-m+2},\ldots,p_n). \tag{7}$$

Evaluating all the partial derivatives at $\bar{\mathbf{z}}(\bar{p})$ and $p_{n-m+1}=p_{n-m+2}=\cdots=p_n=\bar{p}$, we obtain near the fixed point

$$\mathbf{z}_{n+1}-\bar{\mathbf{z}}(\bar{p})=\mathbf{A}(\mathbf{z}_n-\bar{\mathbf{z}}(\bar{p}))+\mathbf{B}^{(m)}(p_{n-m+1}-\bar{p})+\mathbf{B}^{(m-1)}\times(p_{n-m+2}-\bar{p})+\cdots+\mathbf{B}^{(1)}(p_n-\bar{p}), \tag{8}$$

where we have dropped the reference to n in $\mathbf{A}$ and $\mathbf{B}$'s since they are now constant matrix and vectors. It should be noted that, due to the nature of the discrete-time series and delay coordinates used here, Eq. (3) in component form is

$$\begin{pmatrix} z_{n+1}^{(1)} \\ z_{n+1}^{(2)} \\ \vdots \\ z_{n+1}^{(m-1)} \\ z_{n+1}^{(m)} \end{pmatrix}=\begin{pmatrix} z_n^{(2)} \\ z_n^{(3)} \\ \vdots \\ z_n^{(m)} \\ g(\mathbf{z}_n,p_{n-m+1},p_{n-m+2},\ldots,p_n) \end{pmatrix}. \tag{9}$$

Thus most of the entries in the $\mathbf{A}$ matrix and the $\mathbf{B}$ vectors are zero. Specifically,

$$\mathbf{A}=\begin{pmatrix} 0 & 1 & 0 & \cdots & 0 \\ 0 & 0 & 1 & \cdots & 0 \\ \vdots & \vdots & \vdots & \vdots & \vdots \\ 0 & 0 & 0 & \cdots & 1 \\ a^{(m)} & a^{(m-1)} & a^{(m-2)} & \cdots & a^{(1)} \end{pmatrix}_{m\times m} \tag{10}$$

and

$$\mathbf{B}^{(i)}=\begin{pmatrix} 0 \\ 0 \\ \vdots \\ 0 \\ b^{(i)} \end{pmatrix}_{m\times 1}, \tag{11}$$

where $i=1,2,\ldots,m$. The use of Poincaré-map-generated time series reduces our task of obtaining the entire $\mathbf{A}$ and $\mathbf{B}^{(i)}$ to the estimation of only $a^{(1)},a^{(2)},\ldots,a^{(m)}$, $b^{(1)},b^{(2)},\ldots,b^{(m)}$ from the experimental data. We remark that, although it is possible to obtain the values of $a^{(i)}$'s and the $b^{(i)}$'s together at the same time, our experience indicates that the best strategy is to find the $a^{(i)}$'s first based on the unperturbed time series and then to apply the perturbation to calculate the $b^{(i)}$'s. The perturbation is applied in such a way that only one δp is not zero in the time interval spanned by $\mathbf{z}_n$. See Sec. IV for more discussions on the estimation of $a^{(i)}$'s and $b^{(i)}$'s.

Assume that $\mathbf{A}$ in Eq. (10) has u unstable directions and s stable directions $(s+u=m)$ with eigenvalues λ_i satisfying $|\lambda_1|>|\lambda_2|>\cdots>|\lambda_u|>1>|\lambda_{u+1}|>|\lambda_{u+2}|>\cdots>|\lambda_m|$. Let $\mathbf{e}_i$ denote the corresponding eigenvectors. Then a possible control approach is to choose suitable parameter variations according to Eq. (8) to push the trajectory $\mathbf{z}_{n+1}$ into the stable subspace spanned by the stable directions $\mathbf{e}_i$, $i=u+1,u+2,\ldots,m$. However, Dressler and Nistche [6] point out for the $m=2$ case that this strategy may sometimes leads to instabilities in the control parameters. When this happens, one generally needs larger and larger perturbations in p in order to bring the trajectory to stay inside the stable subspace. The control will eventually fail when either the required $\delta p=p-\bar{p}$ exceeds the predetermined maximum control $\delta p_{\max}$ or the value of δp becomes so large that the linear approximation in Eq. (8) is no longer valid. So and Ott proposes an idea to systematically remedy the situation [7]. (A similar approach can be found in [8].) It involves the introduction of a state-plus-parameters system, which includes the regular phase space variable $\mathbf{z}_n$ as well as all the previous variations of the parameter p according to Eq. (3).

The expanded phase space is $2m-1$ dimensional and the state vector $\mathbf{Y}_n$ assumes the form

$$\mathbf{Y}_n=\begin{pmatrix} \mathbf{z}_n \\ p_{n-m-1} \\ p_{n-m-2} \\ \vdots \\ p_{n-1} \end{pmatrix}_{(2m-1)\times 1}.$$

Based on Eq. (8), the linear dynamics around the fixed point

$$\bar{\mathbf{Y}}=\begin{pmatrix} \bar{\mathbf{z}}(\bar{p}) \\ \bar{p} \\ \bar{p} \\ \vdots \\ \bar{p} \end{pmatrix}$$

is [7]

$$\mathbf{Y}_{n-1}-\bar{\mathbf{Y}}=\tilde{\mathbf{A}}(\mathbf{Y}_n-\bar{\mathbf{Y}})+\tilde{\mathbf{B}}(p_n-\bar{p}), \tag{12}$$

where

$$\tilde{\mathbf{A}}=\begin{pmatrix} \mathbf{A} & \mathbf{B}^{(m)} & \mathbf{B}^{(m-1)} & \mathbf{B}^{(m-2)} & \cdots & \mathbf{B}^{(2)} \\ \mathbf{0} & 0 & 1 & 0 & \cdots & 0 \\ \mathbf{0} & 0 & 0 & 1 & \cdots & 0 \\ \vdots & \vdots & \vdots & \vdots & \vdots & \vdots \\ \mathbf{0} & 0 & 0 & 0 & \cdots & 1 \\ \mathbf{0} & 0 & 0 & 0 & \cdots & 0 \end{pmatrix}_{(2m-1)\times(2m-1)}, \tag{13}$$

with $\mathbf{0}$ an m-dimensional row vector of 0's and

$$\tilde{\mathbf{B}}=\begin{pmatrix} \mathbf{B}^{(1)} \\ 0 \\ \vdots \\ 0 \\ 1 \end{pmatrix}_{2m-1\times 1}. \tag{14}$$

We note that the eigenvalues of $\mathbf{A}$ are also the eigenvalues of $\tilde{\mathbf{A}}$ with the corresponding eigenvectors

$$\mathbf{k}_i=\begin{pmatrix} \mathbf{e}_i \\ 0 \\ \vdots \\ 0 \\ 0 \end{pmatrix},$$

$i = 1,2,\ldots,m$. Clearly, the above m vectors are not enough to span the $(2m-1)$-dimensional expanded phase space. To do so one needs additional $m-1$ independent vectors. We argue that these vectors can be found in the null space of the matrix $\bar{\mathbf{A}}^{m-1}$. Specifically, we show in the Appendix that the subspace of the vectors $\mathbf{k}$ satisfying $\bar{\mathbf{A}}^{m-1}\mathbf{k}=\mathbf{0}$ is $(m-1)$ dimensional and more importantly any set of $m-1$ independent vectors denoted $\mathbf{k}_i$, $i=m+1,m+2,\ldots,2m-1$, from this space can be used together with $\mathbf{k}_i$, $i=u+1,u+2,\ldots,m$, to form the basis of the stable subspace $\mathbf{E}_s(\bar{\mathbf{Y}})$ of $\bar{\mathbf{A}}$.

Suppose that at time n the system trajectory falls in the neighborhood of $\bar{\mathbf{Y}}$ called the control region. To stabilize the subsequent motion around this fixed point with u unstable directions, we attempt to apply u small parametric perturbations $\delta p_n, \delta p_{n+1}, \ldots, \delta p_{n+(u-1)}$ in such a way that the deviation $\delta\mathbf{Y}_{n+u}=\mathbf{Y}_{n+u}-\bar{\mathbf{Y}}$ lies entirely [7] in the stable subspace $\mathbf{E}_s(\bar{\mathbf{Y}})$. After that we set the parameter to $\bar{p}$ and the orbit approaches the fixed point under the natural dynamics. Specifically, this control can be achieved as follows. Consider the transpose of $\bar{\mathbf{A}}$ denoted $\bar{\mathbf{A}}^T$. We know that both $\bar{\mathbf{A}}$ and $\bar{\mathbf{A}}^T$ have the same eigenvalue spectrum. Furthermore, as shown in the Appendix, the contravariant unstable eigenvectors $\mathbf{v}_i$ determined by

$$\bar{\mathbf{A}}^T\mathbf{v}_i=\lambda_i\mathbf{v}_i \tag{15}$$

for $i=1,2,\ldots,u$ have the property that they are orthogonal to the stable subspace $\mathbf{E}_s(\bar{\mathbf{Y}})$ of $\bar{\mathbf{A}}$. That is, the dot products $\mathbf{v}_i^T\mathbf{k}_j=0$ for $j=u+1,u+2,\ldots,m,m+1,m+2,\ldots,2m-1$. By choosing the values of $p_n, p_{n+1},\ldots,p_{n+(u-1)}$ such that

$$\begin{aligned} \mathbf{v}_1^T\delta\mathbf{Y}_{n+u}&=0,\\ \mathbf{v}_2^T\delta\mathbf{Y}_{n+u}&=0,\\ &\vdots\\ \mathbf{v}_u^T\delta\mathbf{Y}_{n+u}&=0, \end{aligned} \tag{16}$$

we place the deviation $\delta\mathbf{Y}_{n+u}$ in the stable subspace $\mathbf{E}_s(\bar{\mathbf{Y}})$. In the Appendix we find from the equations in (16) the control law governing the parameter perturbation p_n needed at time n to be

$$p_n=\bar{p}-\left(\sum_{k=1}^{u}\frac{(\lambda_k)^u}{(\mathbf{v}_k^T\bar{\mathbf{B}})\prod_{i=1,i\neq k}^{u}(\lambda_k-\lambda_i)}\mathbf{v}_k^T\right)\delta\mathbf{Y}_n . \tag{17}$$

Although the values of $p_{n+1},\ldots,p_{n+u-1}$ can also be solved together with p_n at time n, the presence of system noise makes it preferable to compute p_n using Eq. (17) at every iterate n.

The contravariant vectors $\mathbf{v}_k$ are also solved explicitly. From Eq. (15), by setting arbitrarily $v_k^{(m)}=1$, we obtain the following recursive relations to determine the other components $v_k^{(i)}$ of the vector $\mathbf{v}_k$:

$$\begin{aligned} v_k^{(1)}&=a^{(m)}/\lambda_k,\\ v_k^{(2)}&=(v_k^{(1)}+a^{(m-1)})/\lambda_k,\\ v_k^{(3)}&=(v_k^{(2)}+a^{(m-2)})/\lambda_k,\\ &\vdots\\ v_k^{(m-1)}&=(v_k^{(m-2)}+a^{(2)})/\lambda_k,\\ v_k^{(m)}&=1,\\ v_k^{(m+1)}&=b^{(m)}/\lambda_k,\\ v_k^{(m+2)}&=(v_k^{(m+1)}+b^{(m-1)})/\lambda_k,\\ v_k^{(m+3)}&=(v_k^{(m+2)}+b^{(m-2)})/\lambda_k,\\ &\vdots\\ v_k^{(2m-1)}&=(v_k^{(2m-2)}+b^{(2)})/\lambda_k . \end{aligned} \tag{18}$$

[Note that the conditions in Eq. (16) imply that the lengths of the vectors $\mathbf{v}_k$ do not play a role. Thus we can set $v_k^{(m)}=1$ for simplicity.] Solving these equations we get

$$\begin{aligned} v_k^{(i)}&=\sum_{j=1}^{i}a^{(m-j+1)}/(\lambda_k)^{i-j+1}, \quad i=1,2,\ldots,m-1,\\ v_k^{(m)}&=1,\\ v_k^{(i)}&=\sum_{j=1}^{i-m}b^{(m-j+1)}/(\lambda_k)^{i-m-j+1},\\ &\qquad i=m+1,m+2,\ldots,2m-1. \end{aligned} \tag{19}$$

We emphasize that all the formulas in Eqs. (17) and (19) needed for implementing the control are expressed explicitly in terms of the variables $a^{(i)}$ and $b^{(i)}$, to be estimated from the experimental time series, and the unstable eigenvalues λ_i of $\mathbf{A}$ in Eq. (10).

For fixed points with one or two unstable directions, a situation likely to be encountered in practice, the control law in Eq. (17) reduces to

$$p_n=\bar{p}-\left(\frac{\lambda_1}{(\mathbf{v}_1^T\bar{\mathbf{B}})}\mathbf{v}_1^T\right)\delta\mathbf{Y}_n \tag{20}$$

for $u=1$ and to

$$p_n=\bar{p}-\left(\frac{(\lambda_1)^2}{(\mathbf{v}_1^T\bar{\mathbf{B}})(\lambda_1-\lambda_2)}\mathbf{v}_1^T+\frac{(\lambda_2)^2}{(\mathbf{v}_2^T\bar{\mathbf{B}})(\lambda_2-\lambda_1)}\mathbf{v}_2^T\right)\delta\mathbf{Y}_n \tag{21}$$

for $u=2$.

C. Stabilizing a period-N orbit

Let a period-N orbit in the original phase space when $p=\bar{p}$ be $\bar{\mathbf{X}}_n(\bar{p}),\bar{\mathbf{X}}_{n-1}(\bar{p}),\ldots,\bar{\mathbf{X}}_{n-N}(\bar{p})=\bar{\mathbf{X}}_n(\bar{p})$. The corresponding scalar time series $\{\bar{x}_n(\bar{p})\}$ is also periodic with a period of N. Suppose at time n the trajectory $\mathbf{z}_n$ in the m-dimensional reconstructed phase space comes near one of the periodic points denoted by $\bar{\mathbf{z}}_n(\bar{p})$. The entire reconstructed periodic orbit is then $\bar{\mathbf{z}}_n(\bar{p}),\ \bar{\mathbf{z}}_{n+1}(\bar{p}),\ldots,\ \bar{\mathbf{z}}_{n+N}(\bar{p})=\bar{\mathbf{z}}_n(\bar{p})$. The Jacobian $\mathbf{A}_n$ in Eq. (6) and the $\mathbf{B}_n$ vectors in Eq. (7) evaluated along the orbit are now functions of n, satisfying the periodic conditions $\mathbf{A}_n=\mathbf{A}_{n+N}$ and $\mathbf{B}_n^{(i)}=\mathbf{B}_{n+N}^{(i)}$. Introducing the expanded state-plus-parameters phase space, we have, close to the periodic orbit, the linear iteration equation

$$\mathbf{Y}_{n+i}-\bar{\mathbf{Y}}_{n+i}=\bar{\mathbf{A}}_{n+i-1}(\mathbf{Y}_{n+i-1}-\bar{\mathbf{Y}}_{n+i-1})+\bar{\mathbf{B}}_{n+i-1}(p_{n+i-1}-\bar{p}), \tag{22}$$

where $i=1,2,3,\ldots$ and $\mathbf{Y}_{n+i}$, $\bar{\mathbf{A}}_{n+i}$, and $\bar{\mathbf{B}}_{n+i}$ are formed in the same way as their counterparts in Eq. (12). Assume that there are u unstable directions associated with the orbit. The control is accomplished by using u small perturbations $p_n,p_{n-1},\ldots,p_{n-u-1}$ to place the deviation $\delta\mathbf{Y}_{n+u}=\mathbf{Y}_{n+u}-\bar{\mathbf{Y}}_{n+u}$ into the stable subspace $\mathbf{E}_s(\bar{\mathbf{Y}}_{n+u})$ of the matrix $\mathbf{J}_{n+u}=\bar{\mathbf{A}}_{n+u-1}\bar{\mathbf{A}}_{n+u-2}\cdots\bar{\mathbf{A}}_{n+u-N}$. Since the eigenvectors change from orbit point to orbit point the control law can no longer be expressed as explicitly as in the case of an $N=1$ fixed point. Below we give a brief description of the steps needed for arriving at the control law.

Let the unstable eigenvalues of the entire periodic orbit be $\lambda_1,\lambda_2,\ldots,\lambda_u$. The stable subspace at the orbit point $\bar{\mathbf{Y}}_{n+i}$ is determined by the matrix

$$\mathbf{J}_{n+i}=\bar{\mathbf{A}}_{n+i-1}\bar{\mathbf{A}}_{n+i-2}\cdots\bar{\mathbf{A}}_{n+i-N}. \tag{23}$$

As in the case of a fixed point there is no need to find this subspace explicitly for the formulation of the control law. Instead we consider the eigenvalue problem

$$\mathbf{J}_{n+i}^T\mathbf{v}_{n+i}^{(j)}=\lambda_j\mathbf{v}_{n+i}^{(j)}. \tag{24}$$

Multiplying Eq. (24) on both sides from the left by $\bar{\mathbf{A}}_{n+i-N-1}=\bar{\mathbf{A}}_{n+i-1}$ we get

$$\mathbf{J}_{n+i-1}^T\bar{\mathbf{A}}_{n+i-1}\mathbf{v}_{n+i}^{(j)}=\lambda_j\bar{\mathbf{A}}_{n+i-1}\mathbf{v}_{n+i}^{(j)}.$$

That is, the vector $\mathbf{v}_{n+i-1}^{(j)}$ is parallel to the vector $\bar{\mathbf{A}}_{n+i-1}^T\mathbf{v}_{n+i}^{(j)}$, namely,

$$\bar{\mathbf{A}}_{n+i-1}^T\mathbf{v}_{n+i}^{(j)}=c_{n+i-1}^{(j)}\mathbf{v}_{n+i-1}^{(j)}. \tag{25}$$

This definition implies the periodic condition $c_n^{(j)}=c_{n+N}^{(j)}$.

Iterating Eq. (22) u times yields

$$\begin{aligned}\delta\mathbf{Y}_{n+u}={}&\bar{\mathbf{A}}_{n+u-1}\bar{\mathbf{A}}_{n+u-2}\cdots\bar{\mathbf{A}}_n\delta\mathbf{Y}_n\\&+\bar{\mathbf{A}}_{n+u-1}\bar{\mathbf{A}}_{n+u-2}\cdots\bar{\mathbf{A}}_{n+1}\bar{\mathbf{B}}_n\delta p_n\\&+\bar{\mathbf{A}}_{n+u-1}\bar{\mathbf{A}}_{n+u-2}\cdots\bar{\mathbf{A}}_{n+2}\bar{\mathbf{B}}_{n+1}\delta p_{n+1}\\&\ \vdots\\&+\bar{\mathbf{A}}_{n+u-1}\bar{\mathbf{B}}_{n+u-2}\delta p_{n+u-2}\\&+\bar{\mathbf{B}}_{n+u-1}\delta p_{n+u-1}.\end{aligned}$$

Choosing the values of $\delta p_n,\delta p_{n+1},\ldots,\delta p_{n+u-1}$ such that

$$(\mathbf{v}_{n+u}^{(j)})^T\delta\mathbf{Y}_{n+u}=0 \tag{26}$$

for $j=1,2,\ldots,u$, we place the deviation $\delta\mathbf{Y}_{n+u}$ entirely in the stable subspace $\mathbf{E}_s(\bar{\mathbf{Y}}_{n+u})$. From Eq. (26), with the aid of Eq. (25), we obtain the u equations

$$\begin{aligned}&(\mathbf{v}_n^{(j)})^T\delta\mathbf{Y}_n\prod_{k=0}^{u-1}c_{n+k}^{(j)}\\&+\sum_{i=1}^{u-1}\left((\mathbf{v}_{n+i}^{(j)})^T\bar{\mathbf{B}}_{n+i-1}\delta p_{n+i-1}\prod_{k=i}^{u-1}c_{n+k}^{(j)}\right)\\&+(\mathbf{v}_{n+u}^{(j)})^T\bar{\mathbf{B}}_{n+u-1}\delta p_{n+u-1}=0,\end{aligned} \tag{27}$$

where $j=1,2,\ldots,u$. We solve these linear equations to obtain the control law governing the parameter perturbation p_n needed at time n to be

$$p_n=\bar{p}+\frac{H}{W}, \tag{28}$$

where $W=\mathrm{Det}(\mathbf{W})$ with $w_{ij}=(\mathbf{v}_{n+j}^{(i)})^T\bar{\mathbf{B}}_{n+j-1}\Pi_{k=j}^{u-1}c_{n+k}^{(i)}$ and $H=\mathrm{Det}(\mathbf{H})$ with $h_{ij}=-(\mathbf{v}_u^{(i)})^T\delta\mathbf{Y}_n\Pi_{k=0}^{u-1}c_{n+k}^{(i)}$ for $j=1$ and $h_{ij}=w_{ij}$ for $j\neq1$. Again, in order to compensate for the effect of noise in experimental applications, we recalculate at each time n the value of p_n, even though by solving the u equations in Eq. (27) simultaneously we can at once obtain parameter perturbations for the future u steps.

For the special case where the period-N orbit has one unstable direction ($u=1$), the control law takes the simple form

$$p_n=\bar{p}-\left(\frac{c_n^{(1)}(\mathbf{v}_n^{(1)})^T}{((\mathbf{v}_{n+1}^{(1)})^T\bar{\mathbf{B}}_n)}\right)\delta\mathbf{Y}_n. \tag{29}$$

Evidently, this equation and Eq. (20) are identical for $N=1$.

We remark that in the above we express the control laws in terms of the unstable directions of the periodic orbit. This approach offers several advantages over expressing control laws using stable directions. First, in the expanded phase space, one tends to have fewer unstable directions than stable ones that include the null space. Second, since the estimated matrix elements of $\mathbf{A}$ and $\mathbf{B}$'s carry inevitable errors, fewer calculations reduce the chance of severe error propagations into the control law that, in turn, affect the control performance. Third, it is an empirical fact that information about unstable directions tends to be more reliably estimated from experimental time series.

III. NUMERICAL RESULTS

A. Formation of time series

In experimental problems, we expect to encounter two classes of continuous-time systems, autonomous and periodically driven. We discuss how to form discrete time series in both cases so that the control laws developed in Sec. II for discrete maps are directly applicable.

First, consider an autonomous system defined as

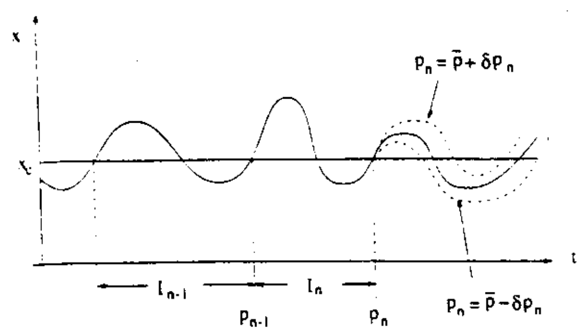

FIG. 1. Schematic illustrating the formation of interspike intervals from a continuous-time series and the effect of control on the intervals.

$$d\mathbf{Z}/dt = \mathbf{G}(\mathbf{Z},p),$$

where $\mathbf{Z} \in R^{k+1}$. Let $x = h(\mathbf{Z})$ denote a scalar observable function. Consider the plot of x versus t. We form the discrete-time series by measuring the intervals I_n between the $(n-1)$th and nth upward (or downward) crossings of some predetermined threshold $x = x_c$ (see Fig. 1). We argue that these variables I_n, which we call interspike intervals, sample the dynamics of some Poincaré map in the original $\mathbf{Z}$ phase space. Specifically, at each crossing in the x versus t plot, the condition $x = h(\mathbf{Z}) = x_c$ is met. This condition defines a k-dimensional Poincaré surface of section in the original $\mathbf{Z}$ space. Thus I_n is also the time between the $(n-1)$th and the nth crossings of the section. Suppose we parametrize this section by a k-dimensional vector $\mathbf{Q}$. Then, the successive crossings of the plane from a given direction by a chaotic trajectory give rise to a Poincaré map

$$\mathbf{Q}_{n+1} = \mathbf{P}(\mathbf{Q}_n, p). \tag{30}$$

Realizing that the interval I_n is uniquely determined by $\mathbf{Q}_{n-1}$, namely,

$$I_n = \Phi(\mathbf{Q}_{n-1}), \tag{31}$$

we complete the analogy between Eqs. (30) and (1) and the analogy between Eqs. (31) and (2).

Traditionally, one measures the continuous-time series x versus t using equally spaced sampling intervals. In the reconstructed phase space one obtains the Poincaré map by examining the crossings of some plane by the reconstructed trajectory. Due to the discreteness of the trajectory one introduces inevitable errors in the resulting Poincaré map through interpolation. In contrast, our way of forming the discrete time series using interspike intervals avoids this problem by monitoring the analog signal and thus detecting the threshold crossing precisely. Furthermore, the reconstructed interspike intervals already obey a Poincaré map. In Fig. 1 we also illustrate the effect of parametric perturbations on the interspike intervals.

Next, we consider a periodically forced system

$$d\mathbf{Z}/dt = \mathbf{G}(\mathbf{Z},t,p),$$

where $\mathbf{Z} \in R^k$ and $\mathbf{G}(\mathbf{Z},t+T,p) = \mathbf{G}(\mathbf{Z},t,p)$. Let $x = h(\mathbf{Z})$ be the scalar observable function. Since by introducing t as an additional variable one can convert a nonautononmous system to an autononmous one, the interspike intervals formation method also applies here. Another more traditional method of forming a discrete-time series $\{x_n\}$ is by measuring x at times $t_n = nT + T_0$ (stroboscopic sampling). From the theorems of [12], the dynamics reconstructed from $\{x_n\}$ in a suitable delay coordinates space represents the dynamics of the Poincaré map $\mathbf{Z}_{n+1} = \mathbf{P}(\mathbf{Z}_n)$ in the original phase space, which, in turn, is equivalent to the continuous-time dynamics described by the differential equations. Below we give two examples of controlling continuous-time chaotic systems using the methods above.

B. Control example 1

Consider the following five-dimensional system of two coupled driven Duffing oscillators:

$$\begin{aligned} &\ddot{x}_1 + \gamma\dot{x}_1 + \alpha(x_1^3 - x_1) + \beta_1(x_1 - x_2) = p_1\sin(\omega t), \\ &\ddot{x}_2 + \gamma\dot{x}_2 + \alpha(x_2^3 - x_2) + \beta_2(x_2 - x_1) = p\sin(\omega t). \end{aligned} \tag{32}$$

For $\gamma = 0.632$, $\alpha = 4.0$, $\beta_1 = 0.1$, $\beta_2 = 0.05$, $\omega = 2.1235$, $p_1 = 1.011$, and $p = \bar{p} = p_1$, Eq. (32) exhibits a chaotic attractor of dimension $D = 3.3$. The scalar observable here is $x = x_1 + x_2$ and we sample the attractor every cycle of the external forcing. The attractor reconstructed using the time series $\{x_n\}$ in an $(m=4)$-dimensional delay coordinates space has a dimension $D = 2.3$. Figure 2(a) shows the attractor projected down to a two-dimensional space. The high-dimensional character of this attractor is apparent.

The reconstructed attractor contains a fixed point $(N=1)$ at $\mathbf{Z}(\bar{p}) = (0.54, 0.54, 0.54, 0.54)^T$ with two unstable directions $(u=2)$. This fixed point corresponds to the synchronized period-1 motion of the coupled oscillators. Our objective is to stabilize this motion. From numerically generated time series we estimate a_i and b_i used in the $\mathbf{A}$ matrix and the $\mathbf{B}$ vectors to be approximately $a^{(1)} = -3.05$, $a^{(2)} = -2.23$, $a^{(3)} = 0.0$, $a^{(4)} = 0.016$ and $b^{(1)} = -0.90$, $b^{(2)} = -0.089$, $b^{(3)} = 0.78$, $b^{(4)} = -0.056$. The two unstable eigenvalues are $\lambda_1 = -1.85$ and $\lambda_2 = -1.20$. Applying the control law in Eq. (17), we stabilize the fixed point as shown in Fig. 2(b), which displays the behavior of the system before and after the control is turned on.

C. Control example 2

Consider the four-dimensional autonomous chemical reaction model [13]

$$\begin{aligned} \dot{x} &= pw/(1+w^{10}) - 0.1x, \\ \dot{y} &= 0.1x - 0.2yz, \\ \dot{z} &= 0.2z(y-w), \\ \dot{w} &= 0.2zw - 0.1w. \end{aligned} \tag{33}$$

For $p = \bar{p} = 2.5$ this system exhibits a chaotic attractor of dimension $D = 2.2$. Assume that the observed scalar variable is x itself. By measuring the times between successive upward crossings of some threshold x_c by the x versus t function we form the interspike interval time series $\{I_n\}$. Reconstructing

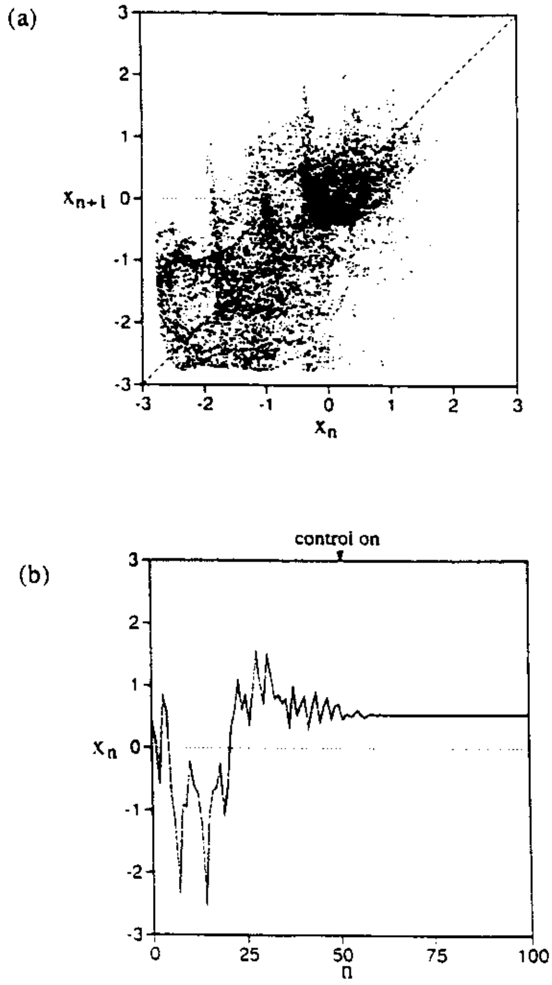

FIG. 2. (a) Two-dimensional ($m = 2$) reconstructed image of the attractor from the coupled Duffing equations, Eq. (32). High-dimensional nature of the dynamics is apparent. (b) The result of applying an $m = 4$ implementation of our control method. Here discrete stroboscopic samples are connected with straight lines.

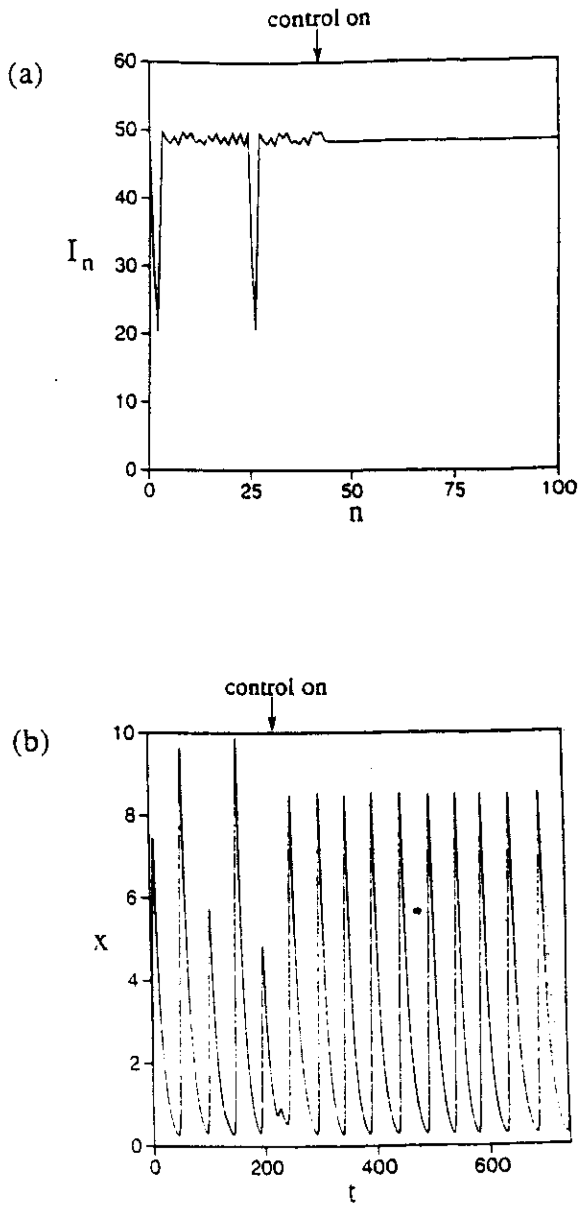

FIG. 3. Results of controlling the unstable period-1 orbit in the chemical reaction model Eq. (33) using an $m = 3$ implementation of the control. (a) The interspike intervals and (b) the corresponding continuous-time series.

this discrete time series in an ($m = 3$)-dimensional delay coordinate space we obtain an attractor of dimension 1.2. In this attractor there is a fixed point ($N = 1$) at $\mathbf{z}_n = (48.40, 48.40, 48.40)^T$ and a period-2 orbit ($N = 2$) cycling between $\bar{\mathbf{z}}_1(\bar{p}) = (47.74, 50.13, 47.74)^T$ and $\bar{\mathbf{z}}_2(\bar{p}) = (50.13, 47.74, 50.13)^T$. Both orbits are found to have one unstable direction ($u = 1$).

First, consider the control of the fixed point. Set $x_c = 1$. From the numerically generated time series we obtain $a^{(1)} = -1.33$, $a^{(2)} = 0.41$, $a^{(3)} = -0.008$ and $b^{(1)} = -1.25$, $b^{(2)} = -3.20$, $b^{(3)} = 1.95$. The unstable eigenvalue is calculated to be $\lambda_1 = -1.59$. The result of applying Eq. (20) is shown in Fig. 3, where the system behavior before and after the control is turned on is displayed. Figure 3(a) is the interspike intervals and Fig. 3(b) gives the corresponding continuous time series.

Next, consider the control of the period-2 orbit. Set $x_c = 3$. From the time series we estimate the elements of the $\mathbf{A}$ matrix and the $\mathbf{B}$ vectors at $\mathbf{z}_1(\bar{p})$ to be $a^{(1)} = -1.56$, $a^{(2)} = 0.042$, $a^{(3)} = 6.0 \times 10^{-5}$, and $b^{(1)} = 1.81$, $b^{(2)} = -3.32$, $b^{(3)} = 1.61$ and at $\mathbf{z}_2(\bar{p})$ to be $a^{(1)} = 2.15$, $a^{(2)} = 0.15$, $a^{(3)} = 2.9 \times 10^{-3}$ and $b^{(1)} = -2.79$, $b^{(2)} = 5.85$, $b^{(3)} = 0.17$. The control law in Eq. (29) is completely determined by these values. In Fig. 4 we show the result of control by displaying the interspike intervals (a) and the corresponding continuous time series (b) for before and after the control is activated.

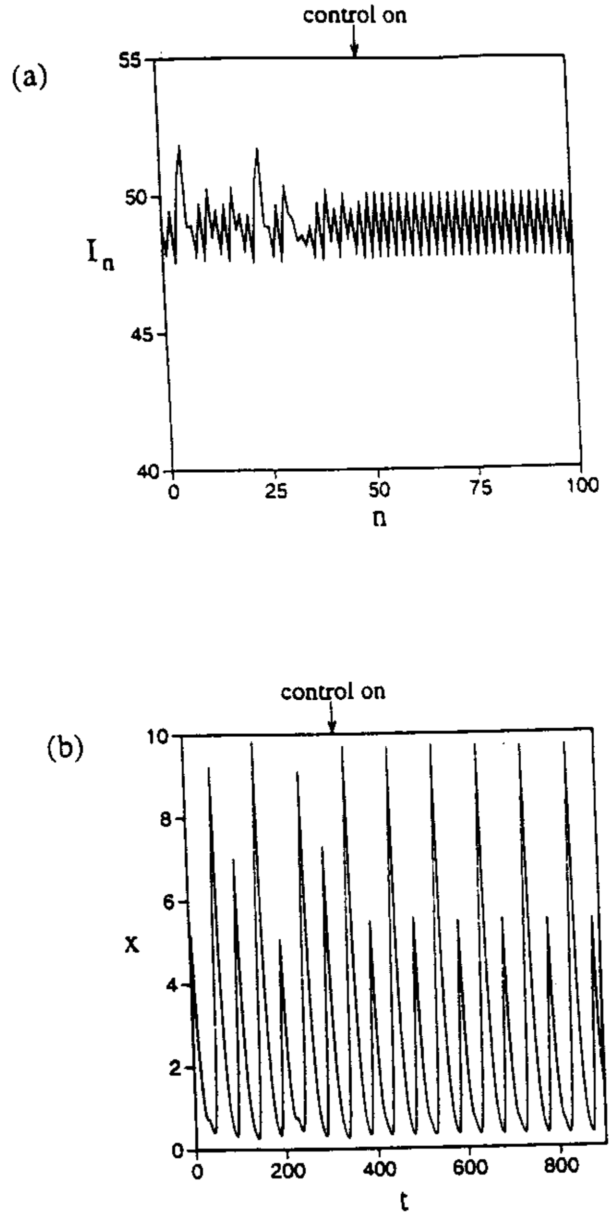

FIG. 4. Results of controlling the unstable period-2 orbit in the chemical reaction model Eq. (33) using an $m=3$ implementation of the control. (a) The interspike intervals and (b) the corresponding continuous-time series.

IV. EXPERIMENTAL RESULTS

A. Setup

Our experimental system consists of a magnetoelastic metal ribbon clamped at its lower end. The ribbon changes its Young's modulus by more than a factor of 10 in response to an external magnetic field and buckles under gravity as a result. This highly nonlinear system is placed vertically within three mutually orthogonal pairs of Helmholtz coils. The two horizontal pairs of the Helmholtz coils are used for counteracting the Earth's magnetic field while the vertical pair is used to supply an approximately uniform field along the ribbon's length. Inside the Helmholtz coils a photonic sensor is used to measure the ribbon's position at a given point. This sensor is mounted a short distance above the base of the ribbon. To obtain chaos, we drive the ribbon with a time-varing magnetic field in the form $H(t)=H_{dc}+H_{ac}\sin(2\pi ft)$, which is applied along the vertical direction. For $f=1.03$ Hz, $H_{ac}=0.961$ Oe, and $H_{dc}=\bar{H}_{dc}=-1.350$ Oe the ribbon exhibits chaotic oscillations. We choose $p=H_{dc}$ as the control parameter.

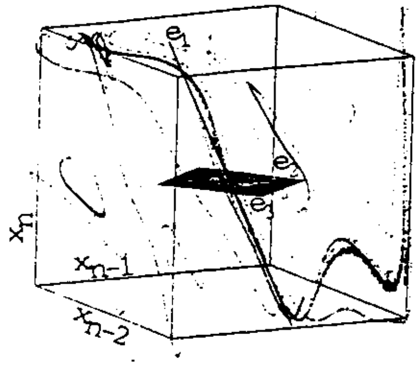

FIG. 5. Time series from the magnetoelastic ribbon reconstructed in a three-dimensional ($m=3$) delay coordinate space. The local dynamics near the fixed point is described by one unstable ($\mathbf{e}_1$) and two stable directions ($\mathbf{e}_2$ and $\mathbf{e}_3$).

Denote the position of the ribbon measured by the photonic sensor every driving period as x_n. From visual inspections of the reconstructed attractor in the $m=2$ space and from some simple estimates it is apparent that the dynamical behavior near the fixed point, which we wish to stabilize, cannot be effectively characterized by one stable direction and one unstable direction. High-dimensional embedding spaces are needed to unfold the local dynamics in this case. This observation is further confirmed by our inability to bring about the desired control using the original Ott-Grebogi-Yorke (OGY) method [2] (see below) as well as using the $m=2$ implementation of our control method, which incorporates the effect of delay coordinates and is equivalent to the Dressler and Nitsche's method [6].

Next we reconstruct the time series in an ($m=3$)-dimensional space as shown in Fig. 5. On the chaotic attractor we identify an unstable periodic orbit of period-1 by looking for saddle points lying on the diagonal. From the experimental data this fixed point is determined to be $\bar{z}(\bar{p})=(6.35, 6.35, 6.35)^T$. To stabilize the system around this unstable fixed point, we choose $p=H_{dc}$ as the control parameter. When the system state point falls in the vicinity of the unstable fixed point, a small time-dependent change was made to this parameter such that the next iterate would fall onto the stable plane defined by the two stable eigenvectors. The perturbation size is calculated according to Eq. (20). To determine the matrix elements $a^{(1)}$, $a^{(2)}$, and $a^{(3)}$ for $\mathbf{A}$ in Eq. (10) we consider a close return event by choosing a point in the close vicinity of the fixed point and finding its preimage and two future iterates. The reason for using the preimage is to better represent the stable directions and the reason for using two future iterates instead of just one is to pick up the negative sign often associated with the unstable eigenvalue. To guard against the detection of a false nearest neighbor in a three-dimensional embedding space we also monitor the delay coordinate map in the $m=4$ and $m=5$ space. From the true nearest-neighbor points we do a least-squares fit to determine $a^{(1)}$, $a^{(2)}$, and $a^{(3)}$ to a high accuracy. Using 20 close return events we find $a^{(1)}=-1.033\,68$, $a^{(2)}=1.7890$, and $a^{(3)}=0.0935$, respectively. From the matrix the unstable eigenvalue was calculated to be $\lambda_1=-1.9338$. The values of $b^{(1)}$, $b^{(2)}$, and $b^{(3)}$ are calculated from the experimental data when a perturbation p_n is applied at time n immediately after a point in the map comes into the vicinity of the unstable fixed point. The perturbation lasts for the full duration of the drive period. When the future section data are measured at time $n+1$, $n+2$, and $n+3$, we calculate the coefficients $b^{(1)}$, $b^{(2)}$, and $b^{(3)}$ according to

$$b^{(1)}=\frac{\delta x_{n+1}-a^{(1)}\delta x_n-a^{(2)}\delta x_{n-1}-a^{(3)}\delta x_{n-2}}{\delta p_n},$$

$$b^{(2)}=\frac{\delta x_{n+2}-a^{(1)}\delta x_{n-1}-a^{(2)}\delta x_n-a^{(3)}\delta x_{n-1}}{\delta p_n},$$

$$b^{(3)}=\frac{\delta x_{n+3}-a^{(1)}\delta x_{n+2}-a^{(2)}\delta x_{n+1}-a^{(3)}\delta x_n}{\delta p_n}.$$

In the experiment we use a constant $\delta p_n=0.038$ Oe every time for perturbation. For a typical run in this experiment the values of $b^{(1)}$, $b^{(2)}$, and $b^{(3)}$ are determined to be 0.001 23 V/Oe, $-0.000\,118$ V/Oe, and $-0.000\,414$ V/Oe, respectively.

B. Results

Using the $m=3$ implementation of our control method with the estimated $a^{(i)}$'s and $b^{(i)}$'s as stated above, we have successfully controlled the chaotic oscillations of the ribbon for almost 200 000 driving cycles (about 54 h) without any loss of control. Figure 6(a) shows a portion of the experimental time series before and after the application of control. The control can be maintained indefinitely. Figure 6(b) shows the perturbations applied to stabilize the period-1 orbit. Notice that the size of the perturbations is very small, typically between ± 0.0054 Oe, or about 0.4% of the nominal dc field $\bar{p}=\bar{H}_{dc}$. Figure 7(a) shows the contrast between the original OGY control [2] and our high-dimensional control with $m=3$ on the same attractor. After 830 iterates the OGY control is turned on and is unable to hold the periodic orbit even though there are numerous attempts on the close returns. The perturbed orbits would come in along the stable direction, but once the orbit reaches the unstable fixed point it starts to depart from the vicinity of the fixed point. In contrast, when our high-dimensional control is activated the system is captured into the period-1 motion rapidly. We note that the $m=2$ implementation of our method, which has the delay coordinates effect taken into account, also failed to achieve proper control. This leads us to believe that for this attractor one needs a higher-dimensional embedding space to unfold the dynamics and implement control.

We have also studied another parameter setting where the local dynamics near the fixed point can be effectively described by one stable and one unstable direction. We are able

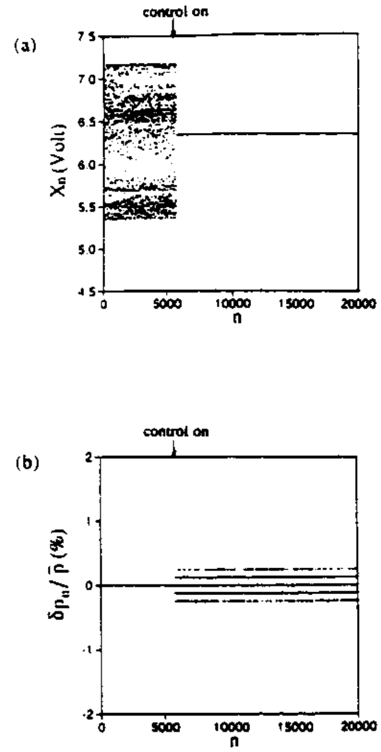

FIG. 6. Results of stabilizing the unstable period-1 orbit using an $m=3$ implementation of our control method. (a) Time series and (b) parameter perturbations. We note that the magnitude of δp_n is about 0.4% of the nominal value of $\bar{p}$, where $p=H_{dc}$ is the dc field.

to control the period-1 orbit in this case with the original OGY method [2]. However, the interesting point is that, by applying the $m=3$ implementation of our method to the same orbit, we are able to achieve control with smaller parameter perturbations compared to the OGY case. This indicates that in some situations, although the low-dimensional control is effective, a higher-dimensional implementation may prove to be more efficient. Details of this result are planned to be presented in a future paper where we consider all the practical aspects of our control technique.

In applications, an important question is the impact of noise on the control performance. The unperturbed ribbon system has about 5% intrinsic noise. Our method is unaffected by this amount of noise. To test the method further, we have also added parametric noise to the system and found that we are able to maintain control even in the presence of about 10% of additional parametric noise, demonstrating the method's robustness. We thus believe that the technique presented in the paper is viable in practical problems where chaos control in high-dimensions is desired. Again we wish to present more detailed results on the issue of noise in a future paper.

V. CONCLUSION

Since Ott, Grebogi, and Yorke published their seminal paper on the control of chaos [2], a great deal of experimental research in nonlinear dynamics has been dedicated to the exploration of various aspects of the OGY algorithm in a

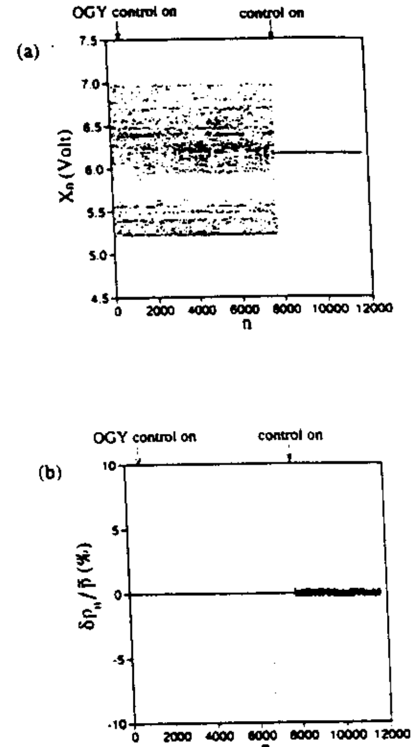

FIG. 7. Comparison of the OGY control and the $m=3$ implementation of our control method. (a) Time series and (b) parameter perturbations.

variety of systems. However, the success of the original OGY theory is limited by the fact that it applies only to systems where the dynamics near the periodic orbit is adequately described by one stable and one unstable direction. In the past few years a number of high-dimensional algorithms have been proposed to address this problem [7–9]. Due to the difficulties in obtaining the coefficients needed for control and sensitivity to noise, these methods are found to be difficult to implement experimentally.

Our main contribution in this paper is the development of a high-dimensional chaos control method that is effective and easy to implement in experiments. Based on the use of time series and delay coordinates, the method requires only small perturbations of a single control parameter to stabilize a periodic orbit in an arbitrary dimensional delay coordinate embedding space with an arbitrary number of unstable directions. In addition, by considering map-based systems our method offers the advantage that the coefficients needed for experimental implementation are easily and reliably estimated from time series data. In this regard, simple methods are proposed to extract such map-based time series from continuous-time systems. The effectiveness of the control method is demonstrated when applied to two examples of ordinary differential equations and to a physical experiment of a magnetoelastic ribbon driven by a sinusoidally varying magnetic field. Robust control is achieved in all cases. Furthermore, we mention that the method is not sensitive to noise and works well even in the presence of substantial noise.

ACKNOWLEDGMENTS

M.D. gratefully acknowledges support from the Office of Naval Research. W.L.D. is supported by the ONR Young Investigator Program. M.L.S. gratefully acknowledges support from the NSWC Independent Research Program and from the Office of Naval Research (Division of Physics and Chemistry).

APPENDIX

1. The null space of $\bar{\mathbf{A}}^{m-1}$

Using matrix blocks we rewrite $\bar{\mathbf{A}}$ defined in Eq. (13) as

$$\bar{\mathbf{A}}=\begin{pmatrix} \mathbf{A} & \mathbf{B} \\ \mathbf{Z}_0 & \mathbf{S} \end{pmatrix},$$

where $\mathbf{B}$ is an $m\times(m-1)$ matrix with $\mathbf{B}^{(i)}$ its column vectors, $\mathbf{Z}_0$ is an $(m-1)\times m$ zero matrix, and

$$\mathbf{S}=\begin{pmatrix} 0 & 1 & 0 & \cdots & 0 \\ 0 & 0 & 1 & \cdots & 0 \\ \vdots & \vdots & \vdots & \vdots & \vdots \\ 0 & 0 & 0 & \cdots & 1 \\ 0 & 0 & 0 & 0 & 0 \end{pmatrix}_{(m-1)\times(m-1)} .$$

It is easy to verify that $\mathbf{S}^{m-1}$ is a matrix of zeros. This means that the eigenvalue problem $\bar{\mathbf{A}}^{m-1}\mathbf{k}=\mathbf{0}$ has m equations for $2m-1$ unknowns from which one can find $m-1$ independent basis vectors to span the null vector $\mathbf{k}$. In other words, the null space of $\bar{\mathbf{A}}^{m-1}$ is $(m-1)$ dimensional.

2. The unstable eigenvectors of $\bar{\mathbf{A}}^T$

We wish to show that $\mathbf{v}_i$ from $\bar{\mathbf{A}}^T\mathbf{v}_i=\lambda_i\mathbf{v}_i$, $i=1,2,\ldots,u$, is orthogonal to the stable subspace spanned by $\mathbf{k}_j$, $j=u+1,u=2,\ldots,2m-1$. Consider $j=u+1,u+2,\ldots,m$. Multiply Eq. (15) from both sides by $\mathbf{k}_j^T$. The left-hand side becomes $\mathbf{k}_j^T\bar{\mathbf{A}}^T\mathbf{v}_i=(\bar{\mathbf{A}}\mathbf{k}_j)^T\mathbf{v}_i=\lambda_j\mathbf{k}_j^T\mathbf{v}_i$. Equating it with the right-hand side $\lambda_i\mathbf{k}_j^T\mathbf{v}_i$ and using $\lambda_i\neq\lambda_j$ we have $\mathbf{k}_j^T\mathbf{v}_i=\mathbf{v}_i^T\mathbf{k}_j=0$. Similarly, one can show that $\mathbf{v}_i^T\mathbf{k}_j=0$, $j=m+1,m+2,\ldots,2m-1$, by considering the eigenvalue problem of $\bar{\mathbf{A}}^{m-1}$ instead of $\bar{\mathbf{A}}$. It is straightforward to see that if the deviation $\delta\mathbf{Y}_{n+u}$ lies entirely in the space of $\mathbf{k}_j$, $j=u+1,u+2,\ldots,m,m+1,m+2,\ldots,2m-1$, then its future evolution asymptotically approaches zero under repeated applications of $\bar{\mathbf{A}}$.

3. The derivation of the control law Eq. (17) from Eq. (16)

Iterating Eq. (12) u times yields

$$\delta\mathbf{Y}_{n+u}=\bar{\mathbf{A}}^u\delta\mathbf{Y}_n+\bar{\mathbf{A}}^{u-1}\bar{\mathbf{B}}\delta p_n+\bar{\mathbf{A}}^{u-2}\bar{\mathbf{B}}\delta p_{n+1}+\cdots$$
$$+\bar{\mathbf{B}}\delta p_{n+u-1}.$$

From Eq. (16) we get

91

$$\lambda_1^{u-1}\delta p_n+\lambda_1^{u-2}\delta p_{n-1}+\cdots+\delta p_{n+u-1}=-\left(\frac{\lambda_1^u \mathbf{v}_1^T}{(\mathbf{v}_1^T\bar{\mathbf{B}})}\right)\delta\mathbf{Y}_n,$$

$$\lambda_2^{u-1}\delta p_n+\lambda_2^{u-2}\delta p_{n-1}+\cdots+\delta p_{n+u-1}=-\left(\frac{\lambda_2^u \mathbf{v}_2^T}{(\mathbf{v}_2^T\bar{\mathbf{B}})}\right)\delta\mathbf{Y}_n,$$

$$\vdots$$

$$\lambda_u^{u-1}\delta p_n+\lambda_u^{u-2}\delta p_{n-1}+\cdots+\delta p_{n+u-1}=-\left(\frac{\lambda_u^u \mathbf{v}_u^T}{(\mathbf{v}_u^T\bar{\mathbf{B}})}\right)\delta\mathbf{Y}_n.$$

These u linear equations contain u unknowns. Using Cramer's rule we express p_n as

$$p_n=\bar{p}+\frac{C}{D},$$

where

$$C=\mathrm{Det}\begin{pmatrix} -[\lambda_1^u\mathbf{v}_1^T/(\mathbf{v}_1^T\bar{\mathbf{B}})]\delta\mathbf{Y}_n & \lambda_1^{u-2} & \lambda_1^{u-3} & \cdots & 1\\ -[\lambda_2^u\mathbf{v}_2^T/(\mathbf{v}_2^T\bar{\mathbf{B}})]\delta\mathbf{Y}_n & \lambda_2^{u-2} & \lambda_2^{u-3} & \cdots & 1\\ \vdots & \vdots & \vdots & \vdots & \vdots\\ -[\lambda_u^u\mathbf{v}_u^T/(\mathbf{v}_u^T\bar{\mathbf{B}})]\delta\mathbf{Y}_n & \lambda_u^{u-2} & \lambda_u^{u-3} & \cdots & 1 \end{pmatrix}_{u\times u} \tag{A1}$$

and

$$D=\mathrm{Det}\begin{pmatrix} \lambda_1^{u-1} & \lambda_1^{u-2} & \lambda_1^{u-3} & \cdots & 1\\ \lambda_2^{u-1} & \lambda_2^{u-2} & \lambda_2^{u-3} & \cdots & 1\\ \vdots & \vdots & \vdots & \vdots & \vdots\\ \lambda_u^{u-1} & \lambda_u^{u-2} & \lambda_u^{u-3} & \cdots & 1 \end{pmatrix}_{u\times u}. \tag{A2}$$

By recognizing that D in (A2) is a slight variant of the standard Vandermonde determinant [14] we find

$$D=(-1)^{(d^2-d)/2}\prod_{1\le i<j\le u}(\lambda_j-\lambda_i).$$

Expanding the determinant in Eq. (A1) about the first column, the resulting cofactors are again variants of the Vandermonde matrix. This leads us to

$$C=\sum_{k=1}^{u}(-1)^{k+(d^2-3d+2)/2}[\lambda_k^u\mathbf{v}_k^T/(\mathbf{v}_k^T\bar{\mathbf{B}})]\delta\mathbf{Y}_n$$

$$\times\prod_{1\le i<j\le u, i\ne k, j\ne k}(\lambda_j-\lambda_i).$$

After some algebra we obtain Eq. (17).

[1] E. Ott, *Chaos in Dynamical Systems* (Cambridge University Press, Cambridge, 1993).

[2] E. Ott, C. Grebogi, and J.A. Yorke, Phys. Rev. Lett. **64**, 1196 (1990).

[3] W.L. Ditto, S.N. Rauseo, and M.L. Spano, Phys. Rev. Lett. **65**, 3211 (1990); E.R. Hunt, *ibid.* **67**, 1953 (1991); R. Roy, T.W. Murphy, T.D. Maier, Z. Gills, and E.R. Hunt, *ibid* **68**, 1259 (1992); A. Garfinkel, M.L. Spano, W.L. Ditto, and J.N. Weiss, Science **257**, 1230 (1992); V. Petrov, V. Caspar, J. Masere, and K. Showalter, Nature (London) **361**, 240 (1993); S.J. Schiff, K. Jerger, D.H. Duong, T. Chang, M.L. Spano, and W.L. Ditto, *ibid.* **370**, 615 (1994); J.E.S. Socolar, D.W. Sukow, and D.J. Gauthier, Phys. Rev. E **50**, 3245 (2994); P. Parmananda, M.A. Rhode, G.A. Johnson, R.W. Rollins, H.D. Dewald, and A.J. Markworth, *ibid.* **49**, 5007 (1994).

[4] E.A. Jackson and A. Hubler, Physica D **44**, 407 (1990); B. Peng, V. Petrov, and K. Showalter, J. Phys. Chem. **95**, 4957 (1991); T. Tel, J. Phys. A **24**, L1359 (1991); K. Pyragas, Phys. Lett. A **170**, 421 (1992); Y.-C. Lai, M. Ding, and C. Grebogi, Phys. Rev. E **47**, 86 (1993); M.A. Matias and J. Guemez, Phys. Rev. Lett. **72**, 1455 (1994); M. Ding, E. Ott, and C. Grebogi, Physica D **74**, 386 (1994); D. Vassiliadis, *ibid.* **71**, 319 (1994); D.J. Christini and J.J. Collins, Phys. Rev. E (to be published).

[5] For reviews, see T.A. Shinbrot, C. Grebogi, E. Ott, and J.A. Yorke, Nature (London) **363**, 411 (1993); W.L. Ditto and L. Pecora, Sci. Am. **269** (8), 78 (1993); G. Chen and X. Dong, Int. J. Bif. Chaos **3**, 1363 (1993); E.R. Hunt and G. Johnson, IEEE Spectrum **30** (11), 32 (1993); R. Roy, Z. Gills, and K.S. Thornburg, Opt. Photon. News **5** (5), 8 (1994); E. Ott and M.L. Spano, Phys. Today **48** (5) 34 (1995).

[6] U. Dressler and G. Nitsche, Phys. Rev. Lett. **68**, 1 (1992); G. Nitsche and U. Dressler, Physica D **58**, 153 (1992).

[7] P. So and E. Ott, Phys. Rev. E **51**, 2955 (1995).

[8] V. Petrov, E. Mihaliuk, S.K. Scott, and K. Showalter, Phys. Rev. E **51**, 3988 (1995).

[9] For a sample of works dealing with chaos control in high dimensions, see F.J. Romeiras, C. Grebogi, E. Ott, and W.P. Dayawansa, Physica D **58**, 165 (1992); D. Auerbach, C. Grebogi, E. Ott, and J.A. Yorke, Phys. Rev. Lett. **69**, 3479 (1992); J.A. Sepulchre and A. Babloyantz, Phys. Rev. E **48**, 945 (1993); G. Hu and K. He, Phys. Rev. Lett. **71**, 3794 (1993); C. Reyl, L. Flepp, R. Badii, and E. Brun, Phys. Rev. E **47**, 267 (1993); P. Colet, R. Roy, and K. Wiesenfeld, *ibid.* **50**, 3453 (1994); G. Hu and Z. Qu, Phys. Rev. Lett. **72**, 68 (1994); I.B. Schwartz and I. Triandaf, Phys. Rev. E **50**, 2548 (1994); A. Namajunas, K. Pyragas, and A. Tamasevicius, Phys. Lett. A **204**, 255 (1995).

[10] Edward Ott (private communication).

[11] J.-P. Eckmann and D. Ruelle, Rev. Mod. Phys. **57**, 617 (1985).

[12] F. Takens, in *Dynamical Systems and Turbulence*, edited by D. Rand and L.S. Young (Springer-Verlag, Berlin, 1981), p. 366; T. Sauer, J.A. Yorke, and M. Casdagli, J. Stat. Phys. **65**, 579 (1991).

[13] G. Baier and S. Sahle, J. Chem. Phys. **100**, 8907 (1994).

[14] R. Bellman, *Introduction to Matrix Analysis* (McGraw-Hill, New York, 1970).

22

PHYSICAL REVIEW E VOLUME 50, NUMBER 5 NOVEMBER 1994

Crisis control: Preventing chaos-induced capsizing of a ship

Mingzhou Ding
Center for Complex Systems and Department of Mathematics, Florida Atlantic University, Boca Raton, Florida 33431

Edward Ott[1,2] and Celso Grebogi[1,3]
[1]*Institute for Plasma Research, University of Maryland, College Park, Maryland 20742*
[2]*Institute for Systems Research and Departments of Physics and of Electrical Engineering, University of Maryland, College Park, Maryland 20742*
[3]*Department of Mathematics and Institute for Physical Science and Technology, University of Maryland, College Park, Maryland 20742*
(Received 11 July 1994)

Responses of many man-made systems, such as ships or oil-drilling platforms, when subject to irregularly time varying environments, can be described by irregularly driven dynamical systems. Consequently, failures of such systems (e.g., capsize of a ship or collapse of a platform), under increasingly severe environmental conditions, come about when the system state escapes from a destroyed chaotic attractor located in some favorable region of the phase space. In this paper we propose a control strategy, based on a previous method of chaos control, which can prevent such failures from taking place. The key feature of our strategy is the incorporation of prediction of the evolution of the environment. This makes possible effective operation of the control even when the temporal behavior of the environment has substantial irregularity. We illustrate the ideas using ship capsizing as an example.

PACS number(s): 05.45.+b

Imagine a ship rolling in lateral ocean waves. Its dynamics can be modeled by the following nonlinear oscillator,

$$\ddot{x}+\nu\dot{x}+\omega^2(x-\alpha x^3)=W(t)\ , \tag{1}$$

where x is a variable characterizing the angle from the ship mast to the vertical direction, ν is the friction coefficient, ω is the eigenfrequency of small vibrations around the origin, α denotes the strength of nonlinearity, and $W(t)$ represents the effect of the ocean waves impinging on the ship. In particular, we shall be interested in the case where the ocean waves have substantial temporal irregularity and drift superposed on their mean periodic time dependence.

In the absence of waves, i.e., $W(t)=0$, for a small displacement in x, the subsequent motion damps out and the ship reverts back to its upright position. For large displacements in x, gravity overcomes buoyancy and x tends to the attractor at $|x|=\infty$. When this occurs we say the ship has capsized. Models of similar type have been used in other studies of ship dynamics [1–3].

We assume that the irregular ocean waves have the following form:

$$W(t)=f(t)[1+\epsilon_a g(t)]\sin\phi(t)\equiv F(t)\sin\phi(t)\ , \tag{2}$$

where $F(t)$ is the amplitude, with $f(t)$ it slowly varying component and $g(t)$ a fast irregularly varying component; the phase $\phi(t)$ is determined by

$$\dot{\phi}(t)=\Omega+\epsilon_p h(t)\ . \tag{3}$$

Here again $h(t)$ is an irregular function of time. In what follows, we (somewhat arbitrarily) model the temporally irregular functions $g(t)$ and $h(t)$ as outputs of well-known chaotic systems. Specifically, we use

$$g(t)=\frac{y(t)-\langle y(t)\rangle}{\sqrt{\langle [y(t)-\langle y(t)\rangle]^2\rangle}}\ ,$$

where $y(t)$ is a solution of the following driven Duffing system:

$$\ddot{y}+0.05\dot{y}+y^3=7.5\cos t\ ,$$

and

$$h(t)=\frac{z_1(t)-\langle z_1(t)\rangle}{\sqrt{\langle [z_1(t)-\langle z_1(t)\rangle]^2\rangle}}\ ,$$

with $z_1(t)$ taken from the Rössler system,

$$\dot{z}_1=-z_2-z_3\ ,$$

$$\dot{z}_2=z_1+0.398z_2\ ,$$

$$\dot{z}_3=2+z_3(z_1-4)\ .$$

The symbol $\langle\ \rangle$ denotes temporal average. Since $g(t)$ and $h(t)$ are normalized, ϵ_a and ϵ_p measure the relative strength of amplitude irregularity and that of phase irregularity, respectively. (We emphasize that our use of low-dimensional chaotic systems to produce the irregularly varying $g(t)$ and $h(t)$ is merely a convenience, and there should be no essential difference in what follows if these functions are stochastic or are produced by some high-dimensional chaotic processes.)

For $\epsilon_a=\epsilon_p=0$ and $f(t)=f_0$, where f_0 is a constant, we have purely sinusoidal waves, and the dynamics in this case will be used as the basis for control later when irregularities are introduced into the system. The evolution of Eq. (1) with increasing wave amplitude f_0 and $\epsilon_a=\epsilon_p=0$ is shown in the bifurcation diagram in Fig. 1. (The values of the system parameters used in the numeri-

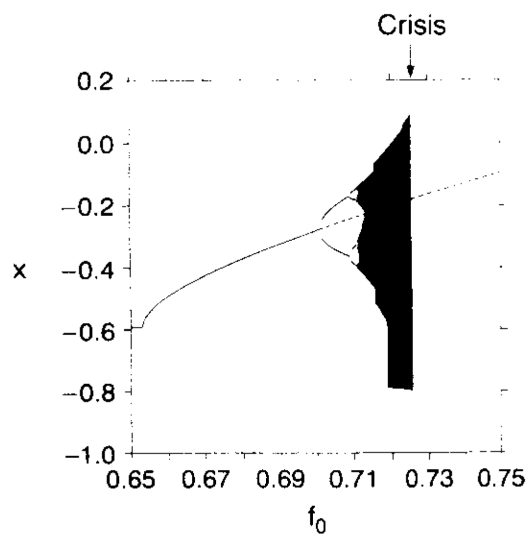

FIG. 1. Bifurcation diagram of Eq. (1). The dashed line indicates the unstable period one orbit after the period doubling bifurcation.

cal computations are quoted in the caption of Fig. 3.) The surface of section here is taken every time $W(t)$ crosses zero with $dW(t)/dt>0$ (i.e., $\Omega t_n=2n\pi$). For $0<f_0<0.7$ the oscillation of the ship is periodic with the period equal to that of the wave. We henceforth call this orbit the period one orbit. Following a period doubling cascade the ship response becomes chaotic. At $f_0\approx 0.726$ a crisis takes place in which the bounded chaotic attractor is destroyed by colliding with its basin boundary. As the wave amplitude increases past this crisis value, since no bounded attractor exists in the system, almost all initial conditions tend to the attractor at $|x|=\infty$ (i.e., the ship capsizes). Also shown in Fig. 1 as a dashed curve is the period one orbit after it loses stability. Now suppose that $f(t)$ is a gradually increasing function of time starting from $f(t)=0$. We anticipate that in the absence of control the ship will capsize some time after $f(t)$ exceeds the crisis value. To prevent this, one starts to apply control to stabilize the period one orbit in Fig. 1 when the wave is still small and continues to do so as the wave increases. As a result, we show that the ship survives waves whose amplitude significantly exceeds the crisis value. More importantly, by incorporating a prediction feature to be detailed below, and suitably modifying the control procedure of [4,5], we are able to prevent capsizing in the presence of substantial wave irregularities.

The equation of motion for the variable x, when control is applied, is again Eq. (1), but with the right-hand side replaced by $W(t)+C(t)$, where $C(t)$ is the control. We take $C(t)$ to be a constant between successive crossings of the surface of section. In practical terms, $C(t)$ can be thought of as the balancing force provided by temporally shifting ballast on the ship, and the value of $C(t)$ is assumed to be bounded between $-C_0$ and C_0, i.e., $-C_0\le C(t)\le C_0$. In fact, we are interested in the case where C_0 is small compared to the force exerted by the waves. We take the surface of section to specify the system state at times $t=t_n$ such that $W(t)=0$ and $dW(t)/dt>0$. Assuming that $f(t)>0$ and that the right-hand side of Eq. (3) is positive this corresponds to $\phi(t_n)=2n\pi$ [see Eq. (2)]. Figure 2 illustrates the prediction and control method. A fixed point of the Poincaré map and its stable and unstable directions are constructed for $\epsilon_a=\epsilon_p=0$ and $f(t)=f(t_n)$. Here we imagine that $f(t)$ can be treated as a constant in the interval $t_n<t<t_{n+1}$. (Note that due to the slow variation of $f(t)$ the fixed point location at $t=t_n$ changes with n [6].) By letting $\epsilon_a\neq 0$ and $\epsilon_p\neq 0$, we introduce irregularity into the wave. The task now is to stabilize the motion around the fixed point. Suppose that at $t=t_n$, the system state is denoted by $\mathbf{z}_n$, where $\mathbf{z}=(x,y=\dot{x})$. From observation of waves propagating toward the ship, we assume that we can make an accurate prediction of $W(t)$ for $t_n\le t\le t_{n+1}$. Integrating Eq. (1) with this predicted $W(t)$, and with various values of $C(t)=\hat{C}$, where $\hat{C}$ is a constant in the interval $[-C_0,C_0]$, we obtain images of the system state on the next surface of section at $t=t_{n+1}$, which form a curve as shown in Fig. 2. The value $\hat{C}=C_n$ of the control that we actually apply to the ship is chosen so that the system state falls on the stable direction of the fixed point.

Figure 3(a) shows part of the wave for $\epsilon_a=0.15$, $\epsilon_p=0.1$, and $f(t)$ a linearly increasing function of t. As shown in Fig. 3(b), in the absence of control, the ship capsizes in several cycles of the ocean waves. Using control with prediction the capsizing is prevented in Fig. 3(b). A more extended controlled orbit is shown in Fig. 3(c). Figure 3(d) shows $C(t)$ as a function of t. Comparing with Fig. 3(a) we see that $C(t)$ is much smaller than the wave amplitude $W(t)$.

In the example above we have tacitly assumed that the wave $W(t)$ can be observed and predicted with certainty in the short term (i.e., from t_n to t_{n+1}). In practice, a more likely situation is that the prediction is imperfect. We now attempt to assess the effect of imperfect prediction. For specificity, we consider only amplitude irregularity in Eq. (2), which we assume to be

$$g(t)=\frac{(1-\gamma)g_o(t)+\gamma g_u(t)}{\sqrt{(1-\gamma)^2+\gamma^2}}\ , \tag{4}$$

where $g_o(t)$ and $g_u(t)$ are two different normalized trajectory realizations (originating from two different initial

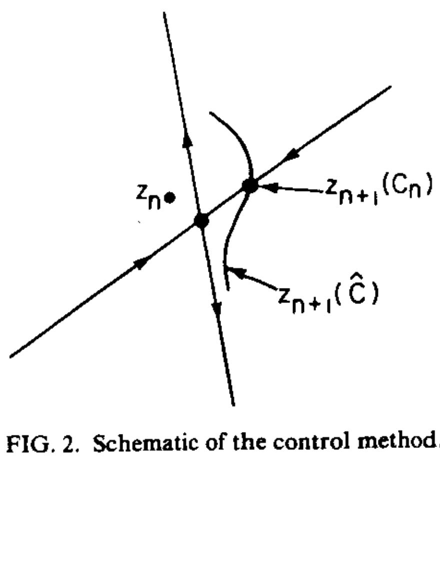

FIG. 2. Schematic of the control method.

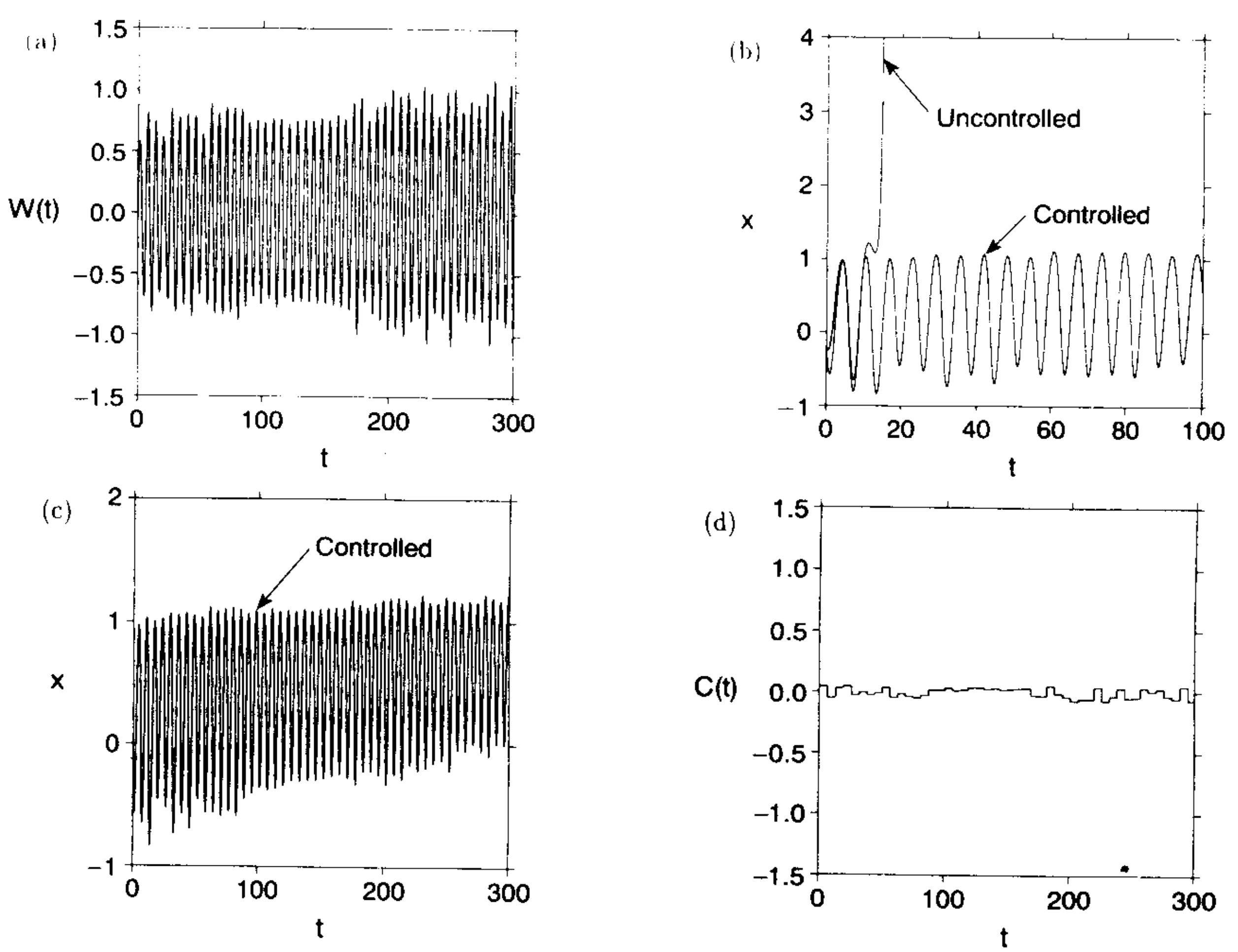

FIG. 3(a) Segment of the irregular increasing wave with $\epsilon_a=0.15$, $\epsilon_p=0.1$, and $f(t)$ a linearly increasing function of t, (b) controlled together with uncontrolled orbit, (c) more extended plot of controlled orbit, and (d) $C(t)$ versus t. The following parameter values are chosen for numerical computations: $\nu=0.5$, $\omega=\Omega=1.0$, $\alpha=1.0$, and integration step size $=2\pi/200$.

conditions) from the same Duffing chaotic attractor, with $g_o(t)$ being the "observed" and $g_u(t)$ the "unobserved" components of $g(t)$, and γ measures the relative strength of these two components. The imperfect prediction of $W(t)$ is assumed to be given by replacing the true $g(t)$ defined in Eq. (4) by $g_o(t)$. To design a control we integrate the equation of motion assuming $g(t)=g_o(t)$. The actual trajectory however is obtained by including $g_u(t)$ in the integration after $C(t)$ has been chosen. Let $\langle T_{\text{survival}} \rangle$ denote the average survival time in wave cycles calculated for ten different realizations of $g_o(t)$ and $g_u(t)$. Our results for $f(t)=f_0=0.9$ and $\epsilon_a=0.1$ are as follows. For $\gamma \leq 0.06$ we have $\langle T_{\text{survival}} \rangle \geq 400$. That is, the control method is robust with respect to less than or equal to 6% of uncertainty. The effectiveness of control deteriorates rapidly as γ increases past 0.06. In particular, we find that $\langle T_{\text{survival}} \rangle \approx 100$ for $\gamma=0.07$, $\langle T_{\text{survival}} \rangle \approx 30$ for $\gamma=0.08$, $\langle T_{\text{survival}} \rangle \approx 20$ for $\gamma=0.1$, $\langle T_{\text{survival}} \rangle \approx 10$ for $\gamma=0.3$, and $\langle T_{\text{survival}} \rangle \approx 2$ for $\gamma=0.0$.

To conclude we remark that, although ship capsizing has been used here to illustrate the ideas of the control strategy, other situations are also candidates for the approach in this paper. In particular, our method is potentially important in applications where a momentary loss of control due to environmental irregularity can result in a catastrophic failure of the system.

This work was supported by the Department of Energy (Office of Scientific Computing, Office of Energy Research), and by the Office of Naval Research.

[1] L. N. Virgin, Appl. Ocean Res. **9**, 89 (1987).

[2] J. M. T. Thompson, R. C. Rainey, and M. S. Soliman, Philos. Trans. R. Soc. London Ser. A **332**, 149 (1990).

[3] A. H. Nayfeh and N. E. Sanchez, Int. Shipbuild. Prog. **37**, 331 (1990).

[4] E. Ott, C. Grebogi, and J. A. Yorke, Phys. Rev. Lett. **64**, 1196 (1990).

[5] T. Shinbrot, C. Grebogi, E. Ott, and J. A. Yorke, Nature **363**, 411 (1993).

[6] An algorithm for tracking and control of unstable periodic orbits is developed by I. Schwartz and I. Triandaf, Phys. Rev. A **46**, 7439 (1992); and implemented in a laser experiment by Z. Gills *et al.*, Phys. Rev. Lett. **64**, 3169 (1992); and in a circuit experiment by T. Carroll, I. Triandaf, I. Schwartz, and L. Pecora, Phys. Rev. A **46**, 6189 (1992).

PHYSICAL REVIEW E VOLUME 49, NUMBER 2 FEBRUARY 1994

Enhancing synchronism of chaotic systems

Mingzhou Ding
Center for Complex Systems and Department of Mathematics, Florida Atlantic University, Boca Raton, Florida 33431

Edward Ott
Institute for Plasma Research and Department of Physics and Department of Electrical Engineering, University of Maryland, College Park, Maryland 20742

(Received 20 August 1993)

Recent work has considered the situation where a state variable (or variables) of a chaotically evolving system is used as an input to a replica of part of the original system. It was found that the replica subsystem often synchronizes to the chaotic evolution of the original system, and it has been suggested that this phenomenon may be used for secure communications. In this paper we point out that exact synchronism may also occur for a large class of systems that are not replicas of part of the original system. This allows greater freedom in choosing synchronizer systems, and we discuss the possibility of using this freedom to choose synchronizer systems with improved performance. Two explicit examples illustrating this statement are given, one where the chaotic system consists of three autonomous differential equations, and the other where the chaotic system is a two-dimensional map.

PACS number(s): 05.45.+b

Recently, Pecora and Carroll [1] have studied the situation where a state variable (or variables) of a chaotic system is used as an input to drive a subsystem that is a replica of part of the original system. They find that the replica subsystem sometimes synchronizes to the chaotic evolution of the original system. The condition for this synchronism to occur depends on the original chaotic system and on the choice of the part of the original system that is used as the replica subsystem. A particularly intriguing aspect of chaos synchronism is its possible application to achieving secure communications (see, for example, [2] and references therein). We list other related works in [3].

Consider a chaotic system, $d\mathbf{Z}/dt=\mathbf{F}(\mathbf{Z})$, where $\mathbf{Z}$ is an m-dimensional vector. Divide the m state variables into two classes via

$$\mathbf{Z}=\begin{bmatrix}\mathbf{x}\\ \mathbf{y}\end{bmatrix},$$

where $\mathbf{x}$ is m_1 dimensional and $\mathbf{y}$ is m_2 dimensional, with $m_1+m_2=m$ (usually $m_1=1$ [1–3]). We refer to $\mathbf{x}$ as the input or drive. Writing the original dynamical system as

$$d\mathbf{x}/dt=\mathbf{G}(\mathbf{x},\mathbf{y}), \tag{1}$$

$$d\mathbf{y}/dt=\mathbf{H}(\mathbf{x},\mathbf{y}), \tag{2}$$

where

$$\mathbf{F}(\mathbf{Z})=\begin{bmatrix}\mathbf{G}(\mathbf{x},\mathbf{y})\\ \mathbf{H}(\mathbf{x},\mathbf{y})\end{bmatrix},$$

the driven replica subsystem is written as

$$d\hat{\mathbf{y}}/dt=\mathbf{H}(\mathbf{x},\hat{\mathbf{y}}). \tag{3}$$

Here we call $\hat{\mathbf{y}}$ the subsystem response, and, in what follows, we use a superscribed circumflex to denote a response variable. We say the subsystem (3) synchronizes to the chaotic evolution of (1) and (2), if

$$\lim_{t\to\infty}|\mathbf{y}(t)-\hat{\mathbf{y}}(t)|=0, \tag{4}$$

for typical $\mathbf{y}(0)\neq\hat{\mathbf{y}}(0)$.

In the context of communication we can imagine that the state variables in the drive vector $\mathbf{x}$ are transmitted from site A to site B. The full state $\mathbf{Z}$ of the system at A is unknown at B, because, although we know $\mathbf{x}(t)$, we do not know $\mathbf{y}(t)$. By feeding the known signal $\mathbf{x}(t)$ into a replica response subsystem (3) located at B, we can then obtain $\mathbf{y}(t)$, if the replica synchronizes with the original system [see (4)], and if we wait long enough for $\hat{\mathbf{y}}(t)$ to closely approach $\mathbf{y}(t)$.

The occurrence of this synchronism is conditioned on whether the largest subsystem Lyapunov exponent is negative [1]. Consider infinitesmal deviations of $\hat{\mathbf{y}}$ from $\mathbf{y}$, i.e.,

$$\hat{\mathbf{y}}(t)=\mathbf{y}(t)+\delta\hat{\mathbf{y}}(t).$$

From (3)

$$d\delta\hat{\mathbf{y}}/dt=\delta\hat{\mathbf{y}}\cdot\partial\mathbf{H}(\mathbf{x},\hat{\mathbf{y}})/\partial\hat{\mathbf{y}}|_{\hat{\mathbf{y}}=\mathbf{y}}, \tag{5}$$

where $\mathbf{x}(t)$ and $\mathbf{y}(t)$ are solutions of (1) and (2). The largest subsystem Lyapunov exponent, denoted $\hat{\Lambda}$, is then given by solving (5) using a typical orbit $(\mathbf{x}(t),\mathbf{y}(t))$ for the original system (1) and (2) and a typical choice for the orientation of $\delta\hat{\mathbf{y}}(0)$,

$$\hat{\Lambda}=\lim_{t\to\infty}\frac{1}{t}\ln\frac{|\delta\hat{\mathbf{y}}(t)|}{|\delta\hat{\mathbf{y}}(0)|}. \tag{6}$$

The point of this paper is that it may be advantageous to use a subsystem that is not a replica of part of the original system. In particular, we note that synchronism is also possible if, instead of the replica system (3), we utilize a nonreplica system of the form

$$d\hat{\mathbf{x}}/dt=\mathbf{K}(\mathbf{x},\hat{\mathbf{x}},\hat{\mathbf{y}}) , \tag{7}$$

$$d\hat{\mathbf{y}}/dt=\mathbf{L}(\mathbf{x},\hat{\mathbf{x}},\hat{\mathbf{y}}) , \tag{8}$$

provided that the functions **K** and **L** satisfy the conditions

$$\mathbf{K}(\mathbf{x},\mathbf{x},\mathbf{y})=\mathbf{G}(\mathbf{x},\mathbf{y}) , \tag{9}$$

$$\mathbf{L}(\mathbf{x},\mathbf{x},\mathbf{y})=\mathbf{H}(\mathbf{x},\mathbf{y}) . \tag{10}$$

We now view the vector,

$$\hat{\mathbf{Z}}(t)=\begin{bmatrix}\hat{\mathbf{x}}(t)\\ \hat{\mathbf{y}}(t)\end{bmatrix} ,$$

as the "response."

Synchronism, $\hat{\mathbf{Z}}(t)=\mathbf{Z}(t)$, then represents a possible solution of (7) and (8). Whether the synchronizing solution is stable depends on the largest Lyapunov exponent for the synchronizer system (7) and (8), which is obtained from

$$d\delta\hat{\mathbf{x}}/dt=\delta\hat{\mathbf{x}}\cdot\nabla_{\hat{\mathbf{x}}}\mathbf{K}(\mathbf{x},\hat{\mathbf{x}},\mathbf{y})|_{\hat{\mathbf{x}}=\mathbf{x}} +\delta\hat{\mathbf{y}}\cdot\nabla_{\hat{\mathbf{y}}}\mathbf{K}(\mathbf{x},\mathbf{x},\hat{\mathbf{y}})|_{\hat{\mathbf{y}}=\mathbf{y}} , \tag{11}$$

$$d\delta\hat{\mathbf{y}}/dt=\delta\hat{\mathbf{x}}\cdot\nabla_{\hat{\mathbf{x}}}\mathbf{L}(\mathbf{x},\hat{\mathbf{x}},\mathbf{y})|_{\hat{\mathbf{x}}=\mathbf{x}} +\delta\hat{\mathbf{y}}\cdot\nabla_{\hat{\mathbf{y}}}\mathbf{L}(\mathbf{x},\mathbf{x},\hat{\mathbf{y}})|_{\hat{\mathbf{y}}=\mathbf{y}} , \tag{12}$$

with $\delta\hat{\mathbf{y}}$ in (6) replaced by

$$\delta\hat{\mathbf{Z}}(t)=\begin{bmatrix}\delta\hat{\mathbf{x}}(t)\\ \delta\hat{\mathbf{y}}(t)\end{bmatrix} .$$

The idea is that there are an infinite number of functions **K** and **L** satisfying (9) and (10) for given **G** and **H**. Thus one is not necessarily constrained to the use of a replica (3) when choosing a system to achieve synchronism. This leads to considerably more flexibility in applications. [We imagine that the original chaotic system, (1) and (2), with the choice of the drive **x** is fixed by the given application.]

We speculate that this added flexibility may facilitate potential improvement in synchronism. Some such improvements might include the following: (1) achieving synchronism when a replica subsystem does not synchronize (i.e., $\hat{\Lambda}>0$ for the replica subsystem); (2) enabling faster convergence to the synchronized state; (3) eliminating or reducing the size of spurious subsystem basins of attraction in which the subsystem does not synchronize; and (4) improving the performance of signal recovery techniques for situations where the chaotic time series is used to mask a small information bearing signal [2].

In what follows we present two examples to illustrate points (1) and (2) for enhancing chaos synchronism mentioned above. The first example is a differential equation system (the Rössler equations) that we investigate numerically. The second example concerns a simple chaotic map that can be solved exactly.

Example 1. The Rössler system we treat in this example can be written as the following set of ordinary differential equations:

$$dx/dt=b+x(y_1-c)\equiv G(x,y_1,y_2) , \tag{13}$$

$$dy_1/dt=-x-y_2\equiv H_1(x,y_1,y_2) , \tag{14}$$

$$dy_2/dt=y_1+ay_2\equiv H_2(x,y_1,y_2) . \tag{15}$$

For $a=0.398$, $b=2$, and $c=4$ (also used in the subsequent calculations), the above system has a chaotic attractor.

Suppose that in a given application we are constrained to transmit only the x component of the above equation with the values a, b, and c as given above. The task is then to attempt obtaining synchronism using this x as a drive. Consider the replica subsystem,

$$d\hat{y}_1/dt=-x-\hat{y}_2 , \tag{16}$$

$$d\hat{y}_2/dt=\hat{y}_1+a\hat{y}_2 . \tag{17}$$

The largest subsystem Lyapunov exponent, assuming $a^2<4$, is

$$\hat{\Lambda}=a/2 . \tag{18}$$

For $a>0$, we have $\hat{\Lambda}>0$, and thus synchronism is not achieved for the parameter values chosen above. Figure 1 shows the times series $y_1(t)$ from the original system plotted together with $\hat{y}_1(t)$ of the response. As we can see, $\hat{y}_1(t)$ diverges from the synchronizing solution as time increases. Here we have chosen, in the numerical calculation, the initial condition for the replica subsystem to be slightly different from that of the original system.

Now we ask, with the same transmitted signal x as a drive, can we achieve synchronism by using a nonreplica response system,

$$d\hat{x}/dt=K(x,\hat{x},\hat{y}_1,\hat{y}_2) , \tag{19}$$

$$d\hat{y}_1/dt=L_1(x,\hat{x},\hat{y}_1,\hat{y}_2) , \tag{20}$$

$$d\hat{y}_2/dt=L_2(x,\hat{x},\hat{y}_1,\hat{y}_2) , \tag{21}$$

with K, L_1, and L_2 satisfying (9) and (10)? We explore this question numerically by taking, for simplicity,

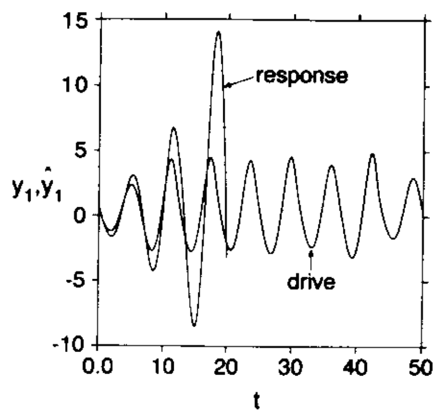

FIG. 1. Trajectories showing the replica subsystem response [(16),(17)] diverging from the solution of the original Rössler system [(13)–(15)].

$$K(x,\hat{x},\hat{y}_1,\hat{y}_2)=G(\hat{x},\hat{y}_1,\hat{y}_2)+\alpha(\hat{x}-x)\ ,$$

$$L_1(x,\hat{x},\hat{y}_1,\hat{y}_2)=H_1(\hat{x},\hat{y}_1,\hat{y}_2)+\beta(\hat{x}-x)\ ,$$

$$L_2(x,\hat{x},\hat{y}_1,\hat{y}_2)=H_2(\hat{x},\hat{y}_1,\hat{y}_2)+\gamma(\hat{x}-x)\ ,$$

which meet the conditions (9) and (10). [We remark that this choice of nonreplica systems, while sufficient for the purpose of this paper, is somewhat arbitrary. Other choices, such as those including terms depending on $\hat{y}_1$ and $\hat{y}_2$, and nonlinearly on $(\hat{x}-x)$, can be made in response to the particular need of the problems at hand.] The new response system is then

$$d\hat{x}/dt=b+x(\hat{y}_1-c)+\alpha(\hat{x}-x)\ , \tag{22}$$

$$d\hat{y}_1/dt=-x-\hat{y}_2+\beta(\hat{x}-x)\ , \tag{23}$$

$$d\hat{y}_2/dt=\hat{y}_1+a\hat{y}_2+\gamma(\hat{x}-x)\ . \tag{24}$$

Greater flexibility in achieving improved performance for this system is rendered by the freedom in choosing the values of the arbitrary parameters α, β, and γ.

Consider a line through the origin in the parameter space spanned by α, β, and γ

$$\alpha/\alpha_e=\beta/\beta_e=\gamma/\gamma_e\ . \tag{25}$$

Here we choose $\alpha_e=-3$, $\beta_e=1$, and $\gamma_e=-5$. In Fig. 2, we plot the numerically calculated largest Lyapunov exponent $\hat{\Lambda}$ for the response system (22), (23), and (24) as a function of β, with α and γ varying according to (25). The value of $\hat{\Lambda}$ generally decreases as β increases, and becomes negative for $\beta>0.27$, indicating the onset of synchronism. Figure 3 shows y_1 and $\hat{y}_1$ calculated using the same initial conditions as that in Fig. 1 but for $\beta=0.7$ ($\hat{\Lambda}=-0.25$). Thus we obtain synchronism using a nonreplica response system for a case where a replica response system does not synchronize.

As mentioned earlier, another possible advantage of using nonreplica response systems is to improve the convergence to the synchronized solution. To illustrate, we show, in Fig. 4, a case of slow convergence for $\beta=0.28$, which is just above the synchronism threshold. In this case, $\hat{\Lambda}=-0.006$, and the two solutions become essentially indistinguishable only for $t>200$. In contrast, as has been seen in Fig. 3, for a different choice of the response system, much faster convergence can be attained.

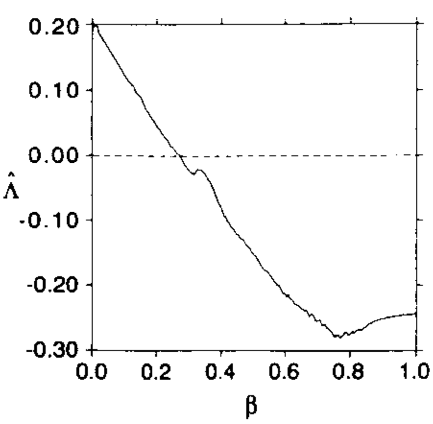

FIG. 2. Numerically evaluated largest Lyapunov exponent $\hat{\Lambda}$ as a function of β for the nonreplica response system (22)–(24).

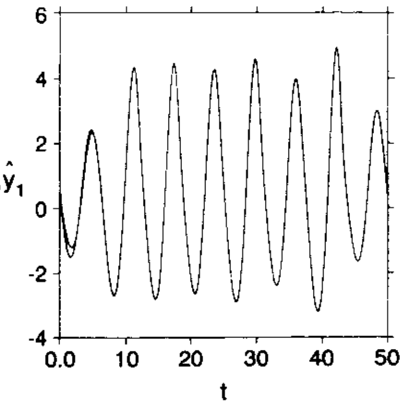

FIG. 3. Trajectories showing the rapid convergence of the nonreplica response system to the synchronizing solution for $\beta=0.7$. $\hat{\Lambda}=-0.25$. Initial conditions used here are the same as those in Fig. 1.

Example 2. In this example, we consider the following two-dimensional area-preserving map:

$$x_{n+1}=(x_n+y_n)\mathrm{mod}1\equiv G(x_n,y_n)\ , \tag{26}$$

$$y_{n+1}=[y_n+Ks(x_n+y_n)]\equiv H(x_n,y_n)\ , \tag{27}$$

where K is a parameter of the system and $s(x)$ is the sawtooth function defined as

$$s(x)\equiv(x\ \mathrm{mod}1)-\tfrac{1}{2}\ .$$

The Jacobian matrix of the system (26) and (27) is constant,

$$\mathbf{J}=\begin{bmatrix}\partial G/\partial x & \partial G/\partial y\\ \partial H/\partial x & \partial H/\partial y\end{bmatrix}=\begin{bmatrix}1 & 1\\ K & 1+K\end{bmatrix}\ . \tag{28}$$

The eigenvalues of this matrix are $[(2+K)$

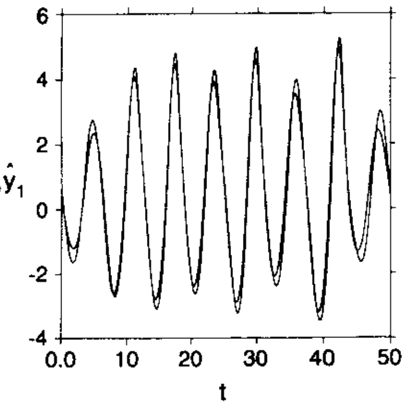

FIG. 4. Slow convergence to the synchronizing solution is encountered when the largest response Lyapunov exponent is negative but small in magnitude. $\beta=0.28$ and $\hat{\Lambda}=-0.006$. Again the same initial conditions as those in Figs. 1 and 3 are used here.

$\pm(4K+K^2)^{1/2}]/2$. If $(4K+K^2)<0$, then the eigenvalues are both complex and of magnitude 1 (no chaos). If $(4K+K^2)>0$, then the eigenvalues are both real, with one of magnitude less than 1 and one of magnitude greater than 1 (chaos). Thus the condition for chaos is $(4K+K^2)>0$, which applies if either

$$K>0 \; , \tag{29}$$

or

$$K<-4 \; . \tag{30}$$

Now let us consider attempting to obtain synchronism using x as the drive and the replica subsystem,

$$\hat{y}_{n+1}=H(x_n,\hat{y}_n) \; , \tag{31}$$

where $H(x,y)$ is given by (27). Since $\partial H/\partial y=1+K$, the replica subsystem Lyapunov exponent is

$$\hat{\Lambda}=\ln|1+K| \; , \tag{32}$$

which is negative only in the range

$$-2<K<0 \; . \tag{33}$$

Comparing (29) and (30) with (33), we see that these conditions are mutually exclusive. That is, where the system (26) and (27) is chaotic, the subsystem (31) does not synchronize.

We now consider whether, with the same drive x_n, synchronism can be obtained by using a nonreplica response system of the form

$$\hat{x}_{n+1}=K(x_n,\hat{x}_n,\hat{y}_n) \; , \tag{34}$$

$$\hat{y}_{n+1}=L(x_n,\hat{x}_n,\hat{y}_n) \; . \tag{35}$$

For this purpose, as in the previous example, we again choose K and L to deviate from G and H by terms linear in $(\hat{x}_n-x_n)$,

$$K(x,\hat{x},\hat{y})=G(x,\hat{y})+\alpha(\hat{x}_n-x_n) \; , \tag{36}$$

$$L(x,\hat{x},\hat{y})=H(x,\hat{y})+\beta(\hat{x}_n-x_n) \; . \tag{37}$$

With this choice the Jacobian matrix of the response system is again constant,

$$\hat{\mathbf{J}}=\begin{bmatrix}\alpha & 1\\ \beta & 1+K\end{bmatrix} \; . \tag{38}$$

The eigenvalues $\hat{\lambda}_1$ and $\hat{\lambda}_2$ of $\hat{\mathbf{J}}$ satisfy

$$\lambda^2-(1+K+\alpha)\hat{\lambda}+[\alpha(1+K)-\beta]=0 \; . \tag{39}$$

Writing (39) as $(\hat{\lambda}-\hat{\lambda}_1)(\hat{\lambda}-\hat{\lambda}_2)=\hat{\lambda}^2-(\hat{\lambda}_1+\hat{\lambda}_2)\hat{\lambda}+\hat{\lambda}_1\hat{\lambda}_2$, we see that $(1+K+\alpha)=\hat{\lambda}_1+\hat{\lambda}_2$ and $\alpha(1+K)-\beta=\hat{\lambda}_1\hat{\lambda}_2$, which can be solved for α and β,

$$\alpha=(\hat{\lambda}_1+\hat{\lambda}_2)-(1+K) \; , \tag{40}$$

$$\beta=[(\hat{\lambda}_1+\hat{\lambda}_2)-(1+K)](1+K)-\hat{\lambda}_1\hat{\lambda}_2 \; . \tag{41}$$

Thus any choice of the response system eigenvalues $\hat{\lambda}_1$ and $\hat{\lambda}_2$ can be realized by setting the values of α and β according to (40) and (41). In particular, we can consider a case where the original system is chaotic [i.e., either (29) or (30) applies], and choose values $|\hat{\lambda}_{1,2}|<1$ yielding synchronism. In contrast, the replica subsystem (31) never synchronizes when the original system is chaotic.

This work is supported by the Office of Naval Research and by the Department of Energy.

[1] L. M. Pecora and T. L. Carroll, Phys. Rev. Lett. **64**, 821 (1990); Phys. Rev. A **44**, 2374 (1991).

[2] K. M. Cuomo and A. V. Oppenheim, Phys. Rev. Lett. **71**, 65 (1993).

[3] H. G. Winful and L. Rahman, Phys. Rev. Lett. **65**, 1575 (1990); R. He and P. G. Vaidya, Phys. Rev. A **46**, 7387 (1992); U. Parlitz, L. Chua, Lj. Kocarev, K. Halle, and A. Shang, Int. J. Bif. Chaos **2**, 973 (1992); Lj. Kocarev, K. Halle, K. Eckert, L. Chua, and U. Parlitz, *ibid.* **2**, 709 (1992); M. de Sousa Vieira, A. J. Lichtenberg, and M. A. Lieberman, Phys. Rev. A **46**, R7359 (1992); M. de Sousa Vieira *et al.*, Int. J. Bif. Chaos **2**, 645 (1992); Y. C. Lai and C. Grebogi, Phys. Rev. E **47**, 2357 (1993).

Synchronizing Hyperchaos with a Scalar Transmitted Signal

J. H. Peng
Department of Physics, Northeast Normal University, Changchun 130024, China

E. J. Ding
CCAST (World Laboratory), P.O. Box 8730, Beijing 100080, China
Institute of Low Energy Nuclear Physics, Beijing Normal University, Beijing 100875, China

M. Ding* and W. Yang
Center for Complex Systems and Department of Mathematics, Florida Atlantic University, Boca Raton, Florida 33431
(Received 17 August 1995)

Recent work has considered the possibility of exploiting the phenomenon of chaos synchronization to achieve secure communication. But theoretical and experimental models studied thus far have been limited to low dimensional systems with one positive Lyapunov exponent. We investigate chaos synchronism in high dimensional systems. In particular, in regard to applications to communication, we show that by transmitting just one scalar signal one can achieve synchronism in chaotic systems with two or more positive Lyapunov exponents.

PACS numbers: 05.45.+b, 89.70.+c

Synchronization of chaotic systems has in recent years become an area of active research [1–7]. Different approaches are proposed and being pursued. Among them is the technique of Pecora and Carroll [2] who show that, when a state variable from a chaotically evolving system is transmitted as an input to a replica of part of the original system, the replica subsystem (receiver) sometimes synchronizes to the original system (sender). They suggest that this phenomenon of chaos synchronism may serve as the basis for new ways to achieve secure communication. Subsequent work enriches and substantiates the claim [3–6]. In a related paper [4] it is pointed out that the receiver subsystem does not need to be a replica of part of the sender system. In fact, allowing the use of nonreplica subsystems adds flexibility and enhances synchronism.

In this work we begin by noting that theoretical as well as experimental studies reported so far concern mainly low dimensional systems with one positive Lyapunov exponent. Perez and Cerdeira [7] show that messages masked by such simple chaotic processes, once intercepted, are sometimes readily extracted. Our objective is thus the implementation of the Pecora-Carroll paradigm of chaos synchronism in high dimensional chaotic systems which takes advantage of the increased randomness and unpredictability. In such systems one generally encounters multiple positive Lyapunov exponents (a situation called hyperchaos [8]). This feature improves security by giving rise to more complex time signals, but at the same time, it also raises the question of whether by transmitting just a single scalar variable, as would be desired in a communication situation, we can still achieve synchronization. Naively, one speculates that the number of variables to be transmitted should be equal to that of positive Lyapunov exponents in order to account for the same number of unstable directions along the chaotic trajectory. In this Letter, using two examples of hyperchaos, one a differential equation and the other a discrete map, we show that such intuition is incorrect, and in fact, chaos synchronism is attained over a broad range of parameters by using a transmitted signal that is expressed as a linear combination of the original phase space variables. We proceed to argue that this approach is general and does not depend on the systems investigated.

Problem formulation.—For specificity, we assume the sender to be a chaotic system in the form

$$d\mathbf{x}(t)/dt = \mathbf{F}(\mathbf{x}(t)), \qquad (1)$$

where $\mathbf{x} \in \mathbf{R}^m$ is an m-dimensional vector. In addition, we take the signal to be transmitted as a scalar variable in the form $u(t) = \mathbf{K}^T\mathbf{x}(t) = K_1x_1(t) + K_2x_2(t) + \cdots + K_mx_m(t)$, with $\mathbf{K}$ a constant column vector. Here T denotes matrix transpose. The receiver subsystem is then written as

$$d\mathbf{y}(t)/dt = \mathbf{F}(\mathbf{y}(t)) - \mathbf{B}(v(t) - u(t)), \qquad (2)$$

where $v(t) = \mathbf{K}^T\mathbf{y}(t)$ and $\mathbf{B} = (B_1, B_2, \ldots, B_m)^T$ is an m-dimensional constant vector.

Observe that if $\mathbf{y}(t) = \mathbf{x}(t)$ is plugged into Eq. (2), the equation is satisfied, meaning that synchronization of chaos is possible for the combined system, Eqs. (1) and (2). The question is whether this solution is attracting so that it can be realized in practice. To answer this question we evaluate the largest Lyapunov exponent for the subsystem Eq. (2) with respect to the trajectory $\mathbf{y}(t) = \mathbf{x}(t)$. Consider infinitesimal deviations of $\mathbf{y}(t)$ from $\mathbf{x}(t)$, i.e.,

$$\mathbf{y}(t) = \mathbf{x}(t) + \delta\mathbf{y}(t).$$

 0031-9007/96/76(6)/904(4)$06.00

From (2),

$$d\delta\mathbf{y}/dt = [\partial\mathbf{F}(\mathbf{y})/\partial\mathbf{y}|_{\mathbf{y}=\mathbf{x}} - \mathbf{B}\mathbf{K}^T]\delta\mathbf{y}. \qquad (3)$$

The largest subsystem Lyapunov exponents, denoted Λ, are then given by solving (3) using a typical orbit $\mathbf{x}(t)$ for the original system (1) and a typical orientation for $\delta\mathbf{y}(0)$,

$$\Lambda = \lim_{t\to\infty} \frac{1}{t} \ln \frac{|\delta\mathbf{y}(t)|}{|\delta\mathbf{y}(0)|}. \qquad (4)$$

When $\Lambda < 0$, for typical $\mathbf{y}(0) \neq \mathbf{x}(0)$,

$$\lim_{t\to\infty} |\mathbf{y}(t) - \mathbf{x}(t)| = 0. \qquad (5)$$

Namely, we observe the occurrence of synchronism.

We note that it is a common practice to transmit a signal that is a phase space variable of the original system. It is found that synchronism is often not attained when this is the case. The problem becomes more acute when the original chaotic system has two or more positive Lyapunov exponents. For such systems, even the use of a nonreplica receiver subsystem as proposed in [4], which has tunable parameters in the **B** vector, can become inadequate. In this regard, our approach outlined above represents an important step in methodology toward remedying the situation. In particular, Λ in Eq. (4) is now a function of the $2m$ parameters contained in both **K** and **B** vectors. This enlarged **K**-**B** space renders greater flexibility not only in designing the characteristics of the transmission but also in choosing the correct parameter combinations to meet the condition for and enhance the performance of synchronism. Specifically, our task is now reduced to that of locating a suitable region in the **K**-**B** space for which Λ is negative. In what follows we demonstrate how this is done and illustrate why it can be done using two examples, one a four variable Rössler equation exhibiting two positive Lyapunov exponents, and the other a coupled map lattice allowing as many positive Lyapunov exponents as the system size.

Example 1.—The hyperchaotic Rössler [8] system we treat here is written as

$$dx_1/dt = -x_2 - x_3, \qquad (6)$$

$$dx_2/dt = x_1 + 0.25x_2 + x_4, \qquad (7)$$

$$dx_3/dt = 3.0 + x_1x_3, \qquad (8)$$

$$dx_4/dt = -0.5x_3 + 0.05x_4. \qquad (9)$$

Numerical evidence indicates that the attractor has two positive Lyapunov exponents, $\lambda_1 = 0.11$ and $\lambda_2 = 0.02$. Choosing $\mathbf{K} = (\sin\theta, 0, \cos\theta, 0)^T$ and $\mathbf{B} = 5.0(\cos\theta, 0, \sin\theta, 0)^T$ somewhat arbitrarily, we plot the largest receiver subsystem Lyapunov exponent Λ

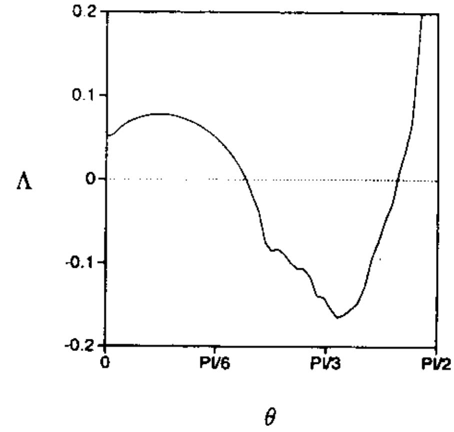

FIG. 1. The largest subsystem Lyapunov exponent Λ for the Rössler system Eqs. (6)–(9) plotted as a function of the parameter θ. It is seen that, over a substantial range of the θ value, Λ is negative, indicating synchronism between the sender and the receiver systems.

as a function of θ in Fig. 1. As can be seen, there is a range of θ values over which Λ is negative. In Fig. 2 we show the result of our synchronization experiment performed on the Rössler system by plotting the difference between x_1 and y_1 for $\theta = \pi/3$. Within the resolution of the figure we obtain chaos synchronism in about 60 time units. We remark that in this example, when a plain phase space variable (i.e., x_i, $i = 1, 2, 3, 4$) is sent as the input to the receiver subsystem, no synchronization is observed.

Clearly, for our approach to be successful we need to resolve the question concerning how to find regions in the **K**-**B** parameter space yielding negative Λ. We propose the following general method as a possible solution. First, for a given system, replace in Eq. (3) the vector **x** and its functions by their average values calculated on the

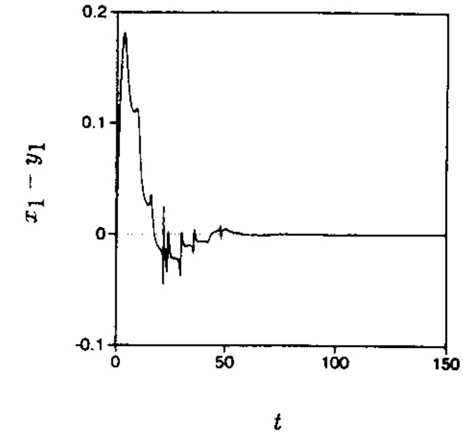

FIG. 2. Result from our numerical synchronization experiment using $\theta = \pi/3$ (see Fig. 1). The difference between the variable x_1 of the sender and the variable y_1 of the receiver asymptotes toward zero as time progresses.

original chaotic attractor. Now Eq. (3) becomes a linear equation of constant coefficients. Second, solve this linear equation and study how the eigenvalues change as the parameters B_i and K_i vary. This will give us a rough indication as to how to locate a favorable region to start our search. Third, beginning in a favorable region obtained above, integrate the full Eqs. (1) and (3), and gradually expand the parameter space exploration until finding a region where the value of Λ is negative. Our experience shows that, in general, the more positive Lyapunov exponents we have in the system, the smaller is such a region. Other ways of searching the parameter space tailored for specific systems are also attempted in our work, and they prove to be effective.

Example 2.—As stressed earlier, achieving synchronism with a scalar transmitted variable is a problem independent of the number of positive Lyapunov exponents involved. To further illustrate, we study a discrete coupled map lattice [9] that can be treated more analytically. In component form, the iteration equation analogous to Eq. (1) is

$$\begin{aligned} x_i(n+1) &= F_i(\mathbf{x}(n)) \\ &= (1 - \epsilon_{i,i-1} - \epsilon_{i,i+1}) f(x_i(n)) \\ &\quad + \epsilon_{i-1,i} f(x_{i-1}(n)) + \epsilon_{i+1,i} f(x_{i+1}(n)), \end{aligned} \tag{10}$$

where i labels the lattice site, n denotes the discrete time, $f(x)$ prescribes the local chaotic dynamics at each lattice site, and $\epsilon_{i,i+1}$ is the coupling strength from site i to site $i+1$, which is the same as that from site $i+1$ to site i, $\epsilon_{i+1,i}$, namely, $\epsilon_{i,i+1} = \epsilon_{i+1,i}$. Here we use nonuniform coupling to simulate a reaction-diffusion equation with space dependent diffusion rate. Let m be the size of the lattice and assume periodic boundary condition. The receiver equation analogous to (2) is

$$\begin{aligned} y_i(n+1) &= F_i(\mathbf{y}(n)) - B_i(v_n - u_n) = (1 - \epsilon_{i,i-1} - \epsilon_{i,i+1}) f(y_i(n)) + \epsilon_{i-1,i} f(y_{i-1}(n)) \\ &\quad + \epsilon_{i+1,i} f(y_{i+1}(n)) - B_i(v_n - u_n), \end{aligned} \tag{11}$$

where $u_n = \mathbf{K}^T \mathbf{x}(n) = K_1 x_1(n) + K_2 x_2(n) + \cdots + K_m x_m(n)$ is the transmitted scalar signal, and $v_n = \mathbf{K}^T \mathbf{y}(n) = K_1 y_1(n) + K_2 y_2(n) + \cdots + K_m y_m(n)$. The linearized equation determining the subsystem Lyapunov exponents is then

$$\delta\mathbf{y}(n+1) = [\partial\mathbf{F}(\mathbf{y})/\partial\mathbf{y}|_{\mathbf{y}=\mathbf{x}(n)} - \mathbf{B}\mathbf{K}^T]\delta\mathbf{y}(n). \tag{12}$$

To facilitate our analysis we restrict ourselves to the special case of $f(x) = 2x \bmod 1$ and $m = 3$. Let $\epsilon_{1,2} = \epsilon_{2,1} = \epsilon_1$, $\epsilon_{2,3} = \epsilon_{3,2} = \epsilon_2$ and $\epsilon_{3,1} = \epsilon_{1,3} = \epsilon_3$. Under these conditions Eq. (12) becomes

$$\delta\mathbf{y}(n+1) = (\mathbf{A} - \mathbf{B}\mathbf{K}^T)\delta\mathbf{y}(n), \tag{13}$$

where $\mathbf{A}$ is a constant matrix taking the explicit form,

$$\mathbf{A} = 2\begin{pmatrix} 1 - \epsilon_1 - \epsilon_3 & \epsilon_1 & \epsilon_3 \\ \epsilon_1 & 1 - \epsilon_1 - \epsilon_2 & \epsilon_2 \\ \epsilon_3 & \epsilon_2 & 1 - \epsilon_2 - \epsilon_3 \end{pmatrix}.$$

For computation, we further fix $\epsilon_1 = 0.1$, $\epsilon_2 = 0.05$, and $\epsilon_3 = 0.15$. With this choice of parameters, $\mathbf{A}$'s eigenvalues are calculated to be 2.0, 1.57, and 1.23. Thus the Lyapunov exponents for the original system are $\lambda_1 = 0.69$, $\lambda_2 = 0.45$, and $\lambda_3 = 0.21$, all being positive.

Now consider the problem of achieving synchronism between Eq. (10) and Eq. (11) in the presence of three positive Lyapunov exponents by transmitting a scalar u_n. To reduce the task of searching the parameter space, we somewhat arbitrarily let $\mathbf{B} = (1, 1.5, 0)^T$ and let $\mathbf{K} = r(4, -2, 3)^T$. In Fig. 3 we plot the value of the largest subsystem Lyapunov exponent Λ as a function of r. Clearly, in the region of $3.51 < r < 4.75$, Λ becomes negative.

This example can be put on a more general footing by recalling a result from control theory [10]. Consider the following discrete control system,

$$\mathbf{z}(n+1) = \mathbf{A}\mathbf{z}(n) + \mathbf{B}p(n), \tag{14}$$

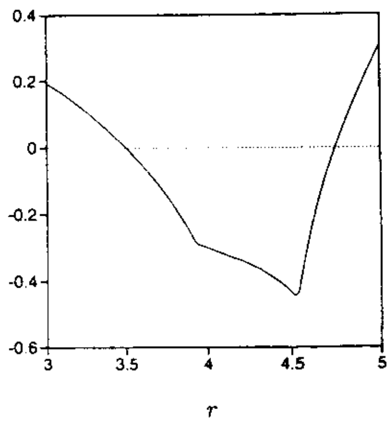

FIG. 3. The largest subsystem Lyapunov exponent Λ for the coupled map lattice Eq. (10) plotted as a function of the parameter r. Synchronism is achieved for r in the range $3.51 < r < 4.75$ over which Λ is negative.

where $\mathbf{z} \in \mathbf{R}^m$, $\mathbf{A}$ is an $m \times m$ constant matrix, $\mathbf{B}$ is a column vector, and $p(n)$ is a scalar control signal. Relating $p(n)$ to the current state of the system $\mathbf{z}(n)$ in a feedback fashion, $p(n) = -\mathbf{K}^T\mathbf{z}(n)$, Eq. (14) becomes

$$\mathbf{z}(n+1) = (\mathbf{A} - \mathbf{B}\mathbf{K}^T)\mathbf{z}(n), \tag{15}$$

which is in the same form as Eq. (13). The question for control theory is how to design a vector $\mathbf{K}$ such that $\mathbf{z} = \mathbf{0}$ becomes an attracting fixed point with any desired degree of stability. It can be shown [10] that, if the vectors $\mathbf{B}$, $\mathbf{AB}$, $\mathbf{A}^2\mathbf{B}, \ldots,$ and $\mathbf{A}^{m-1}\mathbf{B}$ are linearly independent, then for any given set of numbers $\mu_1, \mu_2, \ldots, \mu_m$ one can find a $\mathbf{K}$ so that the matrix $\mathbf{A} - \mathbf{B}\mathbf{K}^T$ has this set of numbers as its eigenvalues. An equivalent way to express the above condition is to construct a controllability matrix $\mathbf{C} = (\mathbf{B} \mid \mathbf{AB} \mid \mathbf{A}^2\mathbf{B} \mid \cdots \mid \mathbf{A}^{m-1}\mathbf{B})$ and require $\mathrm{Det}(\mathbf{C}) \neq 0$.

For the coupled map lattice, the example of $m = 3$ with the set of parameters chosen above the determinant of the controllability matrix has the value of 0.08. This conforms with the finding in Fig. 3, showing that the synchronizing solution can be made stable by selecting suitable values of K_i. It is interesting to note that, if the coupling in Eq. (10) is uniform, i.e., $\epsilon_1 = \epsilon_2 = \epsilon_3$, then the controllability matrix has a zero determinant regardless of how $\mathbf{B}$ is chosen. This means that one will not be able to use a scalar transmitted signal to synchronize the receiver subsystem. But we argue that this is a very rare case in terms of all possible dynamical systems in the form of Eq. (10). A slight deviation from the uniform coupling situation will typically restore the controllability condition and enable again chaos synchronism by a single transmitted scalar signal.

In summary, we have considered the implementation of the Pecora-Carroll synchronization paradigm in high dimensional chaotic systems with two or more positive Lyapunov exponents. In particular, pertaining to the application to communication, we have addressed the issue of whether chaos synchronism is achievable in such systems by transmitting a single scalar signal. We give an affirmative answer to the question by proposing the use of a transmitted signal that is a linear combination of the original phase space variables. This approach provides adjustable parameters in the relative weight of these variables, and proves to be effective when applied to two typical examples of hyperchaos, one a differential equation system and the other a coupled map lattice.

This work is supported by a grant from the Office of Naval Research. E. J. Ding's research is also supported by the Natural Science Foundation of China.

*To whom correspondence should be addressed.

[1] H. G. Winful and L. Rahman, Phys. Rev. Lett. **65**, 1575 (1990); T. Endo and L. O. Chua, Int. J. Bif. Chaos **1**, 701 (1991); V. S. Anishchenko *et al.*, *ibid.* **2**, 633 (1992); N. F. Rulkov *et al.*, *ibid.* **2**, 669 (1992); R. Roy and K. S. Thornburg, Jr., Phys. Rev. Lett. **72**, 2009 (1994); J. F. Heagy, T. L. Carroll, and L. M. Pecora, Phys. Rev. E **50**, 1874 (1994).

[2] L. M. Pecora and T. L. Carroll, Phys. Rev. Lett. **64**, 821 (1990); Phys. Rev. A **44**, 2374 (1991).

[3] R. He and P. G. Vaidya, Phys. Rev. A **46**, 7387 (1992); M. de Sousa Vieira, A. J. Lichtenberg, and M. A. Lieberman, *ibid.* **46**, R7359 (1992); K. Pyragas, Phys. Lett. A **181**, 203 (1992); Y. C. Lai and C. Grebogi, Phys. Rev. E **47**, 2357 (1993); T. C. Newell *et al.*, Phys. Rev. Lett. **72**, 1647 (1994); Phys. Rev. E **49**, 313 (1994); R. Brown, N. F. Rulkov, and N. B. Tufillaro, *ibid.* **50**, 4488 (1994); Lj. Kocarev and U. Parlitz, Phys. Rev. Lett. **74**, 5028 (1995); N. Gershenfeld and G. Grinstein, *ibid.* **74**, 5024 (1995).

[4] M. Ding and E. Ott, Phys. Rev. E **49**, R945 (1994).

[5] K. M. Cuomo and A. V. Oppenheim, Phys. Rev. Lett. **71**, 65 (1993); U. Parlitz *et al.*, Int. J. Bif. Chaos **4**, 973 (1992); Lj. Kocarev *et al.*, *ibid.* **2**, 709 (1992); K. M. Cuomo, A. V. Oppenheim, and S. H. Strogatz, IEEE Trans. Circuits Syst. **40**, 626 (1993).

[6] S. Hayes, C. Grebogi, and E. Ott, Phys. Rev. Lett. **70**, 3031 (1993); S. Hayes, C. Grebogi, E. Ott, and A. Mark, Phys. Rev. Lett. **73**, 1781 (1994).

[7] G. Perez and H. A. Cerdeira, Phys. Rev. Lett. **74**, 1970 (1995).

[8] O. E. Rössler, Phys. Lett. **71A**, 155 (1979).

[9] See K. Kaneko, Chaos **2**, 279 (1992), and other articles in this special focus issue on coupled map lattices.

[10] K. Ogata, *Control Engineering* (Prentice-Hall, Englewood Cliffs, NJ, 1990); for a formulation in terms of discrete dynamics, see, for example, F. J. Romeiras, C. Grebogi, E. Ott, and W. P. Dayawansa, Physica (Amsterdam) **58D**, 165 (1990).

PHYSICAL REVIEW E VOLUME 51, NUMBER 1 JANUARY 1995

Preserving chaos: Control strategies to preserve complex dynamics with potential relevance to biological disorders

Weiming Yang* and Mingzhou Ding

Program in Brain Sciences and Complex Systems, Center for Complex Systems and Department of Mathematics, Florida Atlantic University, Boca Raton, Florida 33431

Arnold J. Mandell

Laboratory for Constructive Mathematics and Department of Mathematics, Florida Atlantic University, Boca Raton, Florida 33431

Edward Ott

Institute for Plasma Research, Institute for Systems Research, and Departments of Physics and of Electrical Engineering, University of Maryland, College Park, Maryland 20742

(Received 24 June 1994)

This paper considers the situation in which an originally chaotic orbit would, in the absence of intervention, become periodic as a result of slow system drift through a bifurcation. In the biological context, such a bifurcation is often undesirable: there are many cases, occurring in a wide variety of different situations, where loss of complexity and the emergence of periodicity are associated with pathology (such situations have been called "dynamical disease"). Motivated by this, we investigate the possibility of using small control perturbations to preserve chaotic motion past the point where it would otherwise bifurcate to periodicity.

PACS number(s): 05.45.+b, 87.10.+e

I. INTRODUCTION

A. Preserving chaos

In this paper we study the following situation. There is a nonlinear system that behaves chaotically when a system parameter p is below some critical value, $p<p_c$. As p increases through p_c, there is a bifurcation in which the chaotic motion is replaced by periodic motion. The problem we address is whether, by using small controls, it is possible to keep the motion chaotic when $p>p_c$. As an example, consider the case of a d-dimensional map,

$$x_{n+1}=\tilde{F}(x_n,p,c_n)\ , \tag{1}$$

where x_n is the d-dimensional state of the system at time n, and c_n denotes the control variable. Roughly, we can think of the control as tuning some "knob" whose setting c_n is at our disposal.

For $c_n \equiv 0$, the map (1) bifurcates from chaos to periodicity as p increases through p_c. The question is how do we program the time dependence of c_n to ensure chaotic dynamics when $p>p_c$. We desire, in addition, that $|c_n|$ be small, and that the control only need to be applied infrequently (i.e., $c_n=0$ most of time).

Past work on controlling chaos has considered the situation where the motion is chaotic and one wishes to modify it to obtain improved system performance by stabilizing a chosen unstable periodic orbit embedded in the chaotic attractor [1,2]. In the present work, however, we regard the complex temporal behavior of the chaotic orbit as "good." Thus we wish to intervene in such a way as to keep it alive in situations where it would naturally be absent. The motivation for this is biological, and is discussed in the next subsection.

B. Biological motivation

It has been known since the 1940's that systems of nonlinear differential equations representative of self-excitatory biological processes, such as the heart beat and neuronal discharge, manifest parameter regions that generate chaotic orbits [3]. In the 1970s, the chaotic behavior of discrete maps also became relevant to biological systems such as population dynamics within ecological context in regimes of high fecundity and nutritional support [4]. Other work suggested that patterns of behavior in biological observables over time better represented some medical diseases than did characteristic structural and/or chemical abnormalities; that bifurcations between dynamical states could be associated with the onset and pathophysiology of a variety of disease states [5]. Since that time, one particularly counterintuitive (and somewhat controversial) theme of a number of studies carried out within the context of "dynamical diseases" is that in some biomedical systems, chaotic dynamical behavior is "normal." Bifurcations to periodic behavior (observed directly or reflected in decreased statistical measures of complexity) are viewed as a pathophysiological loss of the range of adaptive possibilities. The idea was that "getting stuck" can lead to disease states.

A diverse list of examples of emergent pathophysiolog-

*Permanent address: Institute of Theoretical Physics, Academia Sinica, Beijing 100080, China.

1063-651X/95/51(1)/102(9)/$06.00

ical periodicity (and/or decreasing measure indicative of dynamical complexity) in otherwise more irregular, normal time dynamics includes cell counts in hematological disorders [6], stimulant drug induced abnormalities in patterns in time of the behavior of brain enzymes, receptors, and animal explorations of space [7], cardiac interbeat interval patterns in a variety of cardiac disorders [8], the resting record in a variety of signal sensitive biological systems following desensitization [9], experimental epilepsy [10], hormone release patterns correlated with the spontaneous mutation of a neuroendocrine cell to a neoplastic tumor [11], the prediction of immunological rejection of heart transplants [12], the electroencephalographic behavior of the human brain in the presence of neurodegenerative disorders [13], neuroendocrine, cardiac, and electroencephalographic changes with aging [14], and imminent ventricular fibrillation in human subjects [15].

The above references are only a representative list, and it is possible to cite many more illustrating the general thesis that loss of chaos is often associated with disease [16]. Thus we can view the onset of a diseased state as being caused by a slow drift of the parameter p in Eq. (1) through the critical value p_c. As an example suggesting the utility of control in some of these situations we note the recent work [17] that has the goal of preventing epileptic seizures by time dependent stimuli applied to an appropriate region of the brain.

C. Loss regions and control strategy

The three most common bifurcations that can lead from chaotic motion directly to a low period attracting periodic orbit are [18] (1) crises [19], (2) type I intermittency [20], and (3) type III intermittency [20]. In all of the above three cases, for $p > p_c$, one can identify a loss region L, such that, after the orbit falls in L, it is rapidly drawn to the periodic orbit. Before falling in L the orbit motion can exhibit characteristic chaoticlike behavior; that is, it is a chaotic transient.

One strategy to ensure chaos for $p > p_c$ is to consider successive preiterates of L,

$$L_1 = \tilde{F}^{-1}(L,p,0) ,$$
$$L_2 = \tilde{F}^{-1}(L_1,p,0) = \tilde{F}^{-2}(L,p,0) ,$$
$$L_3 = \tilde{F}^{-1}(L_2,p,0) = \tilde{F}^{-3}(L,p,0) ,$$
$$\vdots$$
$$L_m = \tilde{F}^{-1}(L_{m-1},p,0) = \tilde{F}^{-m}(L,p,0) .$$

Thus L_m is the set of points that map to the loss region L in m iterates. Note that as m increases, the width of L_m in the unstable direction (or directions) has a general tendency to shrink exponentially. (There is always at least one unstable direction due to the existence of chaos.) This suggests the following approach. Pick some suitable value of m, which we denote M. Assume that the orbit initially starts outside the regions $L_{M+1} \cup L_M \cup \cdots \cup L_1 \cup L$. If the orbit lands in L_{M+1} on iterate n we apply our control c_n so as to kick the orbit out of L_M on the next iterate. Because L_M is thin, the required c_n can be small. By making M larger we typically make the required size of the control smaller. Thus there is a trade off involving the control size and the number of preiterates M. Consideration of this trade off becomes particularly important if noise is present or if the dynamical system F is not known with absolute precision. After the orbit is kicked out of L_M, it is expected that it will execute a chaotic orbit, until it again falls in L_{M+1}, at which time the small control is again activated, and so on. Thus we achieve the desired result that the control can be set to zero much of the time.

We call the above strategy A. There are also other strategies that can be usefully formulated. These, however, are less general and depend on the type of bifurcation involved (i.e., crisis, type I intermittency, or type III intermittency). We consider some of these other strategies and compare them to strategy A in the subsequent discussions dealing with the relevant bifurcations [21].

In Sec. II, we illustrate our control strategies using one-dimensional map examples exhibiting crisis, type I intermittency, and type III intermittency transitions from chaos to periodicity. Sec. III considers a two-dimensional map example, and Sec. IV focuses on the effect of noise.

We emphasize that, although our discussion is within the context of maps [Eq. (1)], the ideas are also relevant to continuous time dynamical systems (e.g., ordinary differential equations).

II. ONE-DIMENSIONAL MAP EXAMPLES

A. Crisis

We considered the situation shown in Fig. 1 for $c_n \equiv 0$. When $p < p_c$, there is a chaotic attractor in the region $0 \le x \le 1$, and a coexisting attracting periodic orbit of period one located at $x = x_p < 0$; see Fig. 1(a). As p increases through p_c the chaotic attractor is destroyed by a crisis [Fig. 1(b)], and almost all points with respect to the Lebesgue measure that are initialized in $0 \le x \le 1$ eventually go to the periodic attractor. We identify the loss region L as shown in Fig. 1(c). An orbit point in L maps one iterate later to the interval L_+, and one iterate after that to the region $x < 0$, after which it approaches the periodic orbit $x = x_p$ monotonically. Also shown in Fig. 1(c) is the set L_1 of points that map to L on one iterate. Each set L_m consists of 2^m intervals; thus, as shown in Fig. 1(c), the set L_1 consists of two intervals. As a numerical example, assume that the map applying for $x > 0$ is of the logistic form, and that the dependence of $\tilde{F}(x_n,p,c_n)$ on c_n is simply additive,

$$\tilde{F}(x_n,p,c_n) = F(x_n,p) + c_n = p x_n (1 - x_n) + c_n . \tag{2}$$

The critical value of p for Eq. (2) (with $c_n \equiv 0$) is $p_c = 4$. For $p > p_c$ the width of the loss region L is

$$w(L) = [(p - p_c)/p_c]^{1/2} (p_c/p)^{1/2} , \tag{3a}$$

and the width of L_+ is

$$w(L_+) = (p - p_c)/p_c . \tag{3b}$$

To apply strategy A the control c_n is programmed as follows. Suppose that at time n the orbital point x_n falls in one of the 2^{M+1} intervals of L_{M+1} and denote this interval $[x_l^{M+1}, x_r^{M+1}]$. Assume without loss of generality that $F(x_l^{M+1},p,0) < F(x_r^{M+1},p,0)$. We desire $x_{n+1} < F(x_l^{M+1},p,0)$ or $x_{n+1} > F(x_r^{M+1},p,0)$. To do so we choose c_n to be whichever of the following two values has the smaller magnitude,

$$c_n = \begin{cases} 1.1[px_l^{M+1}(1-x_l^{M+1}) - px_n(1-x_n)] , \\ 1.1[px_r^{M+1}(1-x_r^{M+1}) - px_n(1-x_n)] . \end{cases} \tag{4}$$

Figure 2 shows a plot of x_n versus n with strategy A control for the case of $p=4.1$ and $M=1$. Figure 3(a) shows c_n versus n for the same case. Over the time period shown in Fig. 3(a), the largest value of $|c_n|$ is $c_{\max}=0.029$, and the fraction of the time with $c_n \neq 0$ is 0.085. Increasing M to $M=5$, we obtain the plot c_n versus n in Fig. 3(b). By increasing M the largest value of $|c_n|$ is reduced to $c_{\max}=0.0017$ in Fig. 3(b).

We now consider a very simple alternate strategy that works particularly well when p is only slightly bigger than p_c. We note from Eqs. (3) that when p is close to p_c, $w(L_+)$ is smaller than $w(L)$ by the factor $[(p-p_c)/p_c]^{1/2}$. Thus it is easier to kick the orbit out of L_+ than L. Strategy A reduces the kick by making M large enough. Instead, in our alternative strategy we wait until the orbit falls in L, and then apply a c_n so that we kick the orbit from L_+ into the region $x<1$. This can be accomplished, for example, by setting

$$c_n = -(p-p_c)/p_c \tag{5}$$

whenever the orbit falls in L. This has the effect of changing the map from the form shown in Fig. 1(c) to that shown in Fig. 4. Using the same value of p as in Fig. 3(a) and 3(b), the alternate strategy yields the plot of c_n versus n in Fig. 3(c). Note that $c_{\max}$ for strategy A with $M=1$ [Fig. 3(a)] is larger than the value given by Eq. (5) [$c_{\max}=0.029$, as compared to $(p-p_c)/p_c=0.025$], while, when M is increased to $M=5$ [Fig. 3(b)], strategy A yields a much lower value.

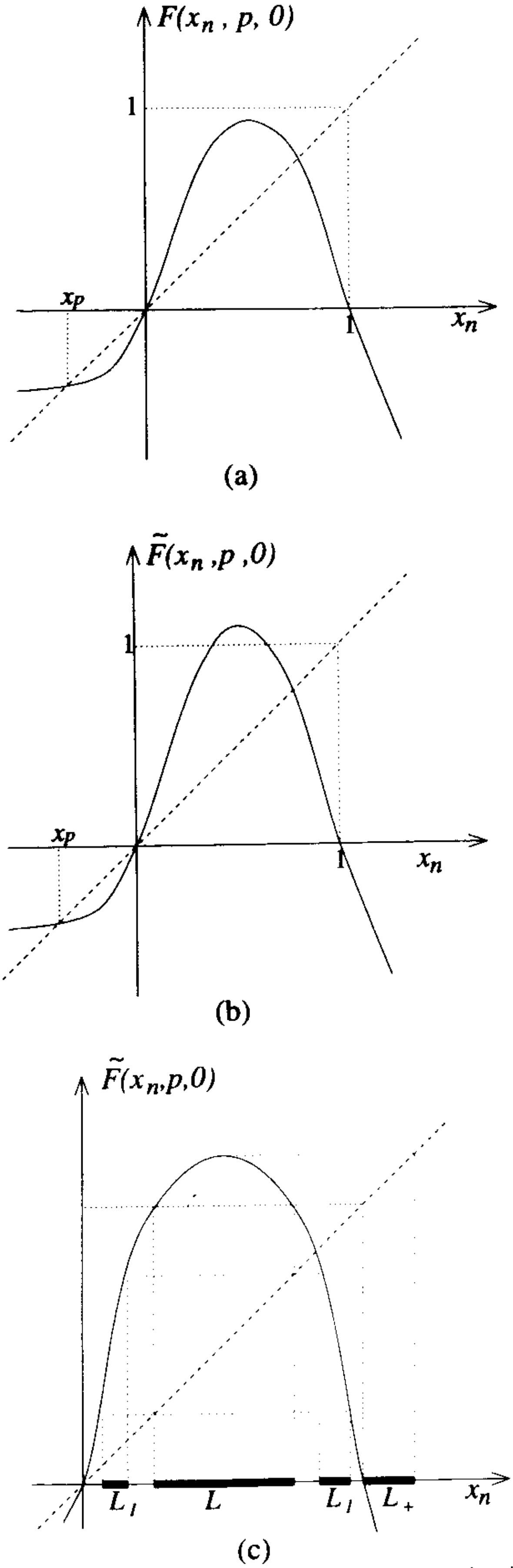

FIG. 1. Illustration of a crisis transition from a chaotic attractor to periodic motion ($x=x_p$).

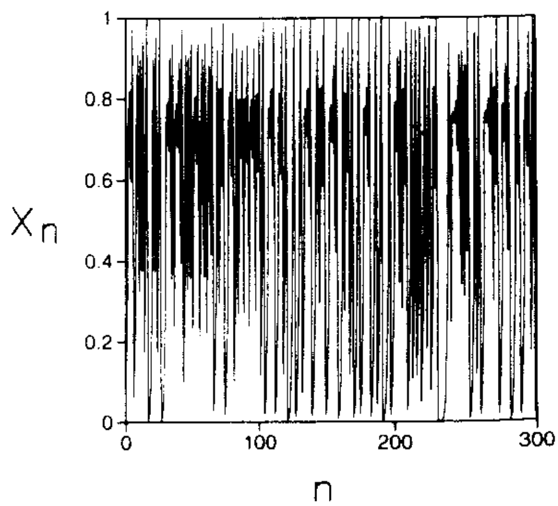

FIG. 2. x_n versus n with control for $M=1$ and $p=4.1>p_c=4$.

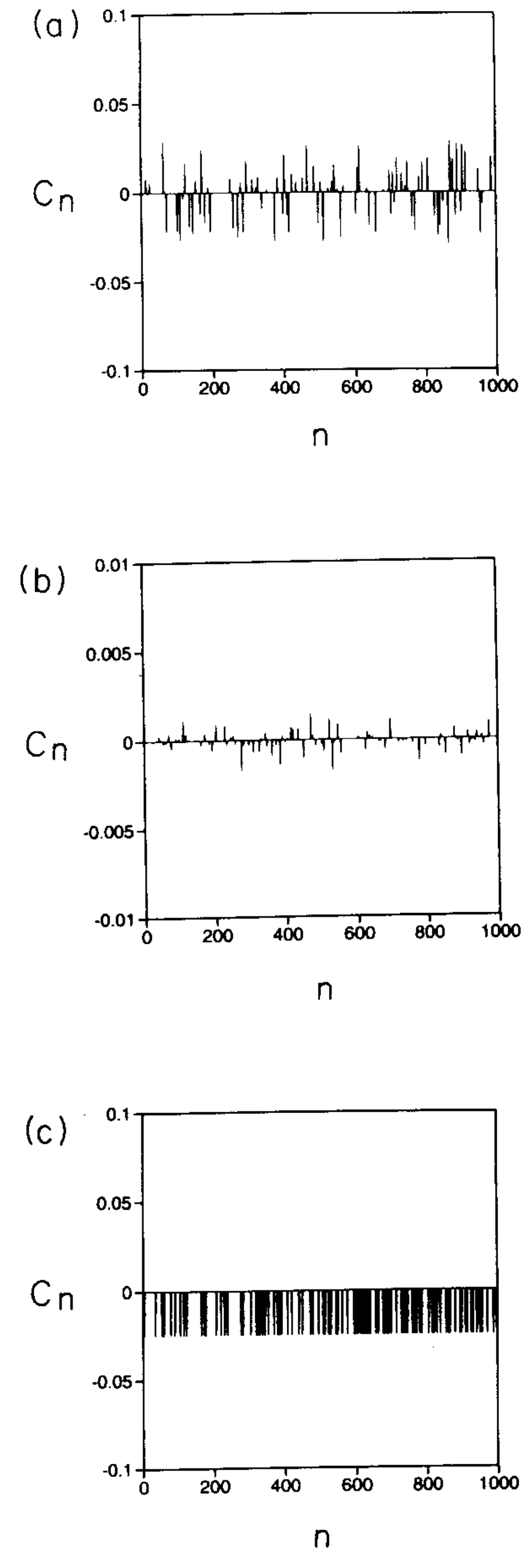

FIG. 3. c_n versus n for $p=4.1$. (a) Strategy A with $M=1$, (b) strategy A with $M=5$, and (c) the alternate strategy.

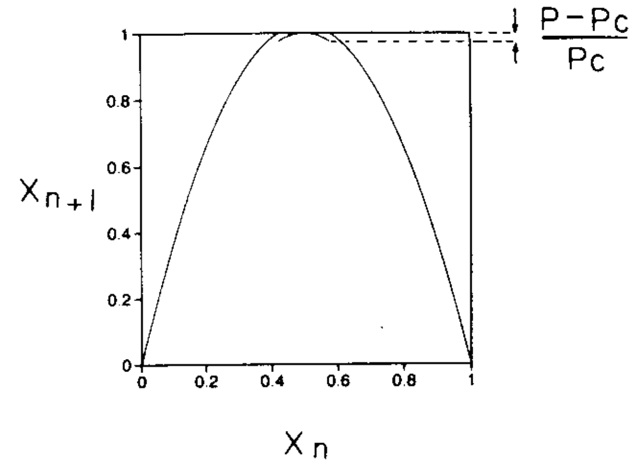

FIG. 4. Effective one-dimensional map associated with the alternate control strategy given by (4) whenever x_n is in L.

B. Type I intermittency

The example we considered is

$$\tilde{F}(x_n,p,c_n)=F(x_n,p)+c_n$$
$$=4px_n(1-x_n)[1-px_n(1-x_n)]+c_n \ . \tag{6}$$

Figure 5(a) shows a plot of $F(x_n,p)$ versus x_n for $p=3.350<p_c=3.375$. In this case there is a chaotic attractor located in $0\le x\le 1$. As p increases through p_c, a tangent bifurcation occurs creating a stable attracting period one orbit $x=x_A$ and a repelling period one orbit $x=x_R$ (see Fig. 6). Figure 5(b) shows a plot of $F(x_n,p)$ versus x_n for $p=3.4>p_c$. (The points x_A and x_R are the new intersections of the diagonal dashed line with F.) A bifurcation diagram for this map is shown in Fig. 7.

Figure 6 shows a schematic identifying the loss region L for this case. Here L is the interval $(1-x_R)<x<x_R$ [$(1-x_R)$ is a preiterate of x_R]. Note that, near the bifurcation (i.e., when $p-p_c>0$ is small), x_A is close to x_R; $x_A=x_R$ at $p=p_c$.

Figure 8(a) shows the orbit x_n versus n for a case without control for $p=3.5>p_c$. Figure 8(b) shows the orbit from the same initial condition as Fig. 8(a) using strategy A control with $M=2$, and Fig. 8(c) shows the resulting c_n versus n. The fraction of the time that the control is activated is 0.08, and the largest $|c_n|$ over the time interval plotted is $c_{\max}=0.01$.

Unlike the crisis case, for type I intermittency the width of L does not approach zero as $p-p_c\to 0^+$. Rather, L appears immediately at $p=p_c$ with nonzero width. On the other hand, for small $p-p_c>0$, the distance (x_R-x_A) is small, namely, $(x_R-x_A)\sim O(\sqrt{p-p_c})$. This motivates the following alternate strategy applicable for p close to p_c. This alternate strategy utilizes a control of order $\sqrt{p-p_c}$ and hence is small if p is close to p_c. If x_n first enters L in the region $x_A<x<x_R$, we apply a positive kick c_n to place x_{n+1} in the region $x>x_R$. Once in this region the orbit is repelled from x_R, moves to the right, and executes a chaotic transient orbit, until it again

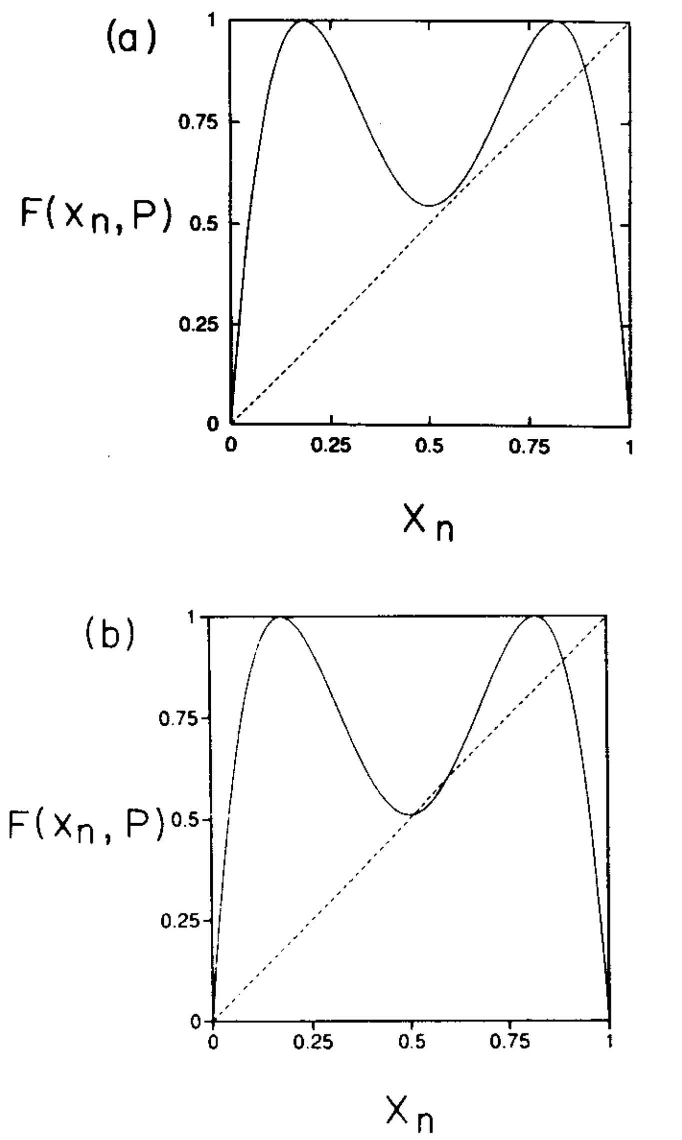

FIG. 5. $F(x_n,p)$ versus x_n for (a) $p=3.35<p_c=3.375$ and (b) $p=3.40>p_c$.

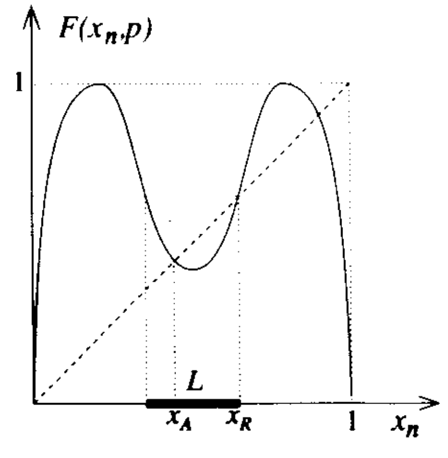

FIG. 6. Schematic identifying the loss region L.

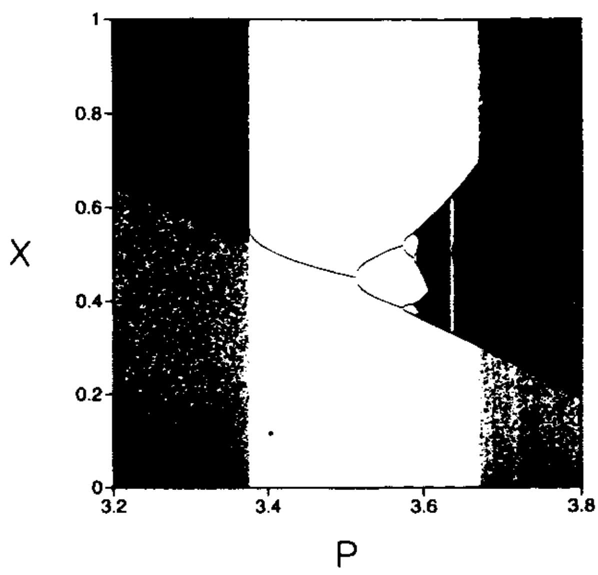

FIG. 7. Bifurcation diagram for $F(x_n,p)$. Note the intermittent transition at $p=p_c=3.375$.

enters L. If x_n first enters L in the region $x<x_A$ with x relatively far from x_A [i.e., $(x_A-x)>O(\sqrt{p-p_c})$], we can wait until it either lands in $x_A<x<x_R$ or else approaches sufficiently close to x_A with $x\leq x_A$. In either case, a kick of order $\sqrt{p-p_c}$ will be capable of placing a next iterate in $x>x_R$.

C. Type III intermittency

We consider the map

$$\tilde{F}(x_n,p,c_n)=F(x_n,p)+c_n$$
$$=x_n[p(12.5-7p)x_n^4-p(11.5-7p)x_n^2+x_n^2-1]+c_n\ . \tag{7}$$

The map $F(x_n,p)$ has a period one orbit at $x=0$. As p increases through $p_c=1$, this period one orbit becomes unstable, experiencing an inverse period doubling bifurcation. The map yields a chaotic attractor for $p>p_c$. (Note that the role of parameter increase here is opposite to the convention used in the previous discussion.) Figures 9(a) and 9(b) show plots of the map $F(x_n,p)$ for $p=1.2>p_c$ (chaotic attractor) and for $p=0.8<p_c$ ($x=0$ being the periodic attractor). We indicate that loss region in Fig. 9(b) as the interval bounded by the two components of the unstable period two orbit created at the bifurcation. For small $(p_c-p)>0$ the width of L scales as $w(L)\sim O(\sqrt{p_c-p}\ )$. (This is similar to the crisis case.) Once an orbit enters L its distance to the period one attractor at $x=0$ decreases monotonically as the orbit flips alternatively from $x>0$ to $x<0$. Also indicated in Fig. 9(b) are the intervals comprising L_1.

Figure 10(a) shows the orbit x_n versus n for a case without control for $p=0.9<p_c$. Figure 10(b) shows the

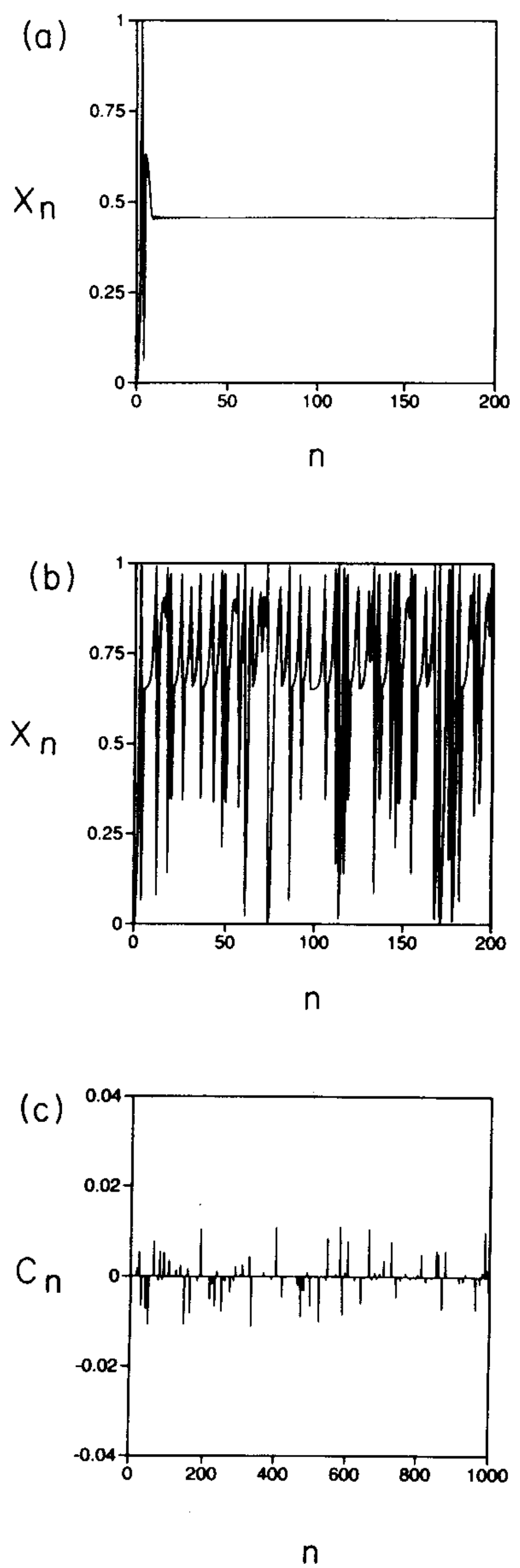

FIG 8. (a) x_n versus n without control for $p=3.5>p_c$. (b) x_n versus n with control and $M=2$ for $p=3.5>p_c$. (c) c_n versus n for the conditions of (b).

orbit from the same initial condition as Fig. 10(a) using strategy A control with $M=2$. Figure 10(c) shows the resulting c_n versus n. The fraction of time the control is activated is 0.03, and the largest $|c_n|$ over the time interval of the plot is $c_{\max}=0.016$.

III. TWO-DIMENSIONAL MAP EXAMPLE

Strategy A can also be applied without the explicit construction of all the L_m. This is particularly useful in the case of two-dimensional maps. Consider the crisis situation schematically illustrated in Figs. 11. For $p<p_c$ there is an chaotic attractor [Fig. 11(a)]. The point A is an unstable saddle on the basin boundary which is the closure of the stable manifold of A. As p increases

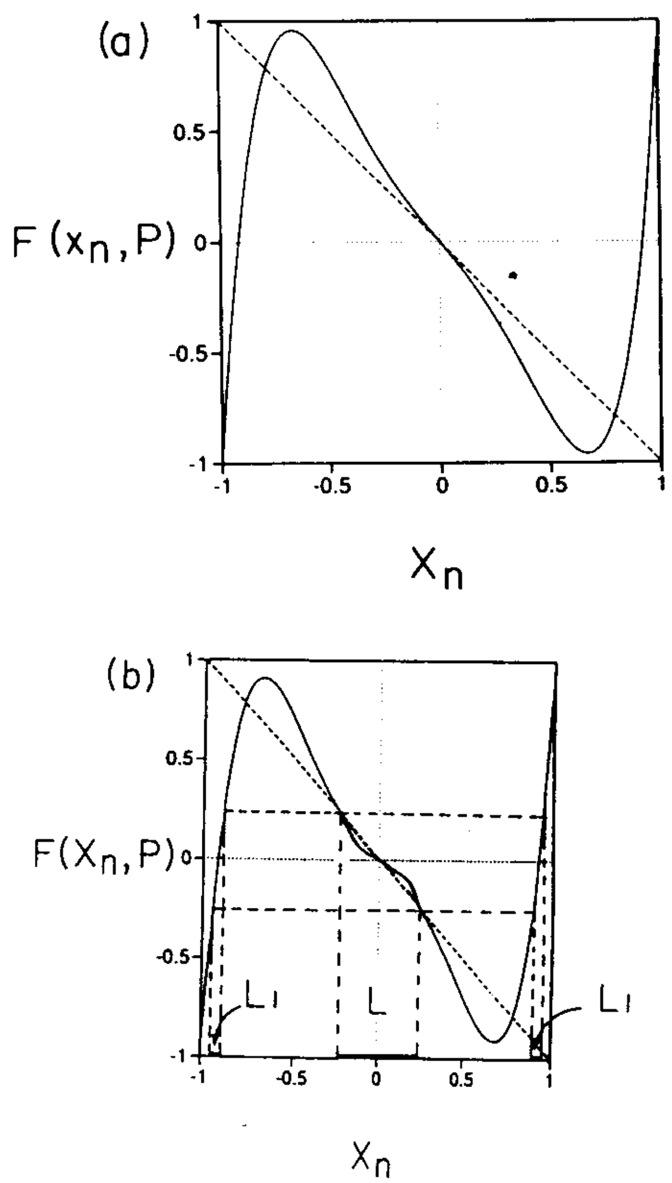

FIG. 9. $F(x_n,p)$ versus x_n for (a) $p=1.2>p_c=1.0$ and (b) $p=0.8<p_c$ (the curvature near the origin is exaggerated for clarity).

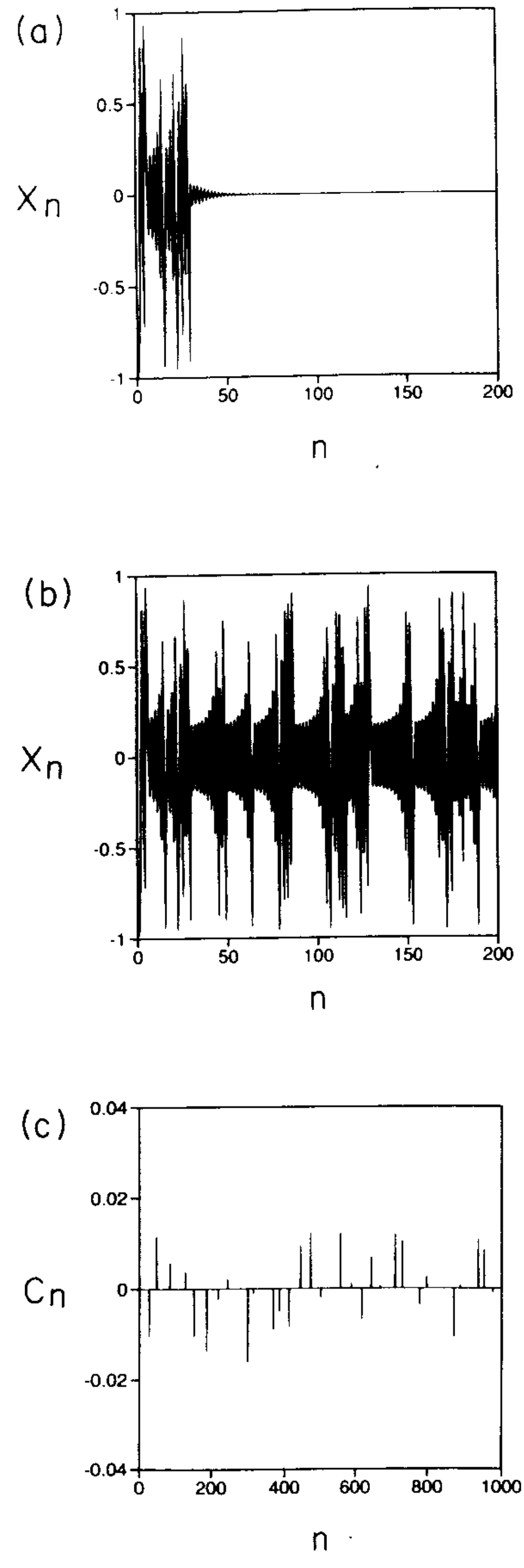

FIG. 10. Results of $p=0.9<p_c$. (a) x_n versus n without control. (b) x_n versus n with strategy A control and $M=2$. (c) c_n versus n.

through p_c, the attractor is destroyed by colliding with the basin boundary, resulting in a situation shown in Fig. 11(b) [22]. We assume that after a chaotic transient almost all points go to a periodic attractor located elsewhere in the phase space. We call the shaded region in Fig. 11(b) L_+ according to the terminology in Sec. II A. Imagine a point x in the former basin of attraction, and examine the $(M+2)$th iterate of x. If this $(M+2)$th iterate falls in L_+, then we say x is in L_{M+1} and apply a kick c_n to the system so that the next iterate of x falls outside of L_M. [By this we mean that the $(M+1)$th iterate of the kicked point without further perturbation falls outside of L_+.] After this we set $c_n=0$ and wait until the procedure needs to be repeated again.

In practice, the above steps can be further simplified. Specifically, we can replace the segment of the stable manifold near the shaded area in Fig. 11(b) by a straight line such that L_+ is to its right. Instead of considering the point falling into the shaded region we can just test whether it is on the right side of this straight line.

Now we use the Hénon map

$$x_{n+1}=p-x_n^2+0.3y_n+c_n\ ,$$

$$y_{n+1}=x_n\ ,$$

as our numerical example to illustrate these ideas. Here $p_c\approx 1.42$ and the straight line mentioned above is chosen to be $10x-y=20$ for $p=2.0$. The value of c_n picked has

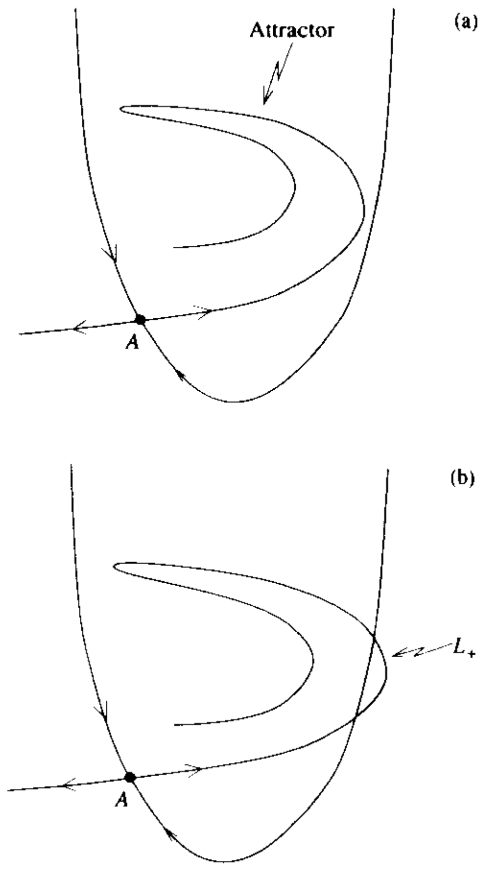

FIG. 11. Schematic of a two-dimensional crisis transition. (a) $p<p_c$ and (b) $p>p_c$.

the smallest amplitude such that the orbit is still kicked out of L_M with $M=5$. Figure 12(a) shows a plot of x_n versus n with strategy A control. A rough sketch of the chaotic saddle can be obtained by plotting (x_n, y_n) [Fig. 12(b)]. For the same case, c_n versus n is displayed in Fig. 12(c). The largest value of $|c_n|$ is $c_{max}=0.034$, and the fraction of time with $c_n \neq 0$ is 0.14.

A simple alternate strategy that can be employed here is to choose $c_n \equiv p_c - p \approx 0.6$ which permanently eliminates the situation in Fig. 11(b). The price one pays here is a much larger control that is on 100% of the time.

IV. EFFECT OF NOISE

The effect of noise is illustrated below for the crisis transition in one-dimensional maps (see Sec. II A). For simplicity we treat uniformly distributed finite amplitude noise whose impact on the map is additive. Namely, we consider

$$x_{n+1} = F_\delta(x_n, p, 0) = p x_n (1 - x_n) + \delta_n + c_n , \tag{8}$$

where $|\delta_n| < \Delta$. In contrast to the situation of Sec. II A, an orbit point, with the presence of noise, can enter L_i

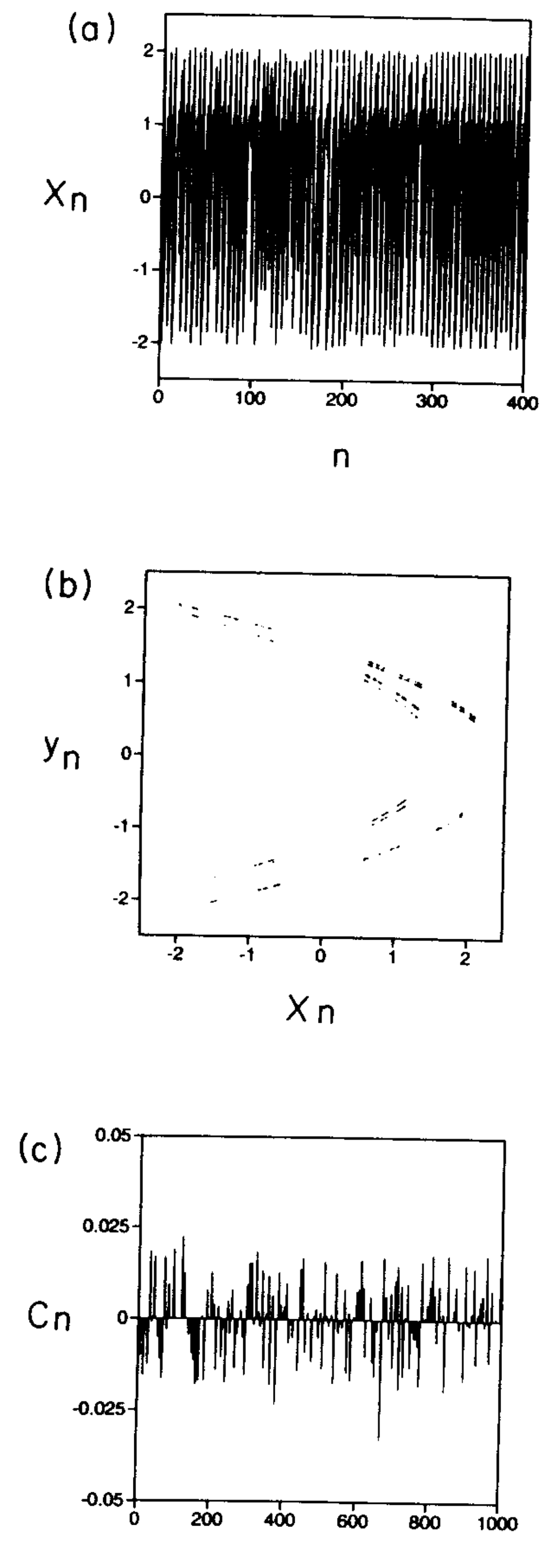

FIG. 12. Results for the Hénon map with $p=2.0$. (a) x_n versus n with control and $M=5$. (b) Sketch of the chaotic saddle with (x_n, y_n). (c) c_n versus n.

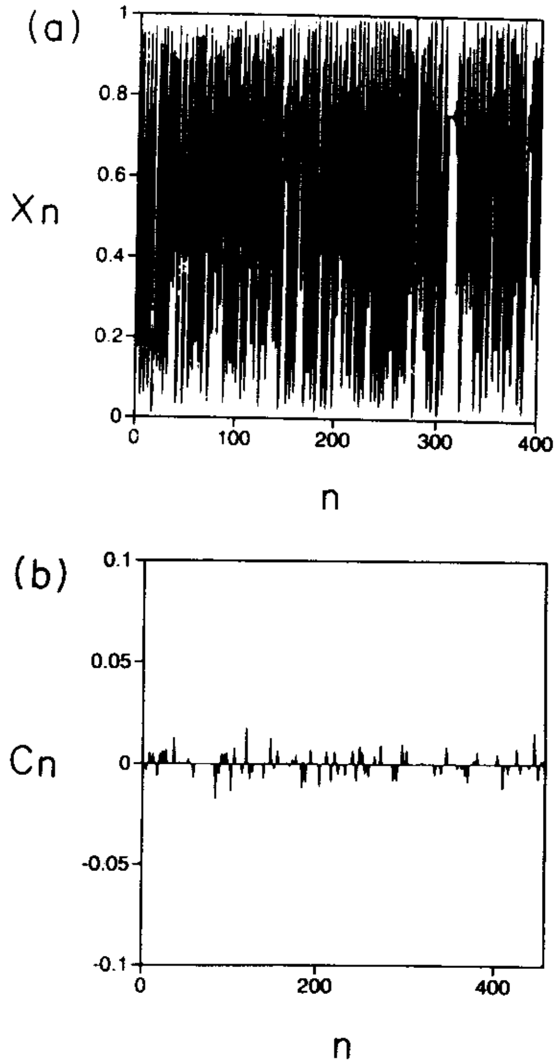

FIG. 13. Results for the noisy logistic map. (a) x_n versus n for $p=4.1$ and $M=2$ and (b) c_n versus n.

without first going through L_j, where $i<j$. To counter this, we first augment every interval in the original L_{m-1} by the amount of Δ on both sides and define the inverse image under F^{-1} of the new set of intervals to be L'_m. Similar to Eq. (4) we choose c_n so that x_{n+1} falls outside of $L'_M \cup L'_{M-1} \cup \cdots \cup L'_1 \cup L'$. Figure 13(a) shows x_n versus n with control for $p=4.1$, $\Delta=0.002$, and $M=2$, and Fig. 13(b) shows c_n versus n. The largest value of $|c_n|$ is $c_{\max}=0.018$ and the fraction of time with $c_n \neq 0$ is 0.1.

Note that, in the noisy case, M cannot be set too large because otherwise intervals in $L'_M \cup L'_{M-1} \cup \cdots \cup L'_1 \cup L'$ will begin to have overlap. This situation becomes more severe as Δ increases. In fact, for $\Delta=0.02$, we find that the simple alternate strategy in Sec. II A with noise modification works more effectively than strategy A. Specifically, if we set

$$c_n = -(p-p_c)/p_c - \Delta$$

whenever the orbit falls in L', the orbit can be controlled with $c_{\max}=0.045$, and the fraction of time with $c_n \neq 0$ is 0.13. On the other hand, if strategy A is implemented for the same conditions, one obtains $c_{\max}=0.063$ with the fraction of time where $c_n \neq 0$ to be 0.5.

V. DISCUSSION

In this paper we have dealt with low-dimensional chaotic systems. The evident biological chaos discussed in Sec. I B above may or may not be low dimensional, and this may also depend on the biological setting. At present, there is controversy as to whether low-dimensional chaos is relevant in biology [23]. Recent evidence suggests low dimensionality in some cases [16,17]. Whether or not the considerations in this paper prove relevant in biology awaits further investigation.

ACKNOWLEDGMENTS

This work was supported by the Office of Naval Research.

[1] E. Ott, C. Grebogi, and J. A. Yorke, Phys. Rev. Lett. **64**, 1196 (1990).

[2] For a review and other references see, T. Shinbrot, C. Grebogi, E. Ott, and J. A. Yorke, Nature **363**, 411 (1993).

[3] M. L. Cartwright and J. W. Littlewood, J. London Math. Soc. **20**, 180 (1945); N. Levinson, Ann. Math. **50**, 127 (1949).

[4] R. M. May, Nature **261**, 459 (1976).

[5] M. C. Mackey and L. Glass, Science **197**, 287 (1977); L. Glass and M. C. Mackey, Ann. N.Y. Acad. Sci. **316**, 214 (1979); A. J. Mandell, Am. J. Physiol. **245**; 14:R484 (1983); M. C. Mackey and J. G. Milton, Ann. N.Y. Acad. Sci. **504**, 16 (1987).

[6] M. C. Mackey, in *Biophysical and Biochemical Information Transfer in Recognition*, edited by J. G. Vassileva-Popova and E. V. Jensen (Plenum, New York, 1979).

[7] A. J. Mandell, K. D. Stewart, and P. V. Russo, Fed. Proc. **40**, 2693 (1981).

[8] A. L. Goldberger, L. J. Findley, M. R. Blackburn, and A. J. Mandell, Am. Heart. J. **107**, 612 (1984); A. L. Goldberger, V. Bhargava, B. J. West, and A. J. Mandell, Physica D **19**, 282 (1986); A. J. Mandell, *ibid.* **27**, 235 (1987); A. L. Goldberger and B. J. West, Ann. N.Y. Acad. Sci. **504**, 195 (1987); A. L. Goldberger, D. R. Rigney, J. Mietus, E. M. Antman, and S. Greenwald, Experientia **44**, 983 (1989); C. K. Peng, J. Mietus, J. M. Hausdorff, S. Havlin, H. E. Stanley, and A. L. Goldberger, Phys. Rev. Lett. **70**, 1343 (1992).

[9] A. J. Mandell, Math. Modeling 7, 809 (1986).

[10] J. Z. Tepper and A. J. Mandell, Ann. N.Y. Acad. Sci. **504**, 88 (1987).

[11] R. C. Guillimin, P. Brazeau, A. Briskin, and A. J. Mandell, in *Synergetics of the Brain*, edited by E. Baser, H. Flohr, H. Haken, and A. J. Mandell (Springer-Verlag, Berlin, 1983); A. J. Mandell, in *Fractals in Physics*, edited by L. Pietronero and E. Tosatti (North-Holland, Amsterdam, 1986).

[12] J. P. Zbilut, G. Mayer-Kress, and K. Geist, Math. Biosci. **90**, 49 (1988).

[13] A. Babloyantz, J. M. Salazar, and C. Nicolis, Phys. Lett. **A111**, 152 (1985); A. Babloyantz and A. Dextexhe, in *From Chemical to Biological Organization*, edited by M. Markus, S. Muller, and G. Nicolis (Springer-Verlag, Berlin, 1988).

[14] A. J. Mandell and M. F. Shlesinger, in *The Ubiquity of Chaos*, edited by S. Krasner (AAAS Press, Washington, D.C., 1990); L. A. Lipsitz and A. L. Goldberger, J. Am. Med. Assoc. **267**, 1806 (1992).

[15] J. E. Skinner, C. M. Pratt, and T. Vybiral, Am. Heart. J. **125**, 731 (1993).

[16] There are also biological situations where periodicity rather than chaos is desired (the opposite to the situation considered here). Thus a recent paper has experimentally investigated the use of chaos control (of the type discussed in Ref. 1 and 2) to achieve periodicity in arrhythmically beating cardiac tissue. The motivation was to suggest the possibility of a "smart" heart pacemaker. [A. Garfinkel, M. Spano, W. L. Ditto, and G. N. Weiss, Science **257**, 1230 (1992).]

[17] S. J. Schiff *et al.*, Nature **370**, 615 (1994).

[18] See, for example, E. Ott, *Chaos in Dynamical Systems* (Cambridge University Press, Cambridge, 1993), Chap. 8.

[19] C. Grebogi, E. Ott, and J. A. Yorke, Phys. Rev. Lett. **48**, 1507 (1982); Physica D 7, 181 (1983); Phys. Rev. Lett. **57**, 1284 (1986).

[20] Y. Pomeau and P. Manneville, Comm. Math. Phys. **74**, 189 (1980). Our considerations of loss regions also apply to type II intermittency, but we do not specifically discuss this case since it involves a transition from chaos to a steady state (via a Hopf bifurcation) rather than a transition to a periodic orbit.

[21] To stabilize motion on a nonattracting chaotic set, Y.-C. Lai and C. Grebogi proposed an alternative but more elaborate control technique in Phys. Rev. E **49**, 1094 (1994).

[22] Crisis scenarios other than the one depicted here also occur. See [19]. The control method we describe is independent of the scenario.

[23] D. Ruelle, Phys. Today, **46** (7), 24 (1994) and references therein.

Trajectory (Phase) Selection in Multistable Systems: Stochastic Resonance, Signal Bias, and the Effect of Signal Phase

Weiming Yang and Mingzhou Ding
Center for Complex Systems and Department of Mathematics, Florida Atlantic University, Boca Raton, Florida 33431

Hu Gang
Center of Theoretical Physics, Chinese Center for Advanced Science and Technology (World Laboratory), Beijing, China and Department of Physics, Beijing Normal University, Beijing 100875, China and Institute of Theoretical Physics, Academia Sinica, Beijing, China

(Received 1 July 1994)

It is common for a periodically driven nonlinear system to have coexistent attractors. Specifically, we are interested in the case where one of these attractors is a limit cycle whose period is an integer multiple of that of the driving. Suppose that in a given application the system is desired to evolve with this limit cycle with a particular phase relative to the driving. In this Letter we propose a technique combining the effect of noise and the effect of a bias periodic signal with a properly chosen phase to accomplish this task.

PACS numbers: 05.45.+b

Introduction.—Periodically driven nonlinear oscillators constitute a class of models that underlies many important applications. It frequently occurs that, in the parameter region of interest, such a system exhibits several coexistent attractors (multistable). Let T denote the period of the forcing. Suppose, for the object of this Letter, that one of these attractors is periodic with mT ($m > 1$) its period. In a given situation this orbit may be wanted for its wave form and spectral properties. If the system is strobed at times $t_n = nT$ ($n = 0, 1, 2, 3, \ldots$) while moving on this attractor, we obtain m discrete surface of section points, repeating every m cycles of the forcing. Thus, starting at $t = 0$, from each of these m points we can have a distinct resulting trajectory, differentiated from one another by their relative behavior with respect to the driving, which we henceforth loosely refer to as the phase; each of these m trajectories has its own domain of initial conditions [1]. Clearly, the existence of multiple basins and domains can be detrimental in such applications as laser arrays or Josephson junctions, where a collection of nearly identical systems with weak coupling is often desired to evolve in synchrony. On the other hand, the richness provided by these phenomena, through proper means of utilization, can also lead to improved system performance.

The above problem was first noted by Pecora and Carroll, who in Ref. [2] proposed a method to drive a multistable system to a preselected trajectory, regardless of where the system is initialized. Their method involves adding a chaotic signal with certain periodic characteristics as part of the drive, and they showed that it works effectively when applied to electronic circuits. Our objective is to present a simpler and more flexible approach, combining the use of noise and a bias signal, to achieve the same result. Specifically, we show that while the random noise, through a mechanism similar to stochastic resonance, is important in eliminating unwanted basins, it is the small periodic bias signal that is crucial in attaining the desired domain. Furthermore, as an additional parameter, the phase of the bias can be tuned in such a way that any one of the m available relative trajectories is selected at will. For a spatially distributed ensemble of multistable systems, this aspect of the technique is especially useful in realizing not only coherent solutions of different phases but also patterns of requisite spatial modulations. We point out that in our approach the combination of noise and signal is activated only for a brief period of time, just long enough to drive an arbitrary initial condition to the target trajectory. After that, it is withdrawn and the system is left to evolve in its natural state. This is in contrast to the method of Ref. [2] where the chaotic drive remains on for as long as the system is operating (i.e., the system is permanently altered). We illustrate our ideas below using two examples, one a differential equation system and the other a circle map.

Example 1.—Consider the driven Duffing equation

$$\ddot{x} + 0.05\dot{x} + x^3 = a + b\cos t + [f_s(t) + f_n(t)], \quad (1)$$

where $f_s(t)$ is the bias signal and $f_n(t)$ represents the effect of random forcing. Specifically, we assume that $f_n(t)$ takes the form $f_n(t) = A_n\eta(t)$, where $\eta(t)$ is Gaussian white noise with $\langle\eta(t)\rangle = 0$ and $\langle\eta(t)\eta(s)\rangle = \delta(t - s)$. The signal $f_s(t)$ is chosen to be in the form $f_s(t) = A_s\sin(\omega t + \phi)$, where ω and ϕ are to be determined by the actual application.

For $f_s(t) = f_n(t) \equiv 0$, $a = 0.15$, and $b = 0.21$, Eq. (1) exhibits three periodic attractors, of period 1, 2, and 3, respectively. Consider a rectangle in the phase space $(x, \dot{x})$ defined by $-0.6 < x < 0.6$ and $-0.2 < \dot{x} < 0.2$.

0031-9007/95/74(20)/3955(4)$06.00

We find that, starting at $t = 0$, about 20% of the points in this region are attracted to the period-3 attractor, while the remaining 80% converge to the period-2 attractor, with equal proportions in the two distinct trajectories denoted α and β. The overlap between the rectangle and the basin of attraction of the period-1 attractor is very small, accounting for less than 1% of the region, and we ignore it for the time being.

Now our task is to obtain a period-2 trajectory with a preselected phase (e.g., the phase α) irrespective of where the system is initialized. We use numerical experiments to illustrate our strategy for achieving this goal. To begin, consider a uniform grid of 70×70 initial conditions on the aforementioned rectangle. For each of the 4900 points, we evolve [3] Eq. (1) for $100T = 200\pi$ units of time, $T = 2\pi$ being the period of the driving, and then reduce the value of $f_s(t)$ and $f_n(t)$ linearly to zero for another $50T$. In the numerical work, this "quenching" process is implemented by setting A_s and A_n to ϵA_s and ϵA_n, and reducing ϵ from one to zero in a ramp. After the removal of $f_s(t)$ and $f_n(t)$, we examine the status of the resulting point $(x, \dot{x})$. The following terms are used for classifying the finding. The values of $L_2(0)$ and $L_3(0)$ denote the numbers of points in the basins of the period-2 and period-3 attractors at $t = 0$. The symbols L_2 and L_3 denote the same quantities at $t = 150T$. We define N_α and N_β to be the numbers of points in domain α and domain β of the period-2 attractor at $t = 150T$; clearly $N_\alpha + N_\beta = L_2$.

First, we study the role of noise. Let $f_s(t) = 0$. In Fig. 1, the horizontal axis is the strength of noise A_n and the vertical axis plots $\mu_1 = L_2/[L_2(0) + L_3(0)]$. As can be seen, the effect of noise increases with A_n, reaching an optimal level when $A_n \approx 0.005$, where almost 100% of the initial conditions are driven to the basin of the period-2 attractor. Upon further increase of A_n, however, the effectiveness of the random perturbation degrades monotonically. The tail portion of the curve indicates that, when the noise level becomes too large, more and more points are actually driven to the period-1 attractor. We note that the length of time for which the noise is activated can have important influence on the details of the curve in Fig. 1. Specifically, if noise is allowed to operate on a time scale much longer than that used in Fig. 1, a range of noise strength can be used to achieve the maximal result (see example 2 below).

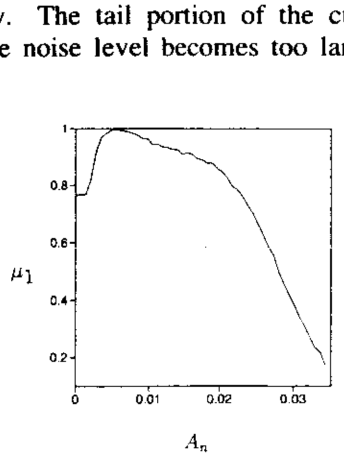

FIG. 1. Plot of $\mu_1 = L_2/[L_2(0) + L_3(0)]$ versus A_n for Eq. (1) with $A_s = 0$. Here μ_1 is the ratio of the number of points found in the basin of the period-2 attractor after the removal of perturbation to the total number of initial conditions in the rectangle $-0.6 < x < 0.6$ and $-0.2 < \dot{x} < 0.2$.

The above observation can be understood in simple terms by considering the one dimensional problem of viscous particles moving in a bounded potential with two minima denoted A and B. Say A is the target attractor which is more stable (i.e., A is a deeper minimum) than B. We draw an analogy between A and the period-2 attractor, and between B and the period-3 attractor. Within a given time scale, if the added random perturbation is weak, most particles initialized in B will remain in B, corresponding to the relatively small value of μ_1 seen in Fig. 1 for small A_n. As the noise becomes stronger, more and more particles will be driven to A, leading to the monotonic rise in the function of μ_1 versus A_n. This process continues until the optimal noise level is attained, beyond which the perturbed particles can jump more and more easily from A to B, giving rise to the monotonic decline portion of the μ_1 versus A_n curve in Fig. 1. If a third, even deeper minimum is present in the system, then large noise will ultimately drive the system toward this new state, corresponding to the tail portion of Fig. 1. Generally, the role of noise is twofold. It generates incoherent random jumps in all directions. But with proper strength, it also induces coherent motion from the less stable attractor (with "shallow" basin) to the more stable one (with "deep" basin). The competition between these two seemingly opposite effects yields the type of curve in Fig. 1. This mechanism is similar to that of stochastic resonance [4,5] where noise can be used to facilitate information processing [6].

Unlike basins of attraction, the definition of domains of initial conditions for periodically forced systems depends on the time when the observation is made. In the case of the period-2 attractor of the Duffing equation, a point in domain α at $t = 0$ maps to domain β at $t = T$, and vice versa. That is, the two domains are symmetric with respect to the time translation $t \rightarrow t + T$. This suggests that random, nondiscriminating perturbations will not be very useful by themselves in driving the system from one domain to another. Our numerical experiments confirm this idea. But imagine that if a judiciously chosen signal, such as an impulse train with period $2T$ and appropriate amplitude, is applied to the system, then the above symmetry is broken and it is conceivable that the trajectory may be led to the preferred domain after certain transient time. In fact, we find on our first choice that the most accessible signal, the sinusoid, works adequately for this purpose, provided its period is twice that of the driving. Specifically, we let $f_s(t) = A_s \sin(t/2 + \phi)$, where ϕ is a tunable phase parameter. Figure 2(a) plots

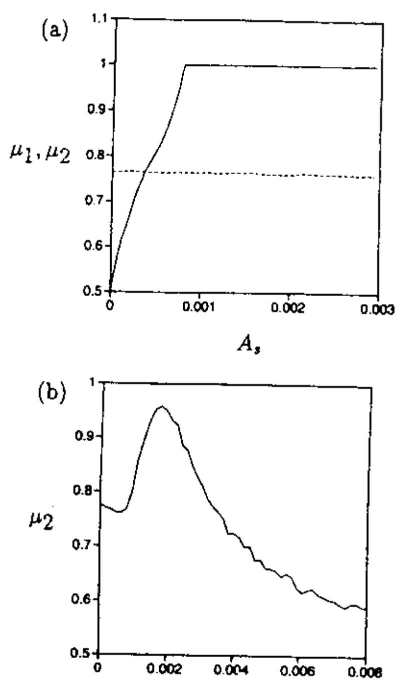

FIG. 2. (a) Plot of $\mu_2 = N_\alpha/[N_\alpha + N_\beta]$ versus A_s (solid line) and $\mu_1 = L_2/[L_2(0) + L_3(0)]$ versus A_s (dashed line) for Eq. (1) with $A_n = 0$ and $\phi = \pi/2$. (b) Plot of μ_2 versus A_n with $A_s = 0.0004$ and $\phi = \pi/2$. The quantity μ_2 gives the ratio of the number of points in domain α to the number of points in the basin of the period-2 attractor after the removal of perturbation.

$\mu_2 = N_\alpha/[N_\alpha + N_\beta]$ against A_s (solid line) with $f_n(t)$ set to zero and $\phi = \pi/2$. Evidently, a very small signal of $A_s = 0.0008$ is already sufficient to produce a 100% conversion from domain β to domain α. Under the same condition, the fraction $\mu_1 = L_2/[L_2(0) + L_3(0)]$ (dashed line) shows no significant change for the given range of A_s. This means that the added bias signal has almost no effect on the basins of the period-2 and period-3 attractors. Figure 2(b) shows the result of combining the signal and noise on the elimination of unwanted domains. We fix $A_s = 0.0004$ and $\phi = \pi/2$. The vertical axis is $\mu_2 = N_\alpha/[N_\alpha + N_\beta]$. Again, we observe a stochastic resonance type of response as A_n increases. Here the noise helps to achieve a higher percentage of conversion compared to the case with signal alone.

We now turn to the role played by the phase ϕ. The result is shown in Fig. 3, where we choose $A_s = 0.002$ and $A_n = 0.004$, and plot $\mu_3 = N_\alpha/[L_2(0) + L_3(0)]$ against ϕ. The main effect is that there are two disjoint intervals of ϕ values for which opposite effects are obtained in terms of selecting a specific domain. In particular, for $\pi/4 < \phi < 4\pi/5$, about 95% of the initial conditions in the rectangle are driven to domain α. In contrast, domain α captures almost no points if $11\pi/8 < \phi < 17\pi/10$. In other words, nearly all the trajectories, except a few that still linger on the period-3 attractor,

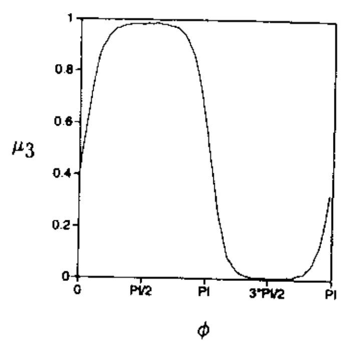

FIG. 3. Plot of $\mu_3 = N_\alpha/[L_2(0) + L_3(0)]$ versus ϕ for Eq. (1) with $A_s = 0.002$ and $A_n = 0.004$. Here μ_3 is the ratio of the number of points found in domain α of the period-2 attractor after the removal of perturbation and the total number of initial conditions in the rectangle $-0.6 < x < 0.6$ and $-0.2 < \dot{x} < 0.2$.

are moved to domain β. This flexibility is an important feature rendered by the phase of the bias signal.

Figure 4 illustrates the combined effect of noise and the bias signal. We let $\phi = 5\pi/6$ and plot $\mu_3 = N_\alpha/[L_2(0) + L_3(0)]$ versus A_n for different values of A_s. The four successively higher curves correspond to $A_s = 0.0004$, 0.001, 0.002, and 0.004. The optimal case occurs when $A_s = 0.004$ and $A_n \approx 0.0044$ where 99% of the points started in the rectangle $-0.6 < x < 0.6$ and $-0.2 < \dot{x} < 0.2$ are driven eventually to the period-2 trajectory of the phase α.

Example 2.—It is often the case that the qualitative dynamics of a periodically driven nonlinear oscillator like Eq. (1) can be adequately modeled by circle maps of the form

$$x_{m+1} = F(x_m) \mod 1, \tag{2}$$

where x is an angular variable and $F(x + 1) = F(x) + 1$. For the purpose of this paper we choose $F(x)$ to be $F(x) = x + A - Bg(x)$ with $g(x) = 4x$ for $0 \le x < 0.25$, $g(x) = 2 - 4x$ for $0.25 \le x < 0.75$, and $g(x) = 4x - 4$ for $0.75 \le x < 1$. The map with the addition of noise and a bias signal is

$$x_{m+1} = x_m + A - Bg(x_m) + A_n \eta_m + A_s S_m \mod 1. \tag{3}$$

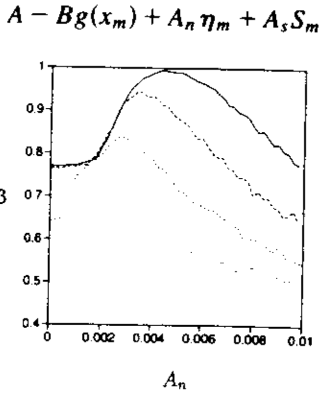

FIG. 4. Plot of $\mu_3 = N_\alpha/[L_2(0) + L_3(0)]$ versus A_n for Eq. (1) with $\phi = 5\pi/6$ where successively higher curves correspond to $A_s = 0.0004$, 0.001, 0.002, and 0.004.

As shown in Ref. [7], this map has a period-2 and a period-3 attractor coexisting for $A = 0.41$, $B = 0.29$, and $A_n = A_s = 0$. Our objective here is to drive an arbitrary initial condition to a particular phase of the period-2 orbit. To this end we assume η_m to be a random number uniformly distributed in $[-0.5, 0.5]$ and $S_m = 0$ if $m =$ odd and $S_m = -1$ if $m =$ even.

From Fig. 2(a) we observe that, if points are initialized in the basin of the period-2 orbit, then with signal alone we can achieve an 100% conversion to the desired phase. This, in combination with Fig. 1, suggests that the noise and the signal can also be applied in two consecutive stages: First, all the points are driven to the basin of the period-2 attractor with noise, and then these points are further moved to the appropriate domain with the signal. We demonstrate this approach with Eq. (3). In the numerical work we begin with 5000 initial conditions distributed uniformly in the unit interval. Then we evolve these points under Eq. (3) for 500 iterates. The next 50 iterates are used to remove the perturbation linearly. In Fig. 5 we show the result of $\mu_1 = L_2[L_2(0) + L_3(0)]$ versus A_n when $A_s = 0$. Note that, since in this case the time scale during which the noise is active is relatively long, a range of noise strength can be applied to achieve the maximal effect. Finally choosing $A_n = 0.015$ and $A_s = 0.005$ and activating the drive in two stages, we convert all the 5000 initial conditions to the desired phase of the period-2 orbit.

In summary, a technique is proposed which eliminates multiple basins as well as domains of attraction in periodically driven systems. The goal is to make the system behave with a periodic trajectory that has a preselected phase relative to the driving. There are three essential components in the technique: noise, a bias periodic signal, and the phase of the signal; the role of each is illustrated with numerical simulations performed on two examples. Our result demonstrates that the technique is flexible and could be easily implemented in experiments. We suggest that an important area of future application is spatiotemporal systems where nearly identical units with weak coupling are desired to evolve in synchrony [8].

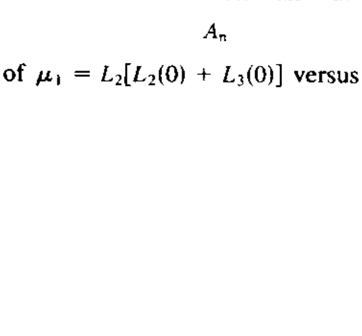

FIG. 5. Plot of $\mu_1 = L_2[L_2(0) + L_3(0)]$ versus A_n for Eq. (3) with $A_s = 0$.

This work was supported by U.S. ONR and by Project Nonlinear Science from National Natural Science Foundation of China.

[1] We henceforth speak about basins and domains of attraction in terms of the surface of sections taken every period of the forcing starting at $t = 0$. Thus the basin of attraction of the period-m attractor is the union of its m domains.

[2] L. M. Pecora and T. L. Carroll, Phys. Rev. Lett. **67**, 945 (1991); Phys. Rev. E **48**, 2426 (1993).

[3] Numerical integrations of the stochastic differential equation (1) are carried out with an algorithm adapted from R. Mannella and V. Palleschi, Phys. Rev. A **40**, 3381 (1989).

[4] R. Benzi, A. Sutera, and A. Vulpiani, J. Phys. A **14**, 453 (1981); C. Nicolis and G. Nicolis, Tellus **34**, 10 (1982).

[5] B. McNamara and K. Wiesenfeld, Phys. Rev. A **39**, 4853 (1989); L. Gammaitoni, F. Marchesoni, E. Menichella-Saetta, and S. Santucci, Phys. Rev. Lett. **62**, 349 (1989); T. Zhou and F. Moss, Phys. Rev. A **41**, 4255 (1990); G. Hu, G. Nicolis, and C. Nicolis, *ibid.* **42**, 2030 (1990); P. Jung and P. Hänggi, *ibid.* **44**, 8032 (1992); M. I. Dykman, R. Mannella, P. V. E. McClintock, and N. G. Stocks, Phys. Rev. Lett. **68**, 2985 (1992).

[6] J. K. Douglass, L. Wilkens, E. Pantazelou, and F. Moss, Nature (London) **365**, 337 (1993).

[7] W. M. Yang and B.-L. Hao, Commun. Theor. Phys. **8**, 1 (1987).

[8] For recent work, see R. Roy and K. S. Thornburg, Jr., Phys. Rev. Lett. **72**, 2009 (1994), and references therein.

Plateau Onset for Correlation Dimension: When Does it Occur?

Mingzhou Ding,[1] Celso Grebogi,[2,3] Edward Ott,[2,4] Tim Sauer,[5] and James A. Yorke[3]
[1]*Center for Complex Systems and Department of Mathematics, Florida Atlantic University, Boca Raton, Florida 33431*
[2]*Laboratory for Plasma Research, University of Maryland, College Park, Maryland 20742*
[3]*Department of Mathematics and Institute for Physical Science and Technology, University of Maryland, College Park, Maryland 20742*
[4]*Departments of Physics and of Electrical Engineering, University of Maryland, College Park, Maryland 20742*
[5]*Department of Mathematical Sciences, George Mason University, Fairfax, Virginia 22030*
(Received 22 February 1993)

Chaotic experimental systems are often investigated using delay coordinates. Estimated values of the correlation dimension in delay coordinate space typically increase with the number of delays and eventually reach a plateau (on which the dimension estimate is relatively constant) whose value is commonly taken as an estimate of the correlation dimension D_2 of the underlying chaotic attractor. We report a rigorous result which implies that, for long enough data sets, the plateau begins when the number of delay coordinates first exceeds D_2. Numerical experiments are presented. We also discuss how lack of sufficient data can produce results that seem to be inconsistent with the theoretical prediction.

PACS numbers: 05.45.+b

The estimation of the correlation dimension [1] of a presumed chaotic time series has been widely used by scientists to assess the nature of a variety of experimental as well as model systems, ranging from simple circuits to chemical reactions to the human brain. It is also known that many factors, such as noise and a lack of data, can hinder the successful application of the dimension extraction algorithm. In this paper, we address two issues related to the understanding of these difficulties, namely, what happens in an ideal situation (i.e., long data string with low noise) and what could be expected when the data set is small. In particular, we focus on the character of the dependence of the estimated correlation dimension on the dimension of the delay coordinate reconstruction space.

Consider an n-dimensional dynamical system that exhibits a chaotic attractor. A correlation integral $C(\epsilon)$ [1] is defined to be the probability that a pair of points chosen randomly on the attractor with respect to the natural measure ρ is separated by a distance less than ϵ on the attractor. The correlation dimension D_2 [1] of the attractor is then defined as $D_2 = \lim_{\epsilon\to 0}\log C(\epsilon)/\log\epsilon$. Assume that we measure and record a trajectory of finite duration L on the attractor at N equally spaced discrete times, $\{\mathbf{x}_i\}_{i=1}^N$, where $\mathbf{x}_i \in \mathbf{R}^n$. The correlation integral $C(\epsilon)$ is then approximated by

$$C(N,\epsilon) = \frac{2}{N(N-1)}\sum_{j=1}^{N}\sum_{i=j+1}^{N}\Theta(\epsilon - |\mathbf{x}_i - \mathbf{x}_j|), \quad (1)$$

where $\Theta(x)=1$ for $x>0$ and $\Theta(x)=0$ for $x\le 0$. In the limit $L,N\to\infty$, $C(N,\epsilon)\to C(\epsilon)$.

The dynamical information of a chaotic experimental system is often contained in a time series, $\{y_i = y(t_i)\}_{i=1}^N$, obtained by measuring a single scalar function $y = h(\mathbf{x})$ where $\mathbf{x}\in\mathbf{R}^n$ is the original phase space variable. From $\{y_i\}_{i=1}^N$ one reconstructs an m-dimensional vector $\mathbf{y}_i$ using the delay coordinates [2,3]

$$\mathbf{y}_i = \{y(t_i), y(t_i - T), \ldots, y(t_i - (m-1)T)\}, \quad (2)$$

where $T>0$ is the delay time and m is the dimension of the reconstruction space. We call the mapping from $\{\mathbf{x}_i\}$ in $\mathbf{R}^n$ to $\{\mathbf{y}_i\}$ in $\mathbf{R}^m$ the "delay coordinate map." Results in Ref. [4] show that, for typical $T>0$ and $m>2D_0$, this delay coordinate map is one to one. Here D_0 is the box-counting dimension of the original chaotic attractor.

Our main focus is to estimate correlation dimension from a time series using delay coordinates [Eq. (2)]. As a point of departure for subsequent discussions, we first report a theorem [5,6] which shows that, for estimating the correlation dimension, $m \ge D_2$ suffices. We emphasize that this result holds true irrespective of whether the delay coordinate map is one to one or not. This is contrary to the commonly accepted notion that an embedding (one to one and differentiable) is needed for dimension estimation, leading to the false surmise that m needs to be at least $2D_2+1$ to guarantee a correct dimension estimation (see [7] for further discussion).

Consider an n-dimensional map $G:\mathbf{R}^n\to\mathbf{R}^n$. Let A be an attractor of G in $\mathbf{R}^n$ with a natural probability measure ρ. For a function $h:\mathbf{R}^n\to\mathbf{R}$, define a delay coordinate map $F_h:\mathbf{R}^n\to\mathbf{R}^m$ as

$$F_h(\mathbf{x}) = [h(\mathbf{x}), h(G^{-1}(\mathbf{x})), \ldots, h(G^{-(m-1)}(\mathbf{x}))].$$

The projected image of the attractor A under F_h has an induced natural probability measure $F_h(\rho)$ in $\mathbf{R}^m$. Furthermore, assume that G has only a finite number of periodic points of period less than or equal to m in A. The following result then applies.

Theorem.—If $D_2(\rho)\le m$, then for almost every h, $D_2(F_h(\rho)) = D_2(\rho)$.

The theorem says that the correlation dimension is preserved under the delay coordinate map with $m \ge D_2(\rho)$. Similar results hold for flows generated by ordinary differential equations. "Almost every" in the statement is understood in the sense of prevalence defined in Ref. [4]; roughly speaking, we can regard this "almost every" as meaning that the functions h that do not give

0031-9007/93/70(25)/3872(4)$06.00

the stated result are very scarce and are not expected to occur in practice. The above dimension preservation result also holds for almost all general projection maps meeting the condition in the theorem. To illustrate, consider a closed curve with a uniform measure in $\mathbf{R}^3$. The dimension of this curve is 1. The projected image of this curve onto the plane still has a dimension of 1 but is generally self-intersecting. Thus the map is not one to one but preserves dimension information. One can further project the image to $\mathbf{R}^1$ and obtain an interval, which again has a dimension of 1 but bears little resemblance to the original curve in $\mathbf{R}^3$.

In applications D_2 is commonly extracted from a time series as follows (see Refs. [8–11] for reviews). First, an m-dimensional trajectory is constructed using Eq. (2). Then, the correlation integral $C_m(N,\epsilon)$ is computed according to Eq. (1), where m indicates the dimensionality of the reconstruction space. From the curve $\log C_m(N,\epsilon)$ vs $\log\epsilon$ one then locates a linear scaling region for small ϵ and estimates the slope of the curve over the linear region. This slope, denoted $\bar{D}_2^{(m)}$, is then taken as an estimate of the correlation dimension $D_2^{(m)}$ of the projection of the attractor to the m-dimensional reconstruction space. If these estimates $\bar{D}_2^{(m)}$, plotted as a function of m, appear to reach a plateau for a range of large enough m values, then we denote the plateaued value $\bar{D}_2$ and take $\bar{D}_2$ an estimate of the true correlation dimension D_2 for the system. From the theorem it is clear that the onset of this plateau should ideally start at $m=\mathrm{Ceil}(D_2)$, where $\mathrm{Ceil}(D_2)$, standing for ceiling of D_2, denotes the smallest integer greater than or equal to D_2.

Our original interest in the current problem was motivated by published reports (see Refs. [12–17] for a sample) where $\bar{D}_2^{(m)}$ plateaus at m values that are considerably greater than $\bar{D}_2$. A particular concern is that, when this happens, what does it imply regarding the correctness of the assertion that $\bar{D}_2$ is an estimate of the true correlation dimension D_2 of the underlying chaotic process? In an attempt to answer this question we have obtained new results on the systematic behavior of the correlation integrals. Based on these behaviors we are able to explain how factors such as a lack of sufficient data can produce results, resembling those seen in the experimental reports cited above, which seem to be inconsistent with the theorem. Furthermore, we find that even in cases where the plateau onset of $\bar{D}_2^{(m)}$ occurs at m values considerably greater than $\mathrm{Ceil}(\bar{D}_2)$, there are situations where the plateaued $\bar{D}_2$ is a good estimate of the true correlation dimension D_2. See Refs. [18–25] for other relevant works addressing the issue of short data sets and noise.

To study the numerical aspects of dimension estimation we use chaotic time series generated by the Mackey-Glass equation [26] $dy(t)/dt=ay(t-\tau)/\{1+[y(t-\tau)]^c\}-by(t)$, where we fix $a=0.2$, $b=0.1$, $c=10.0$, and $\tau=100.0$, and take as the initial condition $y(t)=0.5$ for $t\in[-\tau,0]$. The numerical integration of this equation is done by the following iterative scheme [1]:

$$y(t+\delta t)=\frac{2-b\delta t}{2+b\delta t}y(t)+\frac{\delta t}{2+b\delta t}\left\{\frac{ay(t-\tau)}{1+[y(t-\tau)]^{10}}+\frac{ay(t-\tau+\delta t)}{1+[y(t-\tau+\delta t)]^{10}}\right\}, \tag{3}$$

where δt is the integration step size. We choose $\delta t=0.1$. Equation (3) is then a 1000-dimensional map, which, aside from being an approximation to the original equation, is itself a dynamical system. The time series, generated with a sampling time $t_s=10.0$, are normalized to the unit interval so that the reconstructed attractor lies in the unit hypercube in the reconstruction space. The norm we use to calculate distances in Eq. (1) is the max-norm in which the distance between two points is the largest of all the component differences. To reconstruct the attractor, we follow Eq. (2) and take the delay time to be $T=20.0$ The dimension of the reconstruction space is varied from $m=2$ to $m=25$.

The first time series, used to illustrate the theorem, consists of 50000 points. For each reconstructed attractor at a given m we calculate the correlation integral $C_m(N,\epsilon)$ according to Eq. (1). In Fig. 1 we display $\log_2 C_m(N,\epsilon)$ vs $\log_2\epsilon$ for $m=2$–8, 11, 15, 19, 23. For each m we identify a scaling region for small ϵ and fit a straight line through the region. The open circles in Fig. 2 show the values of $\bar{D}_2^{(m)}$ so estimated as a function of m. For $m\le 7$, $\bar{D}_2^{(m)}\approx m$. For $m\ge 8$, $\bar{D}_2^{(m)}$ plateaus at $\bar{D}_2$ which has a value of about 7.1. Identifying $\bar{D}_2$ with the true correlation dimension D_2 of the underlying attractor, this result is consistent with the prediction by the theorem that the onset of the plateau occurs at $m=\mathrm{Ceil}(D_2)$.

The second time series, used to illustrate the effect

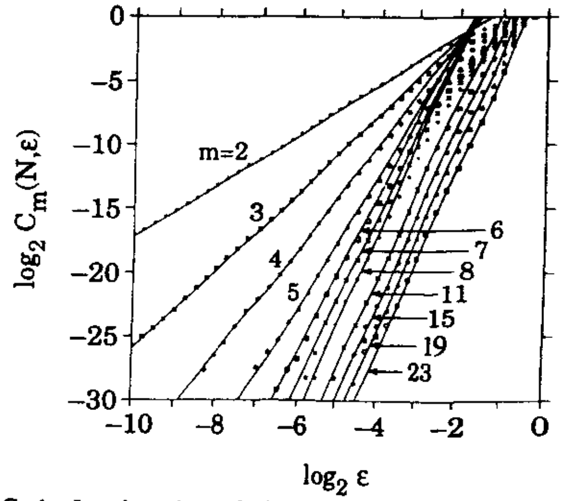

FIG. 1. Log-log plots of the correlation integrals $C_m(N,\epsilon)$ for the data set of 50000 points generated by Eq. (3).

58

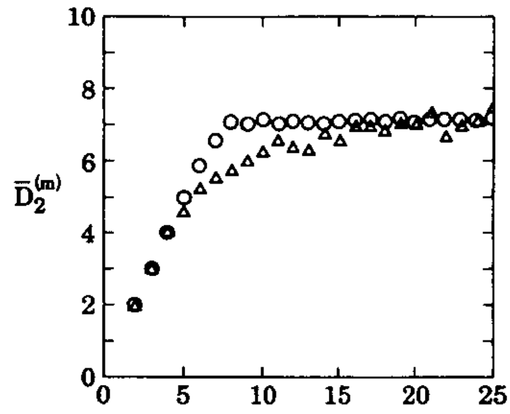

FIG. 2. $\bar{D}_2^{(m)}$ vs m plotted as open circles for the long data set ($N=50000$ and Fig. 1), $\bar{D}_2^{(m)}$ vs m plotted as triangles for the short data set ($N=2000$ and Fig. 3).

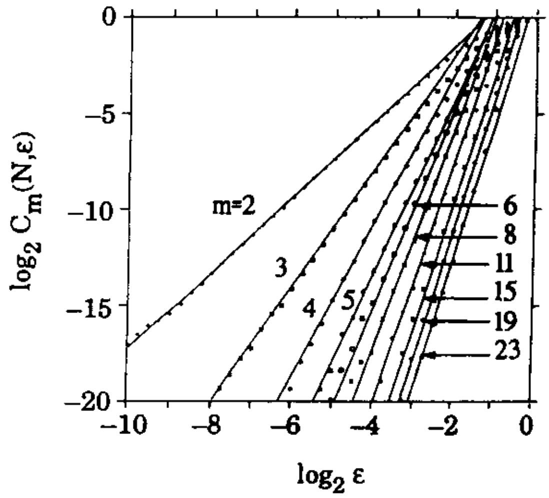

FIG. 3. $\log_2 C_m(N,\epsilon)$ vs $\log_2\epsilon$ for the data set of 2000 points.

due to a lack of data, consists of 2000 points. The $\log_2 C_m(N,\epsilon)$ vs $\log_2\epsilon$ curves are shown in Fig. 3 for $m=2$–6, 8, 11,15, 19, 23. The values of $\bar{D}_2^{(m)}$ in this case are plotted using triangles as a function of m in Fig. 2. This function attains an approximate plateau which begins at $m=16$ and extends beyond $m=25$. The slope averaged over the plateau is about 7.05 which is consistent with the value of 7.1 obtained using the long data set ($N=50000$) plotted as open circles in Fig. 2. But the D_2 estimates for the short data set fall systematically under that for the long data set for $5\le m\le 13$. Thus the plateau does not begin until m is substantially larger than Ceil($\bar{D}_2$). This behavior has also been seen in many experimental studies. In what follows we explain the origin of this apparent inconsistency by exploring the systematic behavior of correlation integrals.

Figure 4 is a schematic diagram of a set of correlation integrals for $m=2$ to $m=13$. A dashed line is fit through the scaling region for each m. For $m\le 5$, $\bar{D}_2^{(m)}\approx m$. For $m\ge 6$, $\bar{D}_2^{(m)}$ plateaus at $\bar{D}_2\approx 5.7$. This value is an estimate of the true D_2 for the system. This figure exhibits several features that are typical of correlation integrals for chaotic systems. The first feature we note is that the horizontal distance between $\log C_m(N,\epsilon)$ and $\log C_{m+1}(N,\epsilon)$ for $m\ge 6$ in the scaling regions is roughly a constant. This constant is predicted, for large m and small ϵ, to be $\Delta h=\Delta v/D_2$, where $\Delta v=TK_2$ with K_2 the correlation entropy [27] and T the delay time in Eq. (2). Two other significant features exhibited by Fig. 4 are as follows. For $m\le 9$, $\log_2 C_m(N,\epsilon)$ increases with a gradually diminishing slope; while for $m\ge 11$, after exiting the linear region, the log-log plots in Fig. 4 first increase with a slope that is steeper than that in the linear scaling region and then level off to meet the point (0,0). These two different trends give rise to an uneven distribution in the extent of the scaling regions for different m with the most extended scaling region occurring at $m=10$.

In Refs. [8,28] arguments are presented to show that the trend observed for relatively small m is due to an "edge effect" resulting from the finite extent to the reconstructed attractor. Ding *et al.* [5] show that the steeper slope observed for relatively large m is caused by foldings occurring on the original attractor. This can be illustrated analytically [5] for the tent map [29]. For $m=1$, the correlation integral for the reconstructed tent map attractor is $C_1(\epsilon)=\epsilon(2-\epsilon)$. For $m=2$, $C_2(\epsilon)$ is written as $C_2(\epsilon)=C_1(\epsilon/2)+R(\epsilon)$. The first term arises because a pair of points y_j and y_l in the time series satisfying $|y_j-y_l|<\epsilon/2$ give rise to a pair of two-dimensional points, $\mathbf{y}_{j+1}=\{y_{j+1},y_j\}$ and $\mathbf{y}_{l+1}=\{y_{l+1},y_l\}$, satisfying $|\mathbf{y}_{j+1}-\mathbf{y}_{l+1}|<\epsilon$. The folding of the tent map at $y=\frac{1}{2}$ leads to situations in which $|y_j-y_l|>\epsilon/2$, but $|y_{j+1}-y_{l+1}|<\epsilon$. Thus the folding in the attractor underlies the correction term $R(\epsilon)$ which is calculated [5] to be $R(\epsilon)=\epsilon^2/2$ for $0\le\epsilon<\frac{2}{3}$ and $R(\epsilon)=3\epsilon-7\epsilon^2/4-1$ for $\frac{2}{3}\le\epsilon\le 1$. For $0\le\epsilon<\frac{2}{3}$, $d\log_2 C_2(\epsilon)/d\log_2\epsilon=1+\epsilon/(2+\epsilon)$. This derivative is 1 when $\epsilon=0$ ($D_2=1$ for the attractor) and increases due to the term $\epsilon/(2+\epsilon)$ whose presence reflects the influence of $R(\epsilon)$ which, in turn, is caused by the folding on the attractor.

From Eq. (1), the range of $C_m(N,\epsilon)$ is $\log_2 2/N^2$

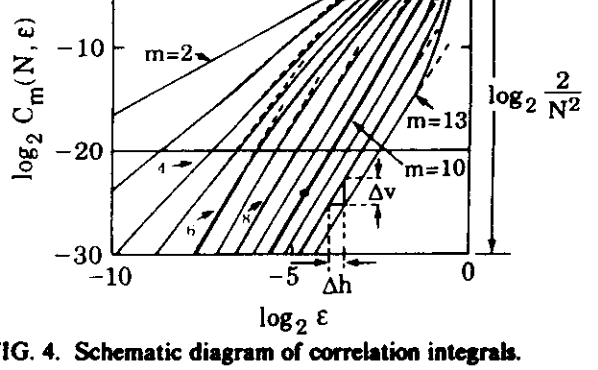

FIG. 4. Schematic diagram of correlation integrals.

Presentation by M. DING

- Controlling Chaos in a Temporally irregular environment to prevent ship capsizing
- Controlling chaos and Tracking in High Dimensions
- Synchronizing high dim. Chaos for Communication
- Trajectory selection in Multistable Systems

Controlling Chaos in a Temporally Irregular Environment: Safe Voyage for a Cargo Ship

M. DING

Florida Atlantic Univ.

with

E. Ott
C. Grebogi
W. Yang

Physica D (1994), PRE (1994)
in preparation

$\leq \log_2 C_m(N,\epsilon) \leq 0$. Imagine a time series of $N=2000$ points generated by the system underlying Fig. 4. The plots of $\log_2 C_m(N,\epsilon)$ vs $\log_2\epsilon$ for this data set roughly correspond to the portion of Fig. 4 above the horizontal line drawn at $\log_2 C_m(N,\epsilon) = \log_2[2/(2000)^2] \approx -20$. Since the upper boundary points of the scaling regions for $m=6$ and 7 are under this horizontal line, the correct dimension is not obtained for $m=6$ and 7. In fact, if we fit a straight line to an *apparent* linear region above $\log_2 C_m(N,\epsilon) = -20$ for $m=6$ we obtain a slope which is markedly smaller than the actual dimension. However, since the upper boundary points of the scaling regions for $m \geq 8$ are above the horizontal line, we can still expect to obtain the correct estimate of $D_2 = 5.7$ for $m \geq 8$. Thus the plateau onset is delayed due to a lack of data.

The same consideration applies to the short data set generated by Eq. (3). In particular, imagine that we restrict our attention to the region $\log_2 C_m(N,\epsilon) > -20$ in Fig. 1 and fit a line through an *apparent* linear range for the $m=8$ data in this region. The slope of this straight line is about 5.9, which is roughly the same as that of 5.8 estimated using 2000 points. Thus, by knowing the correlation integrals for a large data set, we can roughly predict the outcome of a dimension measurement based on a smaller subset of this data.

We remark that if one extends the range of m values beyond what is shown in Fig. 2, at large enough m, $\bar{D}_2^{(m)}$ will start to deviate from the plateau behavior and increase monotonically with m. This is caused by the finite length of the data set and can be understood from the systematic behavior of correlation integrals seen in Fig. 4. A lack of sufficient data will not only delay the plateau onset, but also make the deviation from the plateau behavior occur at smaller values of m, thus shortening the plateau length from both sides. This can again be understood with reference to Fig. 4.

This work was supported by the U.S. DOE (Office of Scientific Computing, Office of Energy Research) and the NSF (Divisions of Mathematical and Physical Sciences). M.D.'s research is also supported in part by a grant from the National Institute of Mental Health.

[1] P. Grassberger and I. Procaccia, Phys. Rev. Lett. 50, 346 (1983); Physica (Amsterdam) 9D, 189 (1983).

[2] J.-P. Eckmann and D. Ruelle, Rev. Mod. Phys. 57, 617 (1985).

[3] F. Takens, in *Dynamical Systems and Turbulence*, edited by D. Rand and L. S. Young (Springer-Verlag, Berlin, 1981), p. 366; R. Mañe, *ibid.*, p. 230.

[4] T. Sauer, J. A. Yorke, and M. Casdagli, J. Stat. Phys. 65, 579 (1991).

[5] M. Ding, C. Grebogi, E. Ott, T. Sauer, and J. A. Yorke, Physica (Amsterdam) D (to be published).

[6] T. Sauer and J. A. Yorke (to be published).

[7] To get a rough idea of how widespread the misconception about the relevance of embedding to dimension estimation is, we conducted a literature search using the Science Citation Index for the years from 1987 to 1992 by looking for papers citing both Ref. [1] and Ref. [3]. We found 183 such papers. We then randomly selected a sample of 22 of these papers for closer examination. The following is what we found. Among the 22 papers there are 15 of them that calculate correlation dimension from time series. Five of these 15 papers make explicit connections between $2D+1$ and dimension estimation. The rest of these papers ignore this issue entirely. Based on this information we estimate that, during the period from 1987 to 1992, there are at least 42 papers (probably many more) where the authors implicitly or explicitly assumed that a one-to-one embedding is needed for dimension calculation. In addition, among the papers we researched for this work, only [8] and [9] imply that $m \geq D_2$ is sufficient for estimating D_2, although no justification is given.

[8] J. Theiler, J. Opt. Soc. Am. A 7, 1055 (1990).

[9] P. Grassberger, in *Chaos*, edited by A. V. Holden (Manchester Univ. Press, Manchester, 1986).

[10] P. Grassberger, T. Schreiber, and C. Schaffrath, Int. J. Bifurcation Chaos 1, 521 (1991).

[11] *Dimensions and Entropies in Chaotic Systems*, edited by G. Mayer-Kress (Springer-Verlag, Berlin, 1986).

[12] J. Holzfuss and G. Mayer-Kress, in *Dimensions and Entropies in Chaotic Systems* (Ref. [11]).

[13] A. Branstater and H. L. Swinney, Phys. Rev. A 35, 2207 (1987).

[14] U. Hübner, W. Klische, N. B. Abraham, and C. O. Weiss, in *Measures of Complexity and Chaos*, edited by N. B. Abraham *et al.* (Plenum, New York, 1990).

[15] K. R. Sreenivasan, in *Dimensions and Entropies in Chaotic Systems* (Ref. [11]).

[16] A. A. Tsonis and J. B. Elsner, Nature (London) 333, 545 (1988).

[17] D. V. Vassiliadis, A. S. Sharma, T. T. Eastman, and K. Papadopoulos, Geophys. Res. Lett. 17, 1841 (1990).

[18] A. Ben-Mizrachi, I. Procaccia, and P. Grassberger, Phys. Rev. A 29, 975 (1984).

[19] J. G. Caputo, in *Measures of Complexity and Chaos*, edited by N. B. Abraham *et al.* (Plenum, New York, 1989).

[20] J. G. Caputo, B. Malraison, and P. Atten, in *Dimensions and Entropies in Chaotic Systems* (Ref. [11]).

[21] J.-P. Eckmann and D. Ruelle, Physica (Amsterdam) 56D, 185 (1992).

[22] N. A. Gershenfeld, Physica (Amsterdam) 55D, 155 (1992).

[23] J. W. Havstad and C. L. Ehlers, Phys. Rev. A 39, 845 (1989).

[24] M. Möller, W. Lange, F. Mischke, N. B. Abraham, and U. Hübner, Phys. Lett. A 138, 176 (1989).

[25] A. R. Osborne and A. Provenzale, Physica (Amsterdam) 35D, 357 (1989).

[26] M. C. Mackey and L. Glass, Science 197, 287 (1977).

[27] P. Grassberger and I. Procaccia, Phys. Rev. A 28, 2591 (1983); Physica (Amsterdam) 13D, 34 (1984).

[28] L. A. Smith, Phys. Lett. A 133, 283 (1988).

[29] The tent map is defined as $y_{n+1} = T(y_n)$, where $T(y) = 2y$ if $0 \leq y < 1/2$ and $T(y) = 2 - 2y$ if $1/2 \leq y \leq 1$.

90

GOAL

- General: Modify the dynamics of a chaotic process to improve performance by using controls.
- Specific: Prevent the capsizing of a ship in irregular waves; eliminate uncertainties in cargo transfer process.

Von Neumann ~ 1950

- All stable* processes we shall predict.
- All unstable** processes we shall control.

* nonchaotic

** chaotic

Ref: F. Dyson "Infinite in ALL Directions"

Attributes of Chaos

- Complex orbit structure
  e.g. Dense set of periodic orbits of all periods
- Sensitive dependence on initial conditions

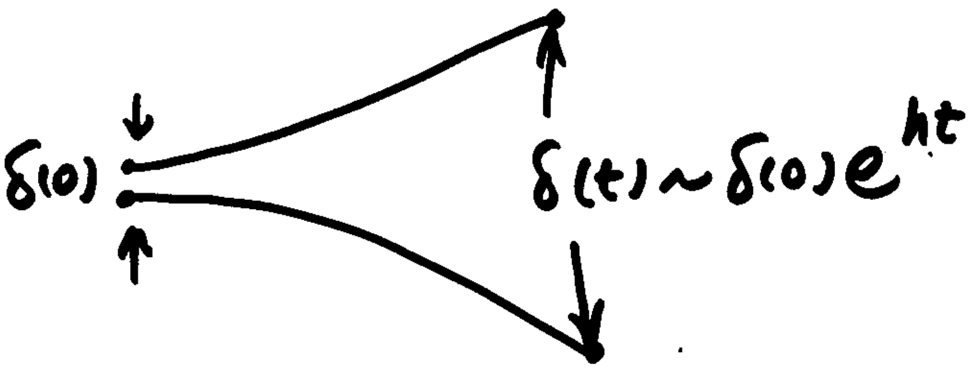

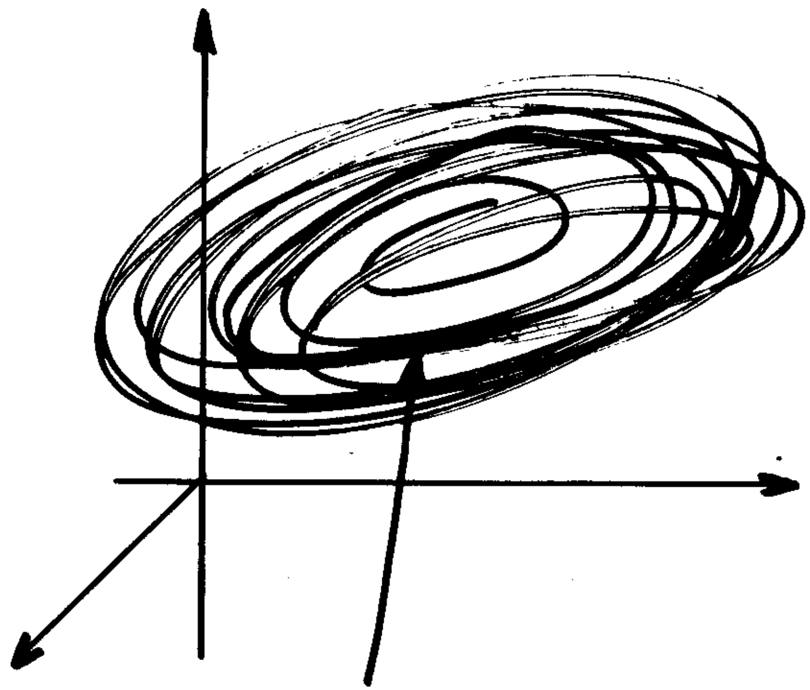

Unstable periodic orbit

Controlling Unstable Periodic Orbit

- In 1990, Ott, Grebogi & Yorke (OGY) observed that an UPO embedded in a chaotic attractor may be stabilized by using SMALL controls in a small neighborhood of the orbit.

- Since dynamics are ergodic orbits eventually enter the desired stabilization neighborhood. Use of targetting helps.

SURFACE OF SECTION

MAP

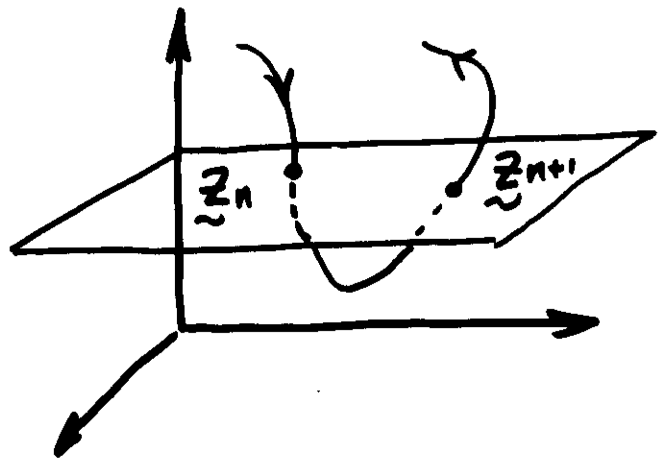

$$\underset{\sim}{z}_{n+1} = \underset{\sim}{F}(\underset{\sim}{z}_n, p)$$

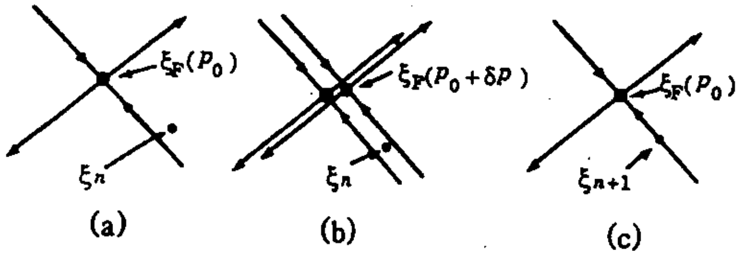

(Ditto, Rauseo, Spano)

Fig. 10

Schematic of original OGY Control

The Control Method

$$\underset{\sim}{Z}_{n+1} = \underset{\sim}{F}(\underset{\sim}{Z}_n, P)$$

$$P \in [P_0 - \delta P, \; P_0 + \delta P]$$

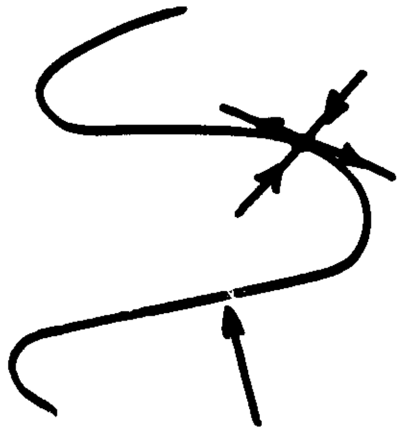

attractor at $P = P_0$

(Ott, Grebogi & Yorke, 1990)

SCT ?

$$\underset{\sim}{z}_{n+1} = \underline{F}(\underset{\sim}{z}_n, p)$$

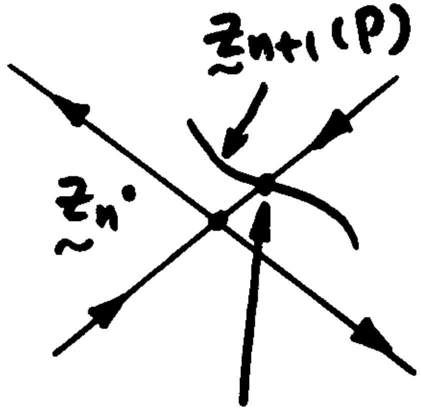

$\underset{\sim}{z}_{n+1}(\bar{p})$

$$p, \bar{p} \in [p_0 - \delta p,\ p_0 + \delta p]$$

choose $\bar{p}$ so that $\underset{\sim}{z}_{n+1}(\bar{p})$ falls on the stable direction of the fixed point.

Preventing Chaos-Induced capsizing of a ship

Chaos, catastrophes and engineering

Applying chaos theory to engineering may seem odd. We expect machines and structures to operate with clockwork predictability. But engineers are now discovering that a sudden disaster may mean there's a fractal in the works

Allan McRobie and Michael Thompson

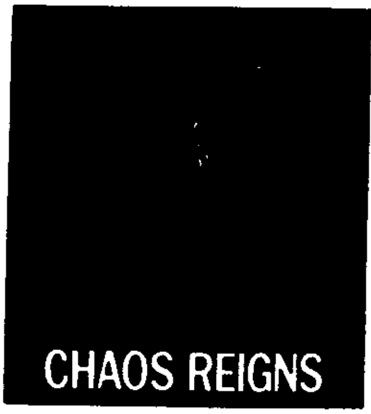

IN FEBRUARY 1974, the Gaul, a trawler from Hull, disappeared in heavy seas off the coast of Norway with the loss of 36 lives. The inquiry into the disaster found that there was nothing wrong with the ship's design: the stability of the vessel against capsize conformed with all required standards. One possible explanation put forward for the loss of the vessel was that it capsized as the result of some transient phenomenon when hit broadside by a short succession of abnormally large waves.

"Transient phenomenon" means that the vessel was moving in an irregular fashion: rocking, swaying, pitching, heaving and rolling. A trawler in a storm is obviously tossed around, so any capsize caused by waves hitting a vessel is a transient phenomenon. Strangely, though, the methods that engineers use to assess how stable a ship is assume that the ship is totally motionless. The methods simply require that the forces on the stationary vessel when tilted at various angles should be such as to try to right it. Various naval engineers at the inquiry pointed out that these tried and trusted methods of stability design might not always be safe. The motion of a ship and the way that it rocks change its stability. Engineers suggested that because of the dynamic nature of capsize a ship's stability should be evaluated when it is moving as well as when it is still.

The word "transient", however, has a stronger meaning than just motion: it is a mathematical term for unsteady motion—motion that has not yet settled down to a steady and regular pattern. The mathematics of transient motions gives equations that are more complicated than the equations of steady rocking, which are often complicated enough. To many engineers, assessing dynamic stability would mean analysing the steady rocking motions. Ships capsize, however, as a result of transient motions so these should be considered as well.

Everything moves, even buildings. Many people in Britain first realised this in recent storms when office workers were

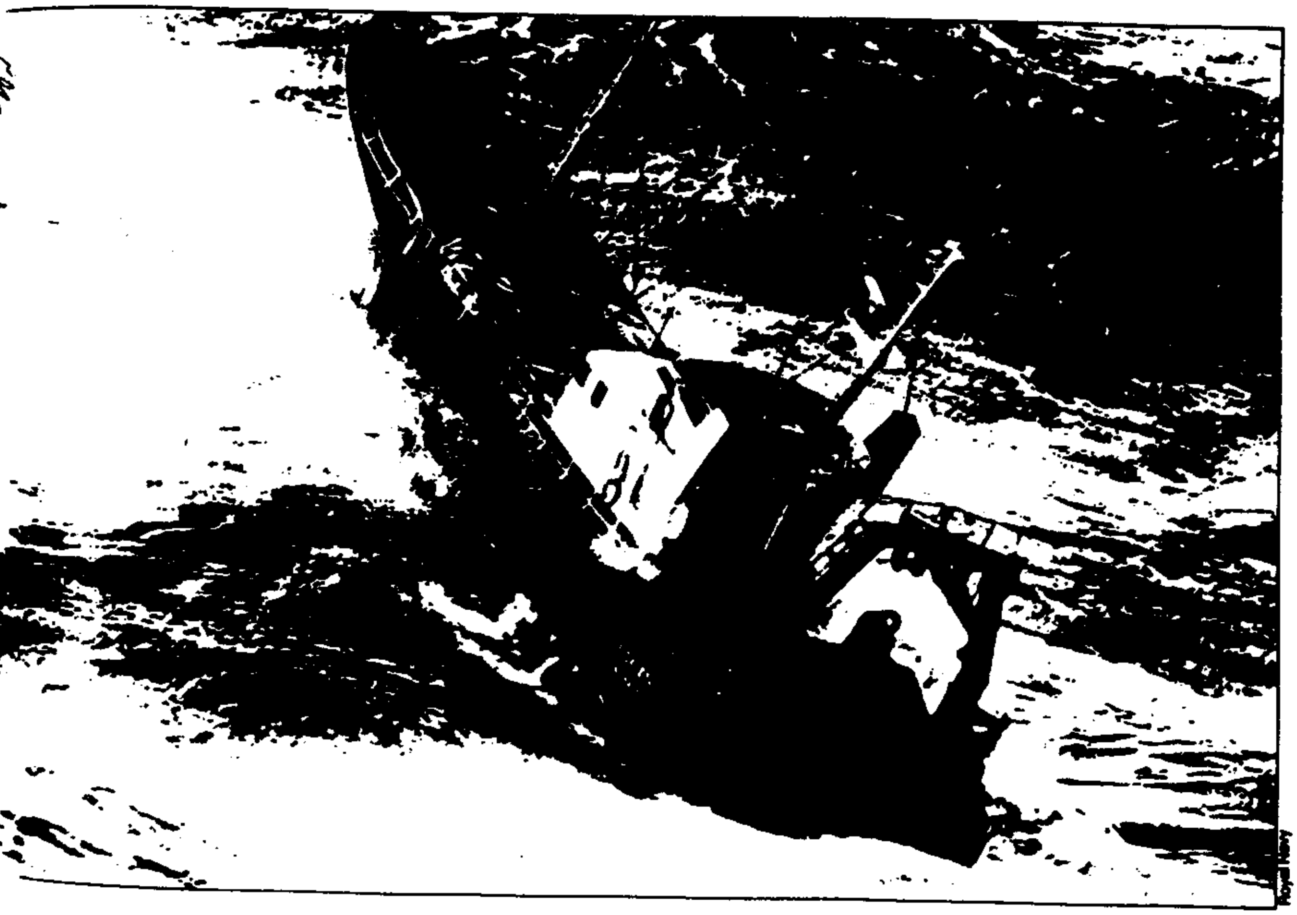

A Ship Model

Rolling motion in a beam sea.

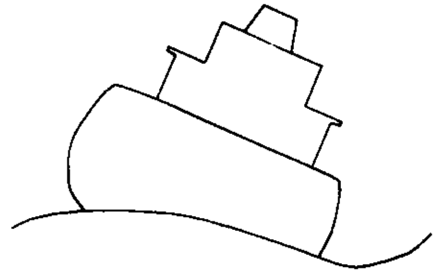

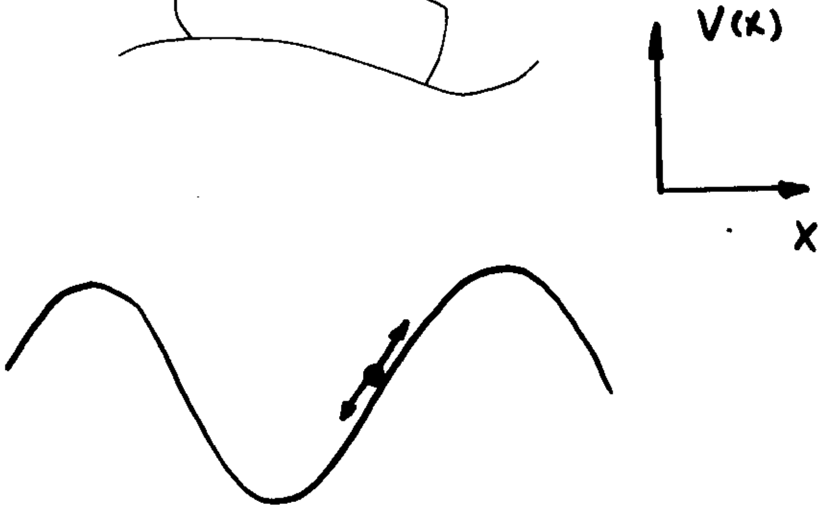

$$\ddot{x} + \nu \dot{x} + \frac{\partial V(x)}{\partial x} = W(t) + C(t)$$

$W(t)$: wave

$C(t)$: control

Dynamics of the System

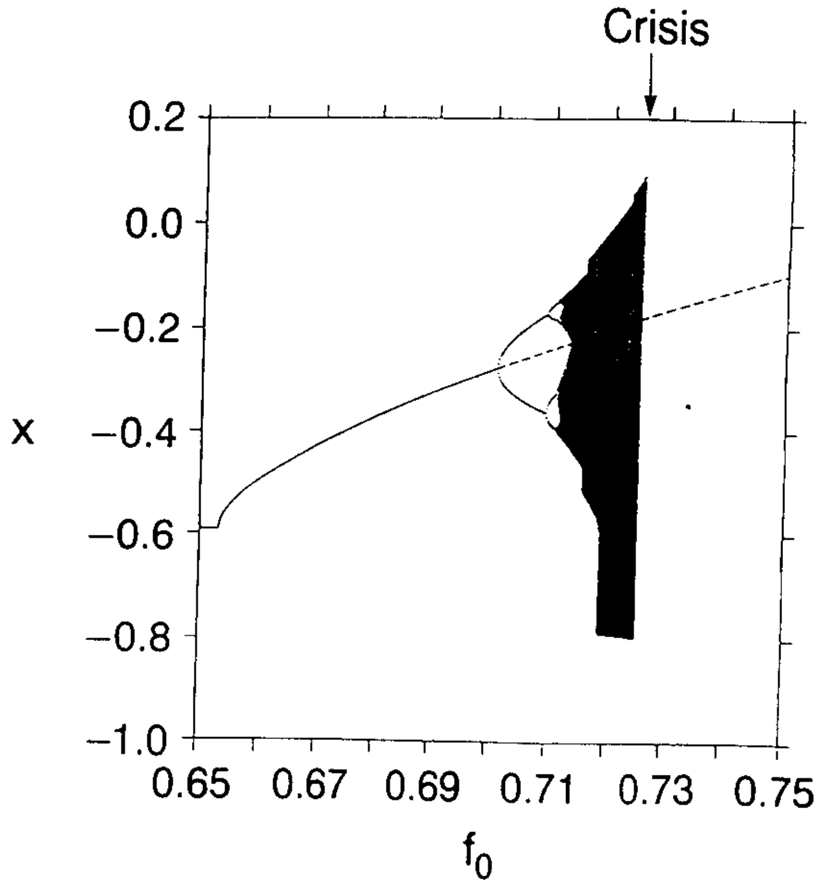

$$\ddot{x} + \nu \dot{x} + x - x^3 = f_0 \sin t$$

$$\nu = 0.5 \qquad t_n = 2n\pi$$

Crisis and Underlying Mechanism

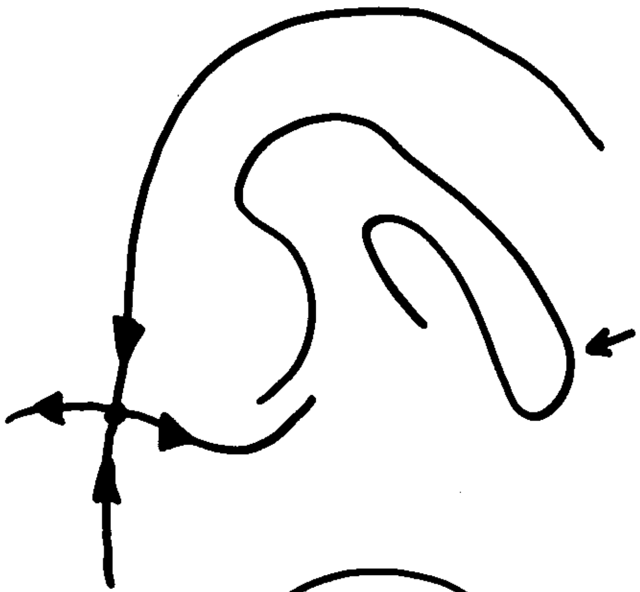

On the surface of sectio

Model of the Wave

$$W(t) = f(t)\left[1 + \epsilon_a g(t)\right] \sin\phi(t)$$

$$\frac{d\phi(t)}{dt} = \Omega + \epsilon_p h(t)$$

$$\langle h(t) \rangle = \langle g(t) \rangle = 0$$

$$\langle h^2(t) \rangle = \langle g^2(t) \rangle = 1$$

$f(t)$: slowly varying amplit.

$g(t)$: Amplitude irregularities

$h(t)$: phase irregularities

$f(t) = f_0$, $\epsilon_a = \epsilon_p = 0$ give periodic wave.

Models of Irregularities

Amplitude

$\sim g(t)$

Duffing Attractor

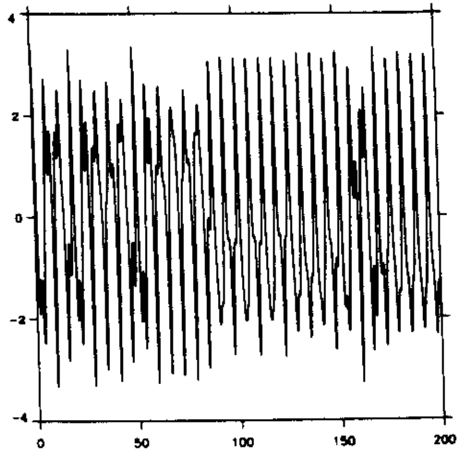

phase

$\sim h(t)$

Rössler Attractor

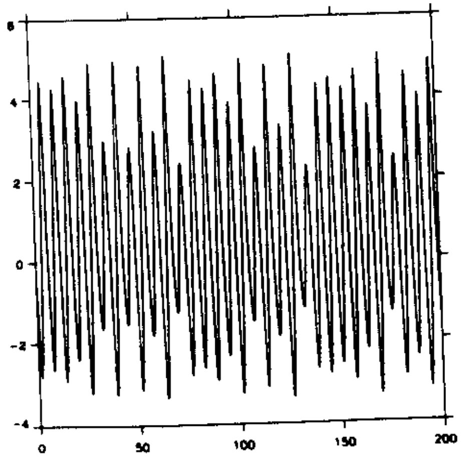

Control with Prediction

Assume that at time t_n we know $W(t)$ for t up to $\sim t_n + \frac{2\pi}{\Omega}$ from observing the sea surface

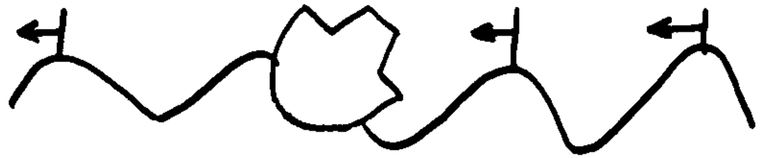

know what is coming at us.

$$\ddot{X} + \nu \dot{X} + \frac{\partial V(x)}{\partial x} = W(t) + C(t)$$

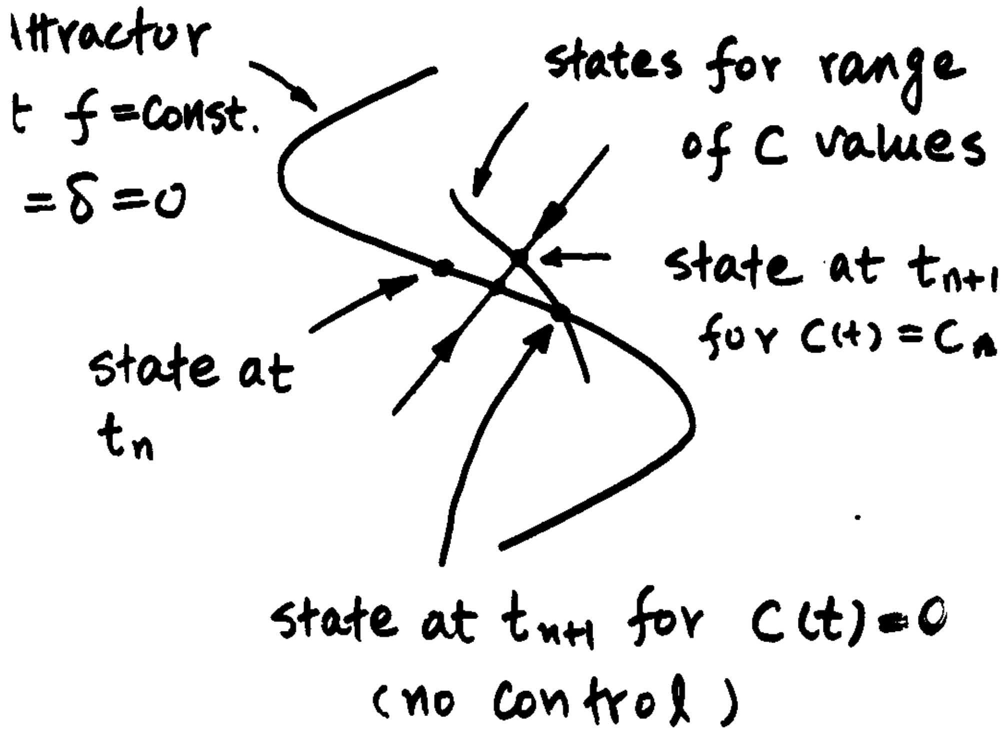

Using knowledge of the regular situation to control the irregular situation.

Controlling Crisis with Increas. Wave Amplitude

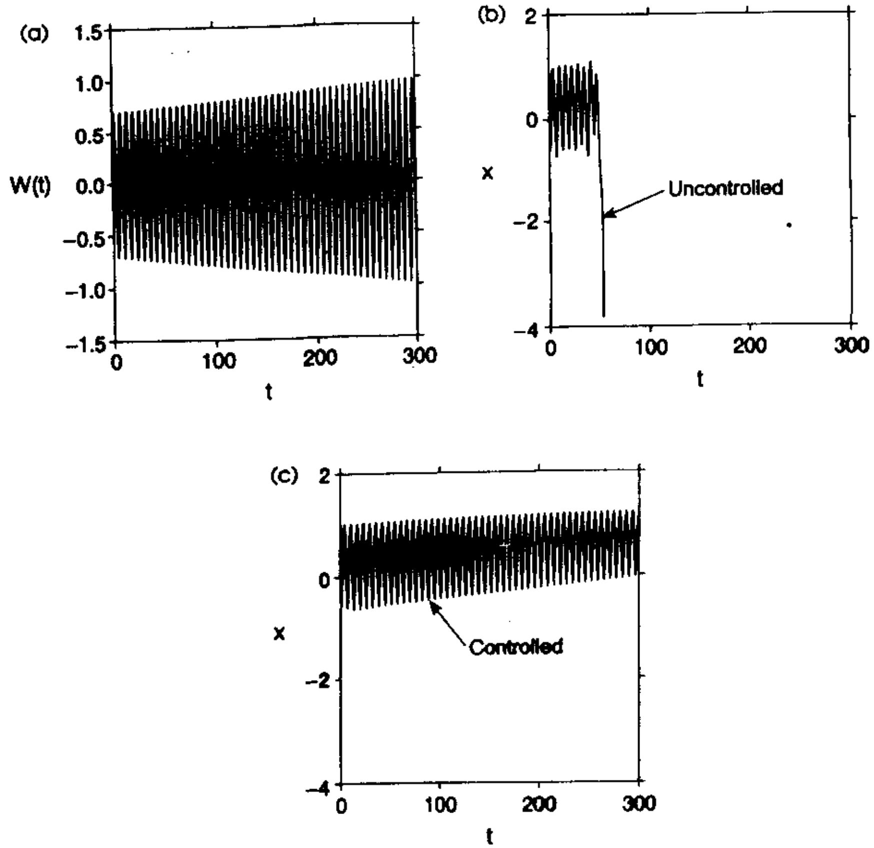

Controlling Amplitude Irregularity

Induced Crisis (I)

$f_0 = 0.72 < f_{crisis}$

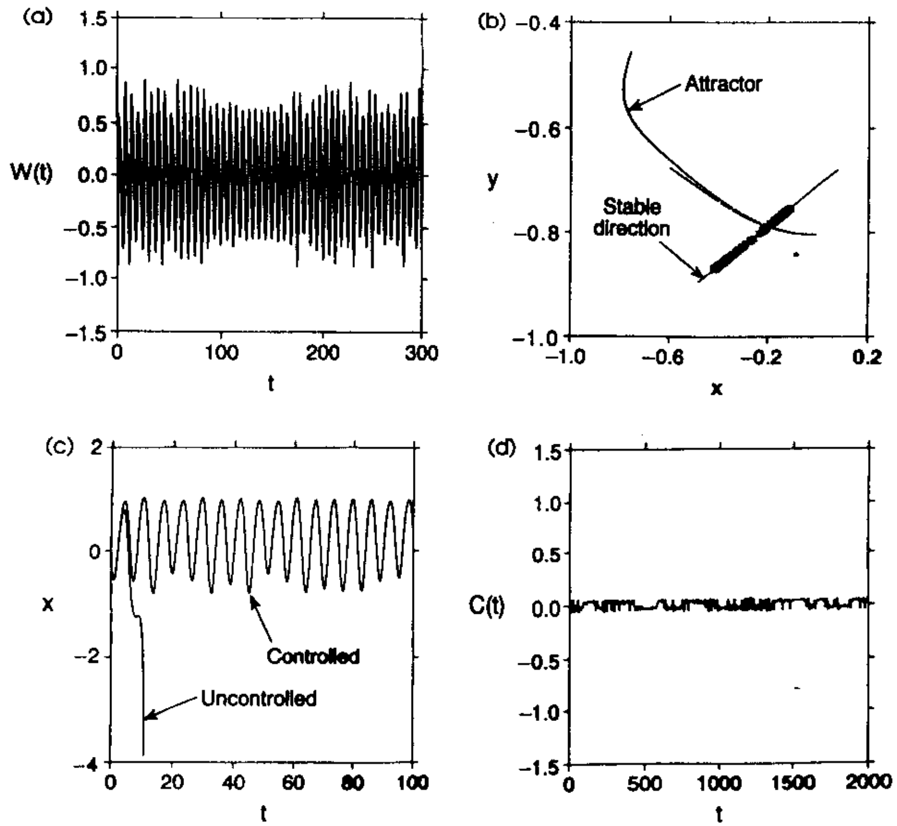

Controlling Amplitude Irregularity

Induced Crisis (II)

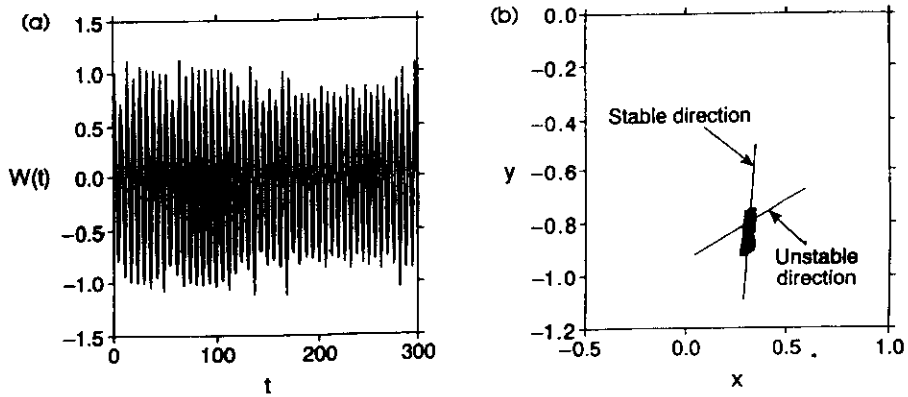

$f_0 = 0.9$

$> f_{crisis}$

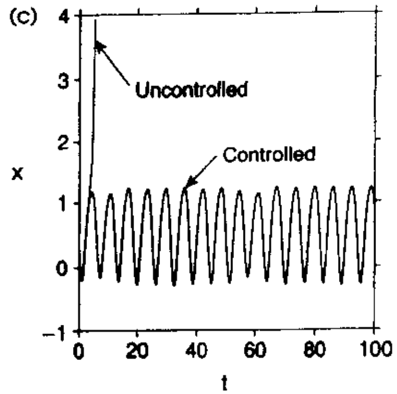

Surface of Section When $\epsilon_p \neq 0$

$$W(t) = f(t)\left[1 + \epsilon_a\, g(t)\right] \sin\phi(t)$$

$$\frac{d\phi(t)}{dt} = \Omega + \epsilon_p\, h(t)$$

$$\frac{d}{dt}\left[\phi(t) - \Omega t\right] = \epsilon_p\, h(t)$$

$$\phi(t_n) = 2n\pi \quad \text{not} \quad t_n = \frac{2\pi}{\Omega} n$$

Wave with phase Irregularity

$\phi(t)$ drifts due to irregularity

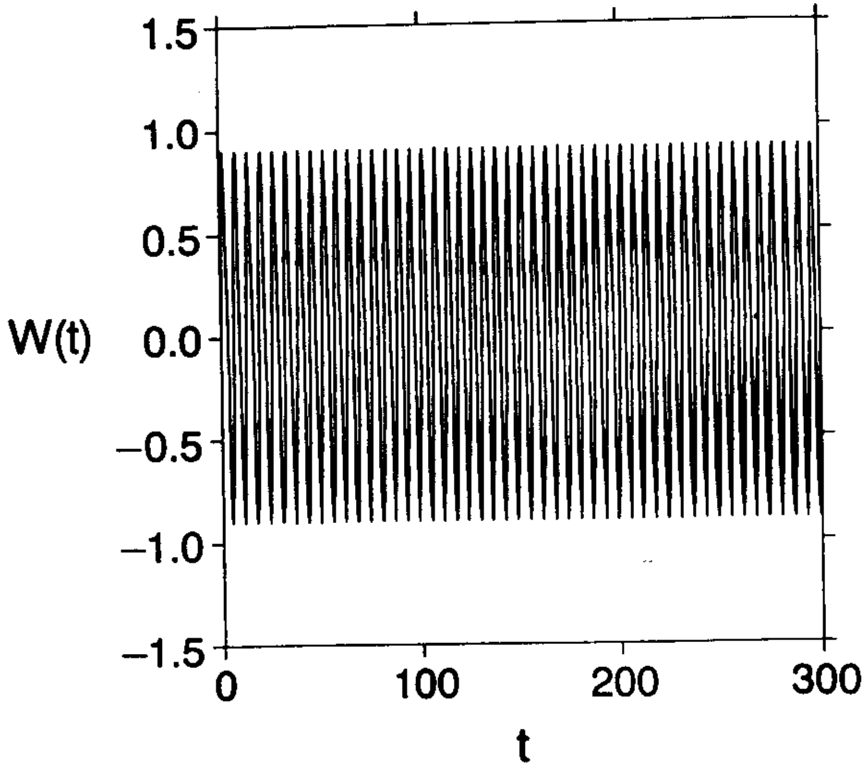

Fig. 6

$t_n = 2n\pi$

$\phi(t_n) = 2n\pi$

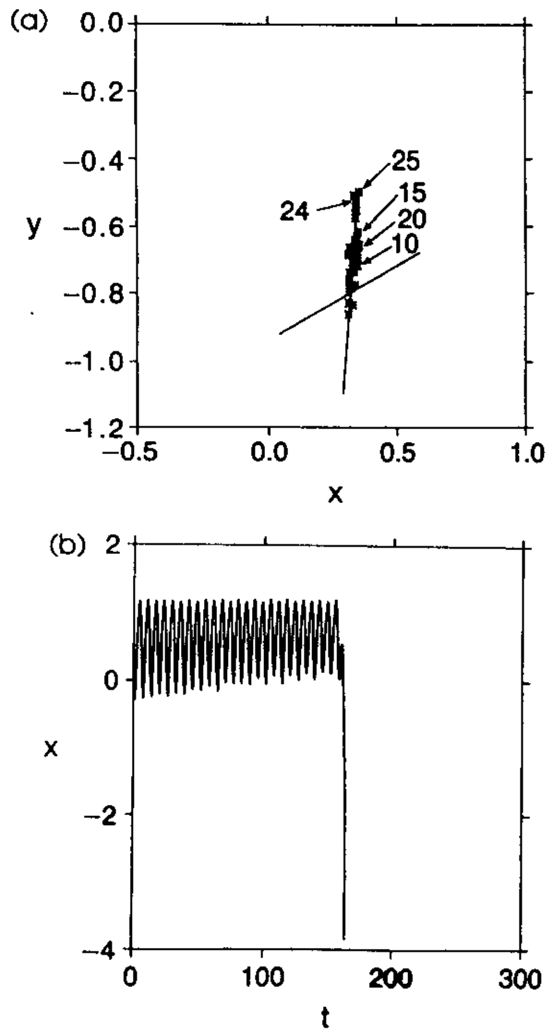

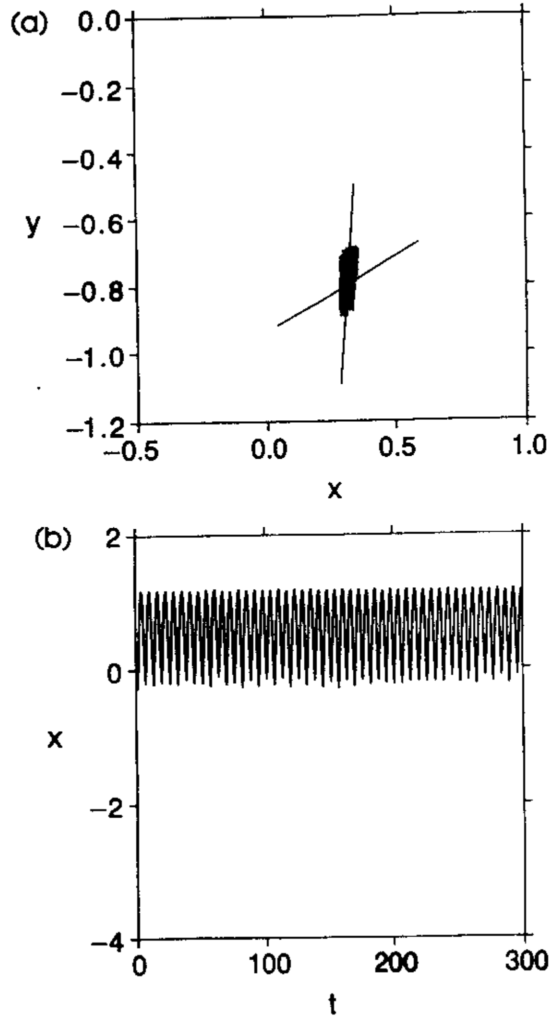

Effect of Imperfect Prediction

$$g(t) = \frac{(1-\gamma)\, g_o(t) + \gamma\, g_u(t)}{\sqrt{(1-\gamma)^2 + \gamma^2}}$$

$\gamma \leq 0.06 \qquad \langle T_{survival} \rangle \geqslant 400$

$\gamma = 0.07 \qquad \langle T_{survival} \rangle \approx 100$

$\gamma = 0.08 \qquad \langle T_{survival} \rangle \approx 30$

$\gamma = 0.10 \qquad \langle T_{survival} \rangle \approx 20$

$\gamma = 0.30 \qquad \langle T_{survival} \rangle \approx 10$

$\gamma = 1.0 \qquad \langle T_{survival} \rangle \approx 2$

Eliminating Chaos-induced Uncertainties with Control in the Cargo Transfer problem

The Model

Double Pendulum

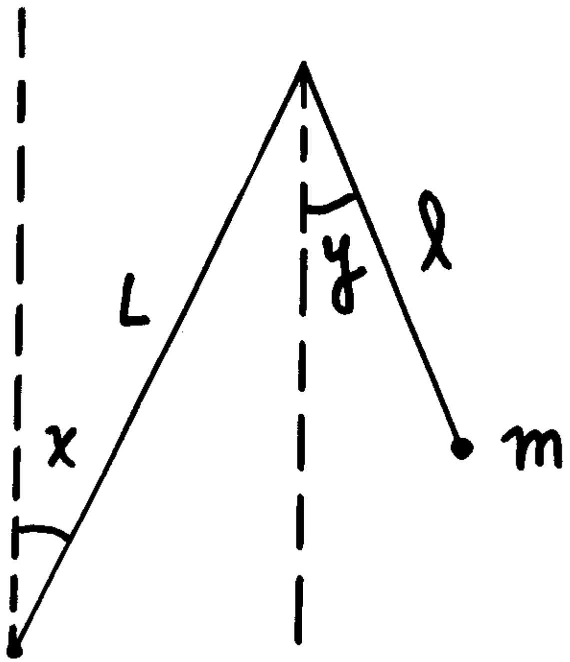

m is not affecting the motion of the base pendulum.

Equations of Motion

$$\ddot{y} + \mu(\dot{x} + \dot{y}) + R\cos(x+y)\,\ddot{x} - R\sin(x+y)\,\dot{x}^2 = -\eta^2 \sin y$$

$$\ddot{x} + \nu\dot{x} + w^2(x - \alpha x^3) = W(t)$$

μ. friction

$R = \dfrac{L}{\ell} > 1$

$\eta^2 = \dfrac{g}{\ell}$; η: eigenfrequency of oscillation of m when $\dot{x} = 0$, $x = 0$.

Response Dynamics

Restricting to Small wave
$f_o < 0.5$

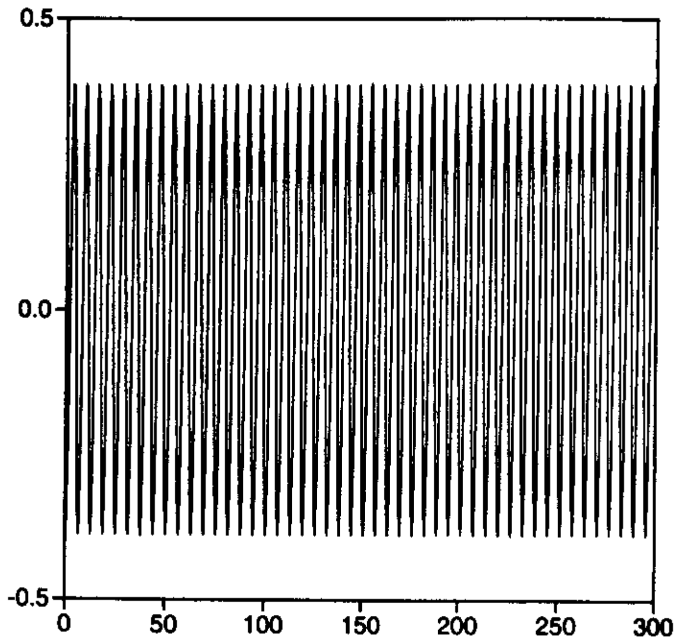

x versus t

$$\ddot{y} + \mu(\dot{x} + \dot{y}) + R\cos(x+y)\,\ddot{x} - R\sin(x+y)\,\dot{x}^2 = -\eta^2 \sin y$$

$R = 1.5$, $\eta^2 = \frac{1}{3}$, $\epsilon_a = \epsilon_p = 0.0$

Bifurcation Diagrams (I)

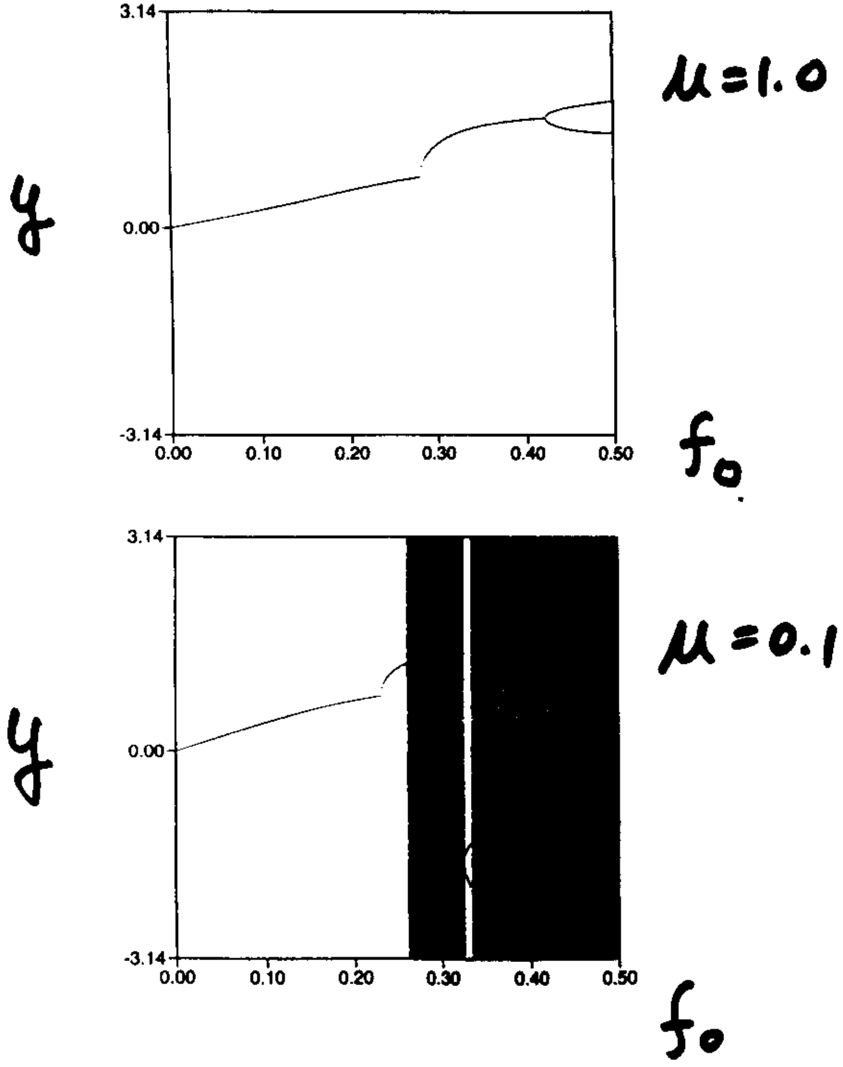

Bifurcation Diagrams (II)

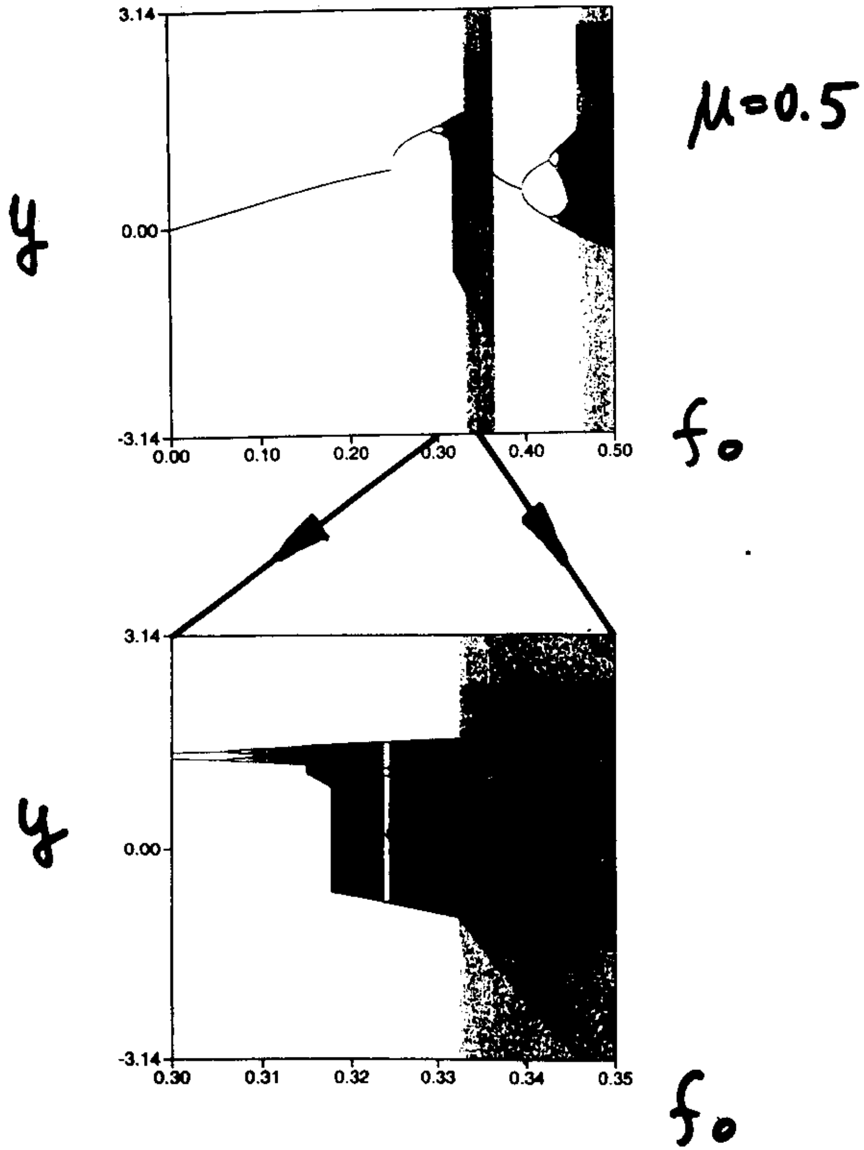

Response of the Mass

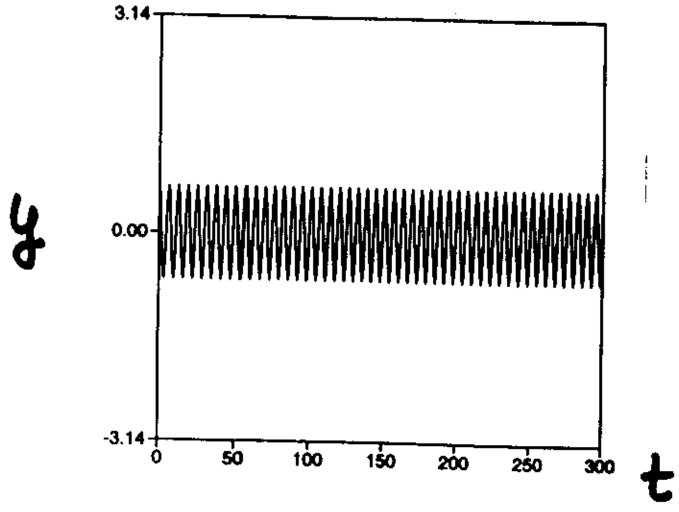

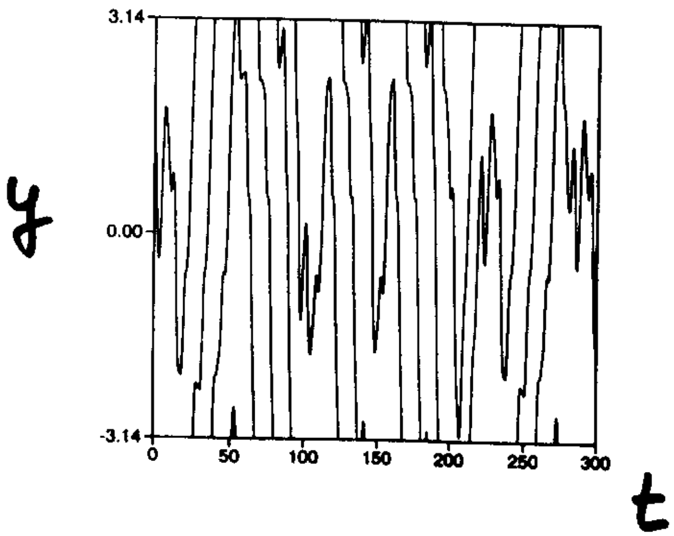

Response of the Mass

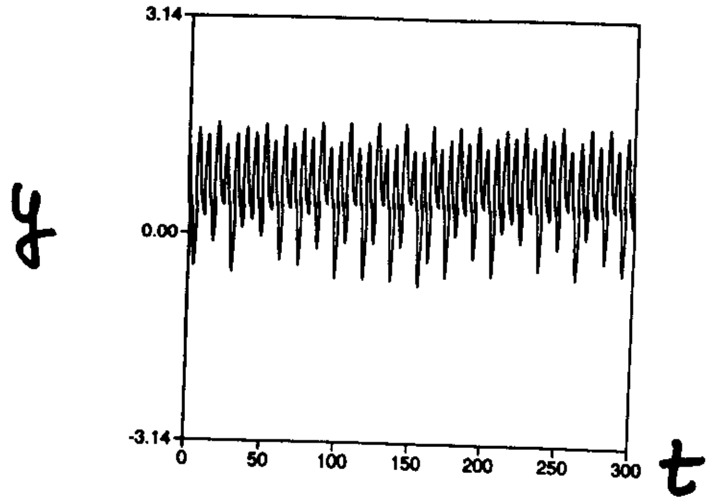

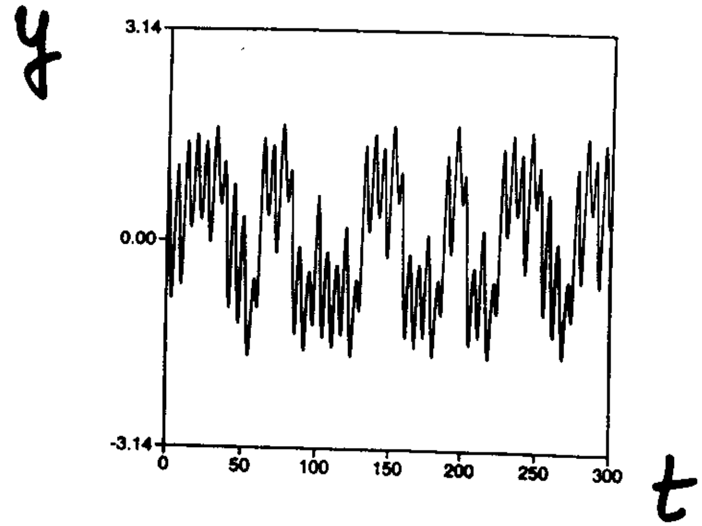

$$\underset{\sim}{Z}_{n+1} = \underset{\sim}{F}(\underset{\sim}{Z}_n, P) + (\text{Irreg.})$$

Ramping wave

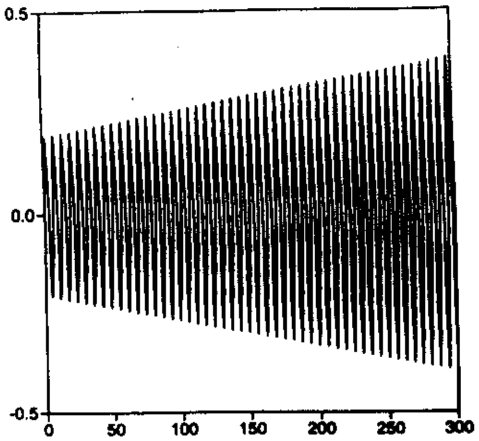

Response of the Mass

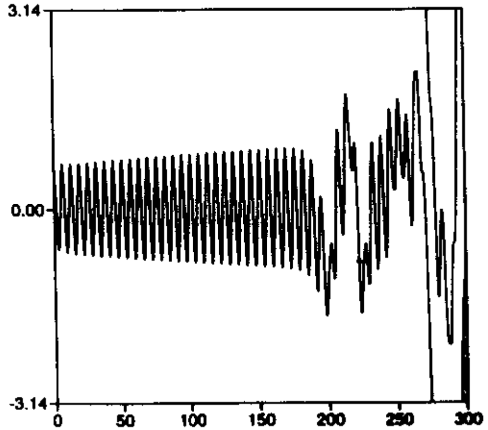

Controlled response

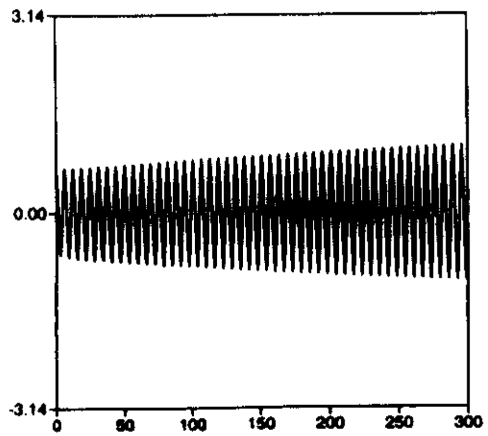

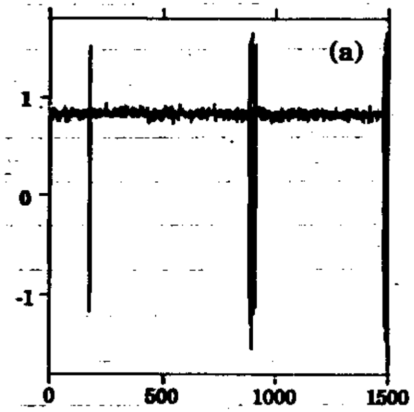

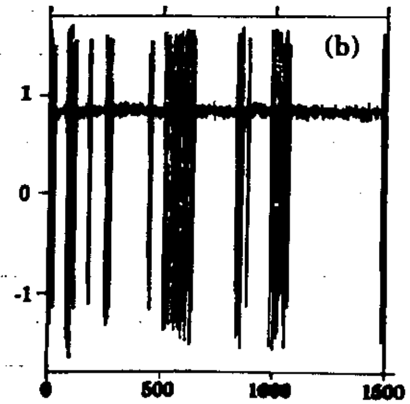

Response Control

- $$\ddot{y} + \mu(\dot{x} + \dot{y}) + \frac{L}{l}\cos(x+y)\ddot{x} - \frac{L}{l}\sin(x+y)\dot{x}^2 = -\eta^2 \sin y$$

- $$\ddot{y} + \mu(\dot{x} + \dot{y}) + \frac{L}{l + \Delta l(t)}\cos(x+y)\ddot{x} - \frac{L}{l + \Delta l(t)}\sin(x+y)\dot{x}^2 = -\eta^2 \sin y$$

$$\ddot{y} + \mu(\dot{x} + \dot{y}) + \frac{R}{1 + \frac{\Delta l(t)}{l}}\cos(x+y)\ddot{x} - \frac{R}{1 + \frac{\Delta l(t)}{l}}\sin(x+y)\dot{x}^2 = -\eta^2 \sin y$$

Let $C(t) = \dfrac{\Delta l(t)}{l}$

Control Method

$z = (y, \dot{y})$ $\qquad -C_0 \le C(t) \le C_0$

$C(t) = C_n$ for

$t_n \le t \le t_{n+1}$

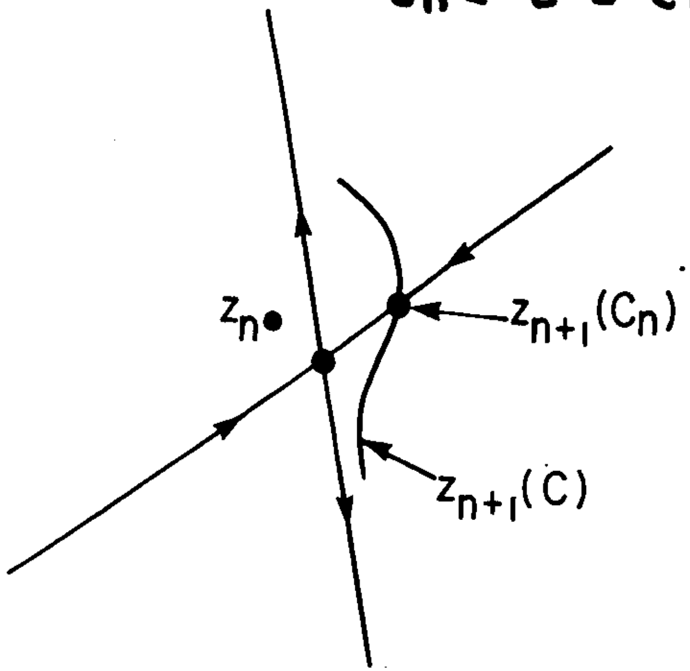

Fig. 2

Control with Prediction

Assume that at time t_n we know $W(t)$ for t up to $\sim t_n + \frac{2\pi}{\Omega}$ from observing and predicting the sea surface

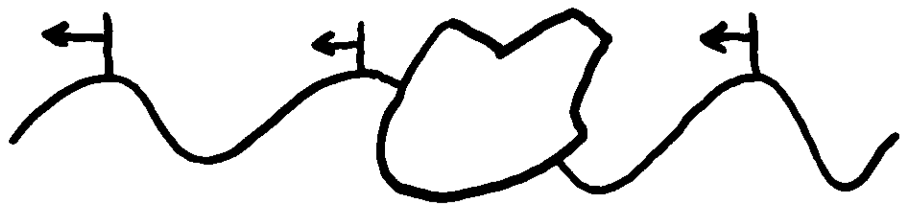

Wave

$f_0=0.34$

$\epsilon_a=0.05$ $\epsilon_p=0$

Uncontrolled orbit

Controlled orbit

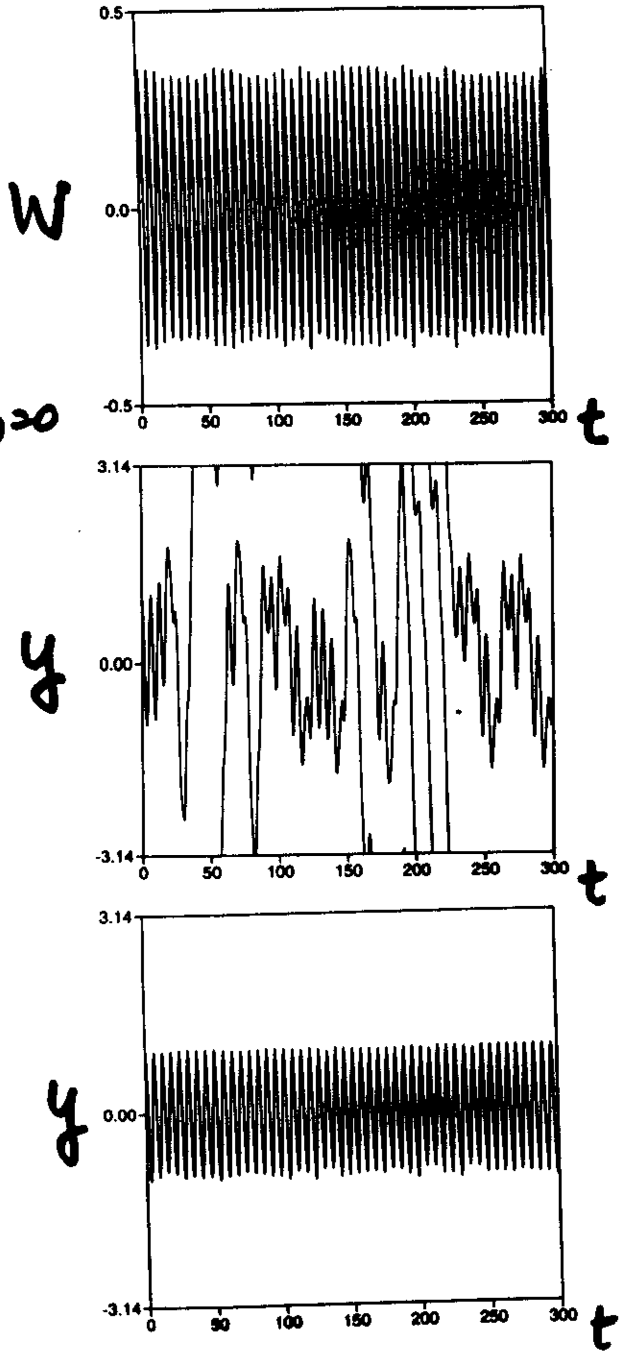

Wave

$f_0=0.34$

$\epsilon_a=0$ $\epsilon_p=0.05$

uncontrolled

Controlled

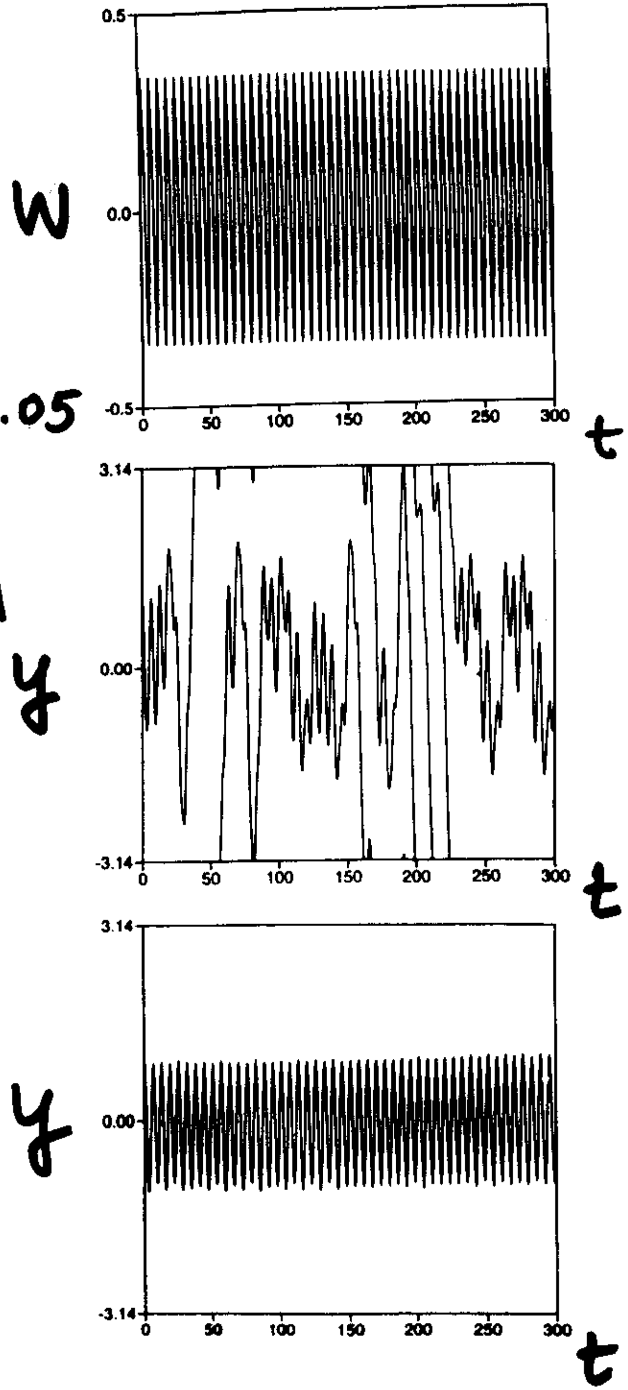

Summary

$f_0 : 0.2 \rightarrow 0.4$

$\epsilon_a = 0.1$

$\epsilon_p = 0.05$

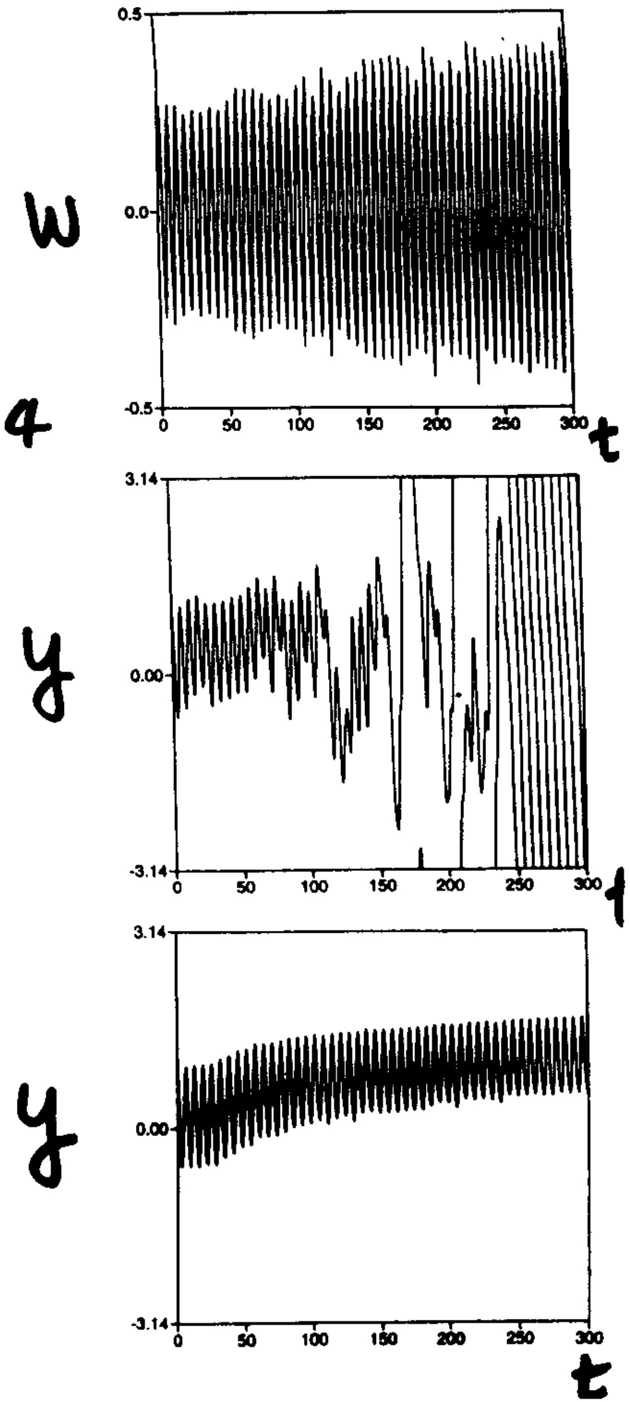

Two sources of uncertainty:

- Chaotic response.
- Abrupt changes in chaotic attractor as parameter drifts.

Using control one can eliminate these problems and convert the system to regular behavior.

Controlling Chaos in High Dimensions

Theory & Experiments

M. DING

Florida Atlantic Univ.

Coworkers:

W. Yang (FAU)
V. In (GA Tech)
W. L. Ditto (GA Tech)
M. Spano (NSWC)
B. Gluckman (NSWC)

Sponsor: ONR

GOAL

- General: Modify the dynamics of a chaotic process to improve performance by using small controls.
- Specific: Develope a high dimensional chaos control method using time series data that is effective, robust against noise and easy to implement in experiments. We assume no model or equations of motion for the system.

Main Results

- Derive explicit control laws for time series produced by maps.
- Introduce simple ways to extract a map-generated time series from a continuous-time series.
- Illustrate the method with two numerical examples.
- Present results on the control of chaos in a physical experiment.

The Method

Assume that the system is described by

$$\underset{\sim}{X}_{n+1} = \underset{\sim}{F}(\underset{\sim}{x}_n, p)$$

$\underset{\sim}{x}_n \in \mathbb{R}^k$, chaotic when $p = \bar{p}$

$x = h(\underset{\sim}{x})$ is the scalar meas.

Reconstructed vector

$$\underset{\sim}{z}_n = \begin{pmatrix} z_n^{(1)} \\ z_n^{(2)} \\ \vdots \\ z_n^{(m)} \end{pmatrix} = \begin{pmatrix} x_{n-m+1} \\ x_{n-m+2} \\ \vdots \\ x_n \end{pmatrix}$$

The discrete map for $\underset{\sim}{z}_n$ is

$$\underset{\sim}{z}_{n+1} = \underset{\sim}{G}(\underset{\sim}{z}_n, p_{n-m+1}, \cdots, p_n)$$

Assume $\underset{\approx}{A}$ has u unstable directions and s stable directions ($s+u=m$) with eigenvalues λ_i satisfying $|\lambda_1| > |\lambda_2| \cdots > |\lambda_u| > 1$

$> |\lambda_{u+1}| > |\lambda_{u+2}| \cdots > |\lambda_m|$

Let $\underset{\sim}{e}_i$ be corresponding eigen vectors. A possible control strategy is to design perturb. to push $\underset{\sim}{z}_{n+1}$ into the stable subspace $\underset{\sim}{e}_{u+1}, \cdots, \underset{\sim}{e}_m$.
Careful consideration rejects it

Note:

$$\underset{\sim}{z}_{n+1} = \begin{pmatrix} z_{n+1}^{(1)} \\ z_{n+1}^{(2)} \\ \vdots \\ z_{n+1}^{(m)} \end{pmatrix} = \begin{pmatrix} x_{n-m+2} \\ x_{n-m+3} \\ \vdots \\ x_{n+1} \end{pmatrix}$$

So in component form

$$\underset{\sim}{z}_{n+1} = \underset{\sim}{G}(\underset{\sim}{z}_n, P_{n-m+1}, \cdots, P_n)$$

is

$$\begin{pmatrix} z_{n+1}^{(1)} \\ z_{n+1}^{(2)} \\ \vdots \\ z_{n+1}^{(m)} \end{pmatrix} = \begin{pmatrix} z_n^{(2)} \\ z_n^{(3)} \\ \vdots \\ g(\underset{\sim}{z}_n, P_{n-m+1} \cdots, P_n) \end{pmatrix}$$

The Method (Continued)

Consider stabilizing a fixed pt

$$\bar{\underset{\sim}{X}}(\bar{p}) = \underline{F}(\bar{\underset{\sim}{X}}(\bar{p}), \bar{p})$$

in the original phase space.

$$\bar{\underset{\sim}{z}}(\bar{p}) = \underset{\sim}{G}(\bar{\underset{\sim}{z}}, \bar{p}, \bar{p}, \cdots p)$$

in the reconstructed space.

Linearize around the f.p.

$$\underset{\sim}{z}_{n+1} - \bar{\underset{\sim}{z}} = \underset{\approx}{A}(\underset{\sim}{z}_n - \bar{\underset{\sim}{z}}) + \underset{\sim}{B}^{(m)}(p_{n-m+1} - \bar{p}) + \underset{\sim}{B}^{(m-1)}(p_{n-m+1} - \bar{p}) + \cdots + \underset{\sim}{B}^{(1)}(p_n - \bar{p})$$

$$\underset{\approx}{A} = \begin{pmatrix} 0 & 1 & 0 & \cdots & 0 \\ 0 & 0 & 1 & \cdots & 0 \\ \vdots & \vdots & \vdots & & \vdots \\ 0 & 0 & 0 & \cdots & 1 \\ a^{(m)} & \cdots & \cdots & & a^{(1)} \end{pmatrix}, \quad \underset{\sim}{B}^{(i)} = \begin{pmatrix} 0 \\ 0 \\ \vdots \\ 0 \\ b^{(i)} \end{pmatrix}$$

In terms of the measured variable x, the linear eq. near the fixed point can be rewritten as

$$\delta x_{n+1} = a^{(m)} \delta x_{n-m+1} + a^{(m-1)} \delta x_{n-m+} + \cdots + a^{(1)} \delta x_n + b^{(m)} \delta p_{n-m+1} + b^{(m-1)} \delta p_{n-m+2} + \cdots + b^{(1)} \delta p_n$$

$$= \sum_{i=1}^{m} a^{(i)} \delta x_{n-i+1} + \sum_{i=1}^{m} b^{(i)} \delta p_{n-i+1}$$

The values of $a^{(i)}$, $b^{(i)}$ need to be estimated from the time series.

The Method (Continued)

Introduce expanded phase space

$$\mathbf{Y}_n = \begin{pmatrix} \mathbf{z}_n \\ p_{n-m+1} \\ p_{n-m+2} \\ \vdots \\ p_{n-1} \end{pmatrix}_{(2m-1)\times 1}$$

So & Ott 1995

Linear dynamics around the fixed point

$$\mathbf{Y}_{n+1} - \bar{\mathbf{Y}} = \tilde{\mathbf{A}}(\mathbf{Y}_n - \bar{\mathbf{Y}}) + \tilde{\mathbf{B}}(p_n - \bar{p})$$

$$\tilde{\mathbf{A}} = \begin{pmatrix} \mathbf{A} & \mathbf{B}^{(m)} & \mathbf{B}^{(m-1)} & \cdots & \mathbf{B}^{(2)} \\ \mathbf{0} & 0 & 1 & \cdots & 0 \\ \vdots & \vdots & \vdots & \vdots & \vdots \\ \mathbf{0} & 0 & 0 & \cdots & 1 \\ \mathbf{0} & 0 & 0 & \cdots & 0 \end{pmatrix}$$

The Method (Continued)

Assume that the fixed point has u unstable directions.

To control, we wish to choose the values of $p_n, p_{n+1}, \cdots, p_{n+u}$ to place $\delta\mathbf{Y}_{n+u} = \mathbf{Y}_{n+u} - \bar{\mathbf{Y}}$ in the stable subspace of $\tilde{\mathbf{A}}$. The control law is

$$p_n = \bar{p} - \left(\sum_{k=1}^{u} \frac{(\lambda_k)^u}{(\mathbf{V}_k^T \mathbf{B}) \prod_{\substack{i=1 \\ i \neq k}}^{u} (\lambda_k - \lambda_i)} \mathbf{V}_k^T \right) \delta\mathbf{Y}_n$$

Note that $\lambda_1, \lambda_2, \cdots, \lambda_m$ are still eigenvalues of $\tilde{\underset{\approx}{A}}$. The corresponding eigenvectors are

$$\underset{\sim}{k}_i = \begin{pmatrix} \underset{\sim}{e}_i \\ 0 \\ \vdots \\ 0 \end{pmatrix}_{(2m-1)\times 1}.$$

It can be shown that the subspace of $\tilde{\underset{\approx}{A}}^{m-1}\underset{\sim}{k} = 0$ is $m-1$ dimensional and it provides the addition $m-1$ independent vectors to span the $2m-1$ dim space.

The stable subspace is spanned by $\underset{\sim}{k}_i$, $i = u+1, \cdots, 2m-1$.

Consider the contravariant unstable eigenvectors determined by

$$\tilde{\underset{\approx}{A}}^T \underset{\sim}{v}_i = \lambda_i \underset{\sim}{v}_i$$

$i = 1, 2, \cdots, u$. We can show that $\underset{\sim}{v}_i$ is orthogonal to the stable subspace of $\tilde{\underset{\approx}{A}}$. Namely,

$$\underset{\sim}{v}_i^T \cdot \underset{\sim}{k}_j = 0, \quad j = u+1, \cdots, 2m-1$$

By choosing values of p_n, $p_{n+1}, \cdots, p_{n+(u-1)}$ such that

$$\underset{\sim}{V}_1^T \, \delta \underset{\sim}{Y}_{n+u} = 0$$

$$\underset{\sim}{V}_2^T \, \delta \underset{\sim}{Y}_{n+u} = 0$$

$$\vdots$$

$$\underset{\sim}{V}_u^T \, \delta \underset{\sim}{Y}_{n+u} = 0$$

we place the deviation $\delta \underset{\sim}{Y}_{n+1}$ in the stable subspace of $\underset{\approx}{\tilde{A}}$.

Interspike Intervals as Discrete Time Series for Autonomous Sys.

$$x = h(\underset{\sim}{X}) = x_c \, , \quad \underset{\sim}{X} \in \mathbb{R}^k.$$

I_n : interspike interval

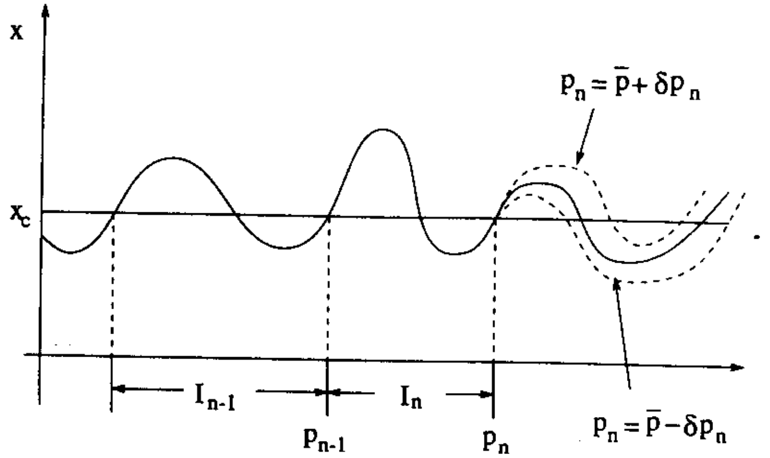

FIG. 1

defines a $k-1$ dimensional hyperplane in the original phase space.

Say that we parametrize the Poincaré surface of section by the variable $\underset{\sim}{Q}$. Then successive crossings of the section give rise to a Poincaré map

$$\underset{\sim}{Q}_{n+1} = \underset{\sim}{P}(\underset{\sim}{Q}_n)$$

The interval I_n is uniquely determined by $\underset{\sim}{Q}_n$, meaning that

$$I_n = \Phi(\underset{\sim}{Q}_n)$$

Spike Generation & Effect of Control

$\dot{\underset{\sim}{x}} = \underset{\sim}{F}_p(\underset{\sim}{x})$, $\underset{\sim}{x} \in \mathbb{R}^m$; $y(t) = h(\underset{\sim}{x}(t))$

e.g. $y(t) = x_1(t)$

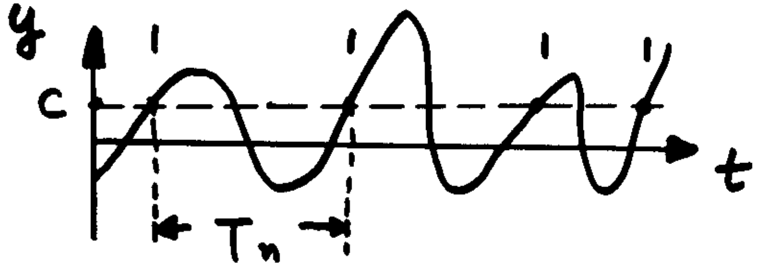

T_n: interspike interval; is also the time between successive piercings of surface section $y = h(\underset{\sim}{x}(t)) = c$ and $\dot{y} > 0$.

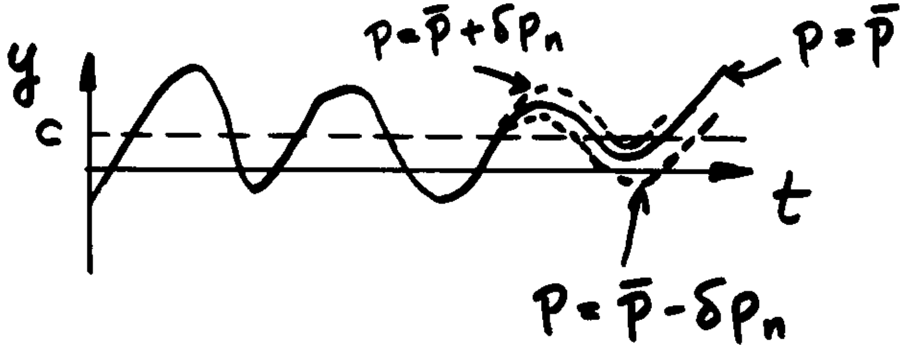

Untitled

Consider noiseless case

Poincaré surface of section in delay coordinate space

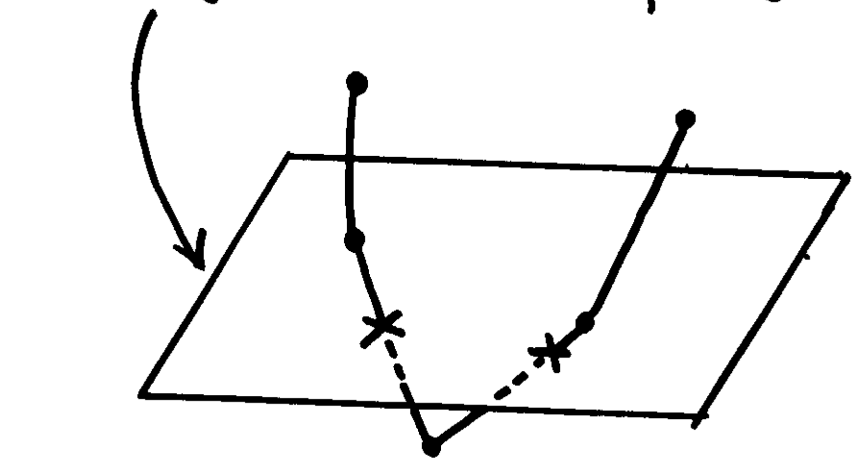

Due to discrete sampling, an error is introduced in the interpolation with the Poincaré surface of section.

Two Numerical Examples

- Nonautonomous system

$$\ddot{x}_1 + \gamma\dot{x}_1 + \alpha(x_1^3 - x_1) + \beta_1(x_1 - x_2) = P_1 \sin\omega t$$

$$\ddot{x}_2 + \gamma\dot{x}_1 + \alpha(x_2^3 - x_2) + \beta_2(x_2 - x_1) = P \sin\omega t$$

- Autonomous system

$$\begin{cases} \dot{x} = \dfrac{pw}{1+w^{10}} - 0.1x \\ \dot{y} = 0.1x - 0.2yz \\ \dot{z} = 0.2z(y-w) \\ \dot{w} = 0.2zw - 0.1w \end{cases}$$

Use ISIs for this system.

Coupled Duffing $x = x_1 + x_2$

$m = 4$

$u = 2$

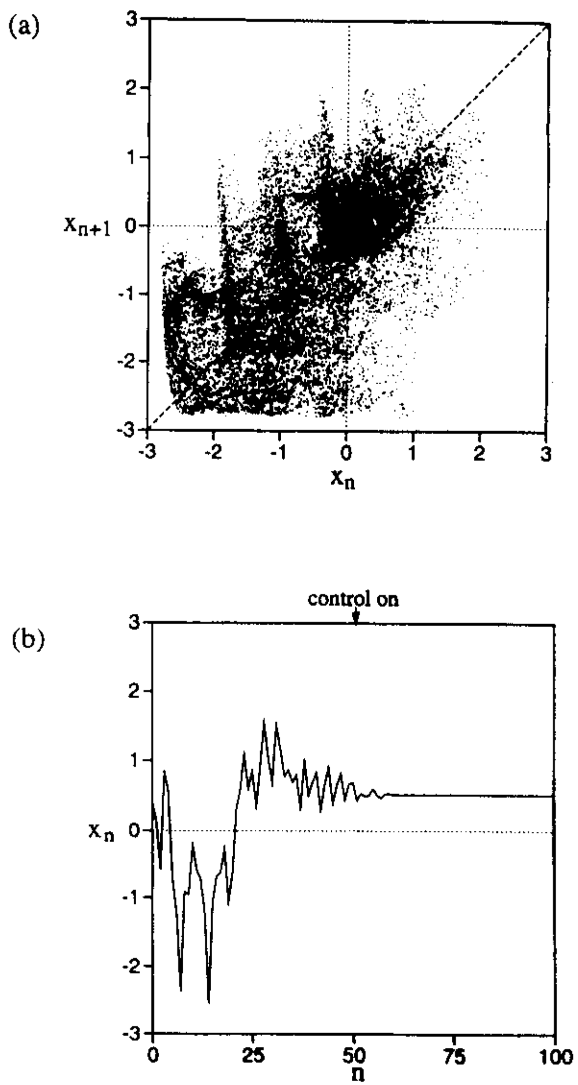

FIG. 2

Chemical Reaction Model

$m = 3$

$u = 1$

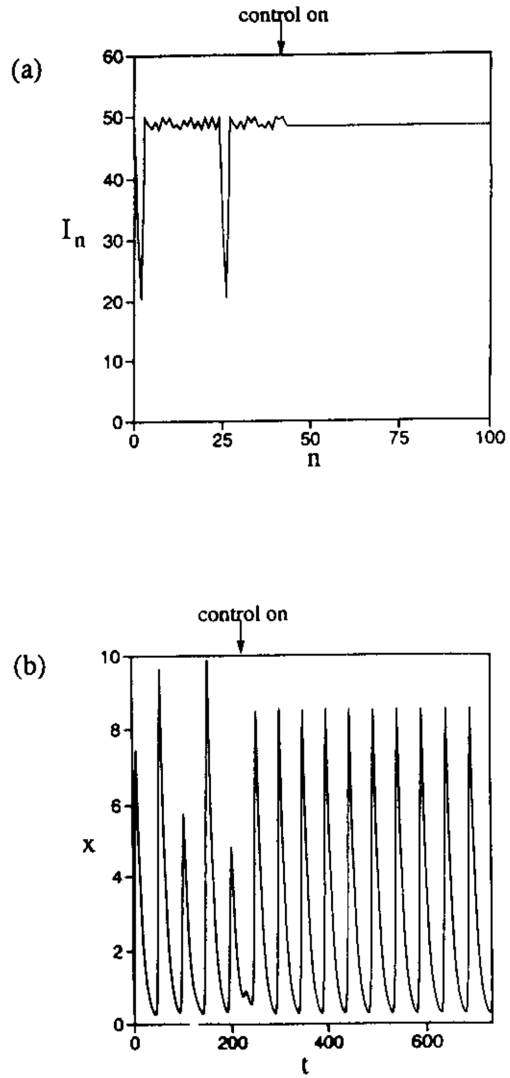

FIG. 3

Chemical Reaction Model

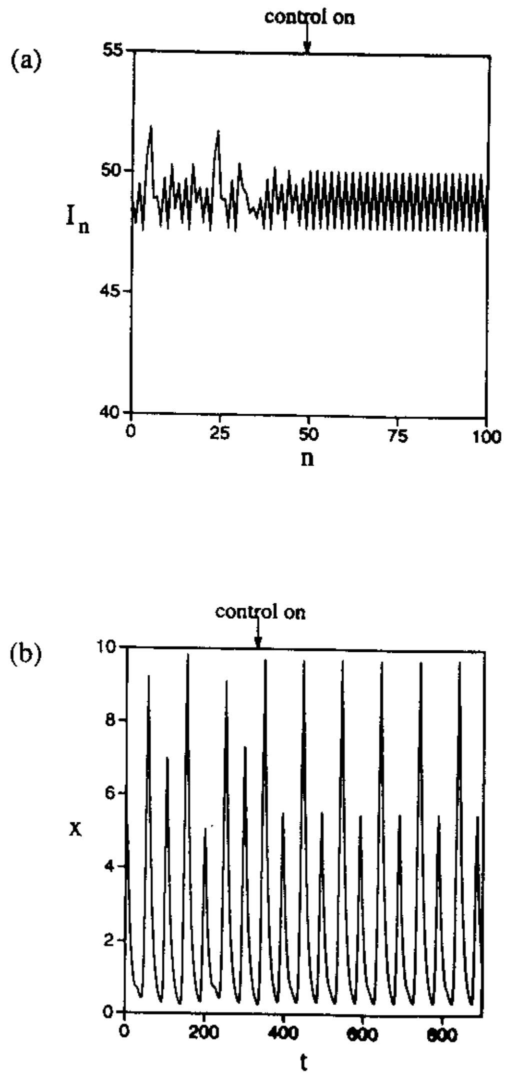

FIG. 4

Two Experimental Examples

1. A magnetoelastic Ribbon
2. A Coupled Duffing circuit

The Magnetoelastic Ribbon

Forcing: $H_0 + H_1 \sin \omega t$

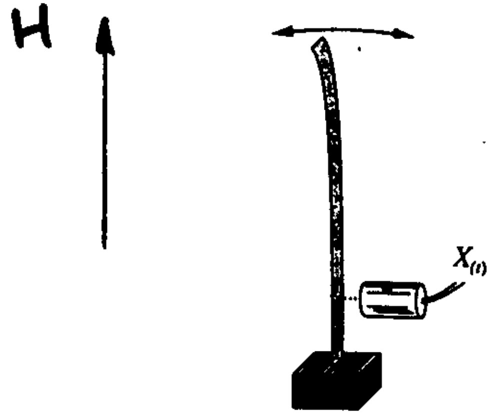

Sampled at $t_n = n \frac{2\pi}{\omega}$

Data from the Ribbon Experiment

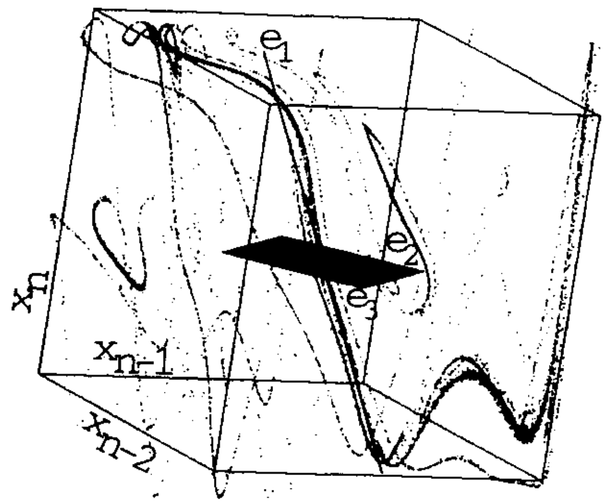

One unstable direction

FIG. 5

Control Result

Comparison with the OGY Method

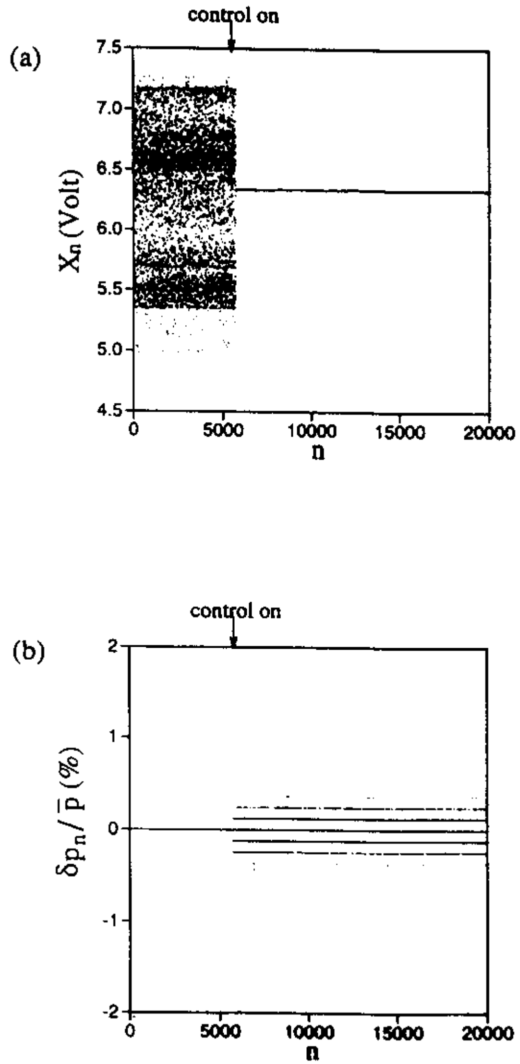

FIG. 6

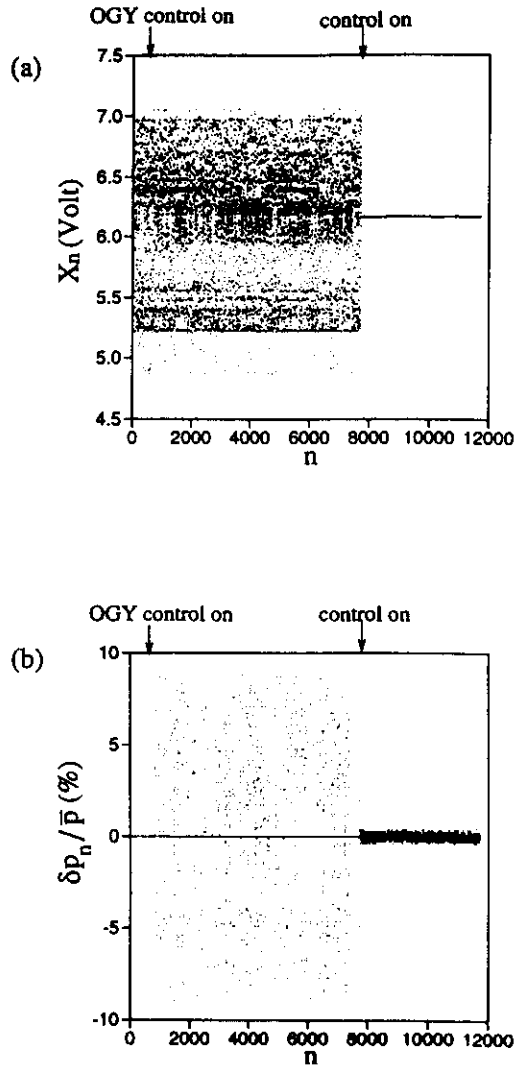

FIG. 7

Coupled Duffing circuit

Tracking Unstable periodic orbits in High Dimensions

u=2?

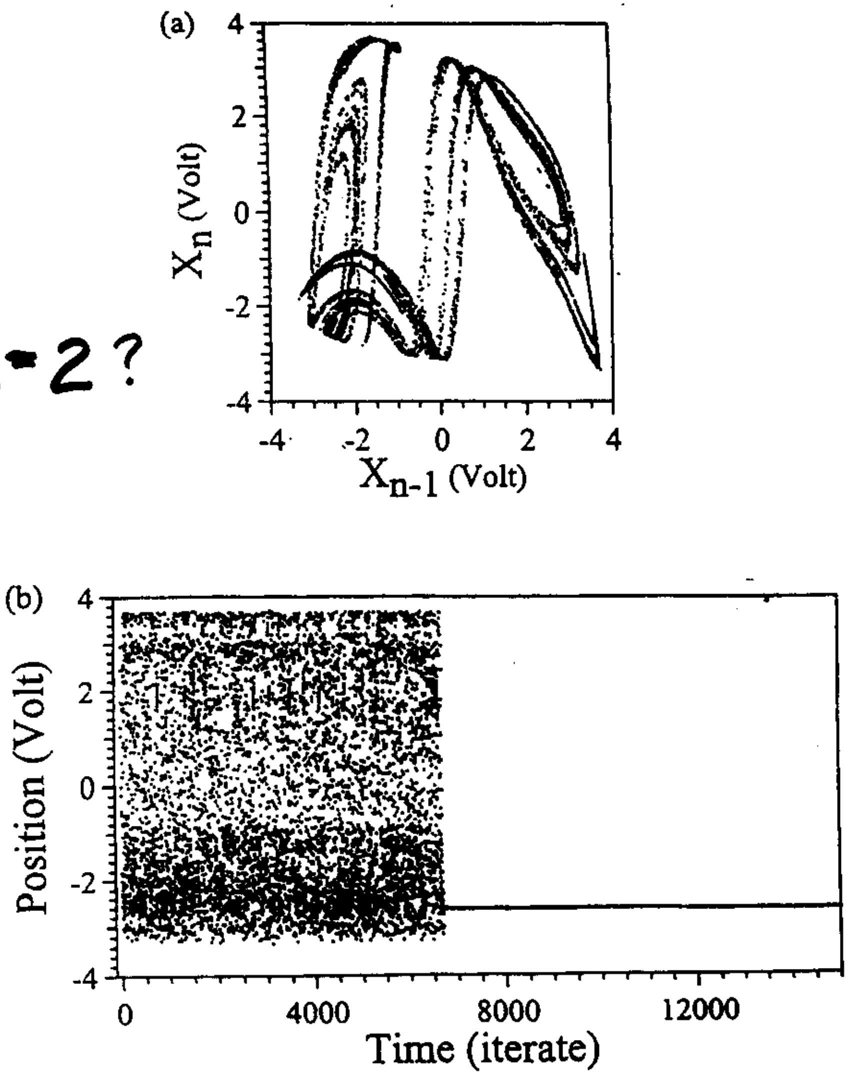

Fig 3 (a), (b)
In, Neff, Ditto, Ding, Yang, Spano and Gluckman

Why Tracking and How ?

- Real world systems are not situated in a static environment.
- You may want to start off when the orbit is stable and then lead the system to the desired operation range while maintaining control.
- Update the periodic orbit position to preserve small control character.
- Update $a^{(i)}$ and $b^{(i)}$.

Updating the Fixed Pt Position

$$X_{n+1} - \bar{X} = \sum_{i=1}^{m} a^{(i)} (X_{n-i+1} - \bar{X}) + \sum_{i=1}^{m} b^{(i)} (p_{n-i+1} - \bar{p})$$

Taking the time average over a history of n_{hist} such equations we have

$$\bar{X} = \langle X_n \rangle + g \langle \delta p_n \rangle$$

where

$$g = \frac{\sum_{i=1}^{m} b^{(i)}}{1 - \sum_{i=1}^{m} a^{(i)}}$$

Updating $a^{(i)}$ and $b^{(i)}$

Again we start with

$$x_{n+1} - \bar{x} = \sum_{i=1}^{m} a^{(i)} (x_{n-i+1} - \bar{x})$$

$$+ \sum_{i=1}^{m} b^{(i)} (p_{n-i+1} - \bar{p})$$

To get good estimates of $a^{(i)}$ and $b^{(i)}$ we need to keep the dynamics alive.

To do that we set a lower boundary for δp_i. I.e.

if $|\delta p_i| < \delta p_{min}$, $\delta p_i = 0$.

Example 1: The Hénon Map

$$\begin{cases} x_{n+1} = p - x_n^2 + 0.3 y_n \\ y_{n+1} = x_n \end{cases}$$

In terms of measured variable x we have

$$x_{n+1} = p - x_n^2 + 0.3 x_{n-1} .$$

For $m = 2$

$$\begin{pmatrix} x_n \\ x_{n+1} \end{pmatrix} = \begin{pmatrix} x_n \\ p - x_n^2 + 0.3 x_{n-1} \end{pmatrix}$$

The fixed pt is at

$$\bar{x} = \frac{-0.7 + \sqrt{0.49 + 4p}}{2}$$

Linearizing around $\bar{x}$ we get

$$\begin{pmatrix} \delta x_n \\ \delta x_{n+1} \end{pmatrix} = \begin{pmatrix} 0 & 1 \\ 0.3 & -2\bar{x} \end{pmatrix} \begin{pmatrix} \delta x_{n-1} \\ \delta x_n \end{pmatrix} + \begin{pmatrix} 0 \\ 1 \end{pmatrix} \delta p_n$$

$$\Rightarrow \quad a^{(1)} = -2\bar{x} = -2 \cdot \frac{-0.7 + \sqrt{0.49 + 4\bar{p}}}{2}$$

$$= 0.7 - \sqrt{0.49 + 4\bar{p}} \; ,$$

$$a^{(2)} = 0.3 \; , \quad b^{(1)} = 1, \quad b^{(2)} = 0$$

Updating fixed pt position but not $a^{(i)}$ and $b^{(i)}$

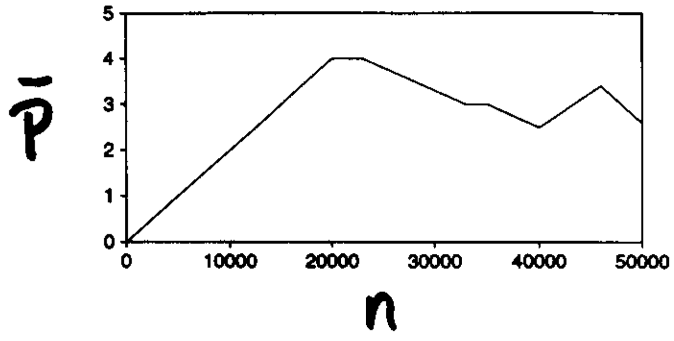

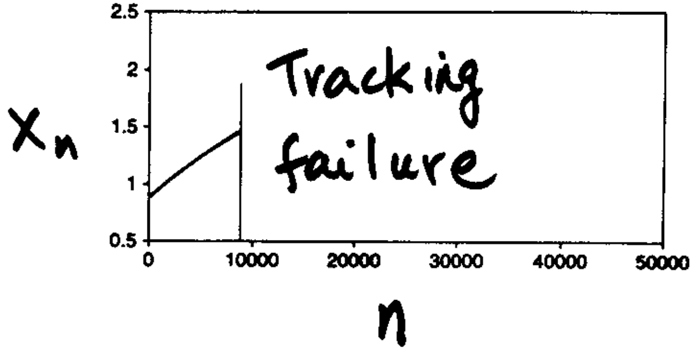

Updating both fixed point and $a^{(i)}$ and $b^{(i)}$

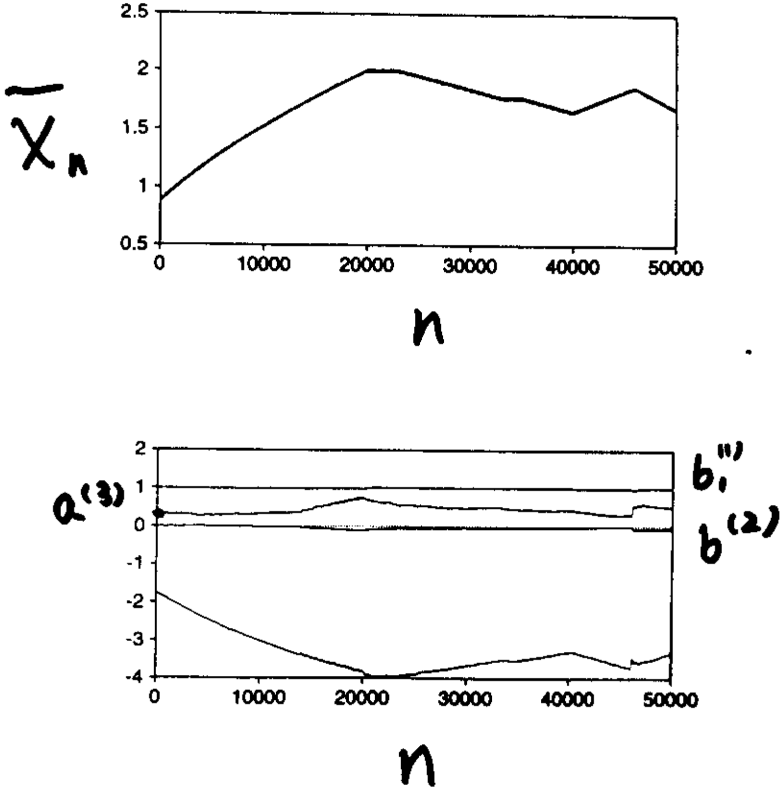

Example 2: The Chemical Model

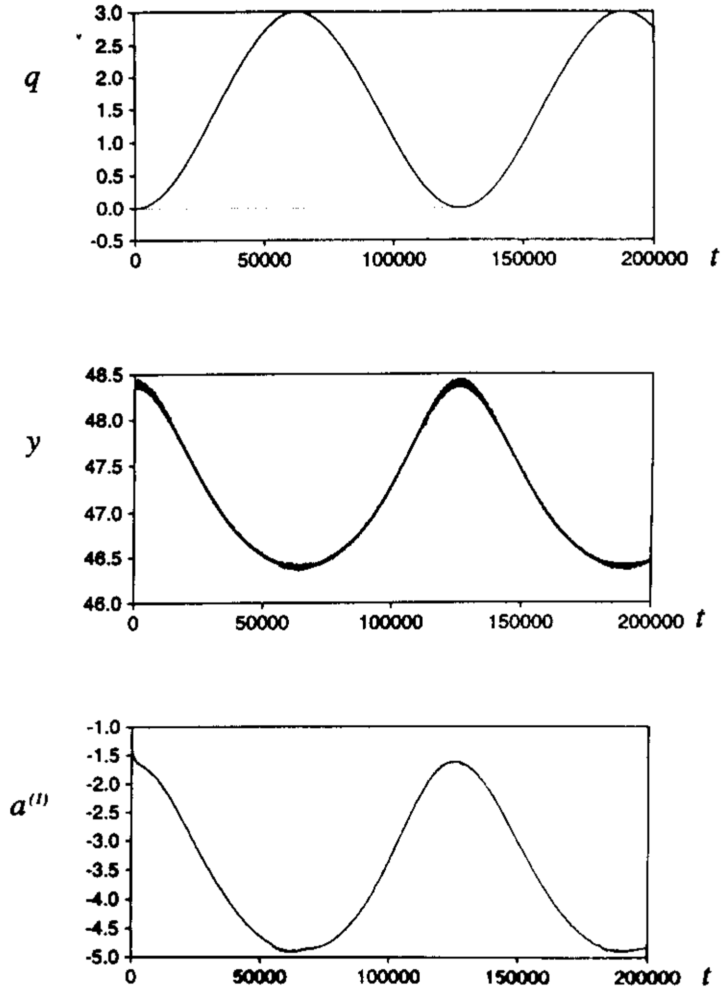

Example 3: The Coupled Duffing Oscillator

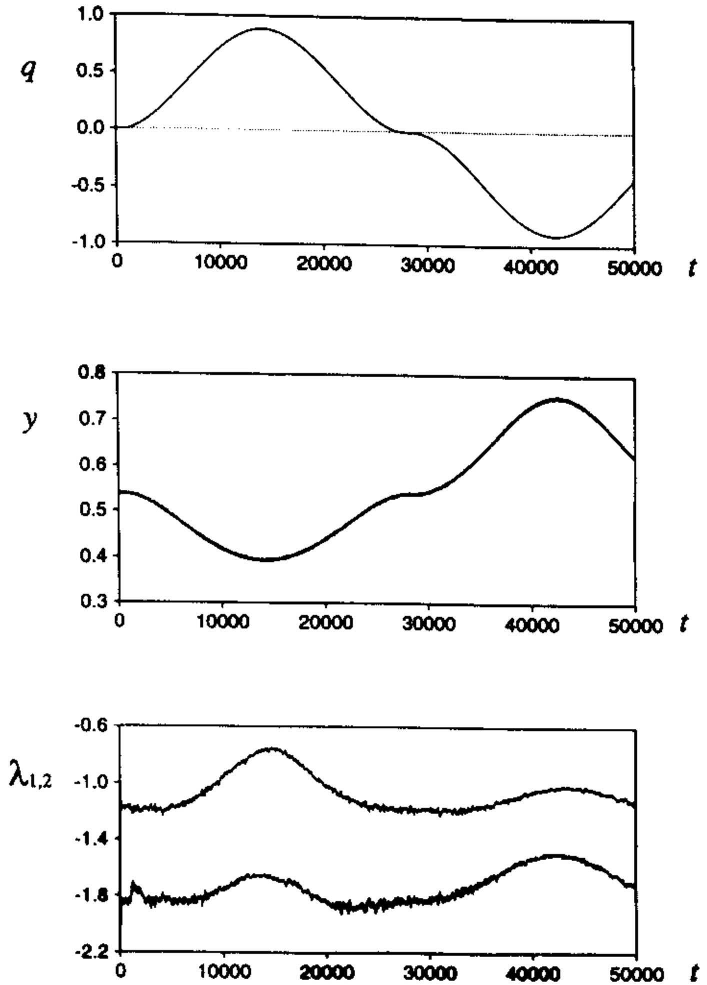

Coupled Duffing system

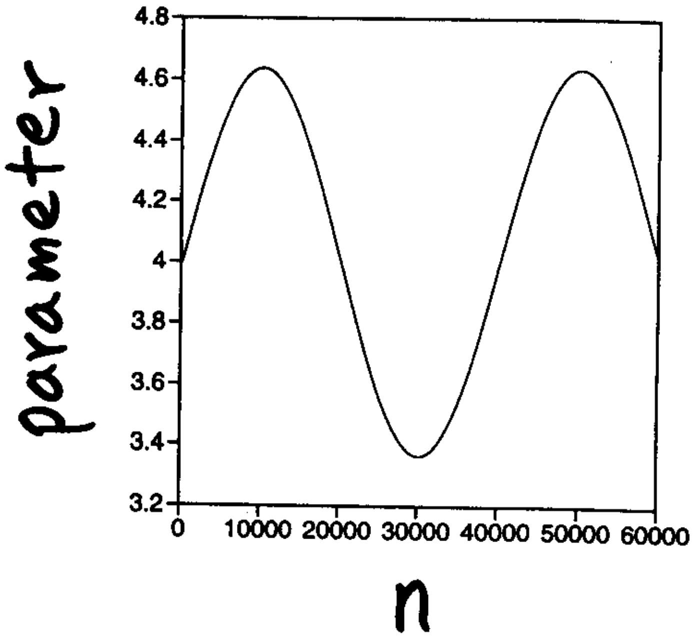

Environment change.

Tracking Result

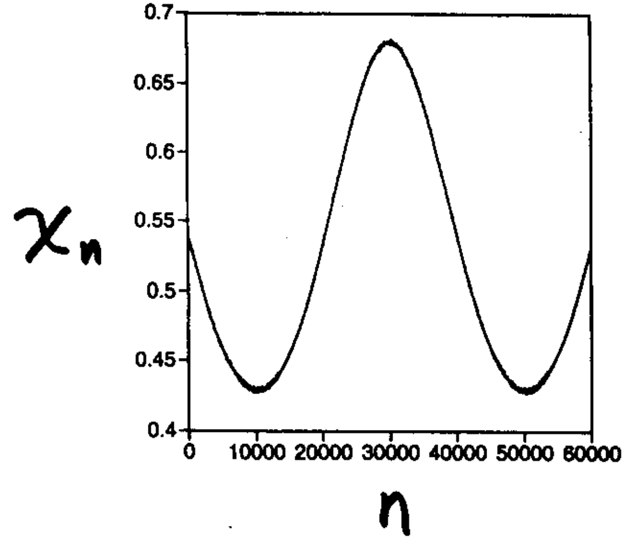

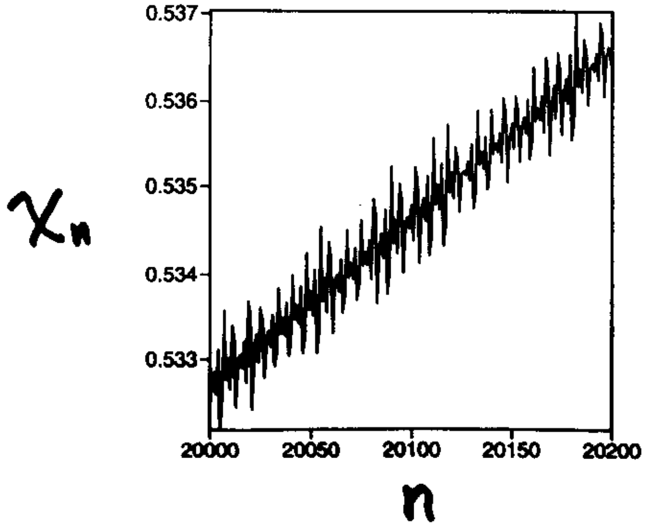

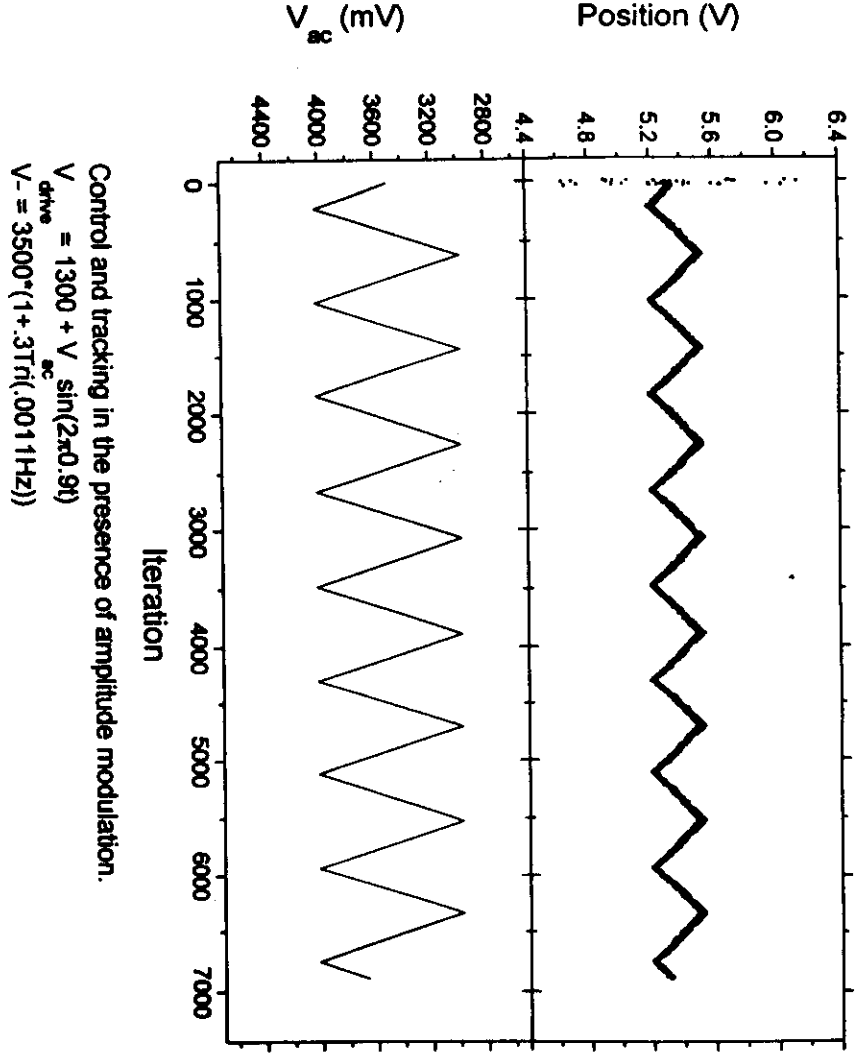

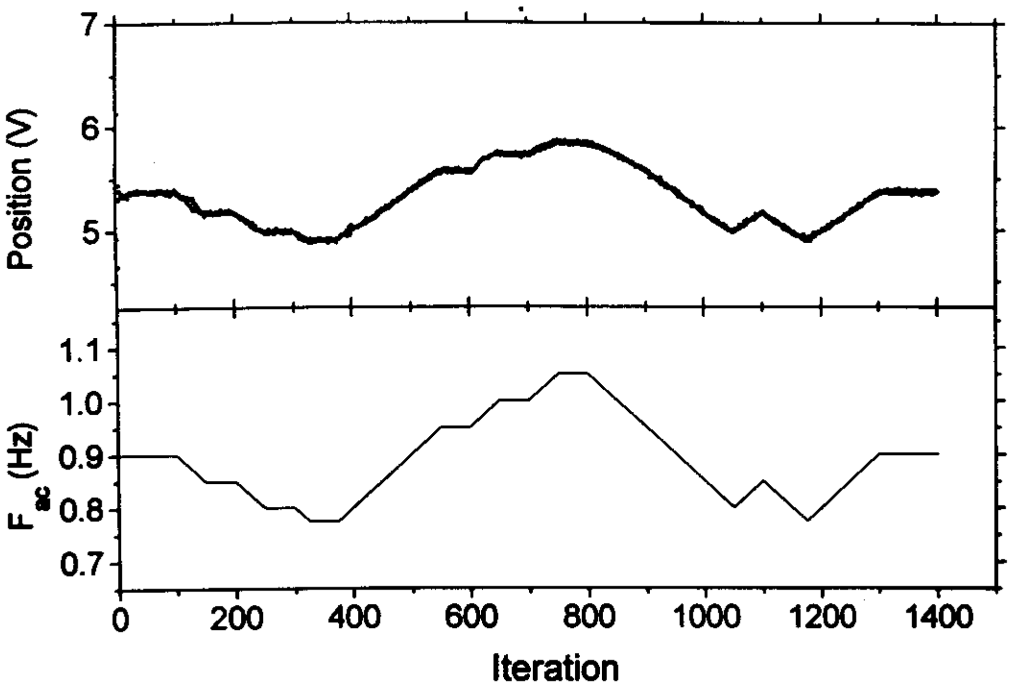

Control and tracking with frequncy variations.
$V_{drive} = 1300 + 3500\sin(2\pi F_{ac} t)$

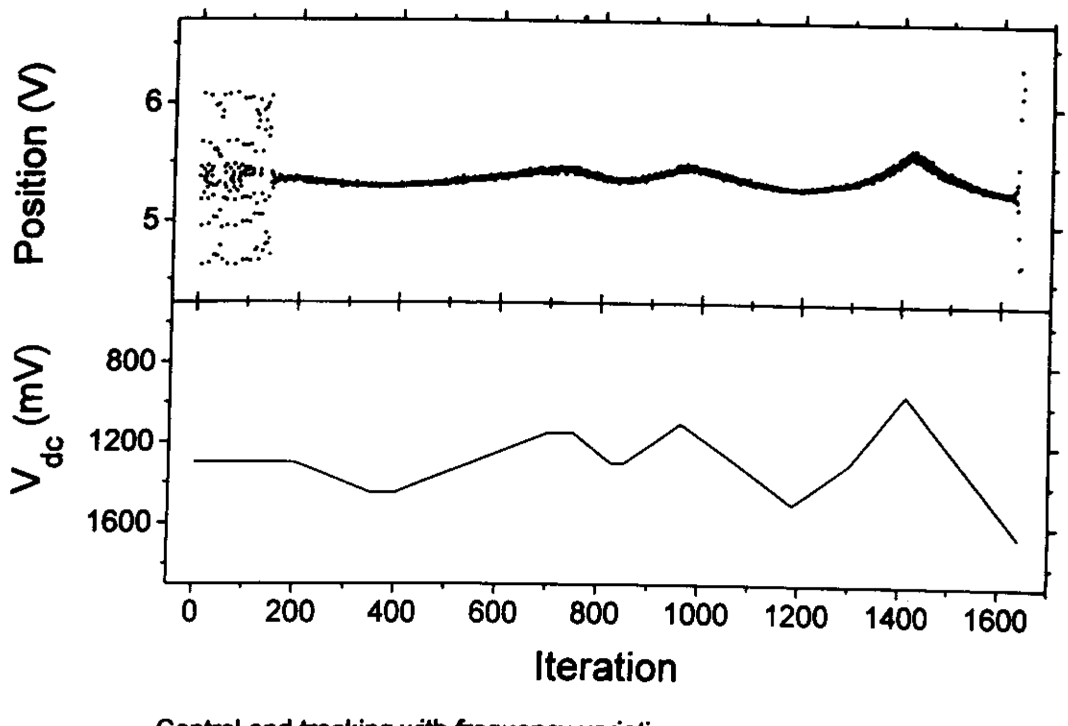

Control and tracking with frequency variations.
$V_{drive} = V_{dc} + 3500\sin(2\pi 0.9t)$

Enhancing Synchronism of Chaotic Systems

M. DING

Florida Atlantic Univ.

with

E. Ott

Phys. Rev. E

(1994)

Basic Idea (Pecora, Carroll)

$$\frac{d\underset{\sim}{Z}}{dt} = \underset{\sim}{F}(\underset{\sim}{Z}), \quad \underset{\sim}{Z} \in \mathbb{R}^{m}$$

$$\underset{\sim}{Z} = \begin{bmatrix} \underset{\sim}{x} \\ \underset{\sim}{y} \end{bmatrix} \qquad \begin{array}{l} \underset{\sim}{x} \in \mathbb{R}^{m_1} \\ \underset{\sim}{y} \in \mathbb{R}^{m_2} \end{array}$$

$m_1 + m_2 = m$ (usually, $m_1 = 1$)

$$\underset{\sim}{F}(\underset{\sim}{z}) = \begin{bmatrix} \underset{\sim}{G}(\underset{\sim}{x}, \underset{\sim}{y}) \\ \underset{\sim}{H}(\underset{\sim}{x}, \underset{\sim}{y}) \end{bmatrix}$$

$$\frac{d\underset{\sim}{x}}{dt} = \underset{\sim}{G}(\underset{\sim}{x}, \underset{\sim}{y}), \quad \frac{d\underset{\sim}{y}}{dt} = \underset{\sim}{H}(\underset{\sim}{x}, \underset{\sim}{y})$$

We consider $\underset{\sim}{z}$ as the driving system and $\underset{\sim}{x}$ as the drive signal.

Receiving system:

$$\frac{d\hat{\underset{\sim}{x}}}{dt} = \underset{\sim}{G}(\hat{\underset{\sim}{x}}, \hat{\underset{\sim}{y}})$$

$$\frac{d\hat{\underset{\sim}{y}}}{dt} = \underset{\sim}{H}(\underset{\sim}{x}, \hat{\underset{\sim}{y}})$$

Synchronization condition

$$\lim_{t\to\infty} |\underset{\sim}{y}(t) - \hat{\underset{\sim}{y}}(t)| = 0$$

for $\underset{\sim}{y}(0) \neq \hat{\underset{\sim}{y}}(0)$

Subsystem Lyapunov Exponent

$$\frac{d\hat{\underset{\sim}{y}}}{dt} = \underset{\sim}{H}(\underset{\sim}{x}, \hat{\underset{\sim}{y}})$$

Clearly, $\hat{\underset{\sim}{y}}(t) = \underset{\sim}{y}(t)$ is a solution. Q: Is it stable?

$$\hat{\underset{\sim}{y}}(t) = \underset{\sim}{y}(t) + \delta\hat{\underset{\sim}{y}}(t)$$

$$\frac{d}{dt}\delta\hat{\underset{\sim}{y}}(t) = \delta\hat{\underset{\sim}{y}}(t) \cdot \left.\frac{\partial \underset{\sim}{H}(\underset{\sim}{x}, \hat{\underset{\sim}{y}})}{\partial \hat{\underset{\sim}{y}}}\right|_{\hat{y}=y}$$

$$\hat{\Lambda} = \lim_{t\to\infty} \frac{1}{t} \ln \frac{|\delta\hat{\underset{\sim}{y}}(t)|}{|\delta\hat{\underset{\sim}{y}}(0)|}$$

$\hat{\Lambda} < 0$: Synchronization

Synchronism With Nonreplica Systems

$$\frac{d\underset{\sim}{\hat{x}}}{dt} = \underset{\sim}{K}(\underset{\sim}{x}, \underset{\sim}{\hat{x}}, \underset{\sim}{\hat{y}})$$

$$\frac{d\underset{\sim}{\hat{y}}}{dt} = \underset{\sim}{L}(\underset{\sim}{x}, \underset{\sim}{\hat{x}}, \underset{\sim}{\hat{y}}).$$

$$\underset{\sim}{K}(\underset{\sim}{x}, \underset{\sim}{x}, \underset{\sim}{y}) = \underset{\sim}{G}(\underset{\sim}{x}, \underset{\sim}{y})$$

$$\underset{\sim}{L}(\underset{\sim}{x}, \underset{\sim}{x}, \underset{\sim}{y}) = \underset{\sim}{H}(\underset{\sim}{x}, \underset{\sim}{y})$$

$$\underset{\sim}{\hat{z}}(t) = \begin{bmatrix} \underset{\sim}{\hat{x}}(t) \\ \underset{\sim}{\hat{y}}(t) \end{bmatrix}$$

$$\underset{\sim}{\hat{z}}(t) = \underset{\sim}{z}(t) + \delta \underset{\sim}{\hat{z}}(t)$$

$$\hat{\Lambda} = \lim_{t \to \infty} \frac{1}{t} \ln \frac{|\delta \underset{\sim}{\hat{z}}(t)|}{|\delta \underset{\sim}{\hat{z}}(0)|}$$

$\hat{\Lambda}$: response Lyapunov exponent.

$$\hat{\Lambda} < 0 \Rightarrow \lim_{t \to \infty} |\underset{\sim}{\hat{z}}(t) - \underset{\sim}{z}(t)| = 0 \quad \text{for } \underset{\sim}{\hat{z}}(0) \neq \underset{\sim}{z}(0)$$

$\Rightarrow$ Synchronization

Potential Advantages

- Achieving synchronism when $\hat{\Lambda} > 0$ for the replica subsystem.
- Enabling faster convergence to the synchronized state.
- Eliminating or reducing the size of spurious basins of attraction.
- Improving the performance of signal recovery technique

Numerical Example

The Rössler system

$$\frac{dx}{dt} = b + x(y_1 - c) \equiv G(x, y_1, y_2)$$

$$\frac{dy_1}{dt} = -x - y_2 \equiv H_1(x, y_1, y_2)$$

$$\frac{dy_2}{dt} = y_1 + a y_2 \equiv H_2(x, y_1, y_2)$$

Replica Subsystem

$$\frac{d\hat{y}_1}{dt} = -x - \hat{y}_2, \quad \frac{d\hat{y}_2}{dt} = \hat{y}_1 + a\hat{y}_2$$

$$\hat{\Lambda} = \frac{a}{2} > 0 \quad \text{for } a > 0$$

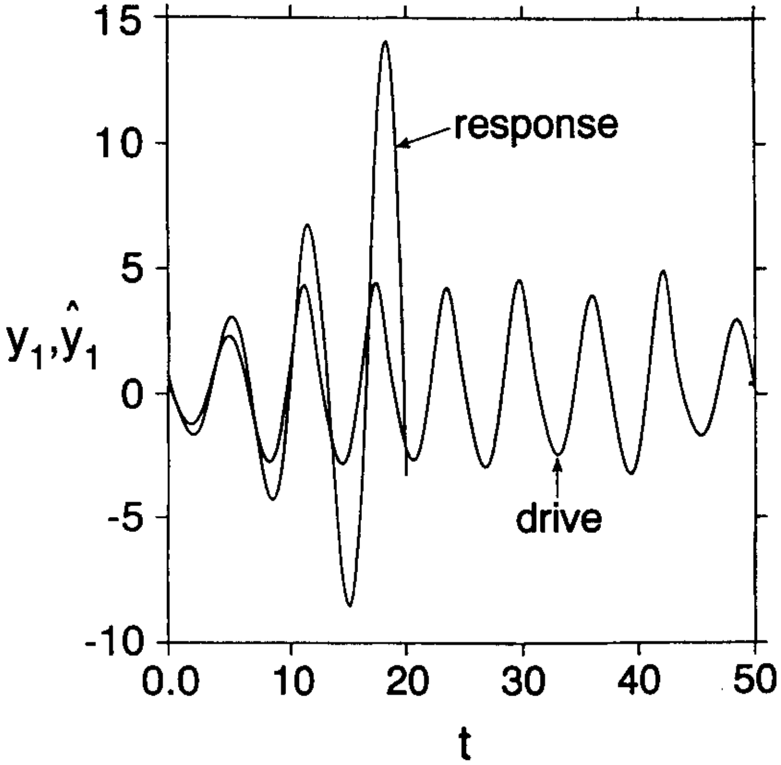

Fig. 1

Nonreplica Response:

$$\frac{d\hat{x}(t)}{dt} = b + x(\hat{y}_1 - c) + \alpha(\hat{x} - x)$$

$$\frac{d\hat{y}_1(t)}{dt} = -x - \hat{y}_2 + \beta(\hat{x} - x)$$

$$\frac{d\hat{y}_2(t)}{dt} = \hat{y}_1 + a\hat{y}_2 + \gamma(\hat{x} - x)$$

Consider the line:

$$\alpha/\alpha_e = \beta/\beta_e = \gamma/\gamma_e$$

$$\alpha_e = -3, \; \beta_e = 1, \; \gamma_e = -5$$

$$0 \leq \beta \leq 1$$

$\beta = 0.7, \quad \hat{\Lambda} = -0.25$

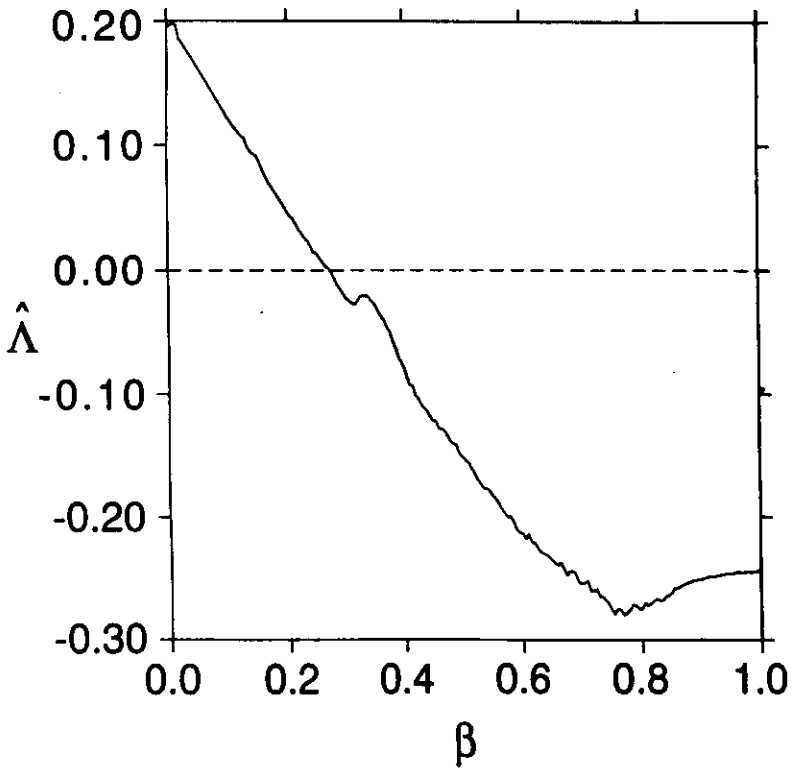

Fig. 2

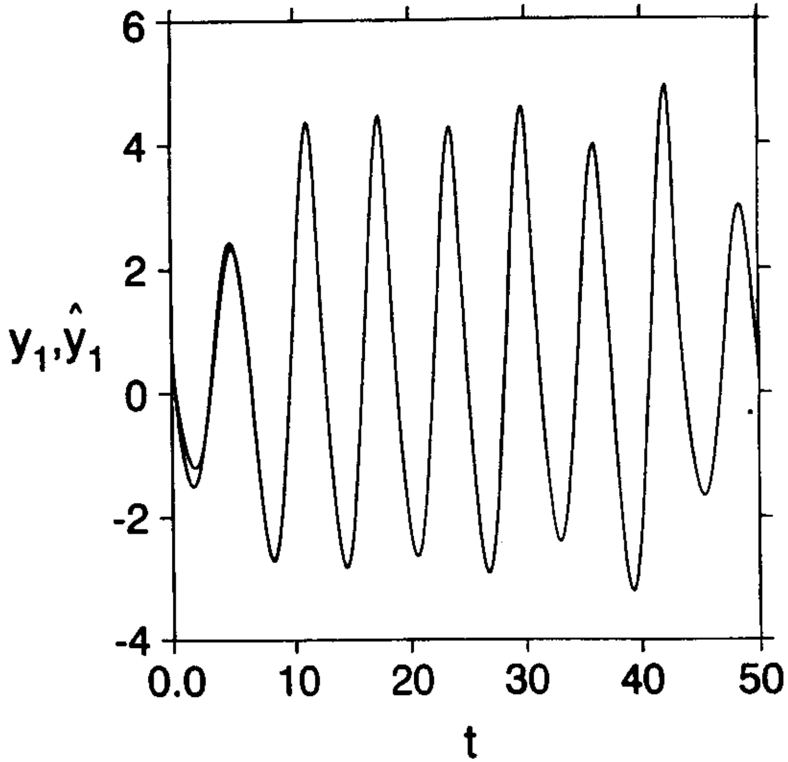

Fig. 3

$\hat{\Lambda} = -0.006$, $\beta = 0.28$

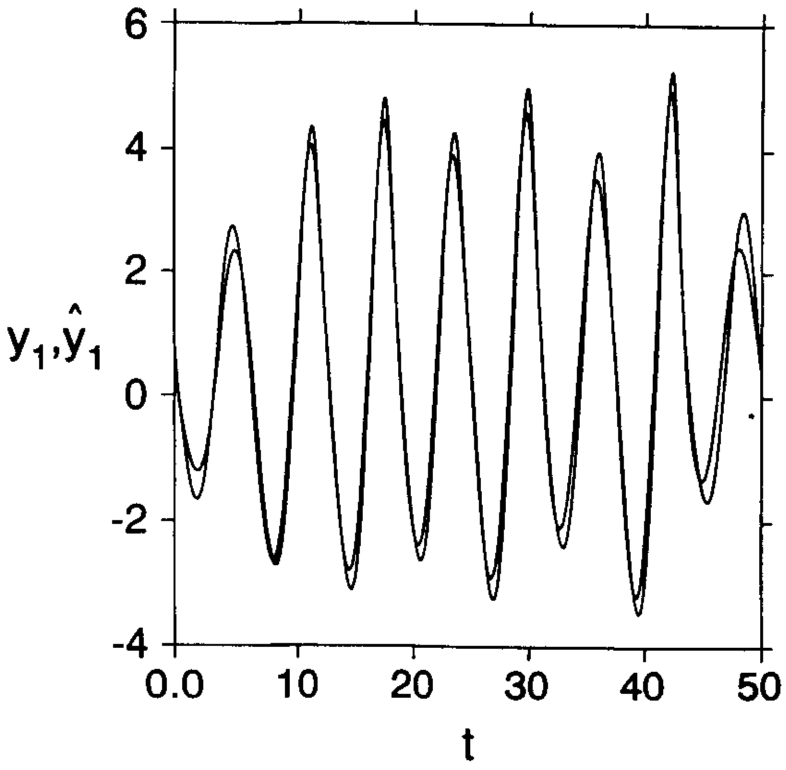

Fig. 4

Synchronizing Hyperchaos With a Scalar Transmitted Signal

M. DING

Florida Atlantic Univ

Coworkers:

E. J. Ding

J. H. Peng

W. Yang

Phys. Rev. Lett.

1996

Using Chaos to Hide Messages: The Cuomo - Oppenheim approach

chaotic sender

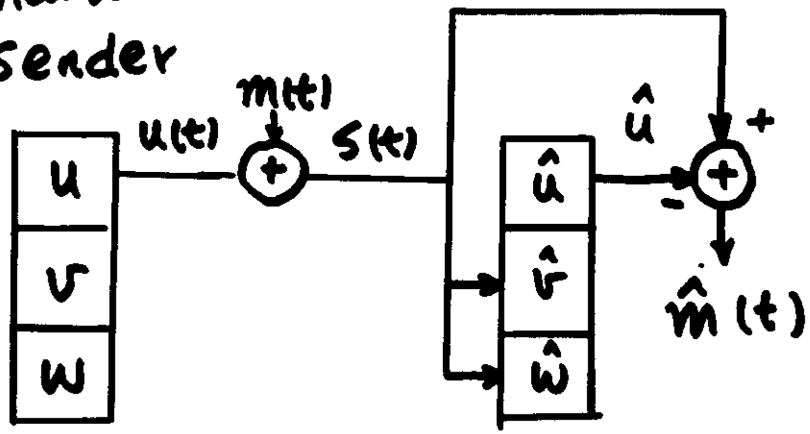

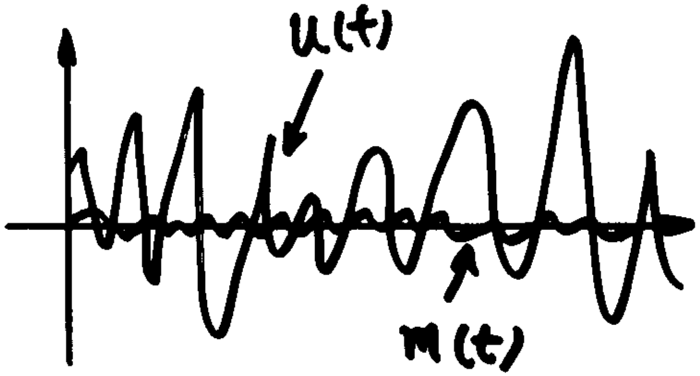

There is a Problem

Theoretical as well as experi. studies reported so far concern mainly with low-dim. systems with one positive Lyapunov exponent. Perez and Cerdeira (PRL, 1995) show that messages often can be extracted if masked by simple chaotic processes.

A Possible Solution

Use high dimensional systems with multiple positive Lyapunov exponents (hyperchaos).

One may speculate that in this case we may need to send as many variables as the number of positive Lyapunov exponents.

Our Approach

Sender:

$$\frac{d\underset{\sim}{x}}{dt} = \underset{\sim}{F}(\underset{\sim}{x}) \qquad \underset{\sim}{x} \in \mathbb{R}^m$$

Transmitted signal:

$$u(t) = \underset{\sim}{K}^T \underset{\sim}{x}(t) = k_1 x_1(t) + k_2 x_2(t) + \cdots + k_m x_m(t)$$

Receiver:

$$\frac{d\hat{\underset{\sim}{x}}}{dt} = \underset{\sim}{F}(\hat{\underset{\sim}{x}}(t)) - \underset{\sim}{B}(v(t) - u(t))$$

$$v(t) = \underset{\sim}{K}^T \hat{\underset{\sim}{x}}(t)$$

$$= k_1 \hat{x}_1(t) + k_2 \hat{x}_2(t) + \cdots + k_m \hat{x}_m(t)$$

For $\underset{\sim}{K} = \begin{pmatrix} 0 \\ \vdots \\ 1 \\ 0 \\ \vdots \\ 0 \end{pmatrix}$ we are back to the first part of the talk.

Stability Problem

Let $\hat{\underset{\sim}{x}}(t) = \underset{\sim}{x}(t) + \delta \hat{\underset{\sim}{x}}(t)$

Then

$$\frac{d}{dt}\delta\hat{\underset{\sim}{x}} = \frac{\partial \underset{\sim}{F}(\hat{\underset{\sim}{x}})}{\partial \hat{\underset{\sim}{x}}}\bigg|_{\hat{\underset{\sim}{x}}=\underset{\sim}{x}} \delta\hat{\underset{\sim}{x}} - \underset{\sim}{B}\,\underset{\sim}{K}^T \delta\hat{\underset{\sim}{x}}$$

$$= \left(\underset{\approx}{J}(\underset{\sim}{x}(t)) - \underset{\sim}{B}\,\underset{\sim}{K}^T \right)\delta\hat{\underset{\sim}{x}}$$

choose $\underset{\sim}{B}$ and $\underset{\sim}{K}^T$ such that

$$|\delta\hat{\underset{\sim}{x}}| \xrightarrow[t\to\infty]{} 0 .$$

A Nonlinear Control Problem

$$\frac{d}{dt}\delta\hat{\underset{\sim}{x}} = (\underset{\approx}{J}(\underset{\sim}{x}(t)) - \underset{\sim}{B}\,\underset{\sim}{k}^T)\,\delta\hat{\underset{\sim}{x}}$$

$$\dot{\underset{\sim}{x}}(t) = \underset{\sim}{F}(\underset{\sim}{x}(t))$$

Choose $\underset{\sim}{B}$, $\underset{\sim}{k}^T$ such that

$$|\delta\hat{\underset{\sim}{x}}| \xrightarrow[t\to\infty]{} 0$$

Numerical Example

Hyperchaotic Rössler System:

$$\begin{cases} \dot{x}_1 = -x_2 - x_3 \\ \dot{x}_2 = x_1 + 0.25\,x_2 + x_4 \\ \dot{x}_3 = 3.0 + x_1 x_3 \\ \dot{x}_4 = -0.5\,x_3 + 0.05\,x_4 \end{cases}$$

$\Lambda_1 = 0.11$, $\Lambda_2 = 0.02$

$$\underset{\sim}{k} = \begin{pmatrix} \sin\theta \\ 0 \\ \cos\theta \\ 0 \end{pmatrix} \qquad \underset{\sim}{B} = 5\begin{pmatrix} \cos\theta \\ 0 \\ \sin\theta \\ 0 \end{pmatrix}$$

Largest Response Lyapunov Exponent

Synchronized Trajec.

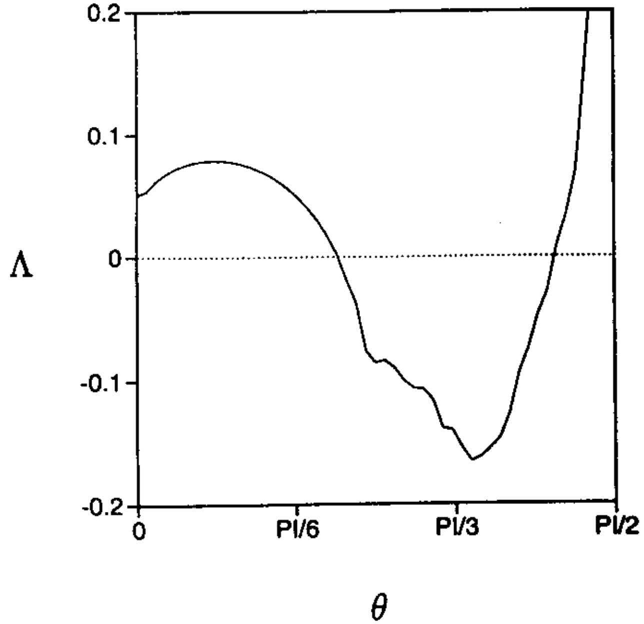

FIG. 1

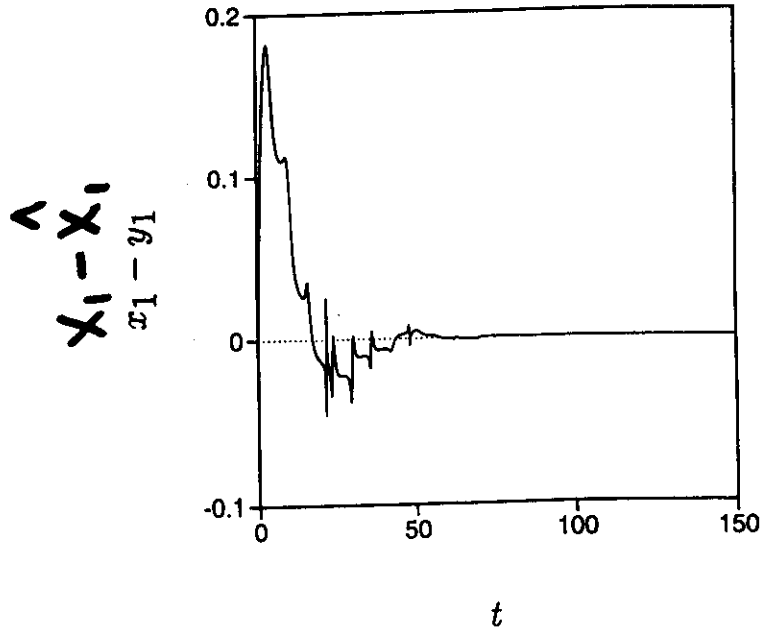

$\Lambda < 0$

FIG. 2

Trajectory Selection in Multistable Systems: Stochastic Resonance, Signal Bias and effect of Signal phase

M. DING

Florida Atlantic Univ.

with

W. Yang

G. Hu

PRL: 1995

Problem & Motivation

$$\ddot{x} + f(\dot{x}, x) = a + b\cos\omega t$$

$$t_n = n\,\frac{2\pi}{\omega}$$

period-Multipled orbit

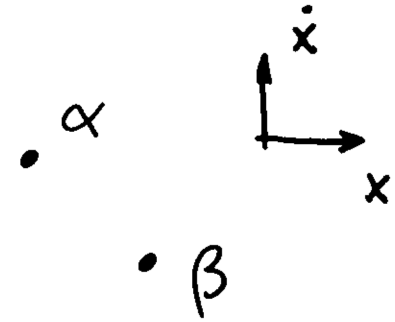

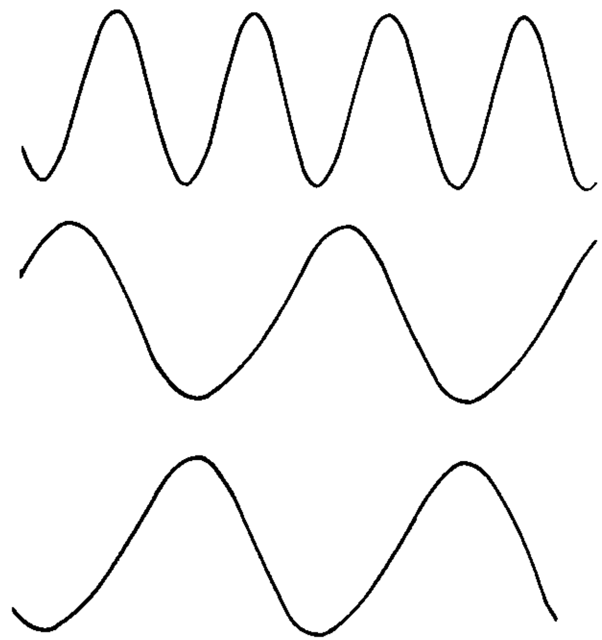

Drive

phase α

phase β

Domain α $\longrightarrow$ phase α

Domain β $\longrightarrow$ phase β

Domain α $\rightarrow$ Domain β

t_n $\quad$ t_{n+1}

Considered under the 2nd iterate of the Poincaré map α and β become fixed point attractors.

Suppose a system of nearly identical units is desired to evolve in synchrony.

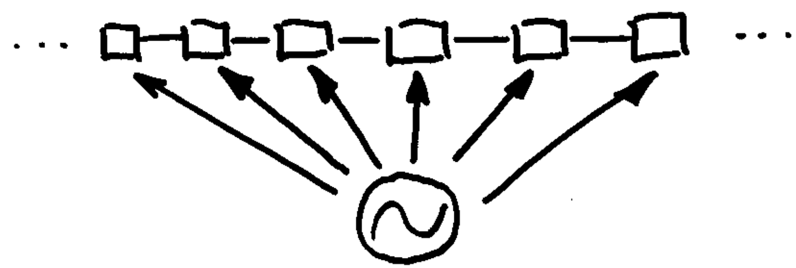

$\square$: $\ddot{x} + f(\dot{x}, x) = a + b\cos\omega t$

Multistability can be detrimental in such applications.

Question is to harness the richness rendered by multistability.

This problem is first noted by Pecora and Carroll (1991, 1993). They propose to add a chaotic signal with certain periodic characteristic as part of the drive.

$$\ddot{x} + f(\dot{x}, x) = a + b\cos\omega t + \epsilon y(t)$$

$y(t)$: chaotic drive

Using Roessler to provide $y(t)$ they demonstrate the method.

Our Approach

$$\ddot{x} + f(\dot{x}, x) = a + b\cos\omega t + f_s(t) + f_n(t)$$

$$f_s(t) = A_s \sin(\Omega t + \phi)$$

$$f_n(t) = A_n \eta(t)$$

$$\langle \eta(t) \rangle = 0, \quad \langle \eta^2(t) \rangle = 1$$

$\eta(t)$: Gaussian White Noise

After being applied for a given period of time, f_s and f_n are removed, and the system evolves in natural state.

Numerical Example

Duffing oscillator:

$$\ddot{x} + 0.05\dot{x} + x^3 = a + b\cos t + f_s(t) + f_n(t)$$

$\dot{x}$

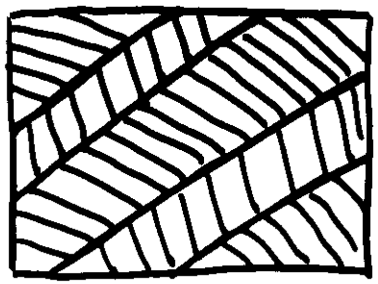

x

$a = 0.15$
$b = 0.21$
$f_s = f_n \equiv 0$

//// : period-2 attractor (Target)

/// : period-3 attractor to be eliminated

Notations

$L_2(0)$, $L_3(0)$: # of pts in period-2 and period-3 basins at $t=0$

L_2, L_3: same quantities after removal f_s and f_n.

N_α, N_β: # of points in Domain α and Domain β after removal of f_s and f_n.

$$N_\alpha + N_\beta = L_2$$

$f_s = 0$

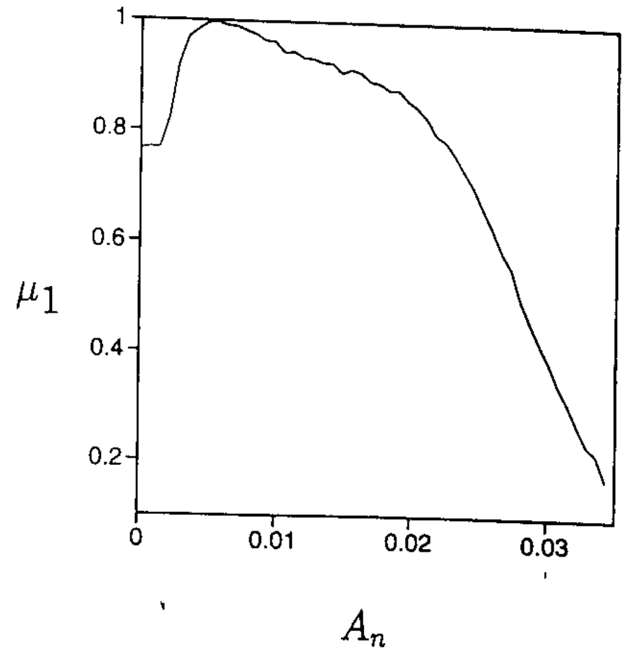

Fig. 1

$$\mu_1 = \frac{L_2}{L_2(0) + L_3(0)}$$

One-dim Analogy

$$\dot{y} = -\frac{\partial V(y)}{\partial y} + \text{noise}$$

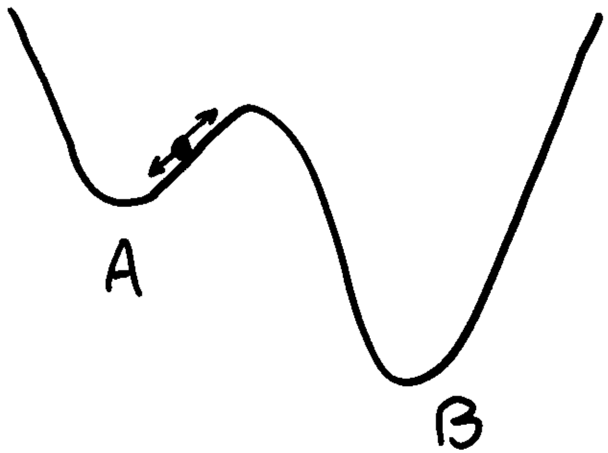

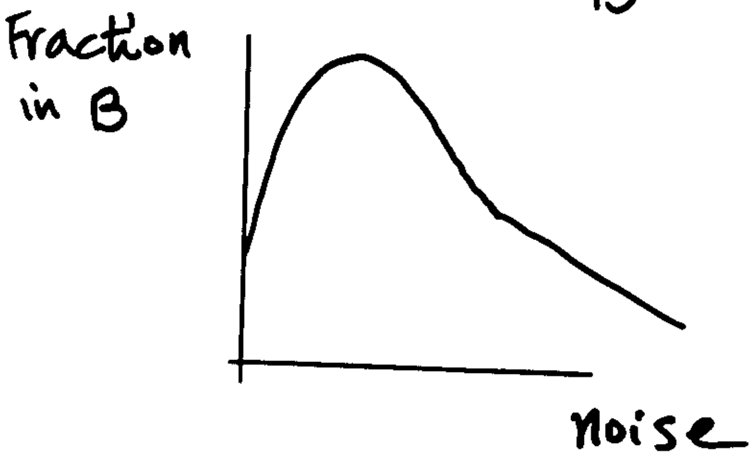

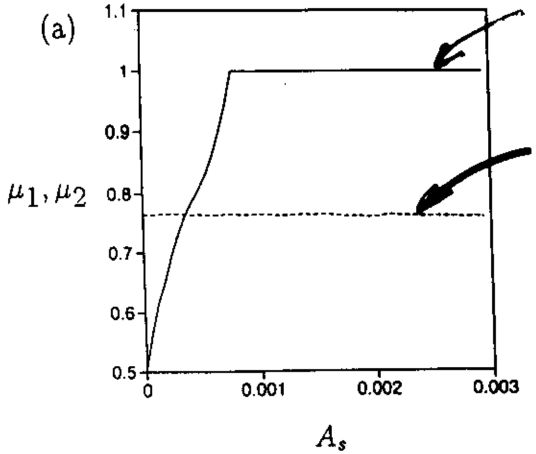

μ_2

μ_1

$A_n = 0$

$f_s(t) =$

$A_s \sin(\frac{t}{2} + \frac{\pi}{2})$

$A_s = 0.002$

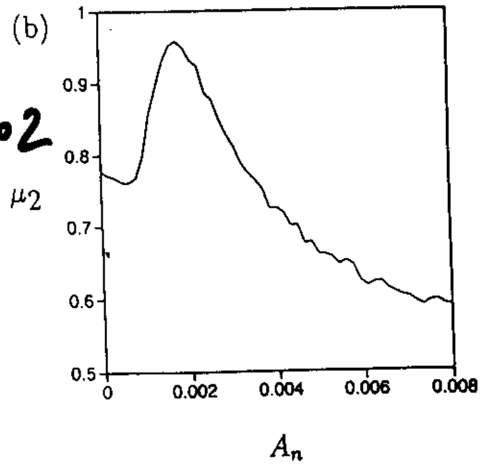

$\mu_2 = N\alpha / (N_\alpha + N_\beta)$

Fig. 2

Effect of Signal Phase

$A_s = 0.002, \quad A_n = 0.004$

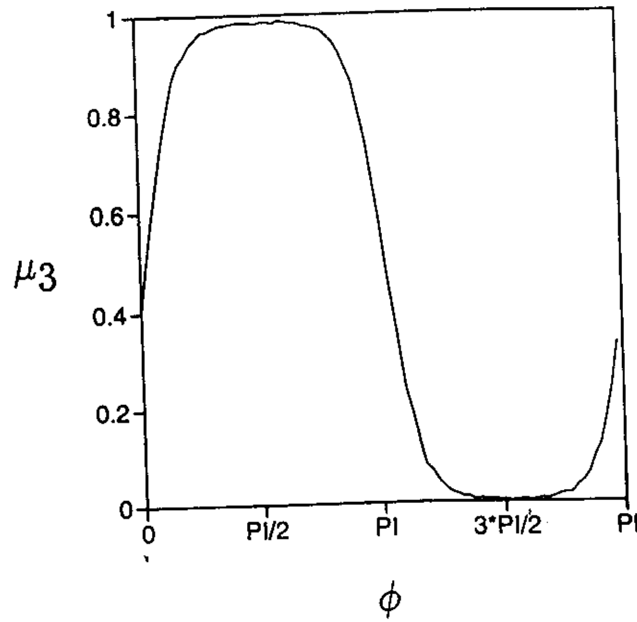

$\mu_3 = N\alpha / (L_2(0) + L_3(0))$

Fig. 3

$\Phi = 5\pi/6$

Example of a Circle Map

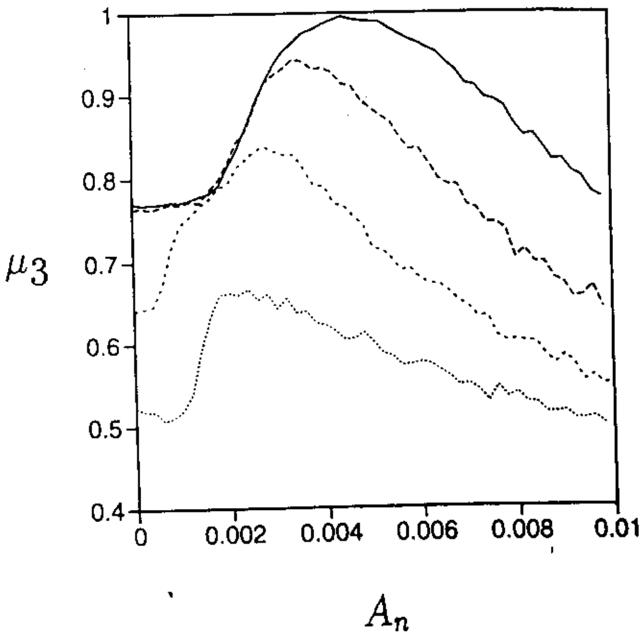

Fig. 4

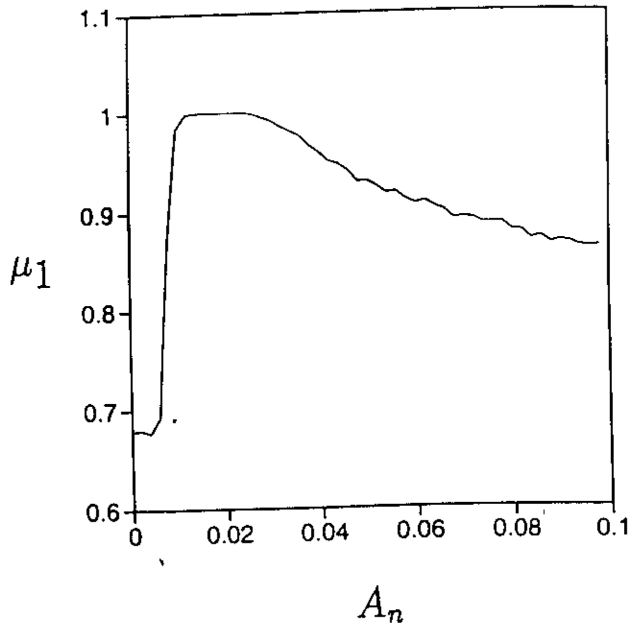

Fig. 5

$A_s = 0.0004, 0.001, 0.002, 0.004$